Universitetet i Stavanger

FACULTY OF SCIENCE AND TECHNOLOGY

MASTER'S THESIS

Study programme/specialisation: Petroleum Geosciences Engineering	Spring semester, 2017 Open
Author: Emera Kamal Aldein Mostafa	…… (signature of author)
Faculty Supervisors: Chris Townsend and Alejandro Escalona	
Title of master's thesis: Subsurface investigation in the Gulf of Corinth (GoC), Greece	
Credits (Ects): 30	
Keywords: Extensional Tectonics Corinth Rift Gulf of Corinth Greece Structural Geology Transfer Faults	Number of pages: …… + supplemental material/other: …… Stavanger,……. date/year

Subsurface investigation in the Gulf of Corinth (GoC), Greece

By

Emera Kamal Aldein Mostafa

Master's Thesis

Presented to the Faculty of Science and Technology

The University of Stavanger

The University of Stavanger

August 2017

Dedication

To the memory of my beloved father`s soul, for his support and being there for me, always.

Emera Mostafa

Acknowledgements

I would like to thank my supervisor Chris Townsend for giving me this opportunity to write this thesis, and for his support, guidance, encouragement and thorough scrutiny of my work, which was always accompanied with constructive feedback and suggestions.

I would also like express to my sincere gratitude to my co-supervisor Alejandro Escalona for all his support and being a constant source of encouragement throughout this thesis. Also, I want to thank Wiktor Weibull, Lisa Watson and Andreas Habel for their technical support.

A further thank is directed to my family, my lovely Mum and my wonderful husband, Aso, for their unwavering support throughout this thesis.

Finally, I would like to express my deepest gratitude to my uncles Camiran, Hassan, and Rizan, for their infinite support and motivation and being there always for me.

Abstract

Subsurface investigation in the Gulf of Corinth (GoC), Greece

Emera Mostafa

The University of Stavanger

Supervisor: Chris Townsend

Co-Supervisor: Alejandro Escalona

The Corinth Rift is an excellent rift laboratory to study the rift processes occurring during the early and late stages of continental extension due to exposure of a series of half-graben structures at the southern margin. Segmentation and lateral variation along the strike in the rift were observed in several studies, where the lateral correlation is hard to obtain as the W-E faults terminated in the valleys and became difficult to trace.

The boundaries between the segments were less emphasized and developed as the main focus of the previous studies was the N-S direction of the rift. The structure geometry is still an going debate and has been interpreted in several ways with some of the studies proposed it to be a relay ramp, and others suggested a transfer zone.

2D seismic, bathymetry, earthquake, and onshore data was used to investigate if the segmentation continues offshore. Furthermore, to reveal the structures the boundaries between the segments, where W-E lines were the main focus throughout this study.

The evidence of the segmentation of the Gulf was substantial as several NNE-SSW faults were traced in W-E seismic lines, some of those faults were correlatable with proposed previous studies boundaries. In total ten transfer faults are proposed; four major, three minor and three sub-minor. The basement structure varies along the strike and today's structures are inherited structure where the stepping of the W-E faults could be related to the structural variation of the basement. The geometry of today structure of the gulf seems to correlate with the proposed transfer faults model by Lister *et al.* (1986), where seismic line presented each segment of the model.

Table of contents

List of figures

List of table

Chapter 1 Introduction

1.1 Background

The Gulf of Corinth (GoC) is a 115 km WNW-ESE oriented extensional basin, that separates the Peloponnesus peninsula from central Main Greece (Figure 1). It is known as one of the most active continental rift systems in the world, initiated around 5 Ma with an extension ratio of 10-16 mm/yr (Clarke *et al*., 1998; Briole *et al*., 2000; Bernad *et al*., 2006). The GoC is described briefly as an E-W striking asymmetrical graben (Moretti *et al*., 2003), with N-dipping normal faults that control the N-S extension and minor S-dipping faults (Roberts and Jackson, 1991; Armijo *et al*., 1996). Initial structures in the central Gulf were controlled by south-dipping faults, but later north-dipping faults became more active and controlled the structures. This change in fault polarity was the main factor in basin geometry formation (Bell *et al*., 2008). The crustal extension in the western part of the rift is estimated to be ~5-13 km, which is less than the central part of ~11-21 km. The difference in the extension rates resulted in higher basement subsidence, higher sedimentation rate and more complex structures with several faults in the central rather than the western part of the basin (Bell *et al*., 2011).

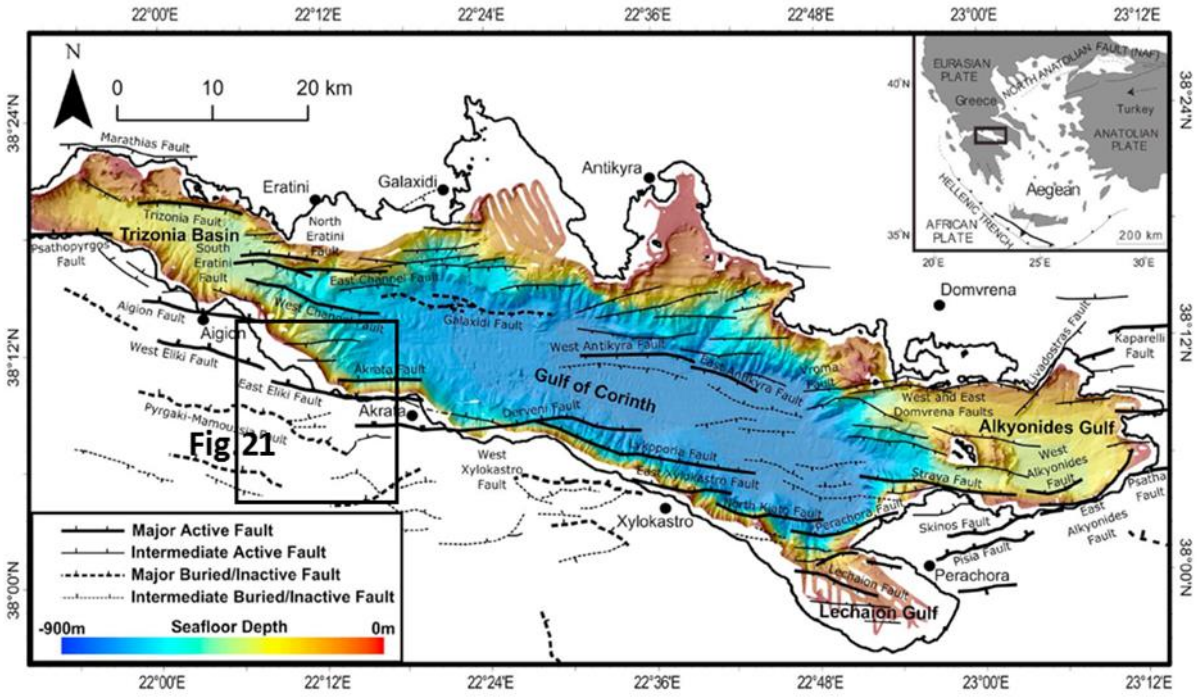

Figure 1 Tectonic map of the GoC showing the main structures in the Corinth Rift. Inset is the tectonic framework of the Aegean showing the main plates and their boundaries with the location of the GoC (Nixon et al., 2016).

1.2 Geological Problem and Objectives

Faults from the early stages of the Corinth rift are preserved onshore, both north and south of the GoC (Ori, 1989; Armijo *et al*., 1996). At the southern margin of the GoC, a series of half-graben structures are exposed, controlled by large displacement N-dipping normal faults. While NNE-SSW river valleys cross-cut these structures perpendicularly. The several major E-W striking faults with average dip angles of 40°-60° and displacement range of 200-1500 meter are difficult to trace from one side of the valley to the other (Dahman, 2015).

The Vouraikos Valley is an example: located in the south western part of the rift system, many of the faults controlling the half-graben structures seem to terminate abruptly on one side of the valley whereas others appear to continue (Dahman, 2015).

Previous work has suggested that the valleys are areas of relay ramps Wood (2013) or transfer zones Dahman (2015). In the case of the transfer zone, Dahman (2015) suggests that the transfer zones are inherited structures from the basement and that they segment the rift system allowing each block to deform independently of the neighbouring block (Lister *et al*., 1986). Furthermore, Wood (2013), related faults step to cross fault or the presence of fault-linking structures.

As the valleys reach the coast, no evidence of their continuity has been documented in the offshore area, as the main focus of previous work has been on E-W striking normal faults controlling the N-S extension of the rift (Bell *et al*., 2011; Taylor *et al*., 2011). However, these N-S structures and segmentation may continue offshore into the northern part of the GoC rift.

Another geological problem is a lateral correlation of the western and eastern sectors of the rift. This is somewhat difficult due to the segmentation of the rift and the major lateral changes in facies and thickness of the syn-rift sediments (Rohais and Moretti, 2016). Lateral variation of the rift structures and stratigraphy was noticed by several authors, and its division has been discussed in numerous studies, but the exact boundaries remain contentious (e.g. Ford *et al*., 2013, Ford *et al*., 2016, Nixon *et al*., 2016).

The overall objective of this thesis is to have the main focus on the W-E direction of the GoC, investigate the boundaries between the segments, and to evaluate if the proposed onshore transfer faults (N-S river valleys) that separate the segmented and tilted blocks continue offshore and into the northern margin of the rift. This study will be carried out using the available 2D seismic in conjunction with earthquake data, existing onshore maps and bathymetry data from the GoC.

1.3 Geological Setting

The relative motion of the African and Eurasian plates has dominated the tectonic evolution of the GoC since the Late Paleozoic. During the Early Cretaceous, the African plate converged with the Eurasian plate resulting in Alpine mountain ranges (Hellenides orogeny) on the northern margin of the Mediterranean and crustal thickening in the Aegean region (McKenzie, 1972; Doutos *et al*., 1988; Taylor *et al*., 2011). From Late Eocene to Early Miocene the Alpine nappe accumulated in western mainland Greece (Figure 2), where the Peloponnesus was positioned due to the westward migration of thrust activity (Fleury, 1980; Richter 1976, and Skourtsosand and Kranis, 2009).

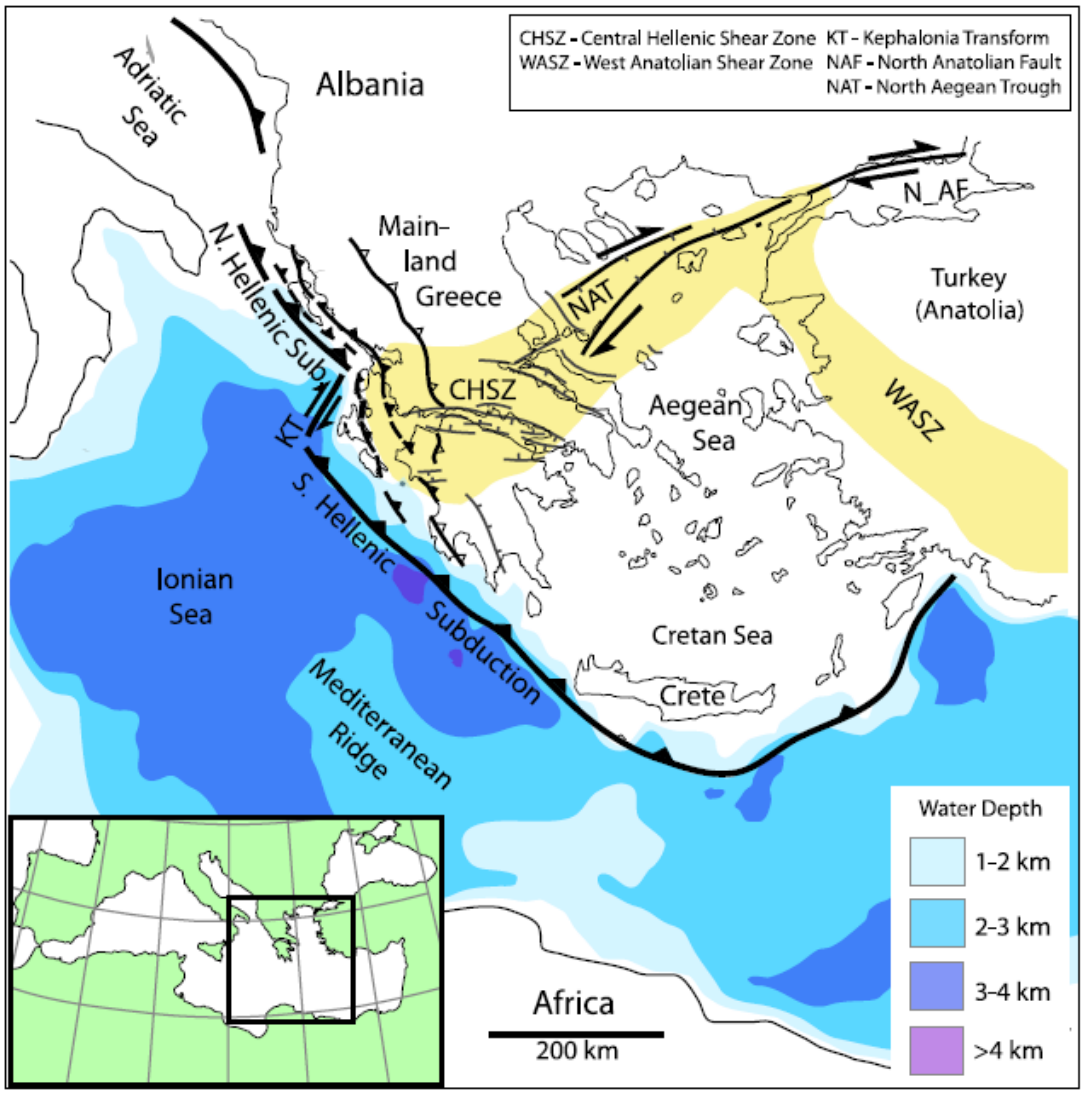

Figure 2 Tectonic setting for GoC and Hellenic subduction zone. NAF, North Anatolian Fault;NAT, North Aegean Trough; CHSZ, Central Hellenic Shear Zone; WASZ, Western Anatolian Shear Zone (Royden and Papanikolau, 2011).

The Zarouchla Complex (ZC) has been defined as the deepest unit of the nappe pile, which consists of a lower metamorphic unit (Phyllites-Quartzite) and an upper unit that corresponds to the Upper Palaeozoic-Upper Triassic Tyros beds (Dercourt 1964; Lekkas and Papanikolaou, 1979; Dornsiepen *et al*., 1986). A tectonic contact separates these two units, later interpreted as a major thrust fault (Lekkas and Papanikolaou, 1979; Dornsiepen *et al*., 2001).

The Pindos Unit is the uppermost part of the Alpine nappe, which consists of Upper Triassic-Upper Cretaceous sediments covered by Tertiary flysch (Degnan and Robertson, 1998; Skourlis and Doutsos, 2000). The Hellenides thrust has been divided into external and internal units (Figure 3) including several NW-SE thrust sheets, where their geometry is inferred at depth. The thrust sheets (Figure 4) consist of mostly sedimentary Paxos, Ionian, Gavrovo-Tripolis and Pindos units in the external Hellenides; and sedimentary as well as crystalline units in the internal Hellenides (Royden and Papanikolaou, 2011).

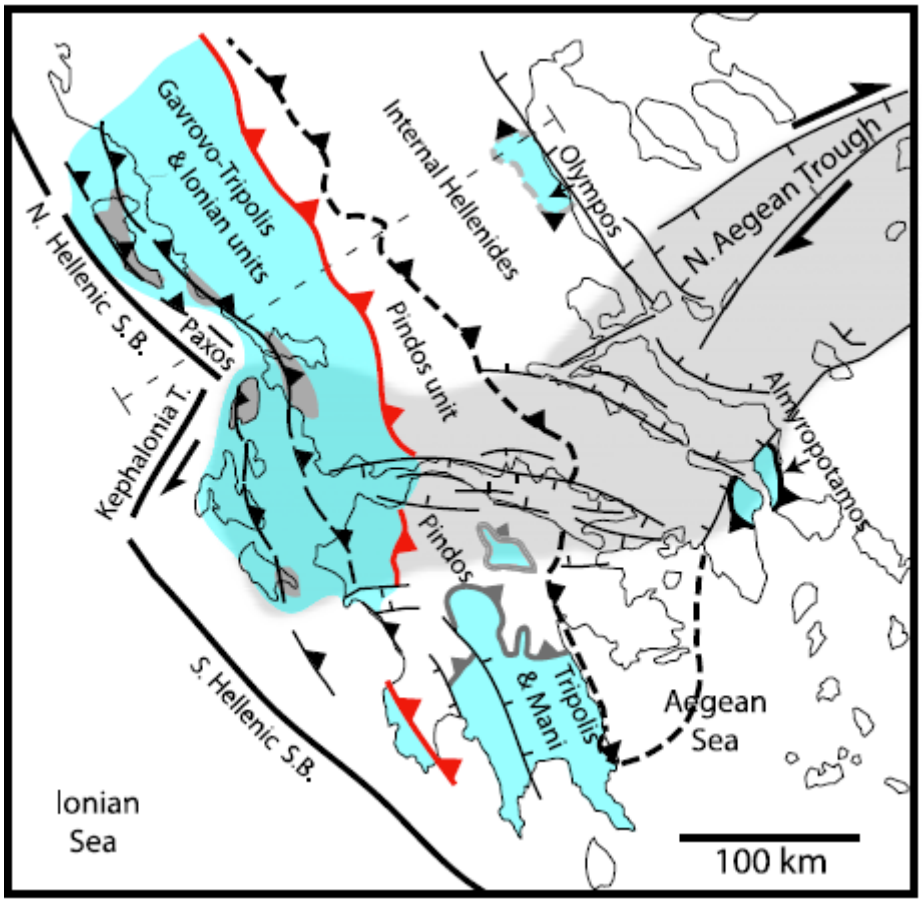

Figure 3 Detailed tectonic structure of the Hellenides thrust belt (Royden and Papanikolau, 2011).

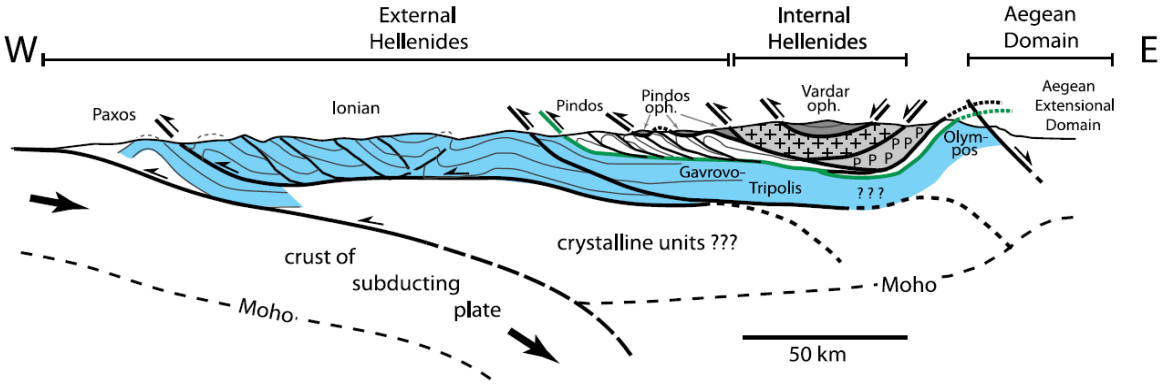

Figure 4 West-east cross section of the northern part of the thrust belt showing the distribution of thrust sheets and their geometry (Royden and Papanikolau, 2011).

In the Late Oligocene, slab rollback of the African plate at the Hellenic Trench resulted in extension in the Mediterranean—more specifically, Aegean back arc extension (McKenzie, 1972; Doutos *et al*., 1988; Taylor *et al*., 2011).

Propagation and strike-slip motion of the Nothern Anatolian Fault (NAF) in a westerly direction had a strong influence on the extensional system in the GoC at ~2-3 Ma (Dewey and Sengor, 1979; Taymaz *et al*., 1991; Armijo *et al*., 1996). This stage resulted in rotation of crustal blocks and crustal collapse due to the increased thickness in the Hellenic Trench (McKenzie, 1972; Horvath and Berckhemer, 1982; Jolivet, 2001). Late Oligocene extension led to rotated fault blocks along the GoC and the Peloponnese peninsula (Ford *et al* ., 2013). This was followed by another extensional regime, which occurred in the Late Pliocene-Pleistocene and established WNW trending rift zones with wide subsidence (Doutsos and Piper 1990).

1.4 Theoretical Background

1.4.1 Transfer Faults

Extensional basins developed due to stretching of the continental lithosphere resulting in passive upwelling and thinning of hot asthenosphere where subsidence and block faulting occurred. The next stage (Figure 5) is the thickening of the lithosphere by heat conduction to the surface, followed by slow thermal subsidence (McKenzie, 1978).

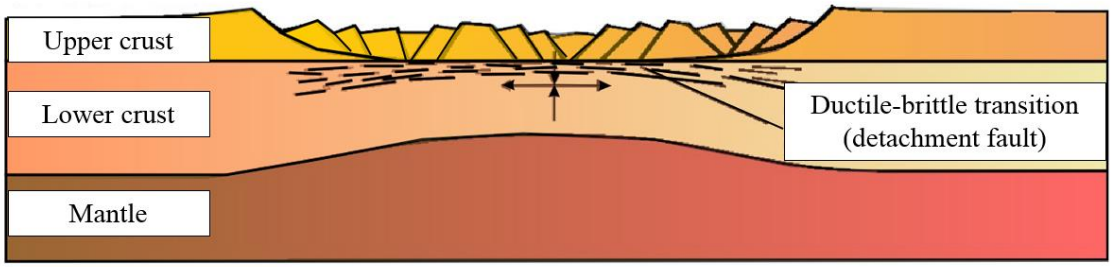

Figure 5 Schematic cross section is showing the pure shear ductile-brittle McKenzie model, modified after Lee et al. (2017).

In contrast to the McKenzie (1978) pure-shear model (Figure 5), Lister *et al*. (1986) proposed a detachment model (Figure 6) and predicted two conjugate passive margins: the upper and the lower plates. The upper plate consists of rocks that are located above the detachment fault and has uncomplicated structures with weakly rotated fault blocks. In contrast, the lower plate consists of deeper crystalline rocks that are overlain by highly faulted remains of the upper plate; its structure is more complex because the faulted blocks are highly tilted and rotated, allowing for more accommodation space.

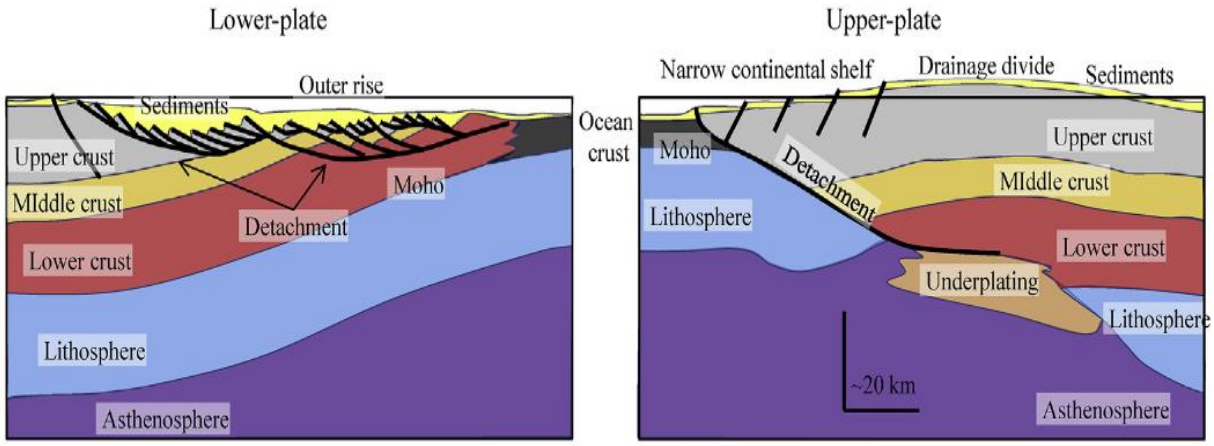

Figure 6 Schematic cross-section showing the Upper plate and Lower plate of Lister et al. (1986), modified by Tasrianto and Escalona, (2015).

According to Lister *et al*. (1986), the termination of main normal faults along shear zones, as well as transferral of displacement and motion from one fault segment to a neighbouring fault segment, is defined as transfer faults. Transfer faults divide the terrane into segments and cause lateral changes in the basin architecture (Figure 7), in addition to possible changes in dip polarity or step in the detachment fault. This stage is associated with a change in the passive margin, from upper-plate to a lower-plate margin.

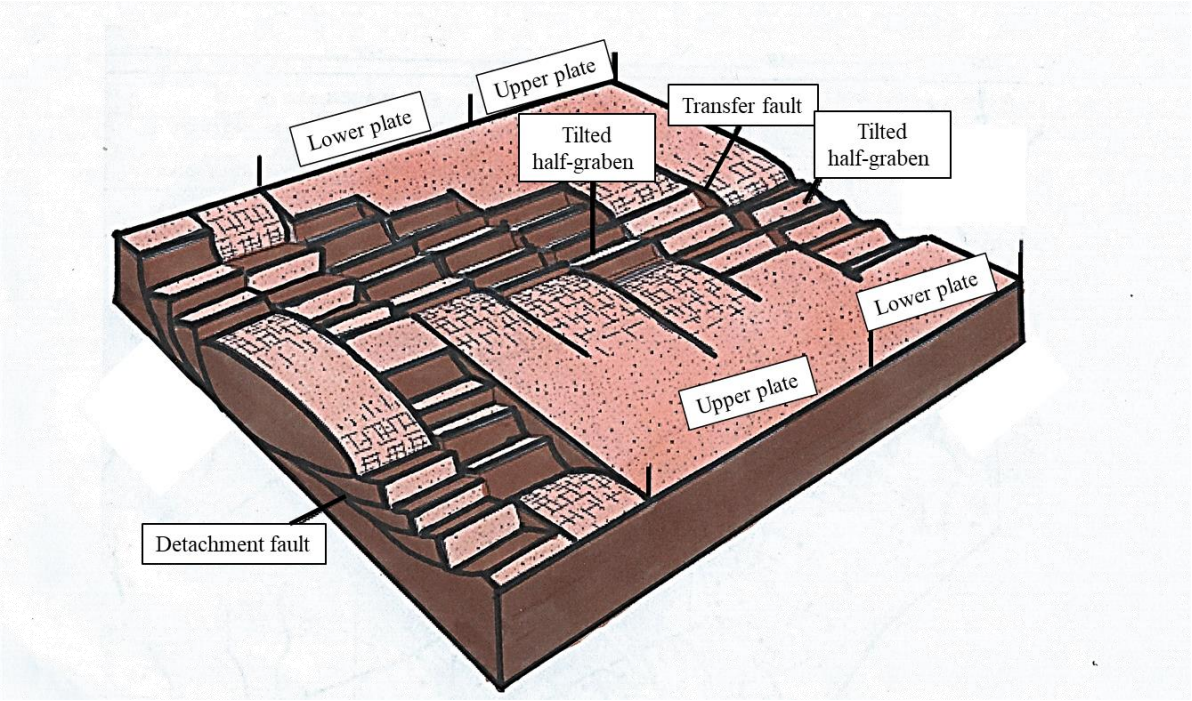

Figure 7 Conceptual 3D model proposed by Lister et al. (1986) showing the architecture of the extensional passive margin including the change from upper to lower plate by transfer faults (modified after Lister et al,. 1986).

Development of detachment faults leads to asymmetrical structure in extensional basins, where transfer faults have an important role in controlling the change from lower-plate to upper-plate margins (Lister *et al*., 1986).

Ancient structural grains may control the geometry of the transfer faults resulting in oblique or lateral transfers, depending on the extensional components of faulting and the relative orientation of the transfer faults (Gibbs, 1984).

Soft-linkage: Relay ramp

A relay ramp forms due to overlapping of faults, where their displacement decreases due to decreased stress at fault tip interaction points (Larsen, 1988) (Figure 8a and 8b). The ramp is a low-stress region connecting the footwall and hanging wall (Larsen, 1988; Foss and Rotevan,2016). Kinematics and fault order control the dip direction of the ramp.Twisting of a relay ramp might occur if the overlapping faults start to propagate (Foss and Rotevan,2016).

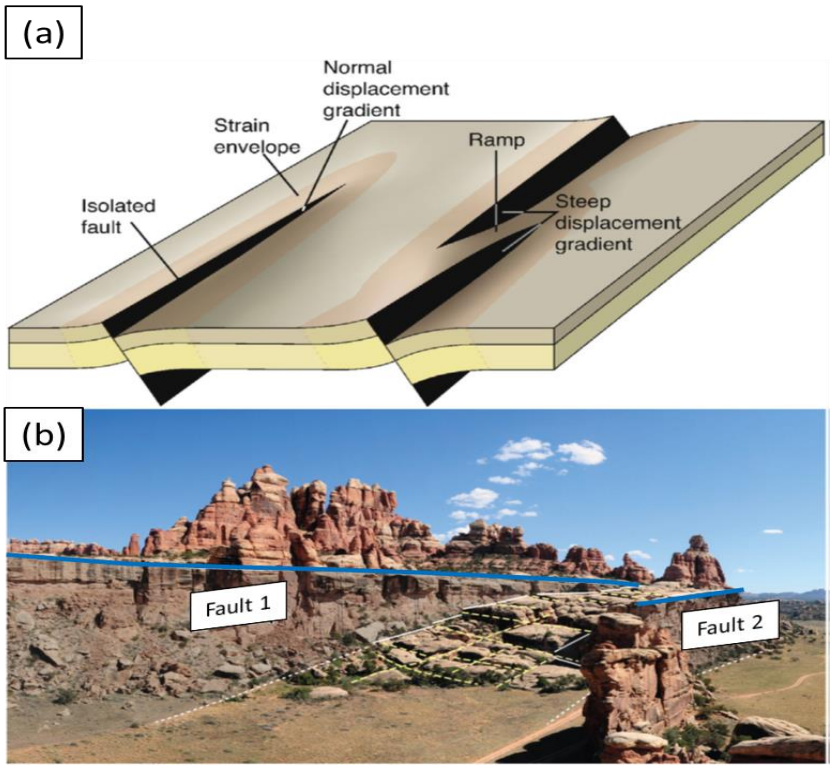

Figure 8 (a) Conceptual 3D model showing how relay ramp structures form, from right to left. (b) Analogue of relay structures in Canyonlands National Park (Fossen and Rotevatn 2016).

In some cases, the ramp is breached completely resulting in a hard-linked transfer fault. The difference between the transfer fault proposed by Lister *et al*. (1986) and a hard linkage transfer fault is illustrated in Figure 9a. In the case of Lister *et al*. (1986), the transfer fault might divide the faults so that displacement is still the same on both sides of the transfer fault (Figure 9a). In contrast, as the hard linked transfer fault is a breached ramp, fault tips will be found on both sides of the transfer fault (Figure 9b).

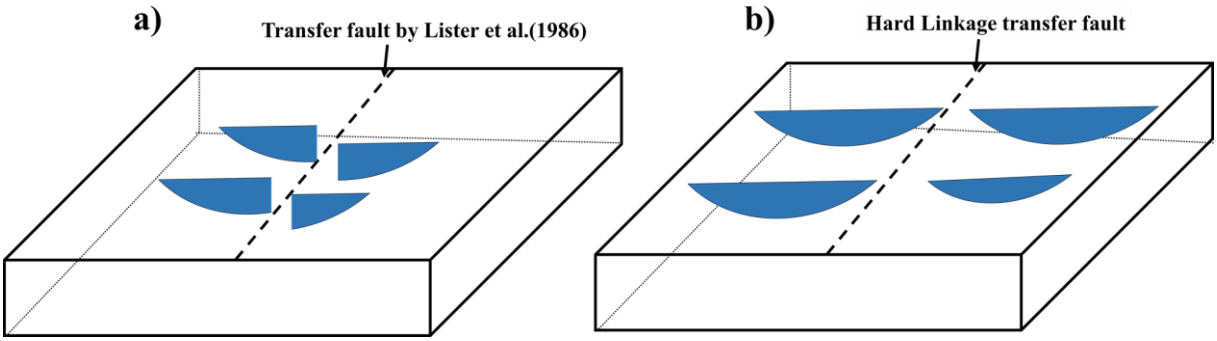

Figure 9 A simplified conceptual models based on previous work: a) transfer fault suggested by Lister et al., (1986); b) hard linkage transfer fault. The blue half circles represent fault displacement, while the dashed line represents a transfer fault.

Structural differences between relay ramps and transfer faults might influence basin development by restricting erosion of syn- and post-tectonic sediments and the way sediments are transferred from the proximal to the distal parts of the sink.

In the case of the transfer fault (Figure 10a), sediments could be transported directly, with the flow orthogonal to the structures. In contrast, the relay ramp (Figure 10b) could control the entry points and the flow direction of sediments (Moustafa and Khalil. 2017). However, some facies variation and drainage patterns have been recognized in the relay zones, where hanging wall depocenters were related to sediment supply. Hence, a relay ramp has a greater drainage basin than a hard linkage setting (Gawthrop and Leeder, 2000; Athmer *et al.*, 2010; Foss and Rotevan, 2016; Moustafa and Khalil. 2017).

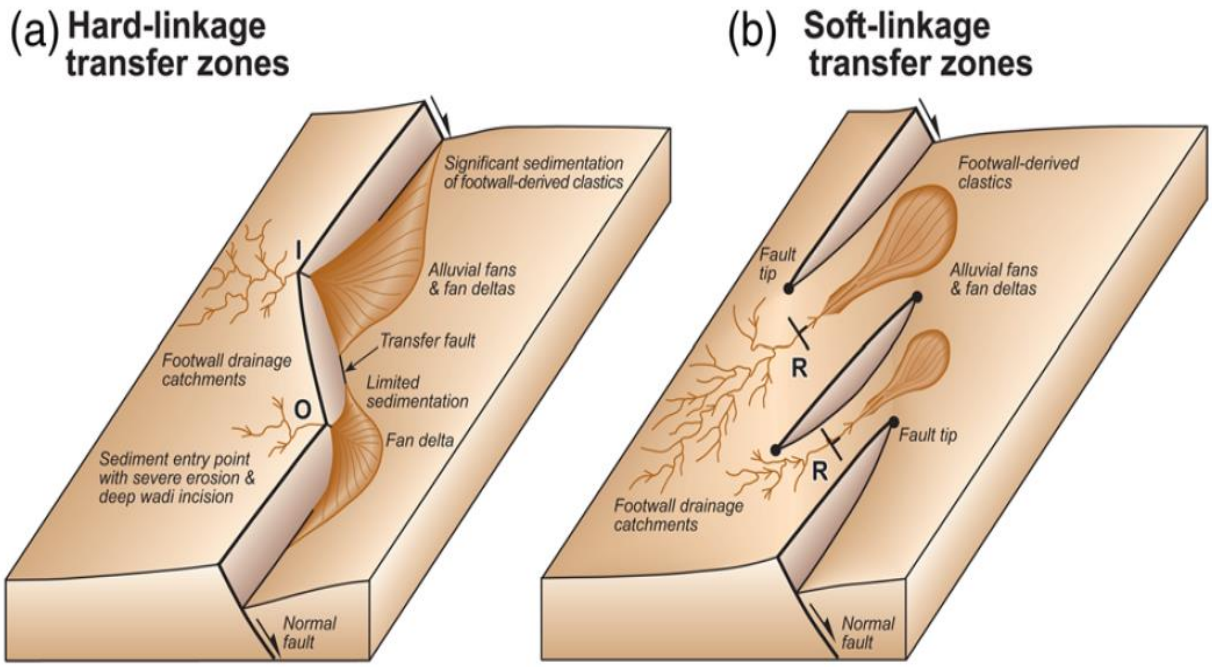

Figure 10 Conceptual 3D models showing the entry points and the locations of the syn- and post-tectonic sediments in two different cases (a) hard-linkage and (b) soft-linkage (I: inward fault kink; O: outward fault kink and R: relay ramp). The difference in the sediment quantity, length of drainage channels and erosion intensity should be noted (Moustafa and Khalil. 2017).

1.5 Previous studies in the Corinth Rift

Over the last few decades, several studies focused on understanding the Corinth Rift geometry and its evolution (e.g., Ori 1989; Doutsos and Piper, 1990; Armijo *et al*., 1996; Sorel, 2000; Bell *et al*., 2008 and Ford *et al*., 2013). In this sub-chapter, previous work is discussed and will be presented based on the geological aspects.

1.5.1 Rift Architecture

1.5.1.1 Simple shear (detachment fault)

Several studies were done to understand rift architecture and the relationship between the Corinth rift and the Miocene metamorphic core complex (e.g., Sorel (2000); Pham *et al*., (2000); Ghisettiand Vezzani (2005); Jolivet *et al*. (2010)). This is largely due to exposure of these low-grade metamorphic rocks (phyllites), which underlie an equivalent metamorphic Ionian unit (Gavrovo carbonate) in the Zarouchla Culmination (ZC) (Ghisetti and Vezzani, 2005).

Sorel (2000), related the difference in dip angle, between N-dipping normal faults in the western part of the Gulf and S-dipping extensional faults in the southern part of the Gulf, to a low-angle detachment fault located in the southern region. This was based on earthquake frequency in the southern part of the Gulf. The detachment fault was active in the early rift stage, followed by the development of N-dipping faults. The southern part of the rift eventually became inactive due to uplifting and tilting. Hence only the northern section remains active.

A similar evolution model for the Corinth Rift, from the pre-rift stage to the present day, has been proposed by Jolivet *et al*. (2010). They described the Corinth rift as an asymmetric structure constructed on a mechanically weak, crustal-scale detachment due to a pressure gap between the Phyllite-Quartzite (PQ) and Gavrovo-Tripolitza napps. It consists of a series of decollements relayed by steeper ramps (Figure 11), based on the retrograde deformation along the shear zone between the two nappes.

In the pre-rifting phase, the PQ nappe formed a dome resulting in an extensional shear zone at the onset of rifting (25 Ma - 15 Ma). Moreover, in the syn-rift stage (3 Ma - 1.5 Ma) the extensional area widened resulting in several normal faults and transferring the detachment from brittle to brittle-ductile transition. In the next syn-rift phase (1.5 Ma -0.7 Ma) the detachment seems to have localized, and no faults are observed toward the north. The last syn-rift stage was dominated by uplift at the southern margin and subsidence at the northern margin, with localization of several large normal faults at the southern margin (Jolivet *et al*., 2010).

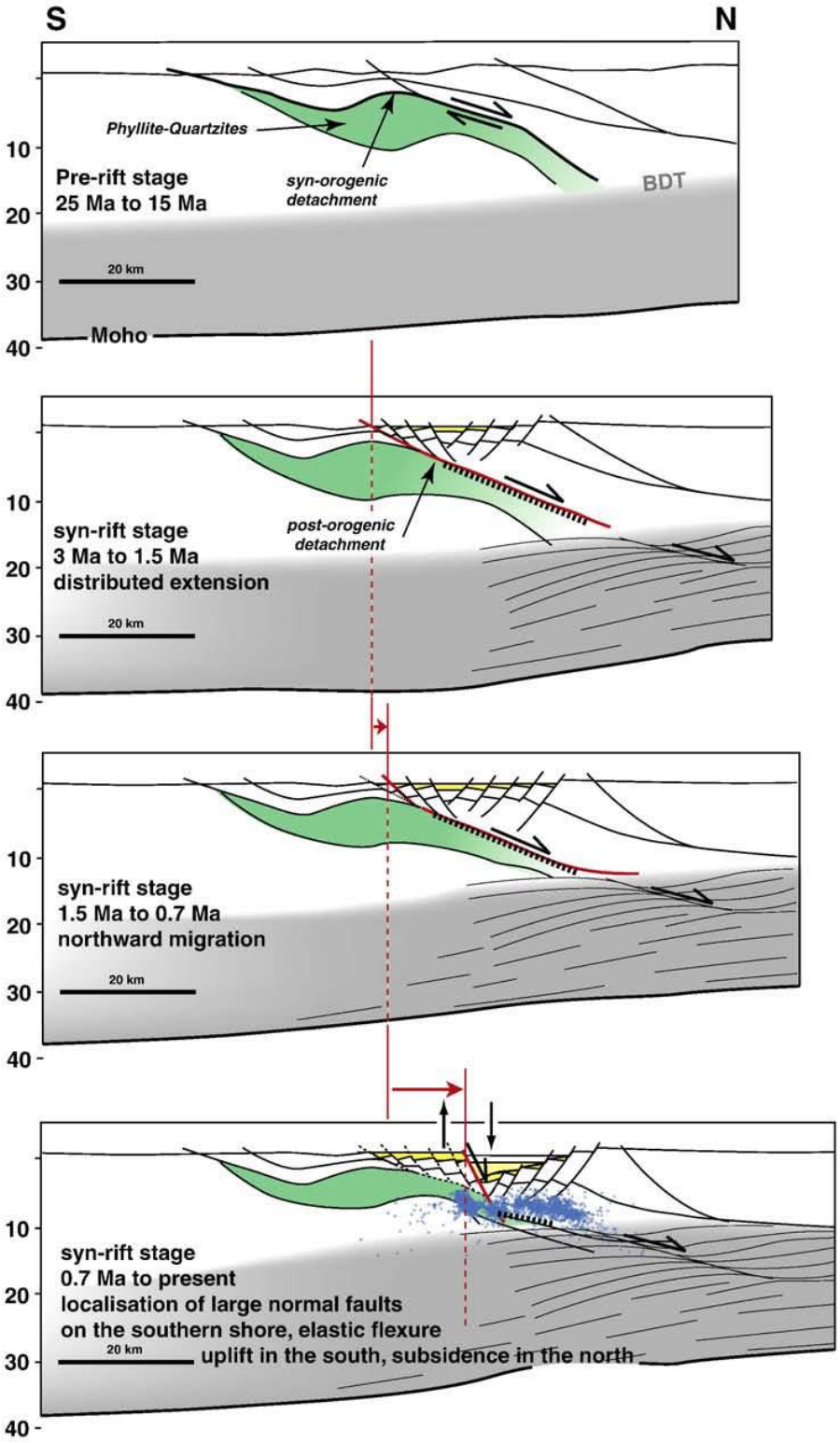

Figure 11 Evolution model of the GoC from pre-to syn-rift stages, as proposed by Jolivet et al. (2010), where PQ (Phyllite-Quartzite) played the main role in basin formation.

1.5.2 Rift Segmentation

Numerous studies have attempted to relate present day rift system structures to pre-existing tectonic grain, drainage systems, and palaeo-topography from the Hellenide fold and thrust belt that formed the N-S oriented mountains (e.g., Ghisetti and Vezzani, 2004; Collier and Jones, 2004; Ghisetti and Vezzani, 2005; Jackson et al., 2006; Ford et al., 2012; Hemelsdaël and Ford, 2016).

Many studies have looked at the N-S extension and its related E-W faults (e.g., Ford et al., 2012; Dahman (2015); Ford et al., 2016; Hemelsdaël and Ford, 2016; Nixon et al., 2016) in the Corinth Rift. However, a lateral miscorrelation of the stratigraphic units were observed in the previous studies along the strike. In contrast, the Corinth rift was divided into either domains (Nixon *et al*., 2016), zones (Ford et al., 2016) or fault segments (Console *et al*., 2013) to represent the lateral structure and sediment variation.

Furthermore, the reason of the miscorrelation has been little emphasized or described as well the boundaries of that subdivision of the Corinth Rift. (exception: Dahman (2015) and Wood (2013)).

In this subchapter, previous studies related to the lateral variation of the Corinth Rift system will be presented.

Ford *et al*. (2016), divided the rift system into several NNE-SSW oriented zones (PG, C5, C4, C3, C2, and C1), where miscorrelation of the stratigraphical units along the strike was noticed, but the boundaries or the reasons were not described or emphasized (Figure 12). However, most previous studies of the seismic data were focused on N-S oriented seismic lines (Nixon *et al*., 2016), where segmentation was neither described nor emphasized.

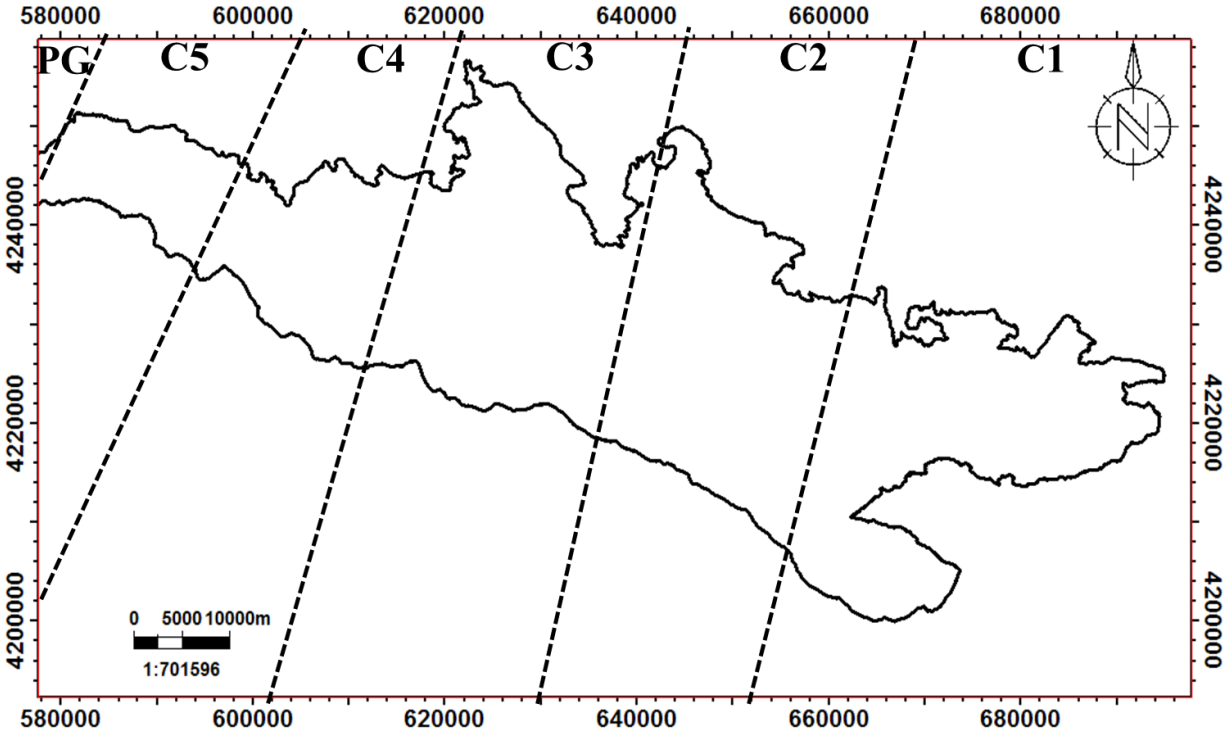

Figure 12 Map of the GoC with proposed NNE-SSW oriented zones by Ford et al. (2016).

1.5.2.1 Segmentation of the rift based on Earthquakes data

The immense amount of seismic activity in the GoC and Central Greece made this an ideal area for geodetic and seismological studies. Based on that, several onshore/offshore seismic arrays have been used to understand the geometry of complex fault structures at depth. According to Console *et al*. (2013), eight along-strike adjacent normal fault segments were identified along the GoC, based on seismic activity data of the last 300 years as well as geological and geophysical features (Figure 13). Furthermore, the change in Coulomb stress along the fault complex segments was an important factor in defining eight segments, each with its own Coulomb stress character (Figure 14).

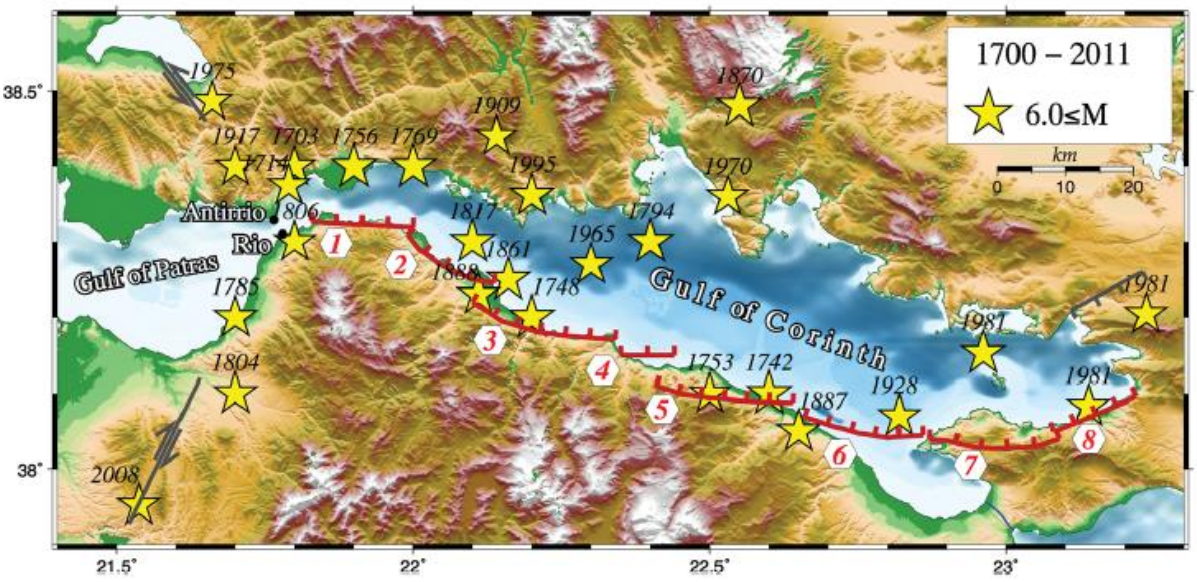

Figure 13 Tectonic map of the GoC showing the eight fault segments. Stars show the location of earthquakes with magnitudes exceeding 6.0 in the period from 1700-2011 (Console et al., 2013).

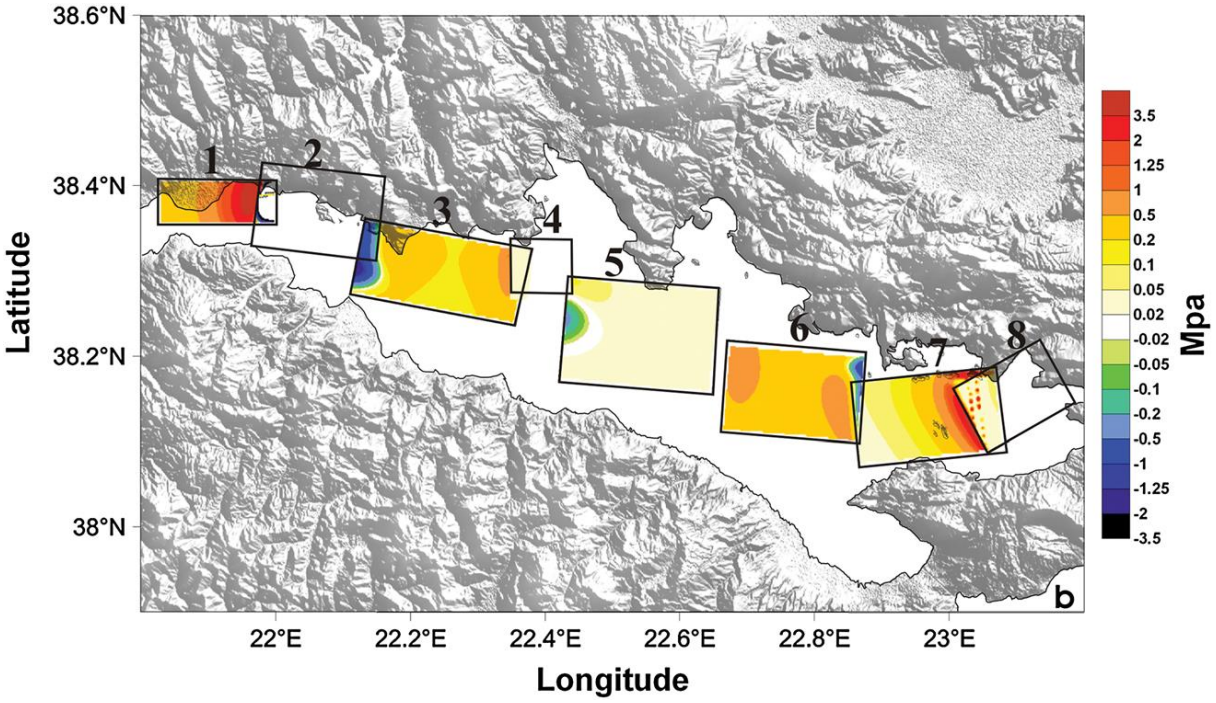

Figure 14 Coulomb stress variation map of the eight segments along the Gulf (Console et al. 2013).

A conductive layer was traced using electrical and magnetic anisotropy at a depth of 10 km in the west (Pirgaki, Helike and Aigion Faults) and 20 km in the east (Xylocastro Fault). This

layer has been related to the low-grade metamorphic basement of the thrust belt (Pham *et al*., 2000).

A possible model for the Corinth rift opening (Figure 15) was proposed based on differences in microseismic activity and strain rates recorded in the area from 1997 to 1999. This model suggests that the lower strain rate and lower microseismicity is a result of loading distribution in the thicker elastic crust (Pham *et al*., 2000). Hence, Ghisetti and Vezzani (2005) suggested that the conductive layer could act as a detachment horizon for the largest normal faults (Figure 16).

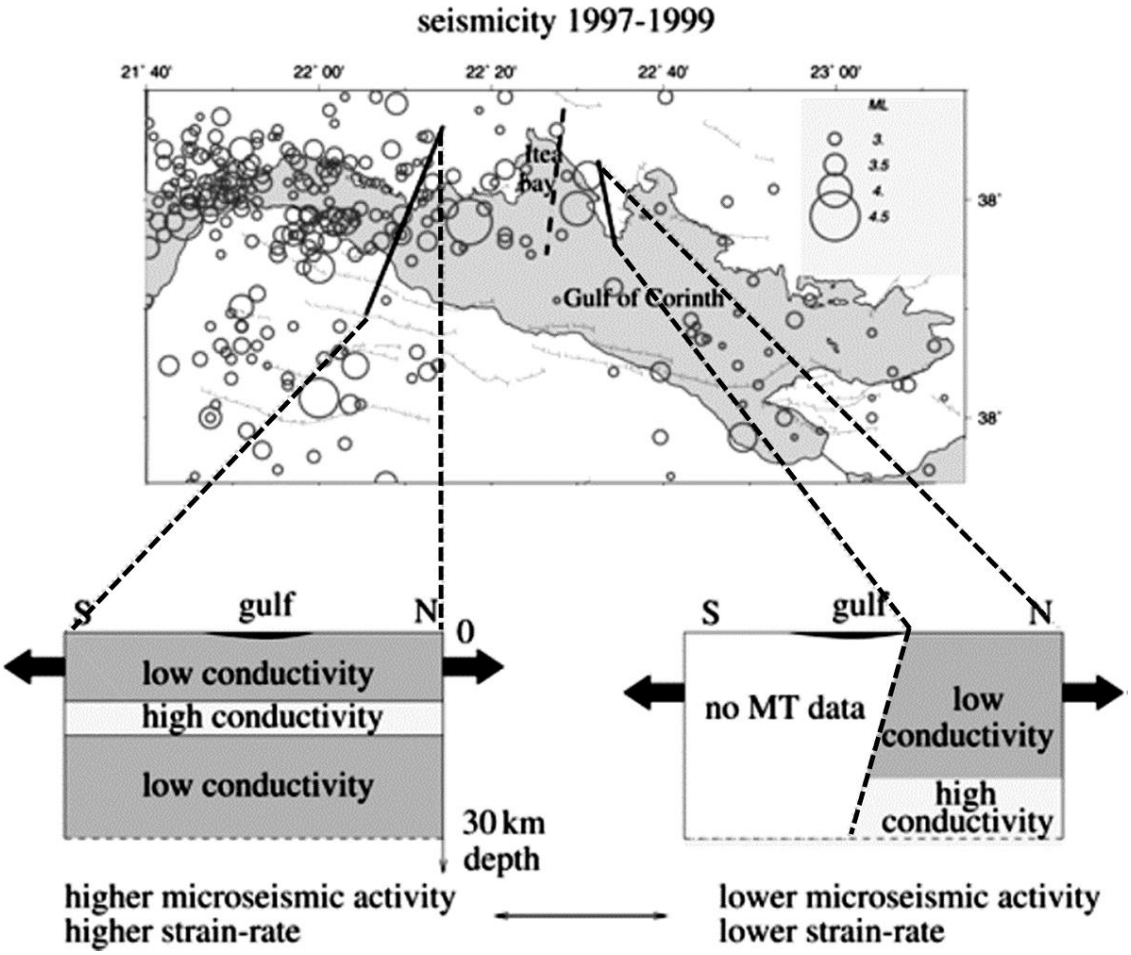

Figure 15 A proposed opening dynamics model of the Corinth rift, based on the difference in microseismic activity for the period 1997-1999 (Pham et al., 2000).

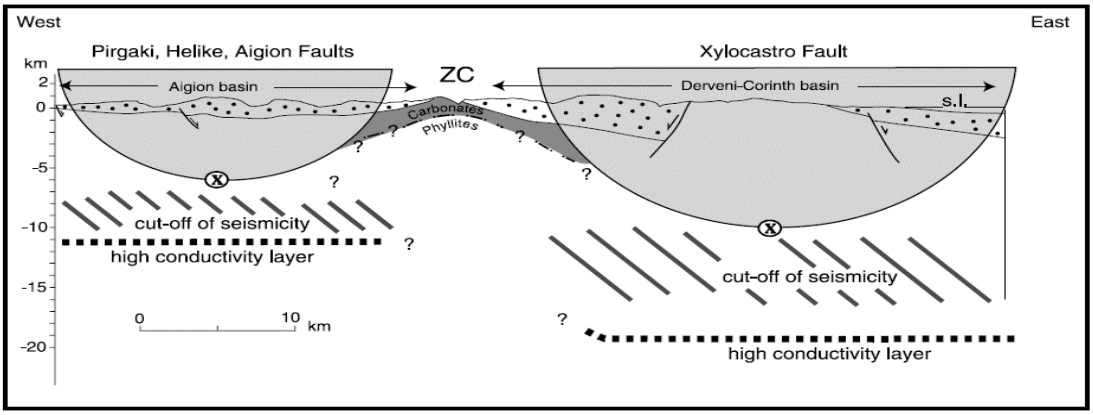

Figure 16: West-east section along Aigion and Derveni-Corinth basins (Trace in Figure16) showing the difference in elevation of the conductive layer, which Pham et al. (2000) traced. The gray half circles indicate the lateral extension of the fault system. The figure is after Ghisetti and Vezzani (2005), and the traced conductive layer is taken from Pham et al. (2000).

Furthermore, a transverse structural culmination was proposed as separating the Aigion and Derveni-Corinth basins. Here (Figure 17), the deepest active normal fault penetration in the eastern region by an NNW-SSE culmination of the Hellenic thrust belt (Zarouchla culmination: ZC), forming two different sub-basins (Aigion and Derveni). There is a major lateral variation in the facies and thickness of syn-rift sediments as well as a difference in the fault architecture across the Krathis River (Figure 18; e.g., Ghisetti and Vezzani, 2005: Rohais *et al*., 2007a; Ford *et al*., 2013).

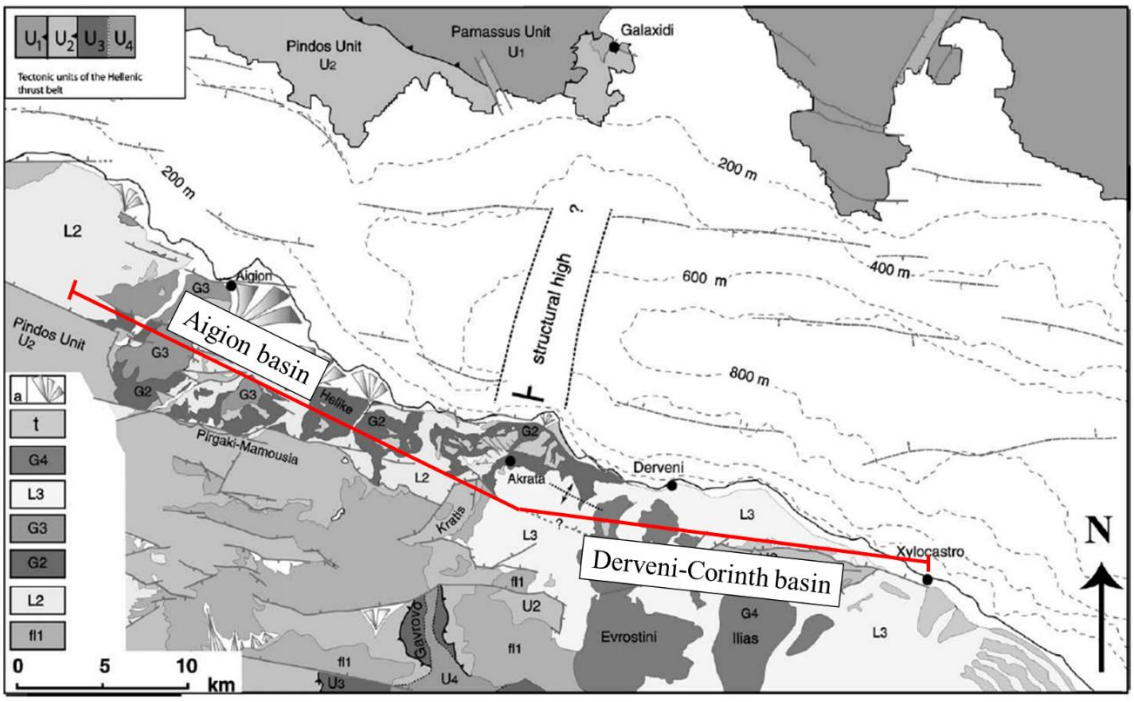

Figure 17 Geological map of the GoC with the suggested structural high in the offshore area based on lateral variations in thickness and facies between the Aigion and Derveni-Corinth basins, after Ghisetti and Vezzani (2004).

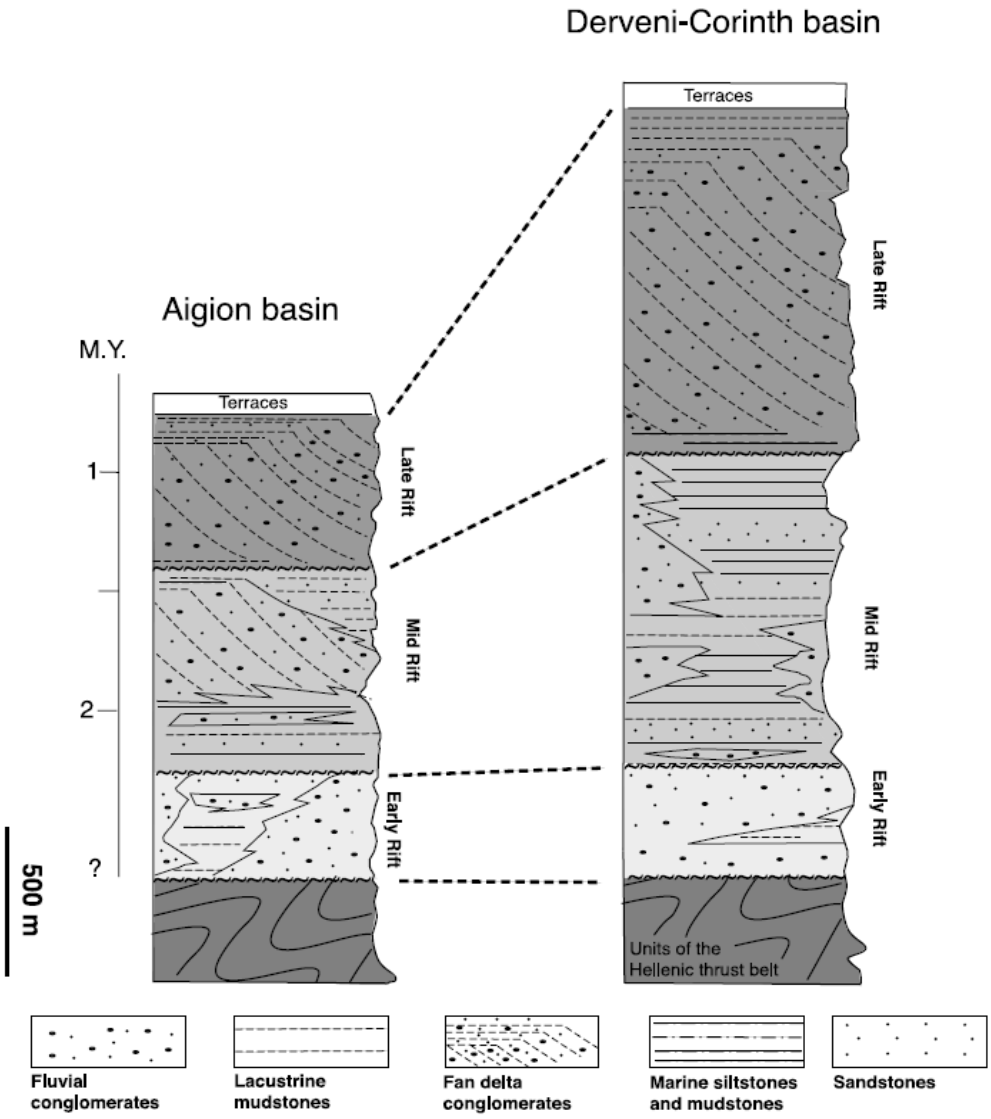

Figure 18 Synthetic stratigraphic columns of syn-rift sediments in Aigion and Derveni-Corinth basins showing the lateral change in facies and thickness (Ghisetti and Vezzani 2005).

Pacchiani and Lyon-Caen (2010), proposed a southwest fault zone which dips northwest relative to the Kerinites Valley (Figure 19a). This was interpreted as a transverse fault based on geological observations: by linking to a 100° N striking normal fault in the Kerinitis Valley (Figure 19b) and by studying the 2001 Agios Ioanis earthquake swarm, together with an analysis of the geometry and spatiotemporal evolution of a high-resolution relocation of multiplets.

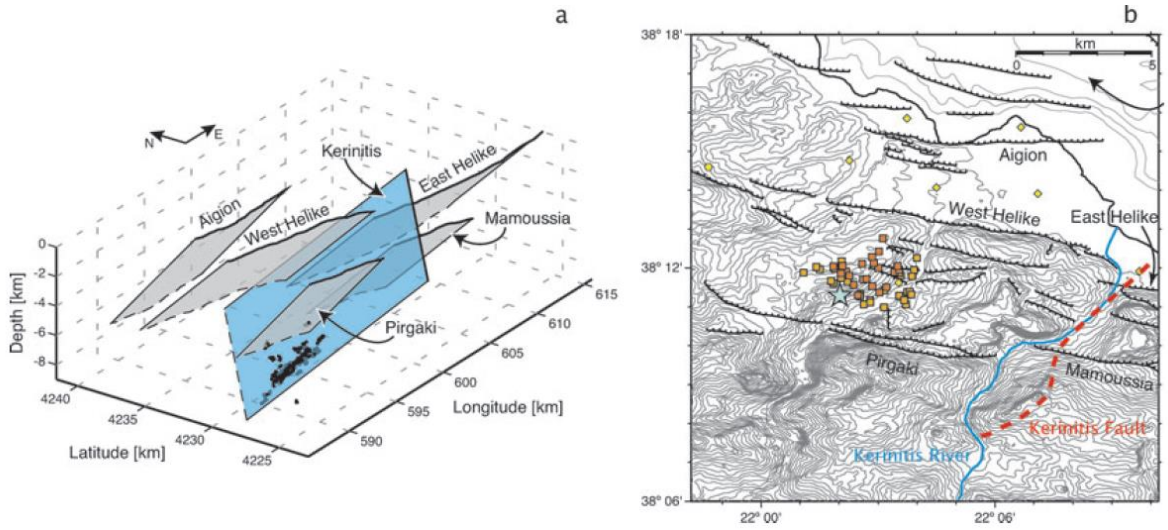

Figure 19 (a) The suggested Kerinitis fault plane together with the major north-dipping normal faults and relocated swarm earthquakes shown in black dots. (b) Elevation contour map of the southern shore of the GoC with the suggested Kerinitis Fault, where the orange squares are the multiples and the light blue star is the Agios Ioanis earthquake (Pacchiani and Lyon-Caen, 2010).

In the same area as the Kerinites Valley, Mrline (2014) produced a gravity model (Figure 20a) based on a gravity survey comprised of 600 gravity points and 140 rock samples. The study concluded that N-S to NNE-SSE transverse faults exist along the steep valleys and the coastal plain between the Aigion and Helike faults.Gravity differences (1997 and 1999) together with earthquake activity (2000 and 2001) were also studied (Figure 20b), and the observed negative gravity change was associated with an increase in extensional stress before the earthquake swarm.

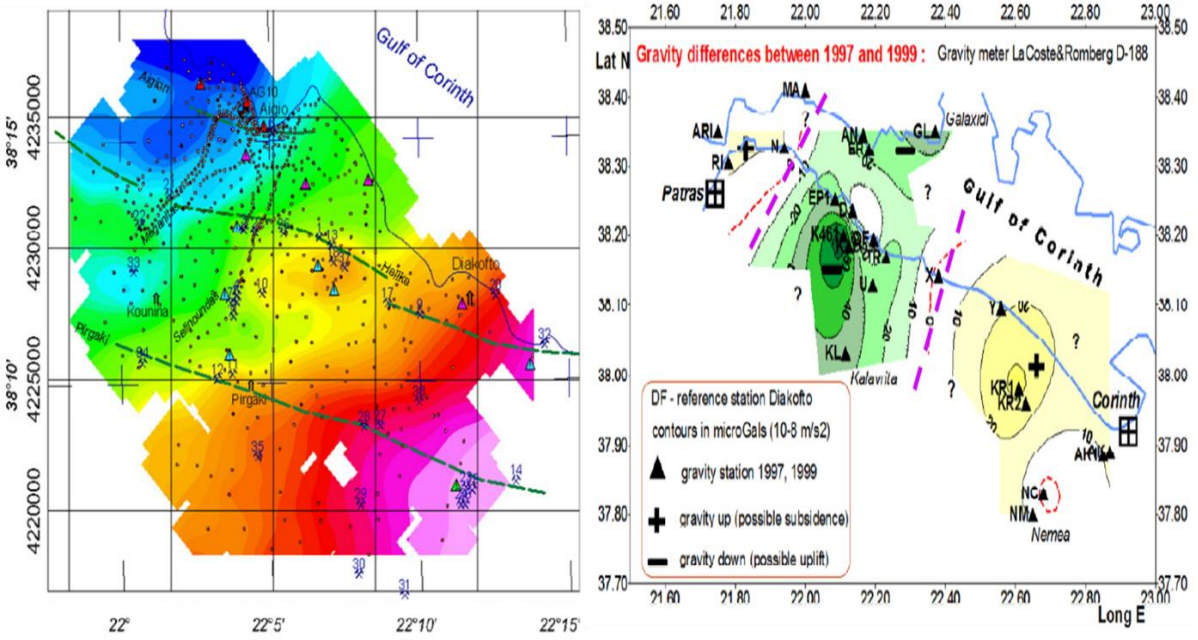

Figure 20 (a) Gravity map with rock sampling locations, survey and monitoring points; the dashed green lines indicate transverse faults. (b) Gravity differences between 1997 and 1999 showing positive gravity changes in eastern part of the Gulf, while negative changes can be seen in the western section. This indicates a possible uplift (Mrlina, 2014).

The transfer fault along the Kerinitis Valley was supported by Dahman (2015), who also proposed two additional transfer faults along the Vouraikos and Ladhopotamos Valleys (Figure 21), based on detailed field mapping and the termination and stepping of the faults across the valleys. These transfer faults segment the rift; they are inherited basement structures acting as a barrier and allowing individual fault blocks to deform independently of neighboring blocks, as suggested by Lister *et al*. (1986).

Ford *et al*. (2013) suggested the N-S interval of miscorrelation is a zone of high relief that was caused by high irregular surface basal unconformity, with palaeo-relief of up to 1000 m thereby concluding that there are no N-S faults.

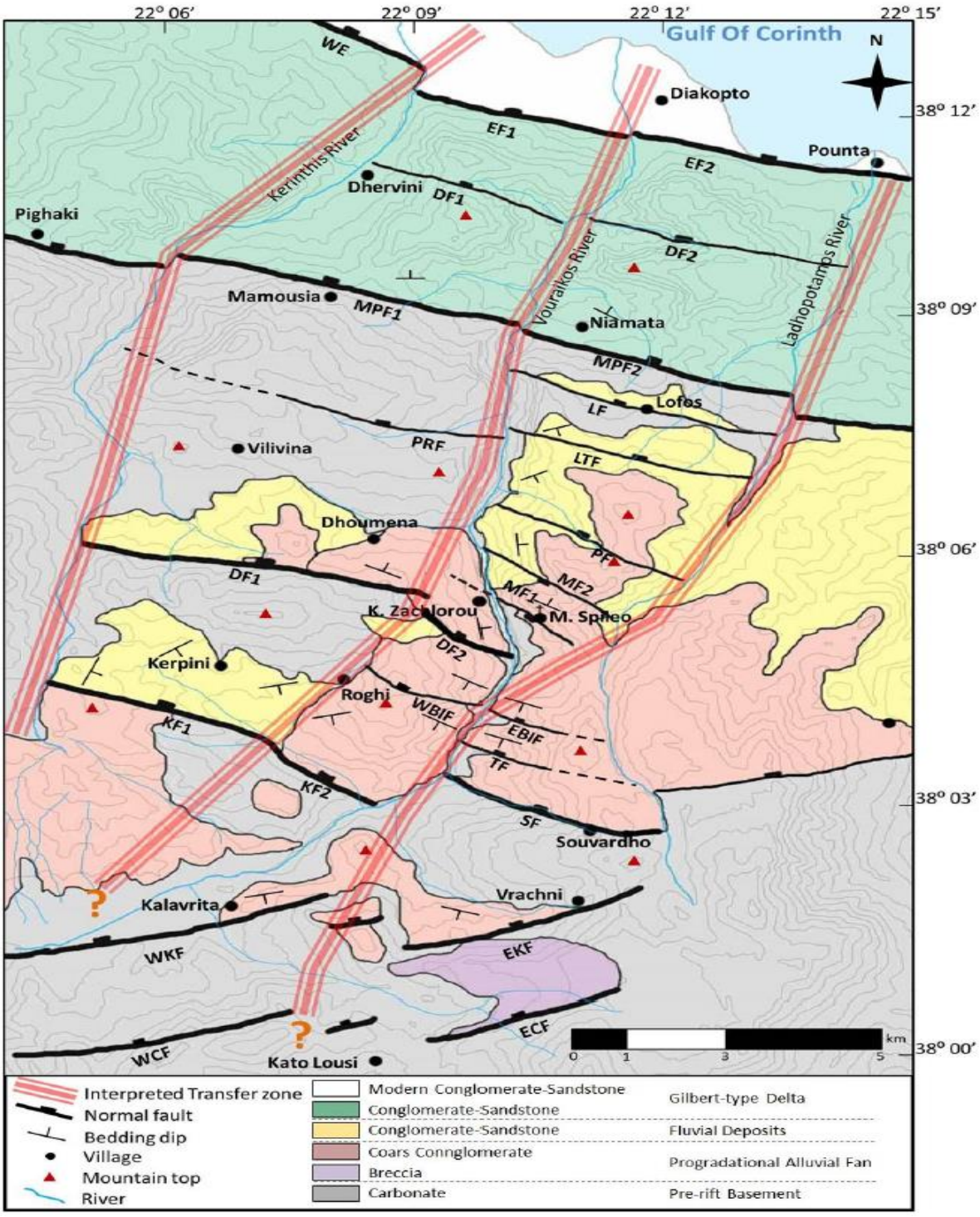

Figure 21: Geological map based on field observations together with the suggested transfer zones (see location in Figure 1), after Dahman (2015).

Wood (2013) proposed a conceptual model, introducing the evolution of the southern onshore margin of the rift, based on three-dimensional geological modeling that included fault-relay and drag geometries constructed from detailed field mapping. Three stages of rifting were suggested: initiation of some fault sets due to an extension, fault sets that were distributed due to the carriage of strain, followed by angular unconformities of the syn-rift sediments in the hangingwall (Wood, 2013). According to Hemelsdaël and Ford (2016), the active normal faults along the southern shore of the GoC show relay zone structures, which separate the uplifted Peloponnese peninsula from the subsided offshore basins. These relay zone structures are eventually breached and exposed, as in the Akrata relay zone (Hemelsdaël and Ford, 2016). This view was also adopted at a larger scale by Nixon *et al*. (2016), to include the S- and N-dipping faults in the GoC (Figure 22).

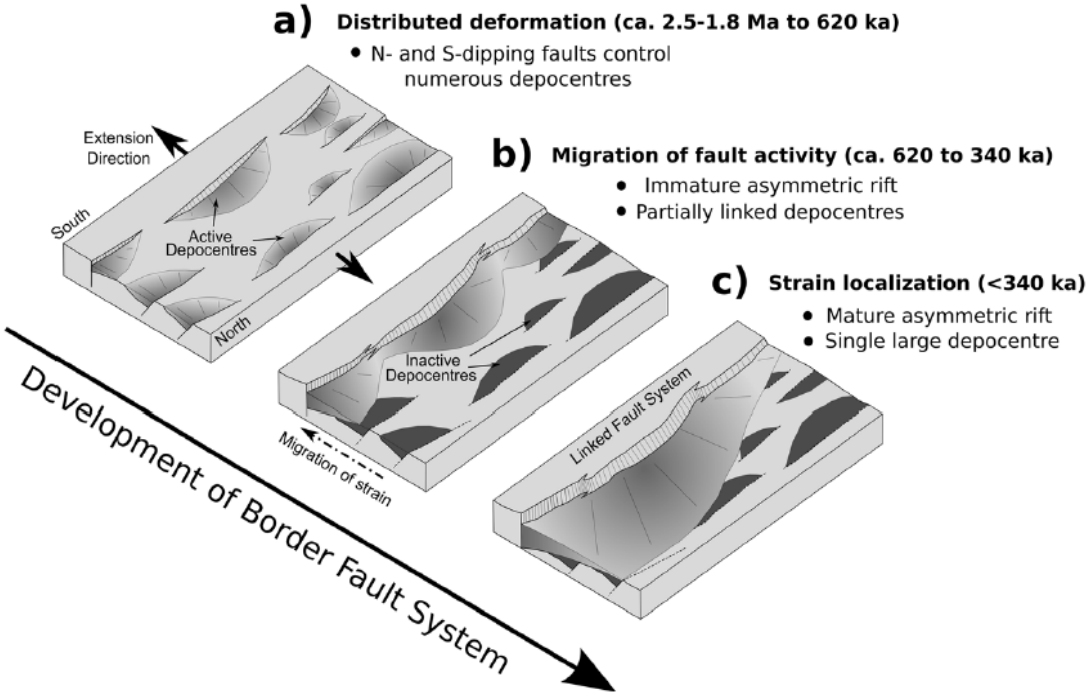

Figure 22 Proposed conceptual evolution model of the GoC (Nixon et al., 2016).

1.5.2.2 Previous studies in the northern margin of GoC

- North Evokios Gulf

The North Evoikos Gulf in the eastern part of central Greece is located between two major stress fields; North Anatolia Fault stress field due to NE-SW extension and Corinth rift which striking WNW-ESE. Due to a complex tectonic framework in the area, Papoulia et al. (2006) did a micro seismicity study. Four different zones of variation of fault orientation and their

connected seismicity have been defined according to Papoulia et al. (2006) based on more than 2000 seismic events with magnitude from 0.7 to 4.5 ML (Figure 23) in 2003. The deformation in those zones increases toward the south where the seismic data align the tectonic and fault trend in the area Papoulia et al. (2006).

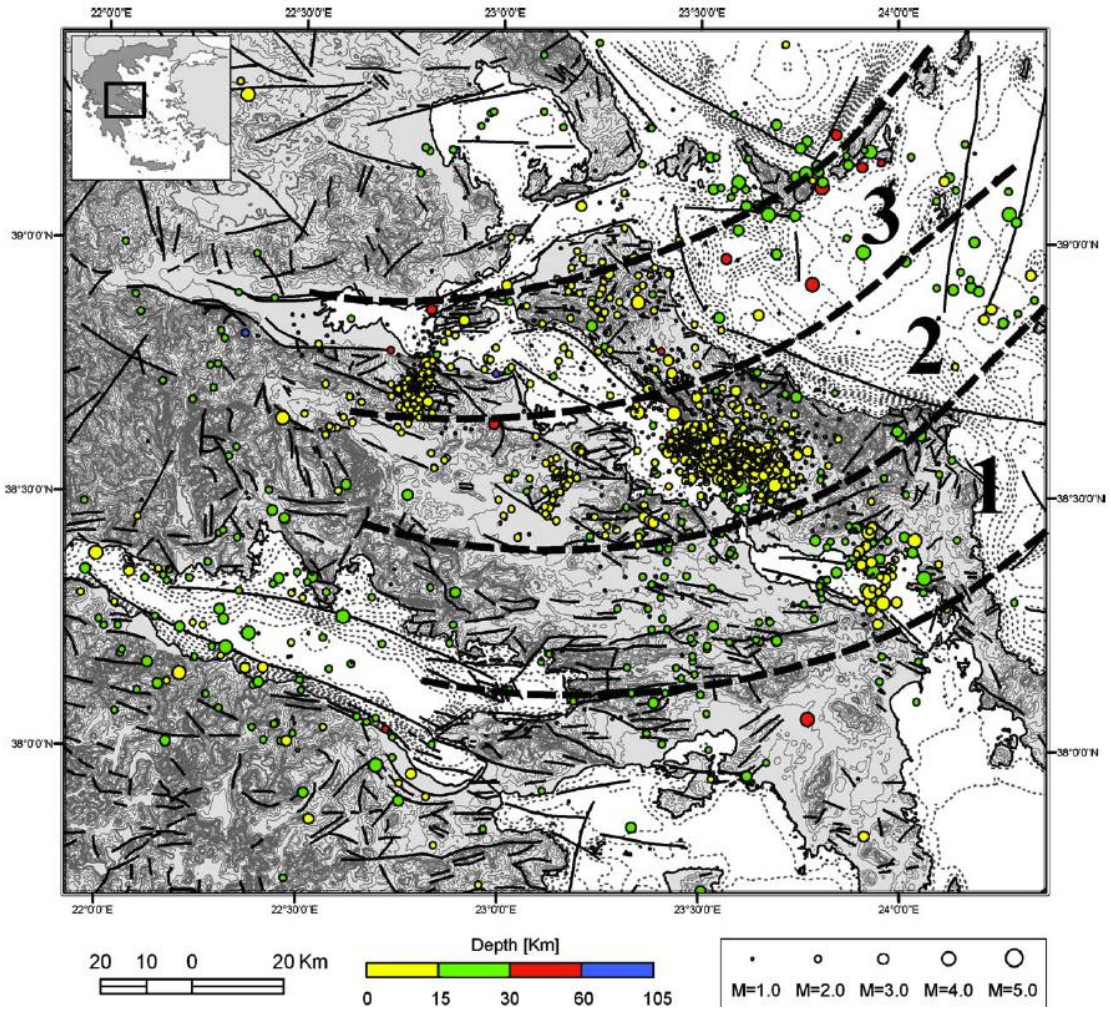

Figure 23 Structural map of Central Greece and Gulf of Corinth shows zones of variation in fault orientation and seismicity Papoulia et al. (2006)

- Northern Evia Island

Palyvos *et al*. (2006), has suggested a major topographic feature Nileas depression (NDpr) in the northern Evia island, which is 17 km long and 15 km wide (Figure 24). The suggestion was made based on geomorphological observations in the northern part of Evia Island.

NDpr is bounded by ENE-WSW to NE-SW strike fault zones (Prokopi-Pelion f.z. (PPFZ) and Kechriae f.z. (KEFZ)). PPFZ and KEFZ strike transverse to the NW-SE active fault zones that bound northern Evia and aligned to transverse structures on the main coast.

Fault zones have been the main active structures during the Middle-Late quaternary resulting uplifting and erosion of NDpr. In contrast, the suggestion of strain accommodation was made based on earthquakes and focal mechanisms in the area.

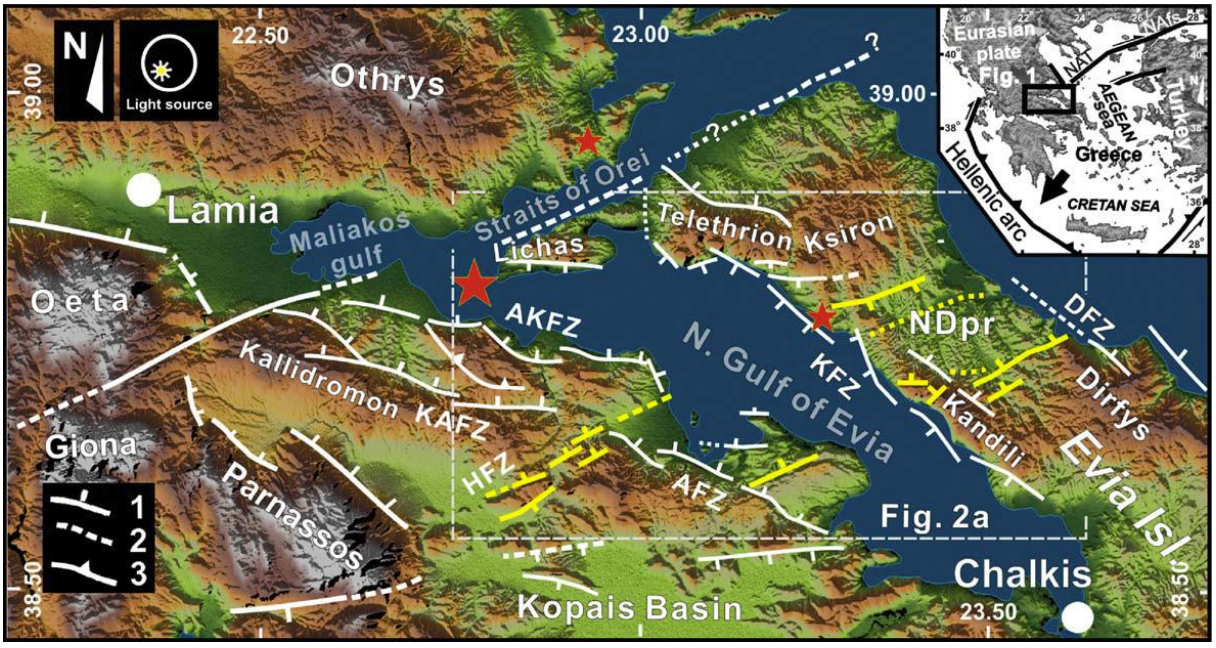

Figure 24 Map of Northern Gulf of Evia and surrounded the area with suggested transverse faults in yellow lines, NDpr: Nileas depression and KAFZ: Kallidromon f.z., 1: (oblique) normal faults, 2: probable f.z. Traces, 3: apparently reverse fault (rotated normal fault) Palyvos et al. (2006).

1.5.3 Offshore interpretation studies

The offshore margin of the Corinth rift was the object of several studies which attempted to reveal the structures, seismic stratigraphy and basin evolution using several seismic profiles (e.g., Sachapazi *et al*., 2003; Leeder *et al*., 2005; Sakellariou *et al*., 2007; Bell *et al*., 2008 and 2009; Taylor *et al*., 2011; Nixon *et al*., 2016; Ford *et al*., 2016).

The structure of the GoC was described as an E-W striking, asymmetric half graben, where N-dipping normal faults on the southern margin control the N-S extension (e.g., Roberts and Jackson, 1991; Armijo *et al*., 1996). In contrast, Taylor *et al*. (2011) divided the Gulf into Western, Central, Eastern and Easternmost sectors and described the faults at the southern margin of the Gulf (i.e., Heliki (HEL), Derveni (DER), Sithas (SIT) and Xylocastro (XYL)) as active right-stepping and dipping toward the north (Figure 25). Moreover, they overlap significantly along strike and are mostly biplanner to listric faults. The dip angles of the faults at the shallow level were proposed to be ~30° at the center and 45-48° in the east of the Gulf.

Furthermore, the faults on the northern margin of the central Gulf were described as S-dipping and active during the early rift phase without any major footwall uplift, as in the Galaxidi fault (Taylor *et al*., 2011). In the central and eastern sector, the structure was described as inherited from the structural grain associated with reactivation of the Parnassos nappe stack in the basement. However, in the western sector, the faults were described as unaffected by the structural grain of the basement (Taylor *et al*., 2011).

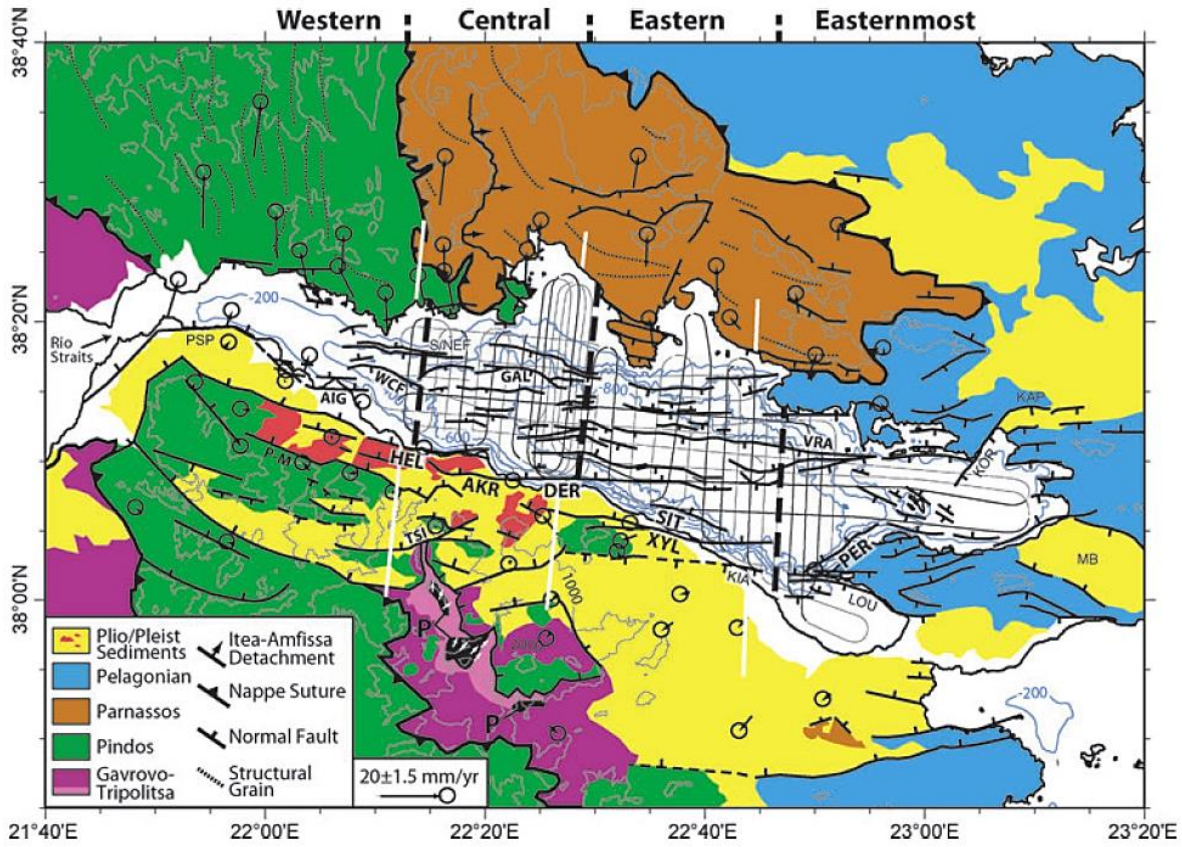

Figure 25 Structural map of the GoC and surrounding areas, offshore faults were interpreted by Taylor et al. (2011) using the EW0108 MCS data (Taylor et al., 2011).

Based on observed variations in the rift architecture along-strike, Nixon *et al.* (2016) divided the Corinth Rift into five domains: West, Central-West, Central-East, East and Alkyonides (Figure 26).West and Central-West domains were described as symmetrical grabens; Central-East, East and Alkyonides domains were described as south thickening half grabens.

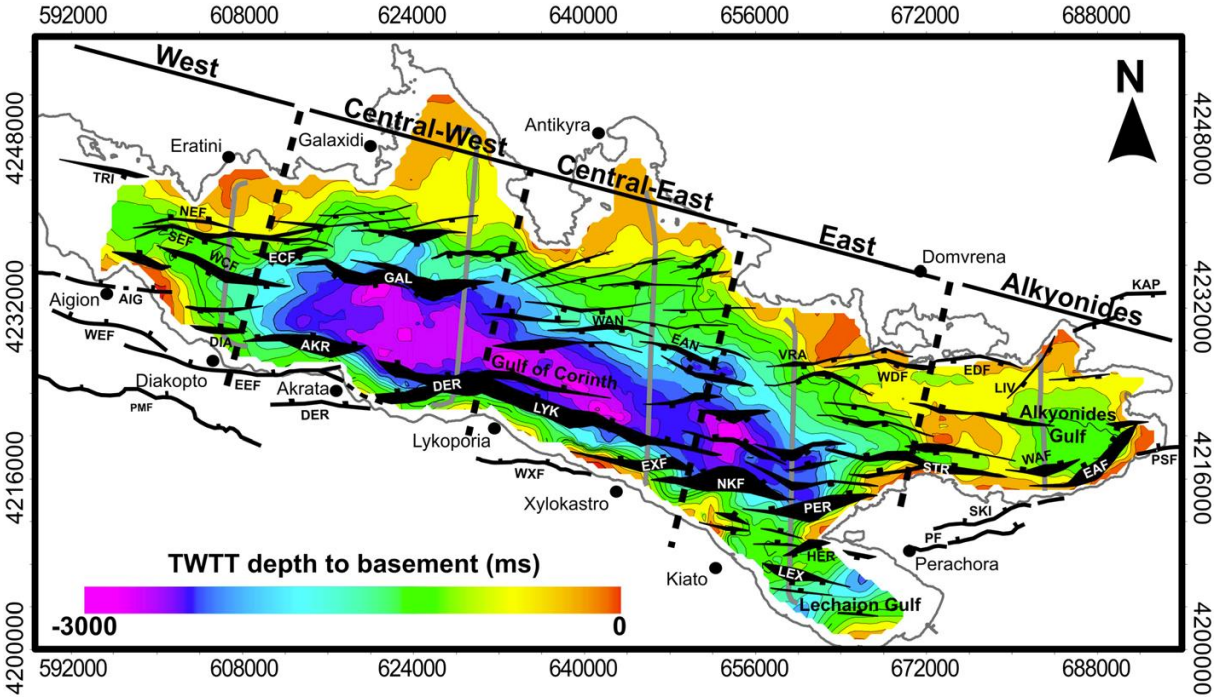

Figure 26 Structural map of the GoC with major faults offsetting seismic basement and proposed domains (Nixon et al., 2016).

1.5.4 Rift Stratigraphy

1.5.4.1 Onshore Stratigraphy

Pre-Rift Sequence

The pre-rift sequence consists of deformed Mesozoic carbonate units, Pindos, which were exposed due to over thrusting and continental collision during the Late Paleogene. It forms the basement to the syn-rift sequences in the Peloponnesus (Collier and Jones, 2004).

Syn-Rift Sequences

Almost 2800 m of syn-rift deposits are exposed on the uplifted southern shore of the GoC and are divided into three groups: Lower, Middle and Upper Group (Figure 27).

Lower Group: Dominated by alluvial and lacustrine sediments, it is characterized by an aggrading trend and is distributed from the Kalavryta Fault Block to the Pirgaki-Mamoussia Fault Block. A major maximum flooding surface separates the Lower and Middle Groups (Ford *et al*., 2013; Rohais and Moretti, 2016).

Middle Group: Consists of alluvial and Gilbert type fan deltas that propagated northward into a brackish to marine basin, combined with lateral distribution of distal turbidites and hemipelagic suspension deposits (Ford *et al*., 2013; Rohais and Moretti, 2016).

Upper Group: Contains mainly uplifted terrace deposits and ancient Gilbert delta conglomerates, deposited mainly on the southern shore and in the Gulf forming today's western coastal plain. The deposition of the Upper group was coincident with uplifting and erosion on the southern coast of the Gulf (Ford *et al*., 2013; Rohais and Moretti, 2016).

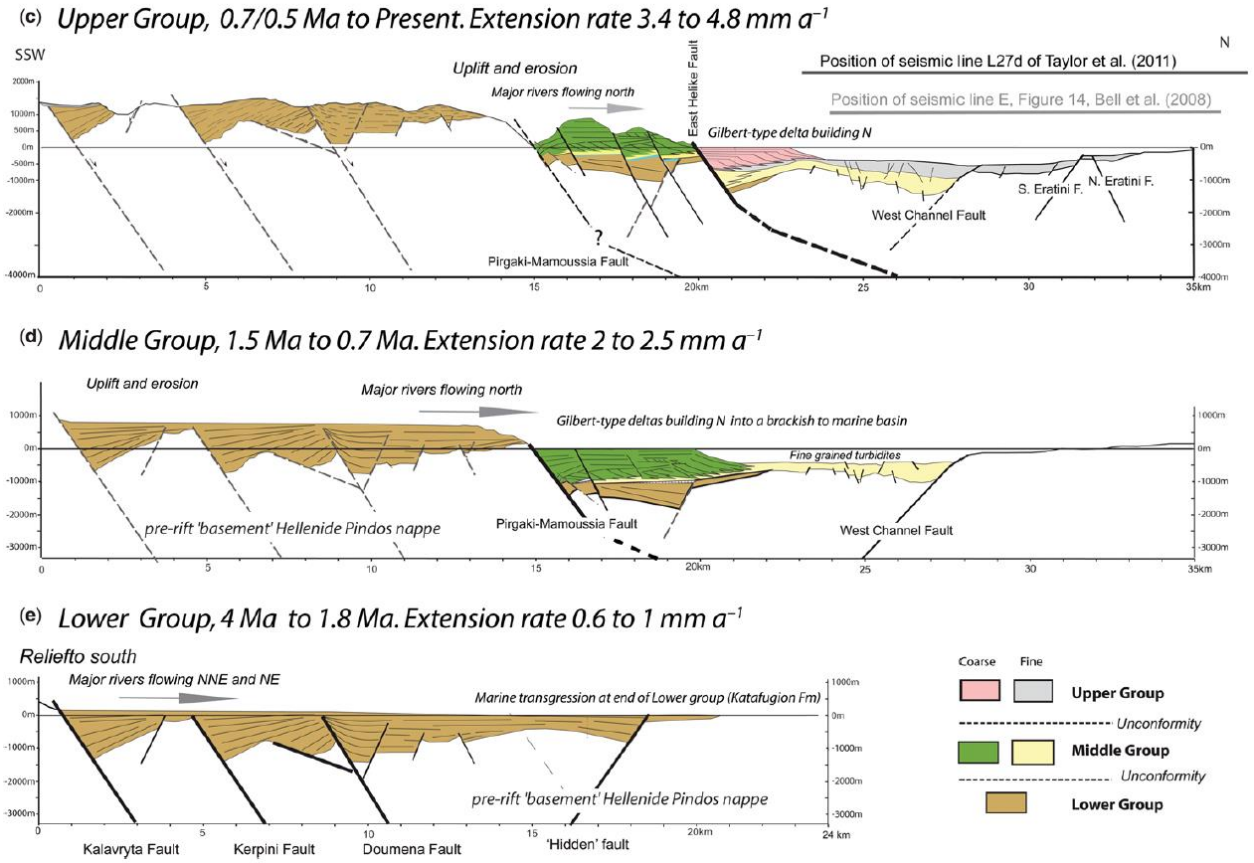

Figure 27 N-S Cross section is showing the structural impact on the syn-rift deposits along the Corinth Rift (Ford et al., 2016).

Structural framework impact on syn-rift deposits in the western section of the GoC

During the deposition of the Lower Group sediments, most of the major normal faults were active, and the depositional system was toward ENE. This then changed toward the south during deposition of the Middle Group, which coincides with northward polarity and the spreading of the rift. Northward progradation of the Gilbert delta was coeval with sea level rise (up to 500 m) and northward migration of fault activity. The last syn-rift phase is associated with the uplifting of the southern margin and tilting of the fan delta system, where the sea level dropped ~600 m (Rohais *et al*., 2007a).

1.5.4.2 Offshore Stratigraphy

The offshore stratigraphy has been subdivided into three sequences: pre-, early- and late rift. The early (Seismic Unit 1: SU1) and late (Seismic Unit 2: SU2) syn-rift sediments are separated by a major unconformity (U), which concurs with the transition from the Middle to Upper Group (Ford *et al*., 2013). SU1 is characterized by low amplitude reflections with the nonexistence of coherency, while SU2 is characterized by high amplitude. According to Hemelsdaël and Ford. (2016), the Lower and Middle Groups are equivalent with the early rift package, while the late-syn-rift corresponds to the Upper Group.

In the absence of drill hole data in the GoC, most previous studies (Taylor *et al*., 2011; Nixon *et al*., 2016) used the 100-ka glacio eustatic cycle proposed by Bintanja and van de Wal (2008) to correlate seismic sequences (Figure 28). The early-rift sequence was divided into six marine and lacustrine packages (H1 to H6; Nixon *et al*. (2016). This view was adapted by Rohais and Moretti (2016) and was used to set up four pseudo-wells in the Eastern section, so as to identify the sedimentation and fault slip rate (Figure 29).

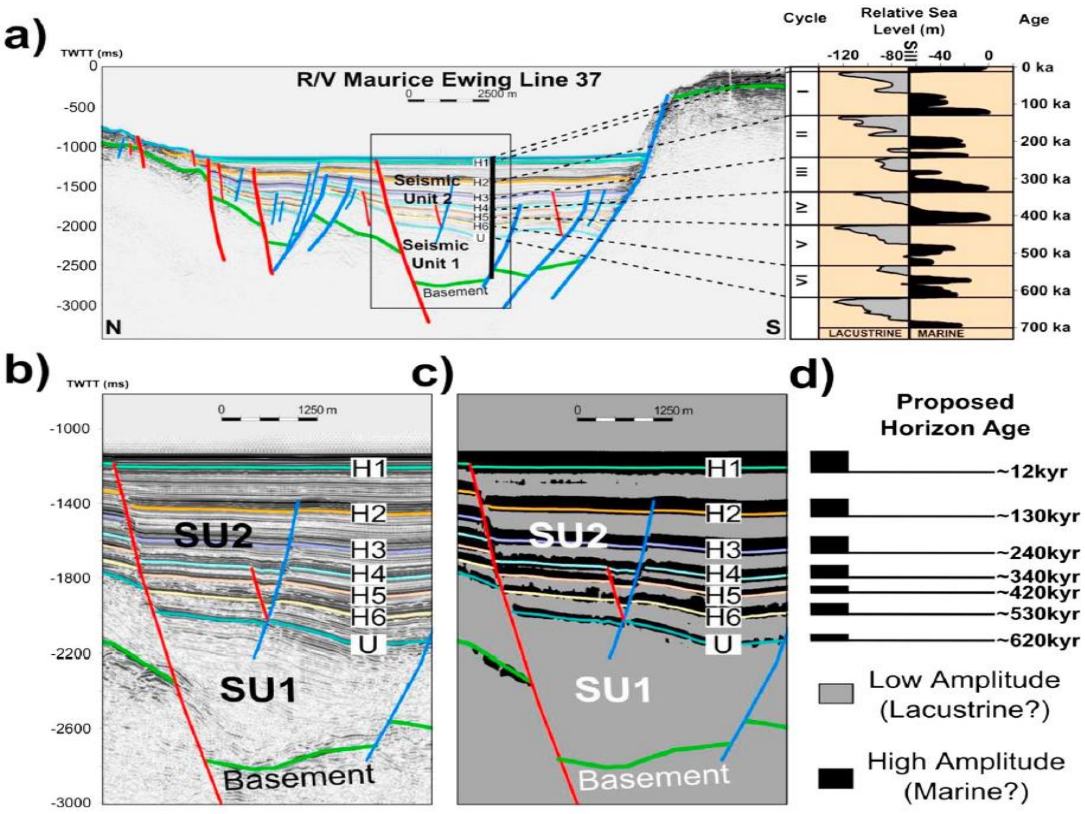

Figure 28 Chronostratigraphic framework of the Corinth Rift based on 100 kyr glacio-eustatic cycles. (Nixon et al., 2016)

Based on the sedimentation and fault slip rate, which are based on transition time between the Middle to the Upper Group (Figure 29) Rohais and Moretti (2016), proposed that the Gulf was very shallow throughout deposition of the Lower Group (0-50 m) and then became deeper (around 200-600 m) during the deposition of the Middle Group. Lastly, the depth was around 600-800 m during deposition of the Upper Group. In addition, the tectonic subsidence was higher during deposition of the late syn-rift sequence. The hypothesis from the sedimentation and fault slip rate show that transition time from Middle to Upper Group was around 0.62-0.71 Ma (Rohais and Moretti, (2016).

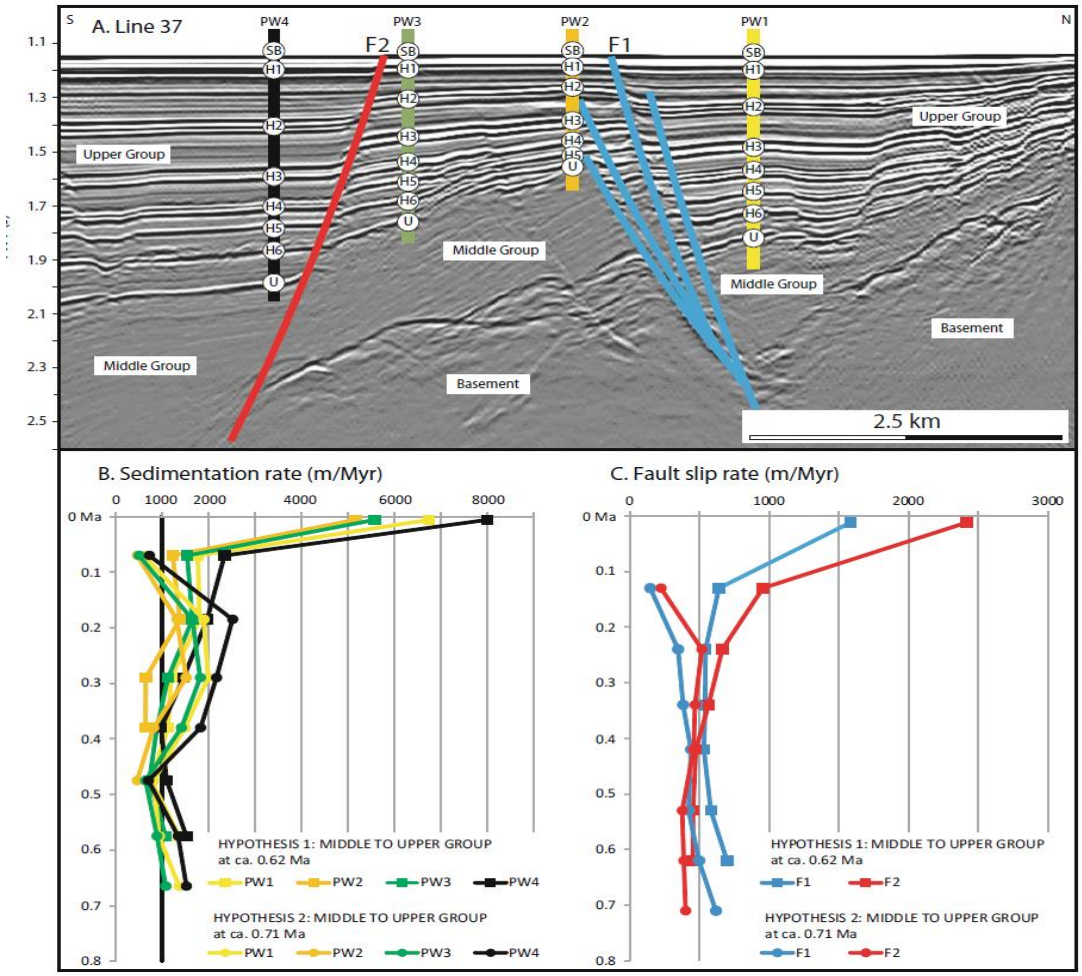

Figure 29(A) Seismic line in the eastern part of the Gulf together with four pseudo-wells (PW). (B) Sedimentation rate hypothesis. (C) Fault slip rate hypothesis (Rohais et al., 2016).

Chapter 2 Data

The workflow of this study is based on 2D seismic interpretation integrated with bathymetry, earthquake and onshore data from previous fieldwork in both offshore and onshore margins.

2.1 2D Seismic

Several seismic reflection profiles were used to study the geometry and stratigraphy of the Gulf (Figure 30). In this study, only the EW0108 seismic reflection profile was available as it was not possible to gain access to the other data sets (e.g., M.V. Vasilios, 2003, R/V AEGAEO, M.V.Vasilios, 1996 and RRS Shackleton, 1982).

Seismic data EW0108 was obtained from the Marine Geoscience Data System (www.ig.utexas.edu). The MCS data was collected in 2001 during a geophysical survey aboard the *R/V Maurice Ewing*. The seismic lines (Figure 31) are trending 33◦N–S and 10◦E–W, with azimuths of ~N005◦E and ~N095◦E, respectively. Several processes were subsequently applied and are summarized in Figure (32).

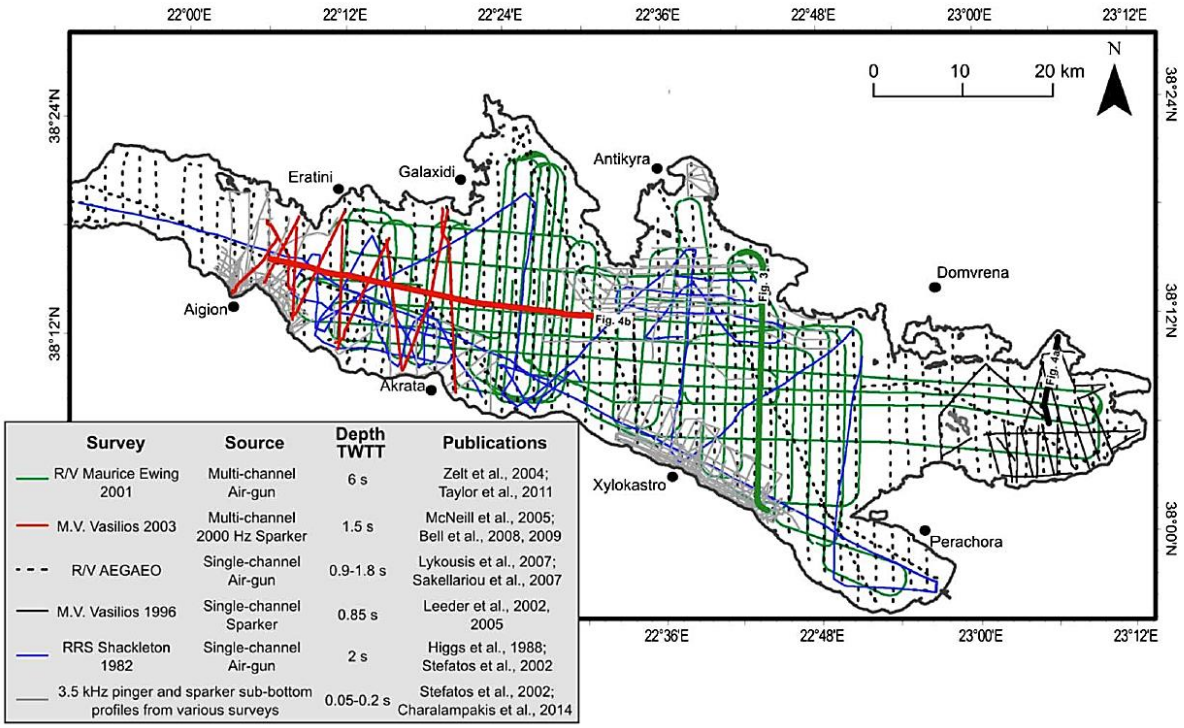

Figure 30 Map of the GoC with seismic reflection profiles that were used in previous studies. The R/V Maurice Ewing 2001 seismic profile is marked with green lines (Nixon et al., 2016).

The seismic source was a 20 air gun, 8445 cu with an interval of 50 m; 16 384 ms of data were recorded for each shot at a 4 ms sample rate. Different streamer lengths were used: a 6 km long

streamer with a group interval of 25 m for lines L1-L23 and a 3 km long streamer with a group range of 12.5 m for the N-S lines L24-L50 (Taylor *et al*., 2011).

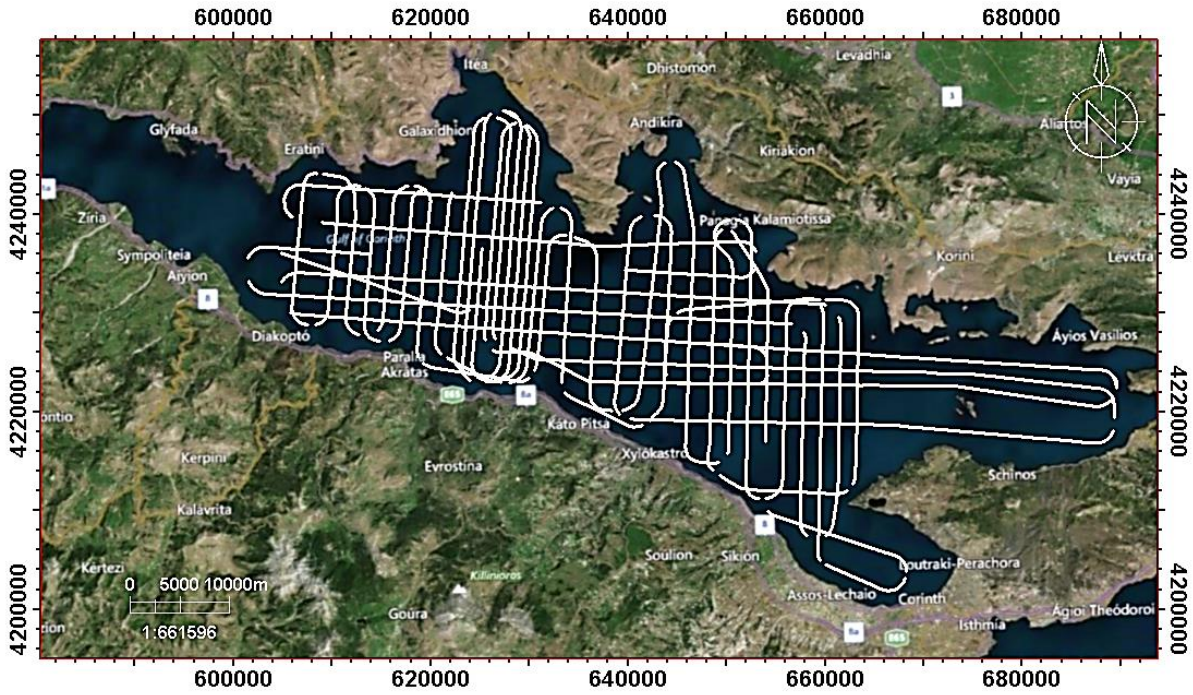

Figure 31 GoC boundary with seismic lines used in this study

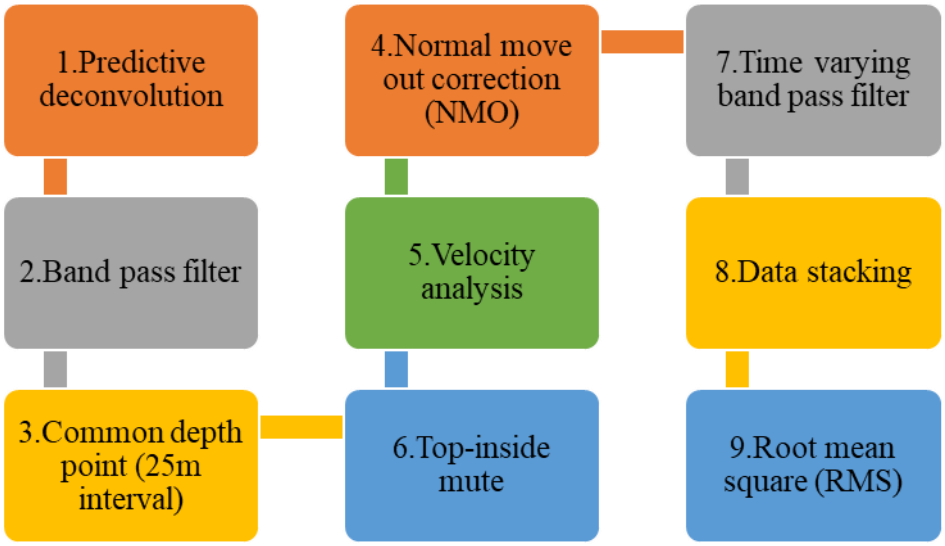

Figure 32 List of the processes that have been applied to the 2D seismic line.

The area not covered by seismic was marked by a polygon to avoid extrapolation in the surface output (Figure 33), as it is a zone of no-data. This is because the sea is too shallow to collect seismic data, and any geological interpretation in this area would be speculative.

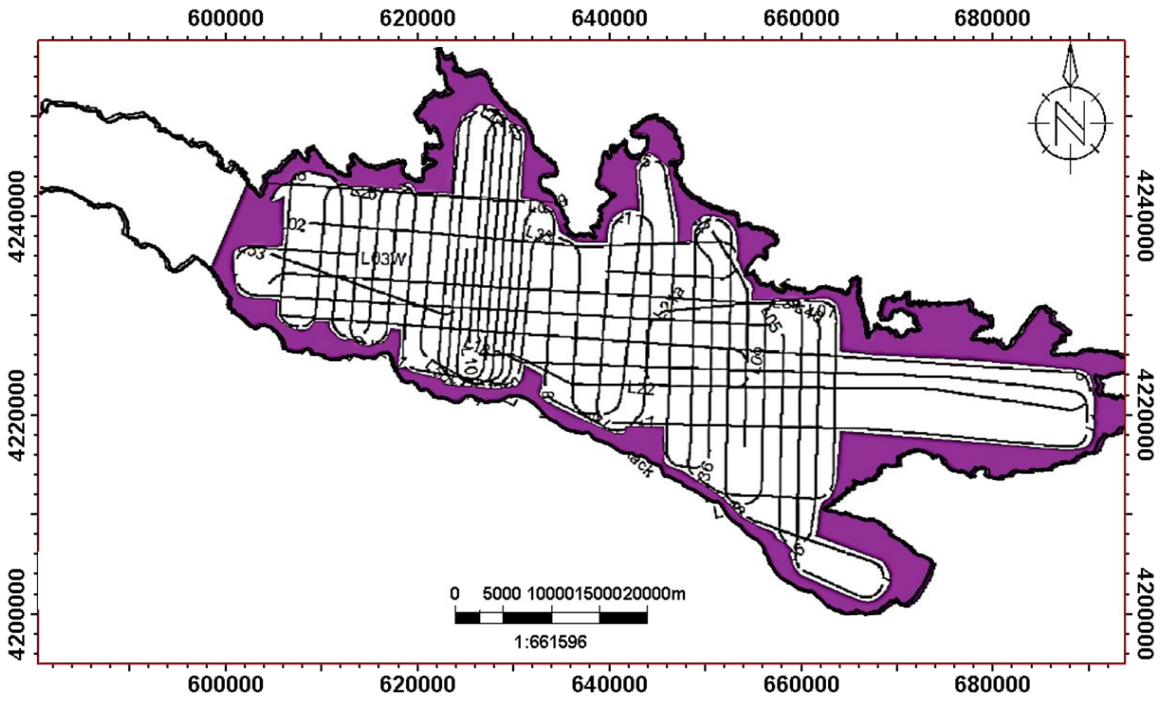

Figure 33 Boundary map of the GoC with marked zone of no data in purple.

2.2 Bathymetry

The available Multibeam bathymetry data covers only western part of GoC (Figure 34).The data was collected on board MV Vassilios G on July 2003 under the direction of the Universities of Southampton, Patras (Greece) and Leeds. A Reson Seabat 8160 50 kHz multibeam echosounder with a 1508 swath across the track using 126 beams was used. A 10 m cell size was used to grid the multibeam data, and navigation was calculated using an inertial navigation system and differential global positioning system (McNeill *et al*., 2005).

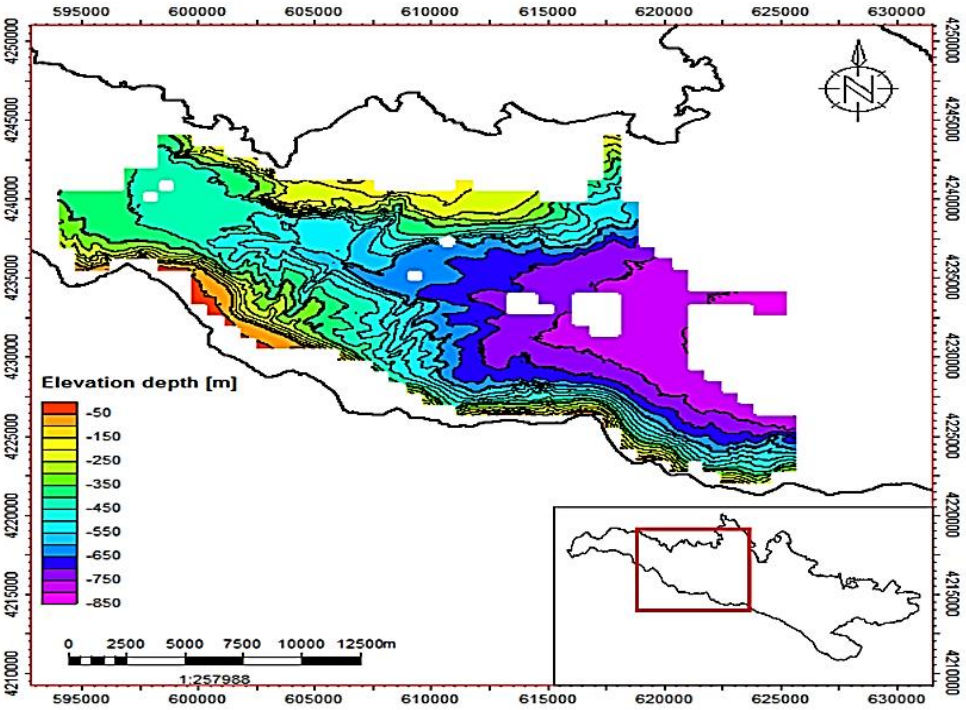

Figure 34 Bathymetry map of the western section of the GoC provided from McNeill et al. (2005).

Chapter 3 Observation and Interpretation

The interpretation was done using Petrel 2016. Seismic lines captured from Petrel are presented in this thesis with some loss of detail due to a lower resolution in the exported and printed versions. All N-S and W-E interpreted and non-interpreted lines were added to Appendix I to improve image resolution. The interpretation was previously done with a focus on the N-S features; therefore, in this study, the W-E lines are interpreted and presented. The identification and geometry of the segments, as well as lateral variation, was emphasized during interpretation. While the primary focus was the main packages (Pre-rift, Early, and Late Syn-rift) and faults.

3.1 Seismic Stratigraphic frame work used in this study

Three units were interpreted throughout the offshore rift pre-rift (basement), Early and Late syn-rift packages. The interpretation was carried out by the same method used in previous studies (Taylor *et al*., 2011 and Nixon *et al*., 2016), especially distinguishing the Early and Late syn-rift sequences.

The Early Syn-rift sequences are characterized by low amplitude reflectors where it was difficult to trace the horizons as the reflectors were discontinues and chaotic. In the absence of clear seismic amplitude, the early-rift sequences have been interpreted as one package (Figure 35).

The Late-rift section is characterized by high amplitude and mostly continuous reflectors. It is divisible into six seismic horizons (Figure 35). However, each horizon is composed of two or three high amplitude reflectors except the first unit which is characterized by semi-transparent amplitudes.

The nomenclature previously established by Nixon *et al*. (2016) was adopted in this study for the six horizons observed: H1, H2, H3, H4, H5, and H6. This was done for practical and comparative purposes since those interpretations were most similar to the observations made here. Those horizons were not observed along the whole Gulf, as the reflectors became discontinues in some parts along the Gulf, Figure (36), shows where those horizons were interpreted without extrapolation.

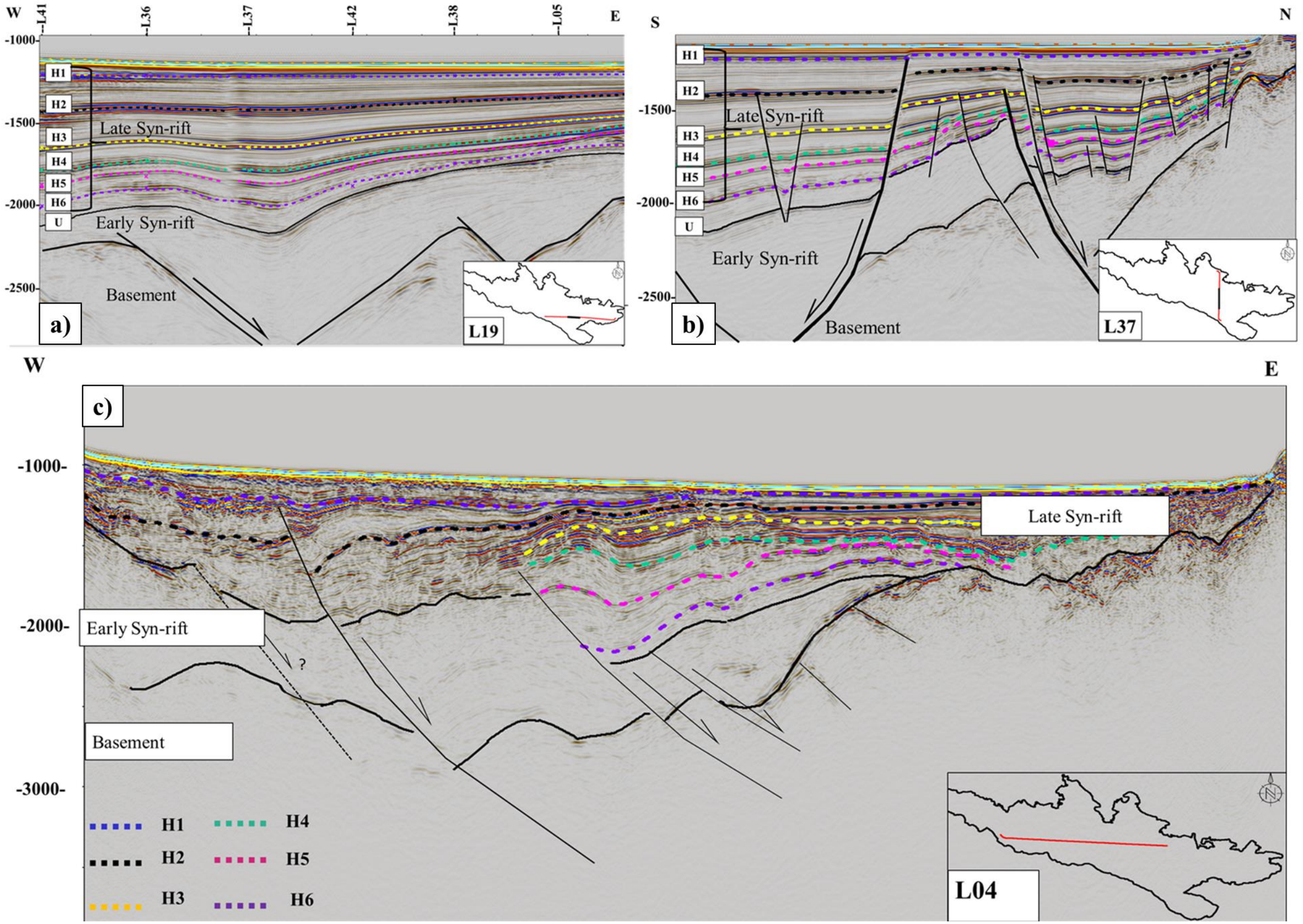

Figure 35Stratigraphic framework of the Gulf in this study showing: a) a small portion of the seismic framework of L19 with clear reflection, b) a small portion of the seismic framework of L37 with clear reflection, c) the W-E line that covers the eastern part of the West domain up until the boundary of the Central-East domain. The main packages were traced throughout the Gulf, while the reflection of sub-sequences of the Late rift were not clear and became chaotic toward the Central-West and West domains. The vertical scale is TWT in msec.

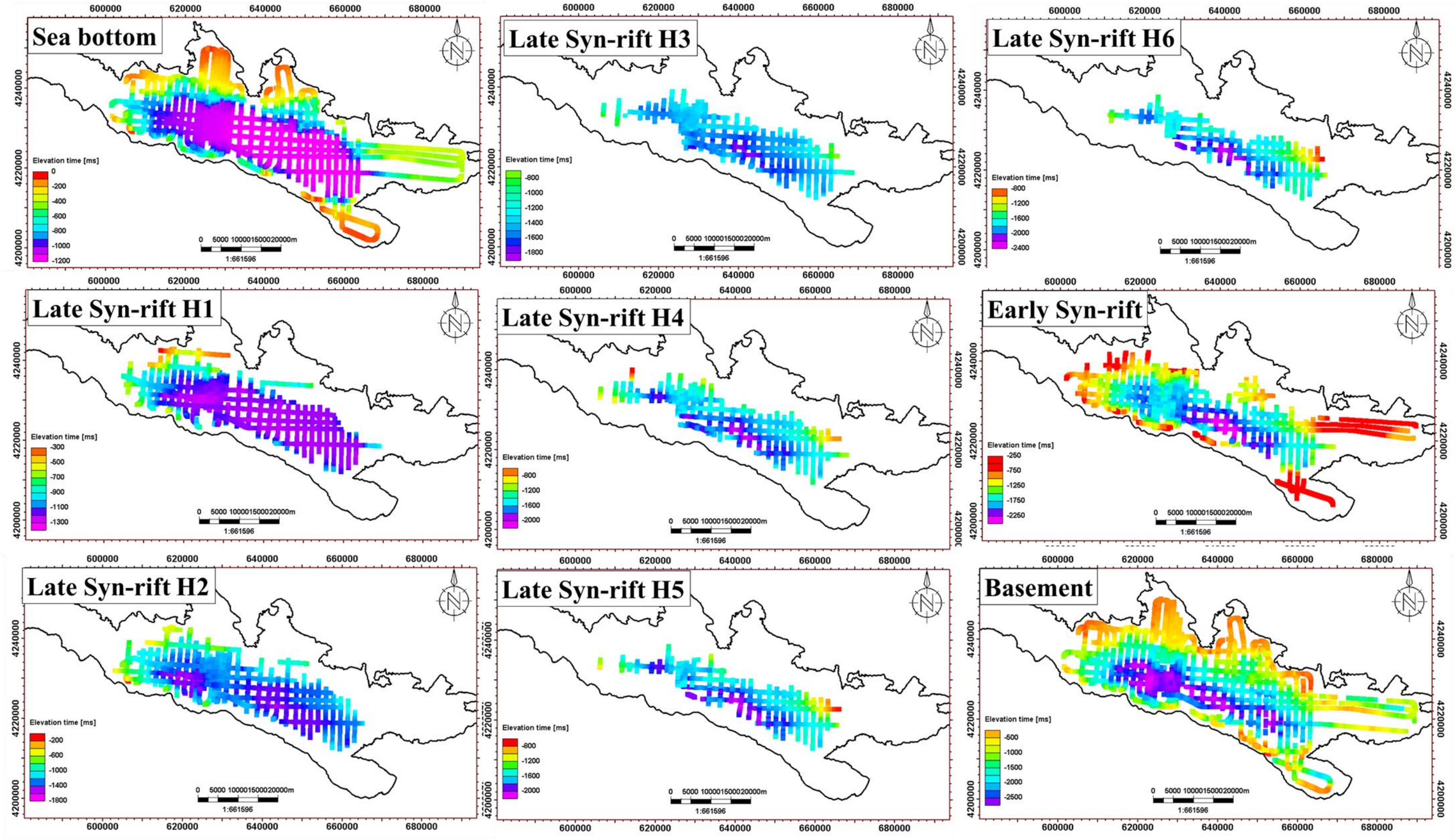

Figure 36 The distribution of interpreted horizons along the GoC in this study, without extrapolation or interpretation.

3.2 Structural and stratigraphic variation along strike

In this sub-chapter, all W-E seismic lines are described individually in order of appearance from north to south.

L01: is located in the western part of the northern margin of the Gulf, the seismic profile shows identified basement at shallow level with a Late syn-rift package along with the whole section (Figure 37).

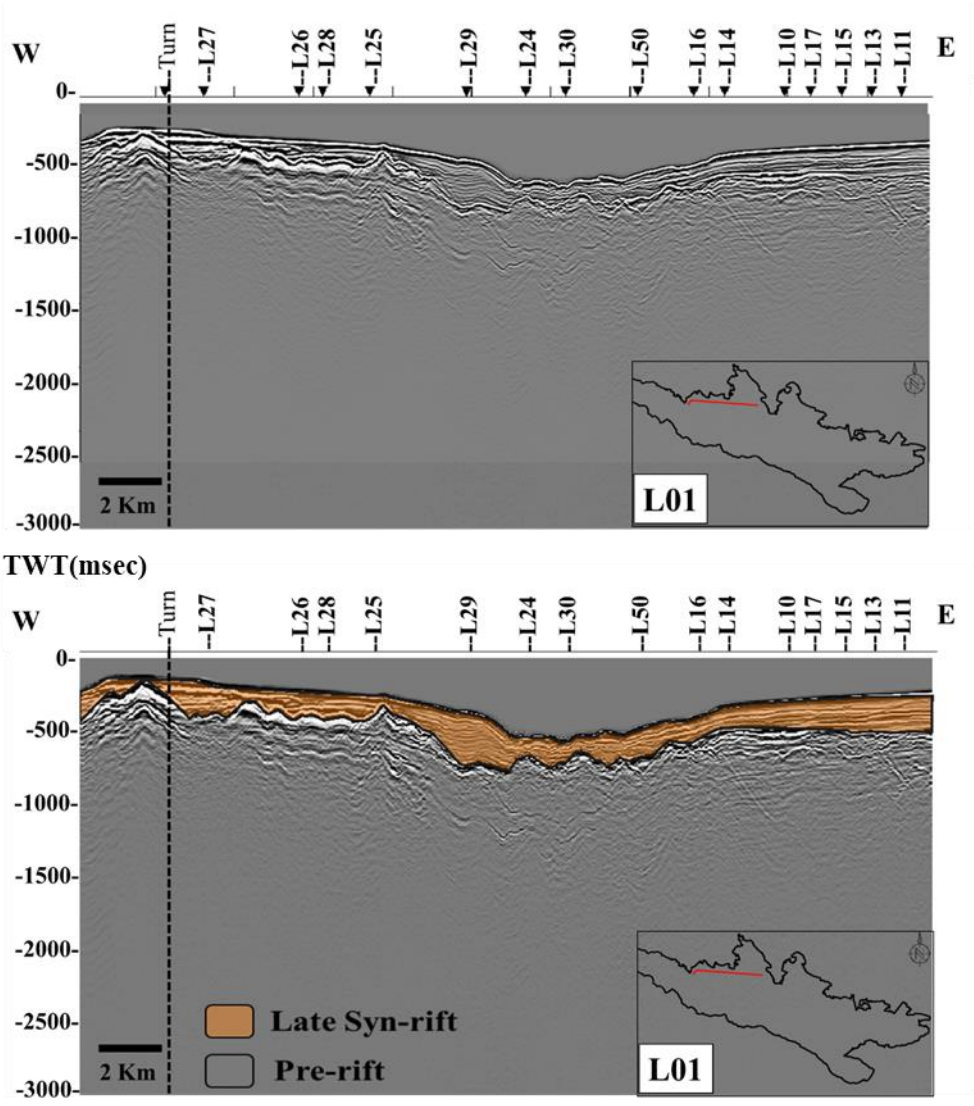

Figure 37 Uninterpreted and interpreted seismic profile of L04.

L02: is located in the northern margin of the central Gulf. Three major faults were interpreted (Figure 38), two west dipping and one east dipping. Fault 1, with a displacement of ~2.1 km and dip angle ~40°, fault 2 is dipping ~40° with a displacement of ~3.4 km, and fault 3 with a displacement of 2.4 km and dip angle ~45°. Those faults seem to be active during the Early Syn-rift time. Both Early and Late syn-rift sequences were observed; the thickness of the Early rift is greater than the Late-rift sequence, and both packages get thinner to the west and east,

with the thickest package located at the center of the profile. Compressional features are observed in the section, especially for the Early syn-rift where the unit seems to have a divergent fill combined with compression.

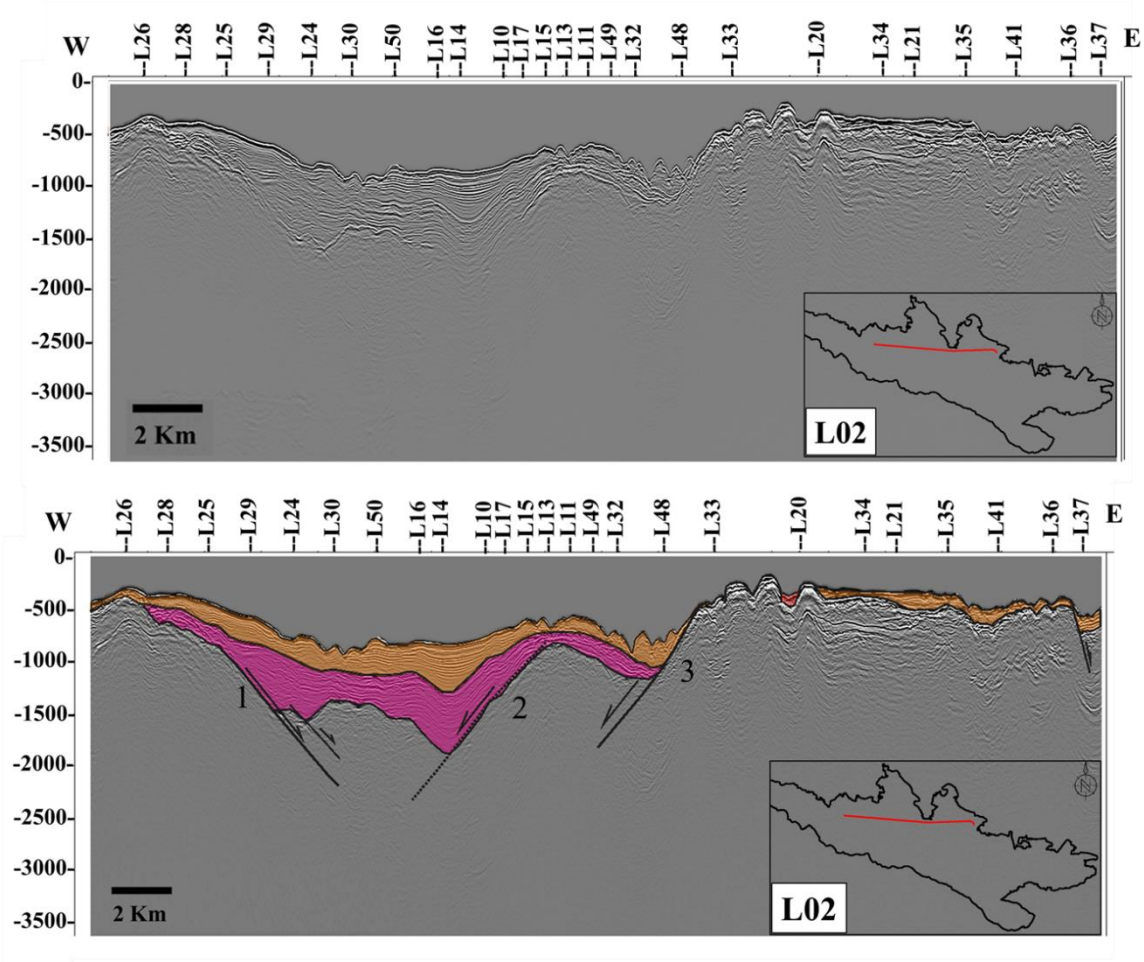

Figure 38 Uninterpreted and interpreted seismic profile of L02, the vertical scale is TWT(msec).

L03W: is in the western section of the Gulf (Figure 39) where several faults were traced;. These faults interact with the basement and a part of the Early Syn-rift section fault 1 is dipping 41 ° toward the east with a displacement of 3.1 km, and fault 2 is dipping toward the west with a displacement of 0.9 km and dip angle of 33°.

The thickness of the Early rift is not homogeneous: it is thicker in the eastern section of the line, filling the small basin formed by 1 and 2; and, before the seismic line turns, erosion of the Early-rift is observed on the hanging wall. The Late-rift sequence overlays the Early rift in the whole section, and it shows a significant change in thickness.

L03E: is located in the Central-East domain and has a half-graben structure (Figure 39), where two East dipping faults are traced. The major fault 1 cross-cuts the basement, Early and Late

Syn-rift sections with a displacement of 4 km and dip angle of 45 ° and seems to be active in pre-rift and during the deposition of syn-rift package with clearly growth strata in syn-rift packages. Fault 2 interacts with both basement and Early-rift sections, only with a displacement of 1.6 km and dip angle of 38 ° and seems to be active during the pre-rift and early-syn rift. The Early Syn-rift package filled this small basin and is thinner than the Late Syn-rift package. The Late syn-rift package overlies the Early rift package and has its maximum thickness at the center of the section, in the basin and flank out towards the NE and SE.

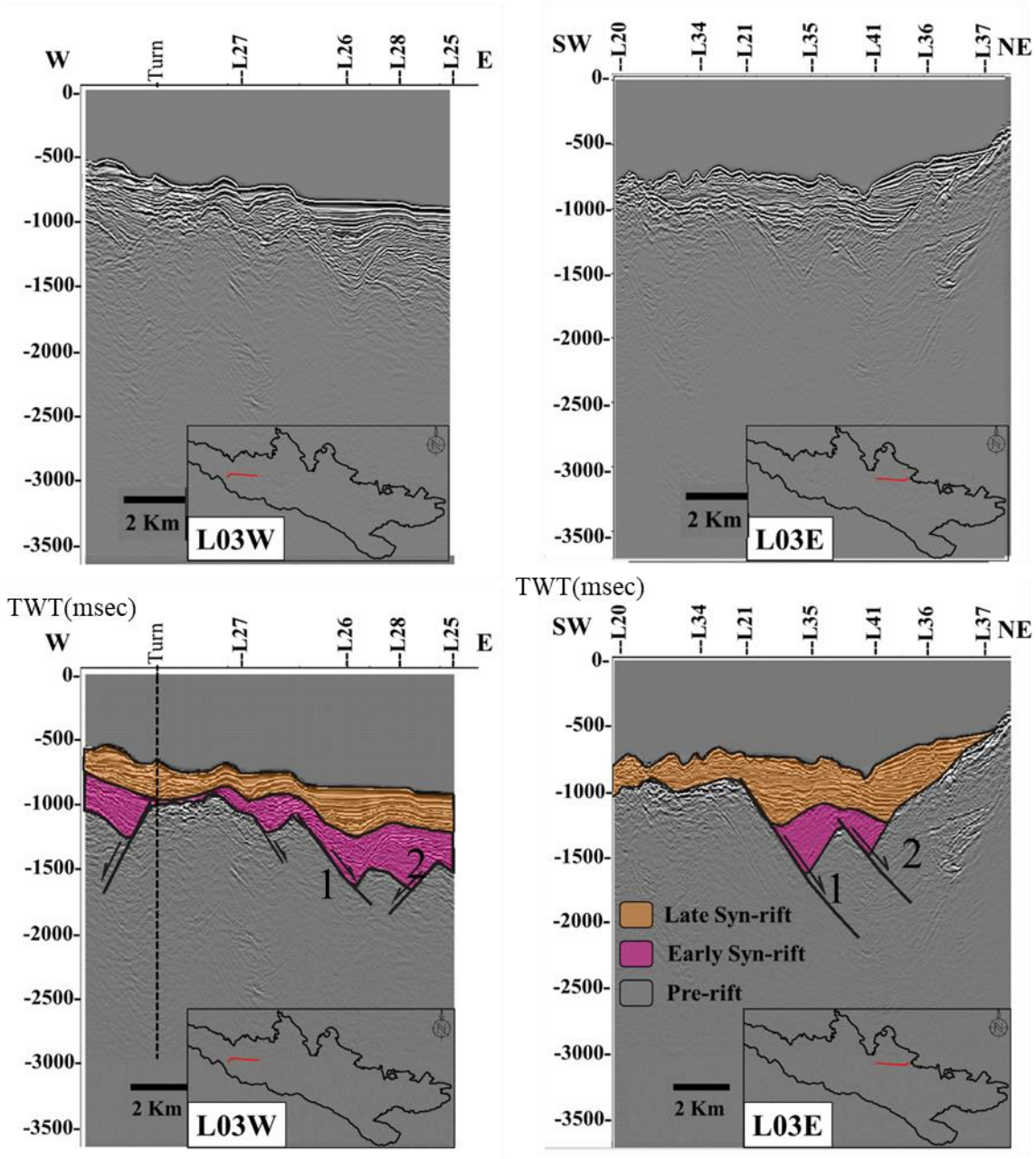

Figure 39 Non-interpreted and interpreted seismic profile L03W and L03E.

L04: is crosses the eastern part of the West domain, as well as both Central-West and East domains (Figure 40). Six major faults were traced, all of which dip toward the east and interact with the basement and the Early rift section with variation of displacement and dipping angle (Table 1). Only four of these faults cross the Late rift section, three of which have a listric shape. Two faults formed a roll over structure in the Late Syn-rift sequence recording two events, as there exists a major roll-over that includes a smaller roll-over, as marked in the Figure (40). Faults 3,4, and 5 seem to be active in the Pre-, Early-, and Late rift, while others seem to be active only in Pre- and Early-rift. Additionally, the Late Syn-rift horizons (H1& H2) were traced along the whole seismic profile, while the high amplitude reflections of horizons H3, H4, H5 &H6 became chaotic and difficult to trace in the Central-West section. Therefore, the termination of these horizons was marked across the listric fault.

Table 1 Shows displacement and dip angle information of faults in L04.

Fault	1	2	3	4	5	6
Dip angle	~40°	~33°	~40°	~38°	~30°	~32°
Displacement (km)	~2.9	~2.9	~1.3	~2.2	~3.3	~1.1

The thickness of the Late and Early Syn-rift packages varies along the section: the thickest package of the Early-rift is located on the footwall of listric fault 5 with thickness of ~5.1 km in the form of growth strata, while the thickest package of the Late-rift is located on the footwall of listric fault 4 with thickness of ~4.9 km. At the eastern part of the section, small faults were traced in the basement, where the basement is shallower.

L07: crosses the eastern part of the West domain, as well as both Central-West and East domains further north of L04 (Figure 41). Three faults that cross the basement, Early and Late -rift sequences were interpreted, as well as four faults interacting with the basement and Early Syn-rift sections. (Table 2), shows displacement and dip angle range of faults. All faults are dipping toward the east, and one additional small fault dipping toward the west in the eastern section were interpreted as well. This west dipping fault crosses the basement and syn-rift sequences. Faults 4, 5, and 6 seem to be active during the whole rift period, where growth strata are observed in Early- and Late-rift, while others faults seem to be active only in the early-rift period. Thickness variation of the Syn-rift sequences is observed along the whole section, the maximum depth of which is located in the Central-West and pinches out toward the west and

the east. The Late Syn-rift horizons were correlatable only in the central section of the seismic profile, while horizons H1, H2 & H3 were traced along the whole seismic profile.

Table 2 Shows faults displacement and dip angle in L07.

Fault	1	2	3	4	5	6
Dip angle	~30°	~30°	~33°	~38°	~46°	~46°
Displacement (km)	~2.6	~1.8	~4.2	~0.8	~1.6	~0.8

L08 & 23: These lines cross at the southern margin of the Gulf (Figure 42), along with the eastern part of West domain as well as Central (West& East), East, and Alkyonides domains.

Five normal faults, including one listric, were observed crossing the basement and Syn-rift sequences, in addition to two smaller faults crossing the basement and Early-rift sequence in the eastern section of the line. Table (1), shows displacement and dip angle range of faults in order from west to east, growth strata was observed toward fault 4 of the whole syn-rift package,The thickness of the Early-rift package varies along strike: it is thinner in the west, thicker toward the centre of the section, gets thinner where the basement is at shallow level and fills a smaller basin that pinches out toward the east. In contrast, the basement became shallower and was at shallow level in L23, followed by three faults: one minor, one east and one west dipping. In the Eastern section of L23 where two faults are located, a compressional feature was also noticed in the thick Early rift package, in the form of two small anticlines where the top boundary is eroded forming an angular unconformity.

Table 3 Shows displacement and dip angle values of faults in L08&23.

Fault	1	2	3	4	5	6
Dip angle	~38°	~40°	~40°	~35°	~30°	~30°
Displacement (km)	~6.0	~6.0	~1.6	~2.8	~0.4	~3.2

The Late-rift sequence thickness varies too; it is thinner on the flanks and is thickest in the Central domain. The horizons H1 and H2 were traced along L08; while H3, H4, H5, and H6 were only traced along the Eastern section of L08, as the reflection became chaotic and hard to interpret.

w

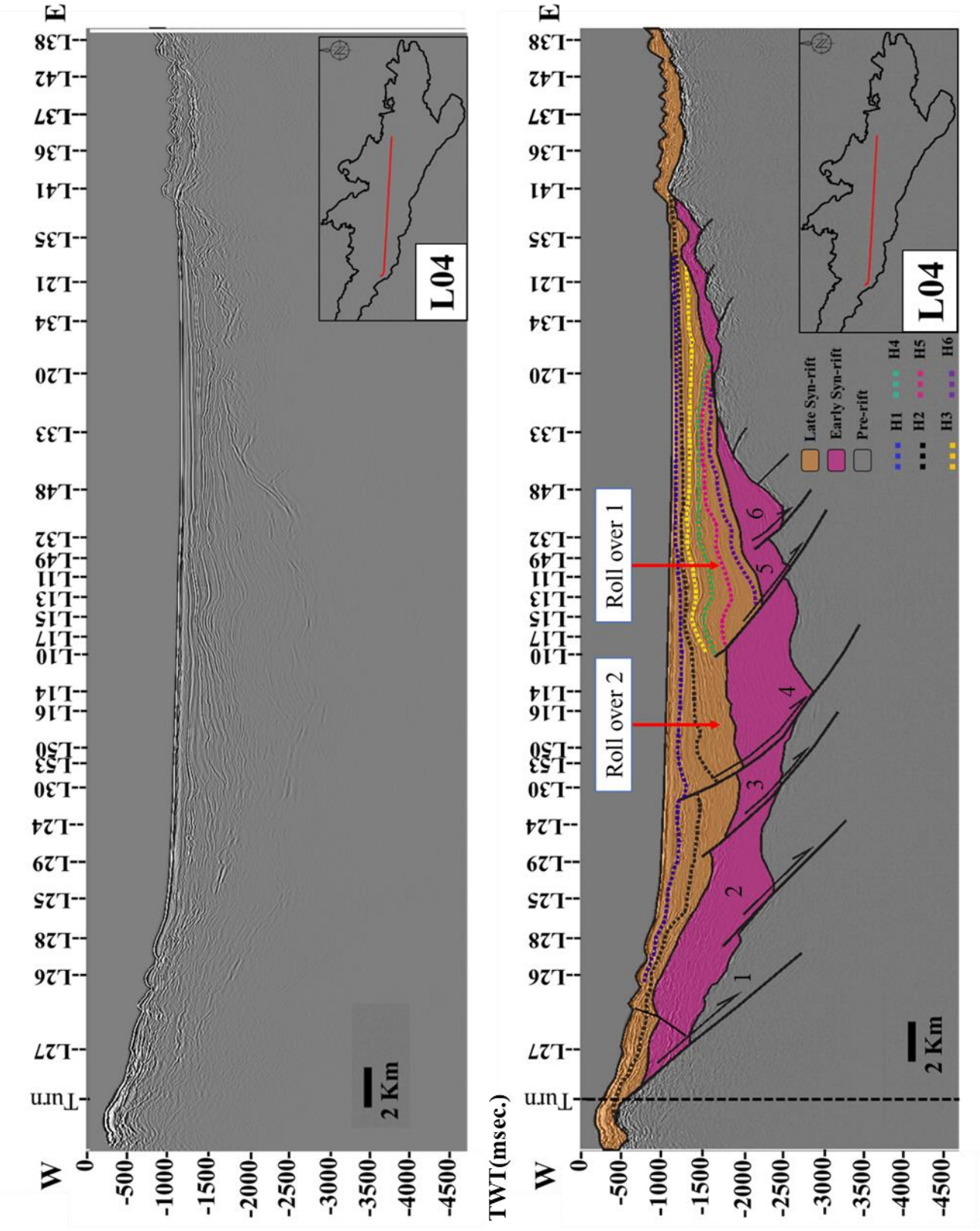

Figure 40 Non-interpreted and interpreted seismic profile of L04 with two marked roll-over structures.

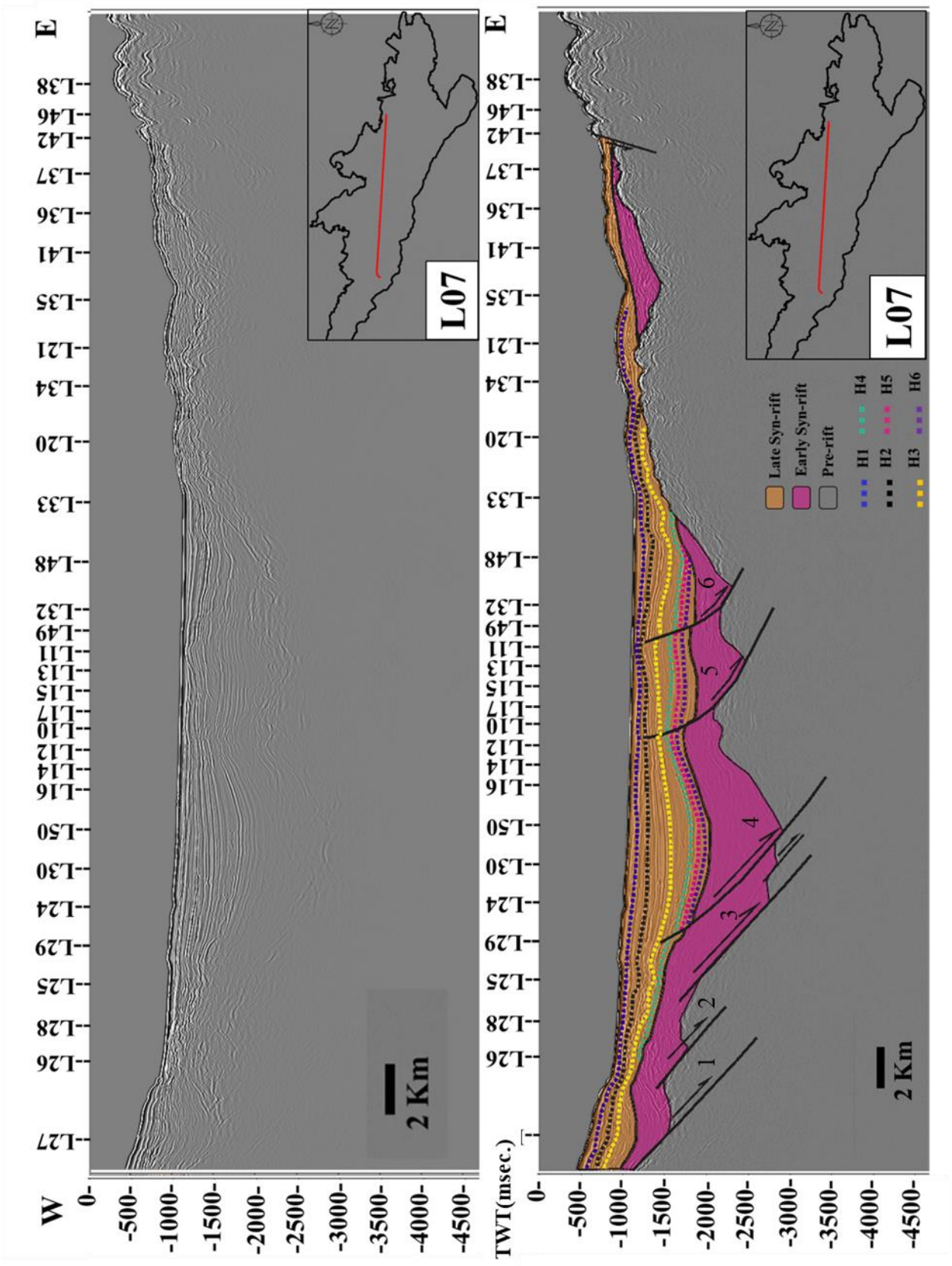

Figure 41 Non-interpreted and interpreted seismic profile L07.

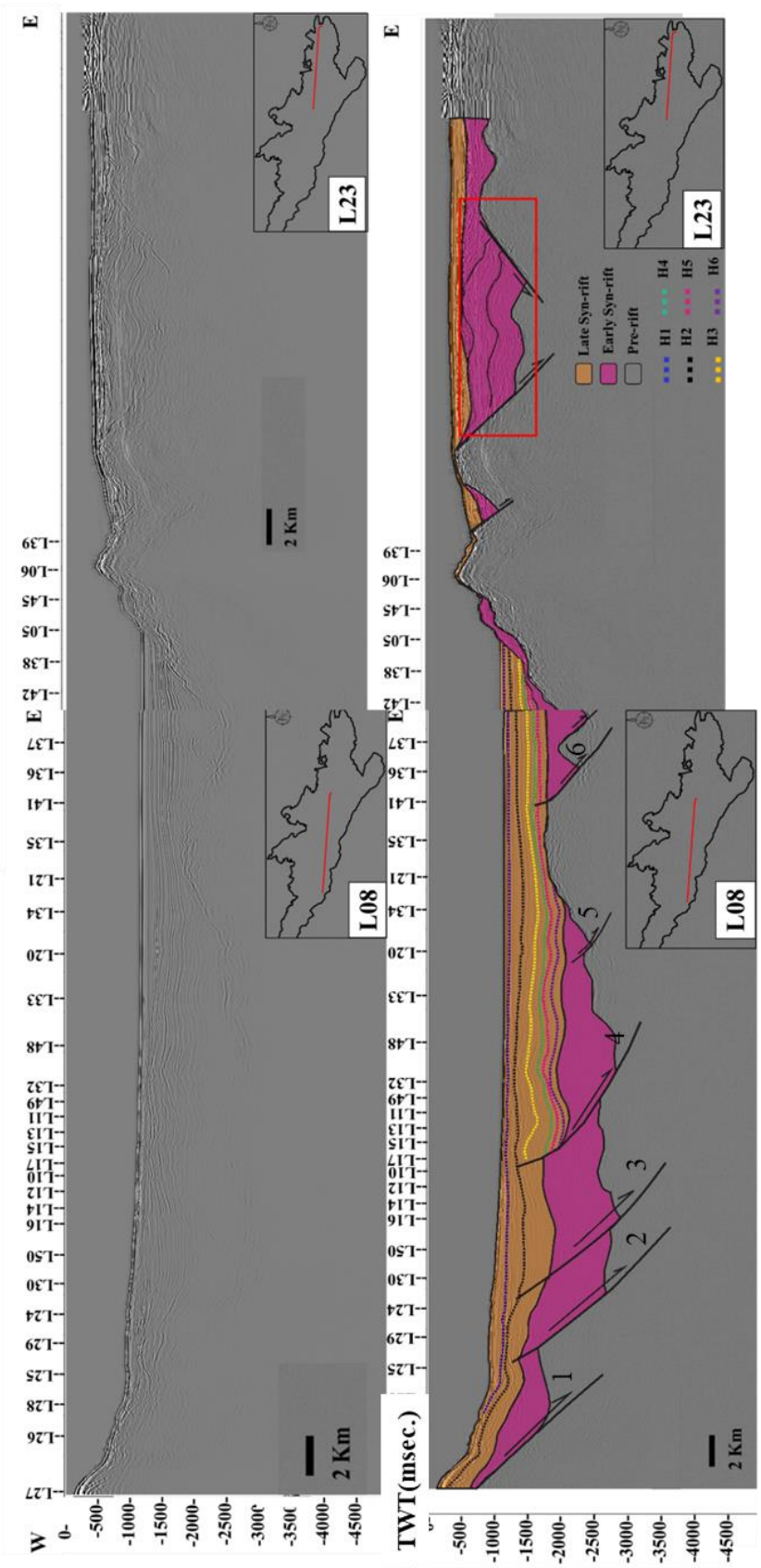

Figure 42 Uninterpreted and interpreted seismic profiles L08 and L23 with marked compressional feature in the redbox.

L53: is a W-E line across the eastern section of the West domain and Central-west domain (Figure 43). Three east dipping major normal faults were interpreted; two of which interact with the basement, Early and Late rift sequences and the third with only the Early-rift sequence and the basement. Table (4), shows the displacement and dip angle range of faults, growth strata of early syn-rift was observed toward fault 2 with a thickness of ~2.0 km.

Table 4 Shows displacement and dip angle of faults in L53.

Fault	1	2	3
Dip angle	~25°	~25°	~28°
Displacement (km)	~1.7	~1.5	~0.9

The Early rift package is thinner in the west and increases in thickness toward the east. It decreases briefly where line 29 intersects the seismic line, but starts to increase again toward the east. H1 and H2 sub-sequences were traced only along the section; the Late syn-rift section thins out toward the west.

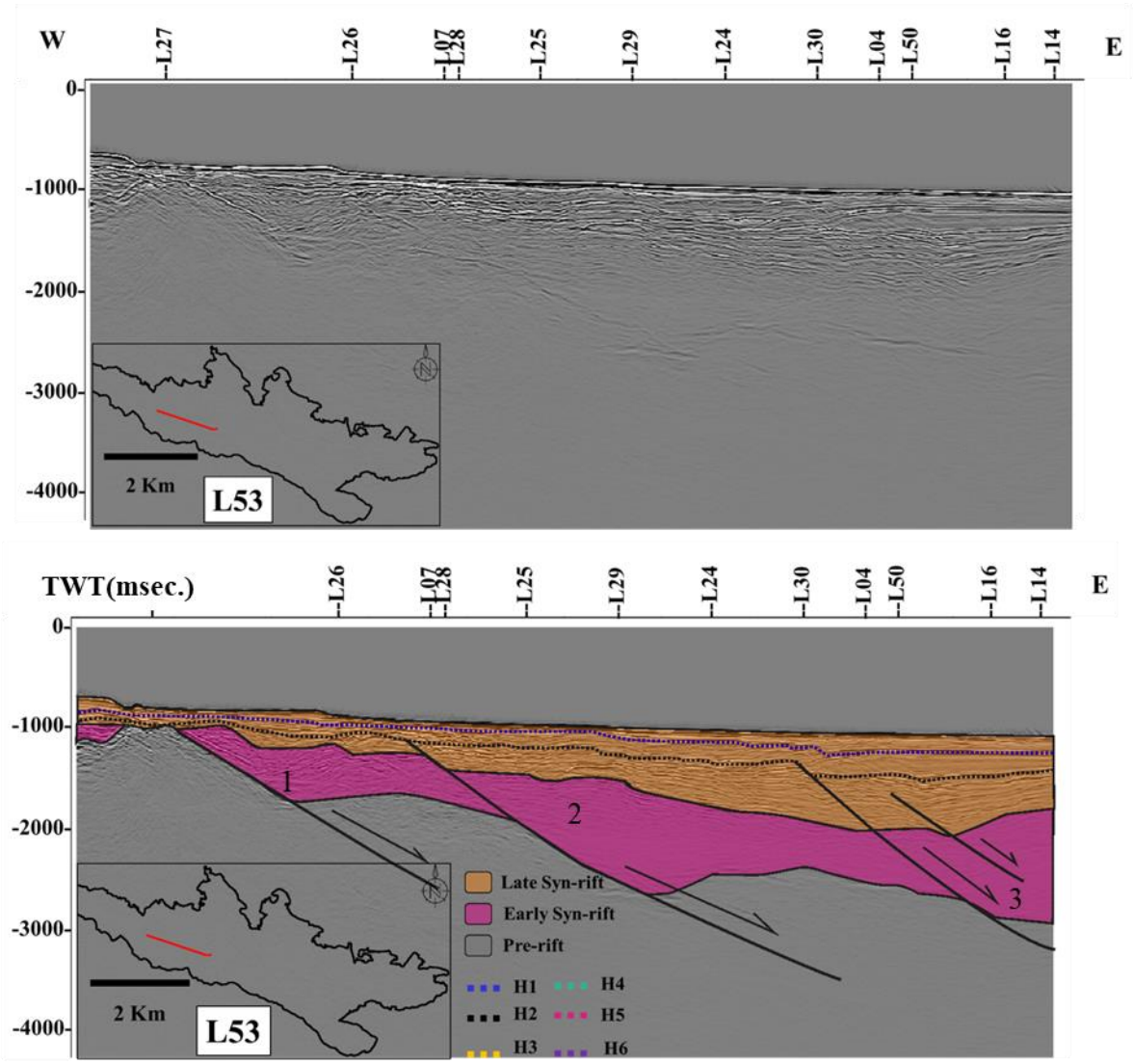

Figure 43 Non-interpreted and interpreted seismic profile L53.

L09&22: are located at the southern margin and cover the eastern part of the Central-West, Central East, East and Alkyonides domains, together with line22 (Figure 44). Four east dipping normal faults with rotated blocks, which interact with the basement and Early rift packages, were observed in the L09. Table (4), shows the values of their displacement and dip angle, these faults seem to be active during pre-and early-rift, growth strata of the Early-rift sequence was observed toward faults 2, 3, and 4. The thickness of Late-rift is greater than the Early rift and both pinch out toward the East, the thickest package of late syn-rift is ~5.0 km, while in early syn-rift is ~3.0 km. All Late-rift horizons were traced along L09.

Table 5 Shows displacement and dip angle values of faults in L09&22.

Fault	1	2	3	4
Dip angle	~28°	~30°	~30°	~30°
Displacement (km)	~2.0	~0.8	~1.0	~0.6

The whole Syn-rift package has a wavy shape in the Eastern part of the line. In L22 the basement is at a shallow level, and a thin layer of Syn-rift sediment covers it as it pinches out, before it fills a smaller basin in the eastern section of the line. Two small faults were recognized in L22: the first is an east dipping normal fault, while the second is a more significant west dipping fault. Both faults cross-cut the basement and Early-rift package.

L18: the structures are more or less similar to L09; the difference is that there is no west dipping fault (Figure 45). In contrast, all of the faults are east dipping including three faults in the eastern part of the line, values of their displacement and dip angles are presented in Table (6). These faults seem to be active during pre- and early-rift, where growth strata feature was observed in the early syn.rift toward all interpreted faults.

Table 6 Shows displacement and dip angle values of faults in L18.

Fault	1	2	3	4
Dip angle	~25°	~30°	~30°	~30°
Displacement (km)	~1.0	~1.25	~1.5	~1.7

L19: is located at the southern margin of the Central-East, East and Alkyonides domains. Six faults were observed (Figure 46): a major east dipping normal fault 1 which crosses the pre-and Syn-rift packages, three east dipping normal faults 2,3, and 4 that interact with the basement and Early-rift package, a west dipping fault 5, and a minor fault that only cross-cuts the basement beside fault 5.

Table 7 Shows displacement and dip angle values of faults in L19.

Fault	1	2	3	4	5
Dip angle	~42°	~30°	~30°	~28°	~50°
Displacement (km)	~7.0	~6.0	~2.3	~1.3	~2.7

Fault 1 is controlling the depositional structure of the whole syn-rift package as it is deposited in the form of growth strata toward fault 1 with a thickness of ~6.0 km. Early-rift package is thicker than the Early syn-rift package in average, and both are pinching out toward the east where the basement is high. In contrast, faults 2, 3, 4, and 5 were active during the pre- and early-rifting stages.

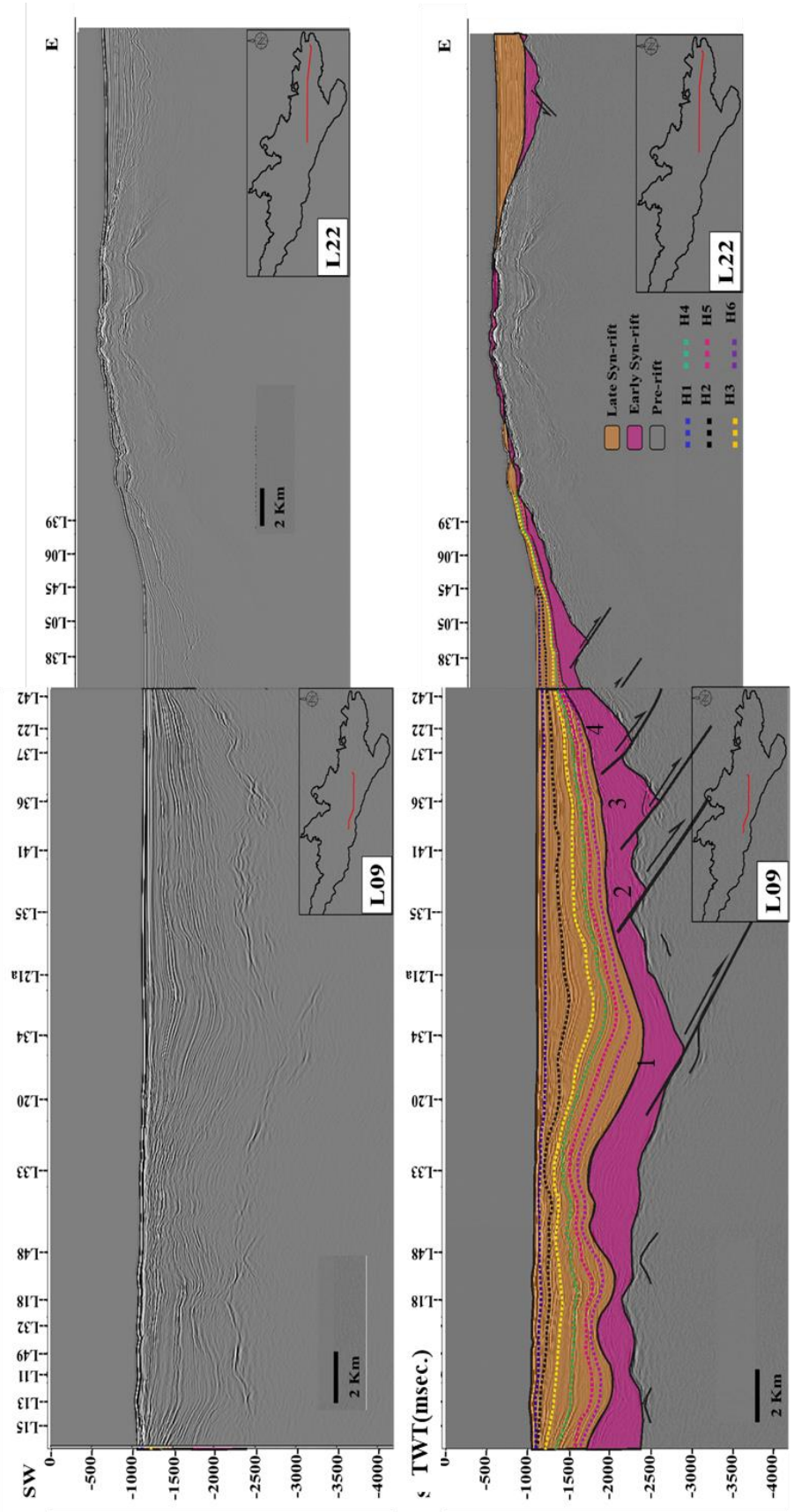

Figure 44 Non-interpreted and interpreted seismic profiles L09 and L22.

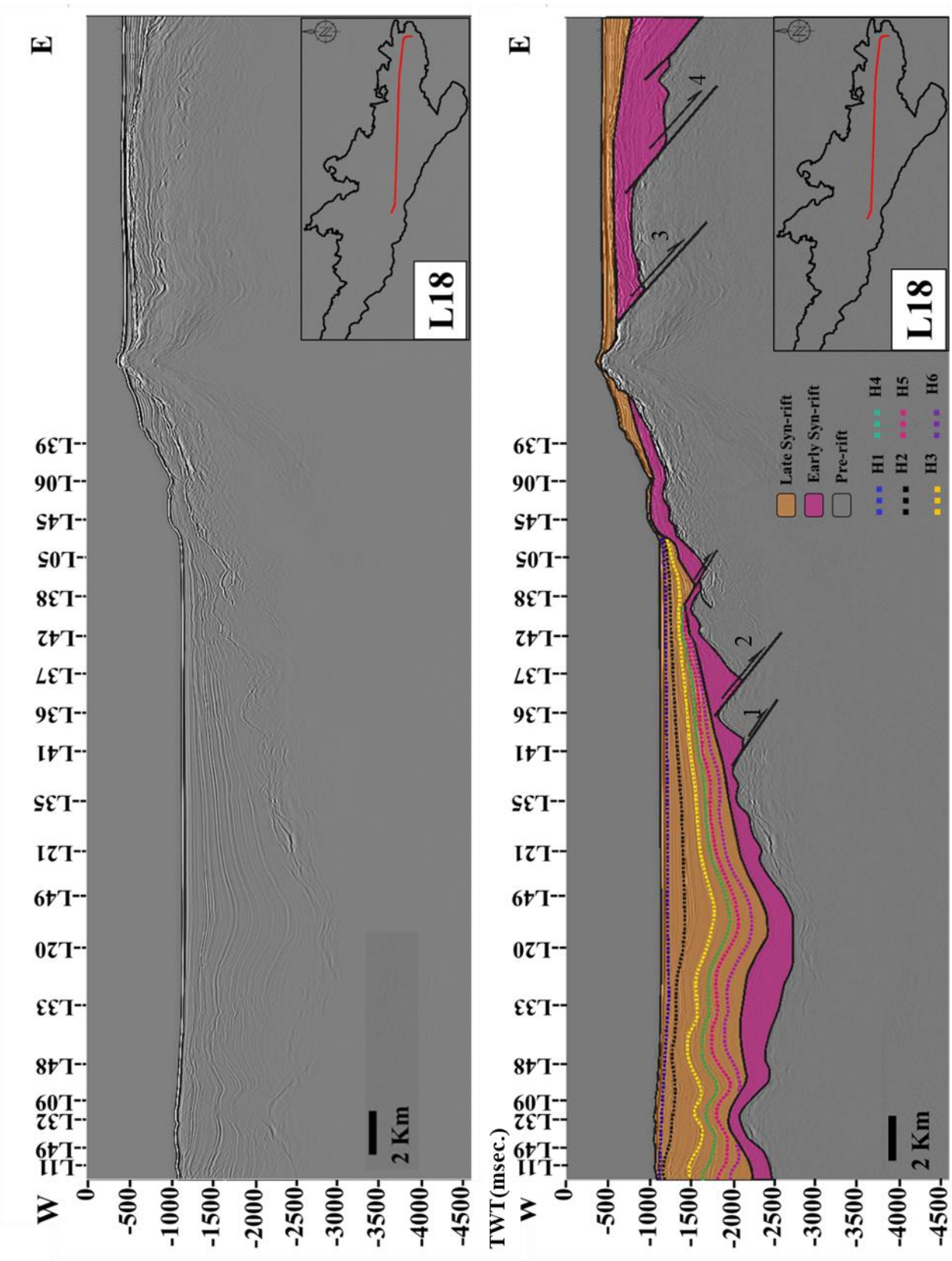

Figure 45 Non-interpreted and interpreted seismic profile L18.

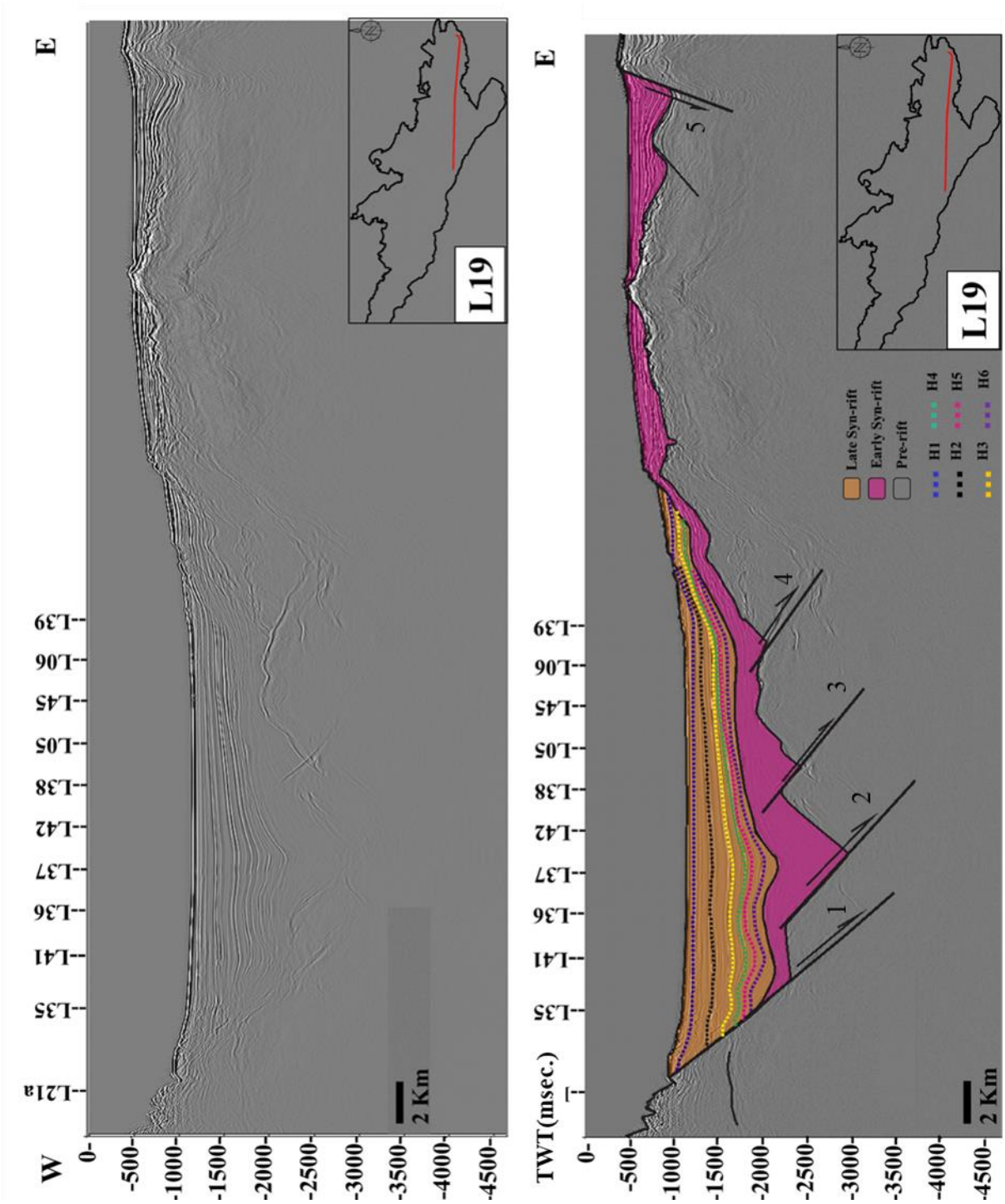

Figure 46 Non-interpreted and interpreted seismic profile L19.

L31: is located at the southern margin of Central-West domain (Figure 47). An east normal dipping fault was traced at the center of the line with a displacement of 1.6 km and dip angle of 40° and seems to be active during pre-, early-, and late stage of rifting. Growth strata was observed in the whole syn-rift package. The Early-rift sequence has a mostly homogenous thickness at the center of the section, but it pinches out toward the east and thickens in the

west. The Late-rift sequence pinches out toward the west and the east and is thickest in the footwall of the fault.

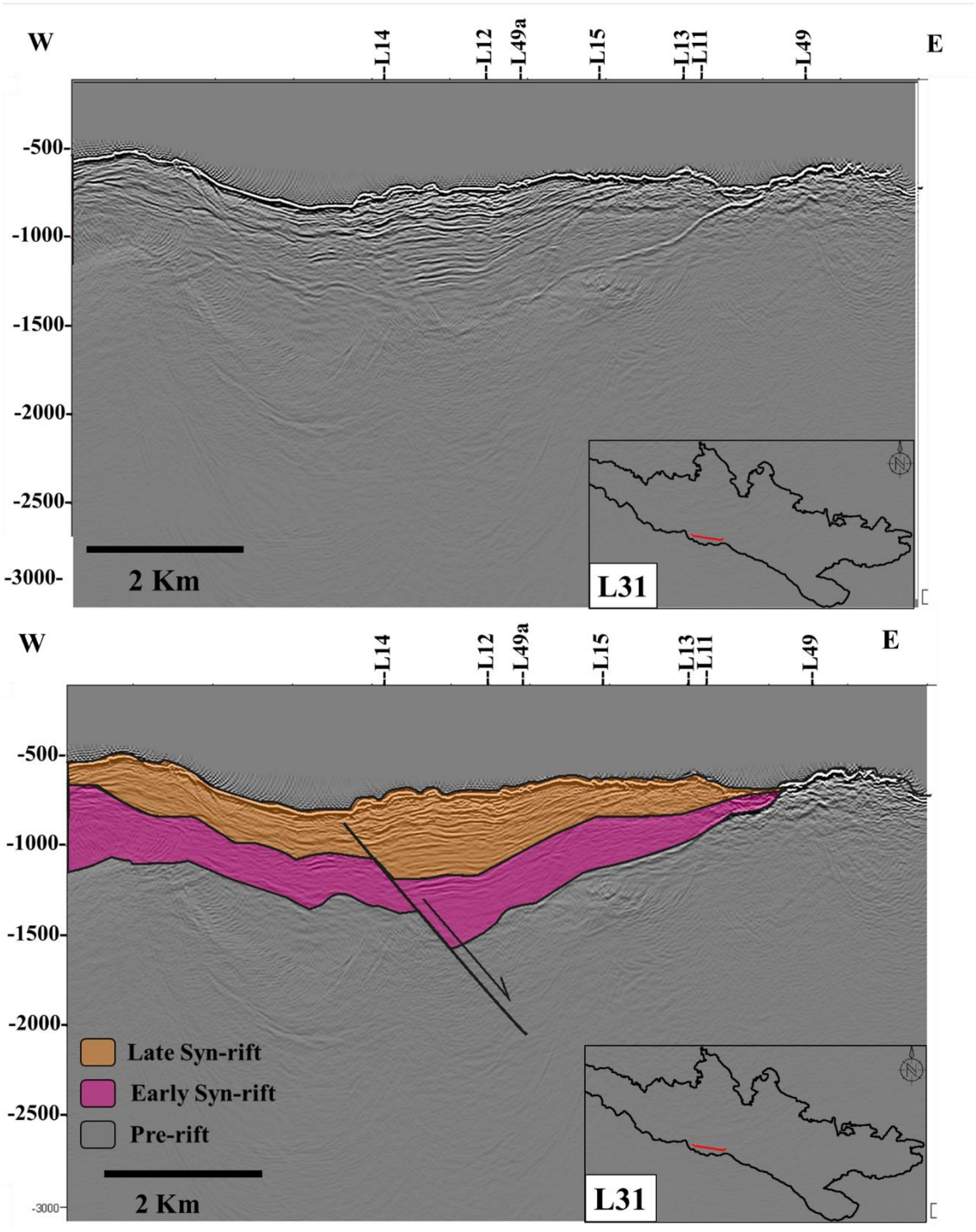

Figure 47 Non-interpreted and interpreted seismic profile L31.

L40: is located at the southern margin of the East domain (Figure 48). It consists of only basement and Early-rift sections with an ~30° east dipping normal fault with a displacement of ~1.7 km. The Early-rift package thins out toward the west and east; this shape character could

be caused possibly by a submarine erosion. In the western section, a prominent canyon was observed with wide of ~320m and depth of ~240 m incising the Sea floor.

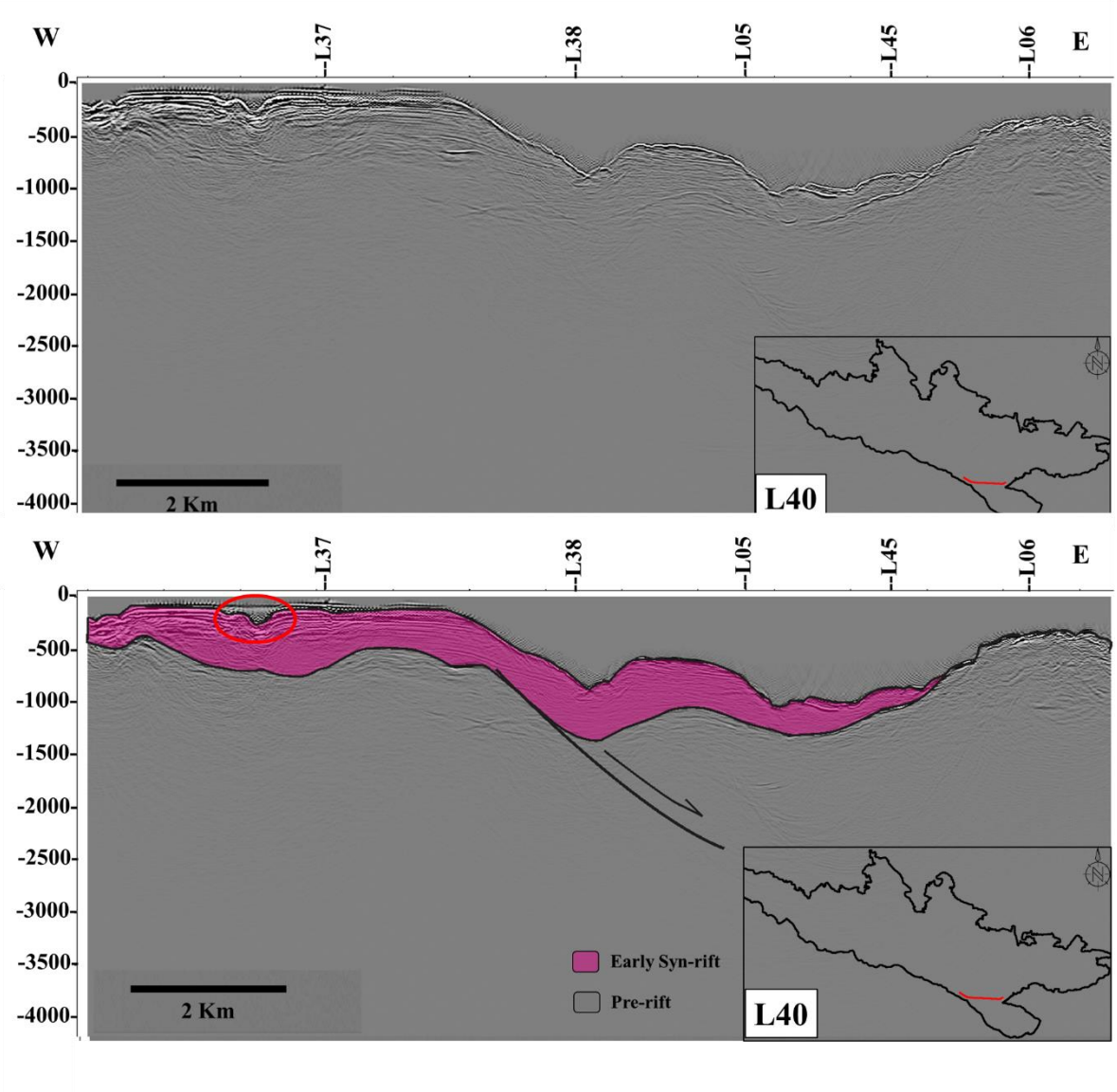

Figure 48 Non-interpreted and interpreted seismic profile L40 with the marked canyon in the red circle.

L43: is also located at the southern margin of the East-domain (Figure 49). Syn-rift packages and basement were traced, as well as an NW dipping normal fault. A prominent canyon incising the Sea floor with depth ~300 m and ~600 m wide is observed in the line, which is just located on a major step of the basement caused by faulting with a displacement of ~2 km and dip angle ~29°. Canyons from Line 40 and 43 were mapped in Figure 50 to show the exact location. The basement is deepest toward SE where a thick package of Early-rift sediment is deposited with a thickness of ~2.2 km. The thickness of the Late syn-rift sequence is more or less homogeneous along the line.

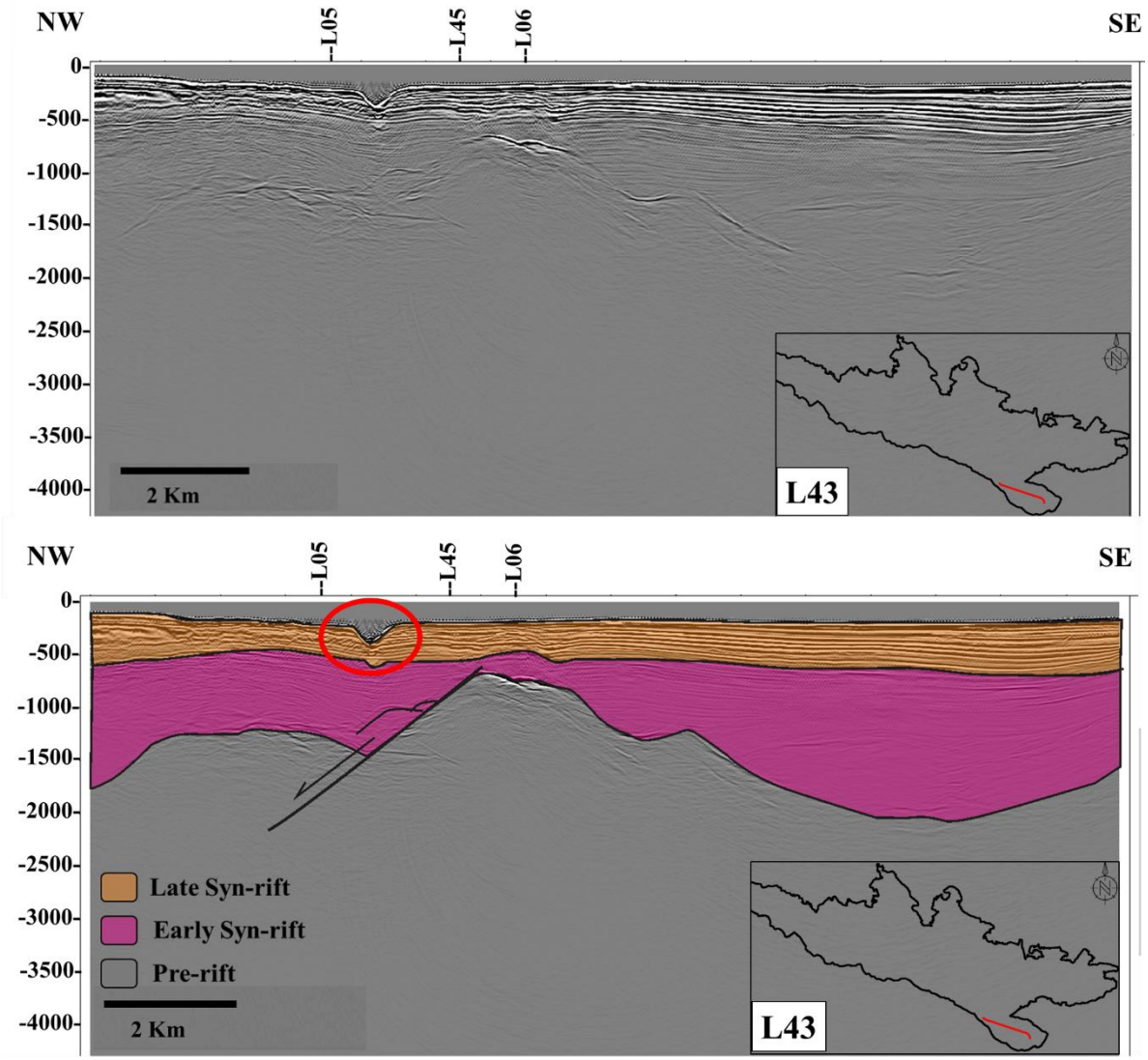

Figure 49 Non-interpreted and interpreted seismic profile of L43 with interpreted canyon marked in the red circle.

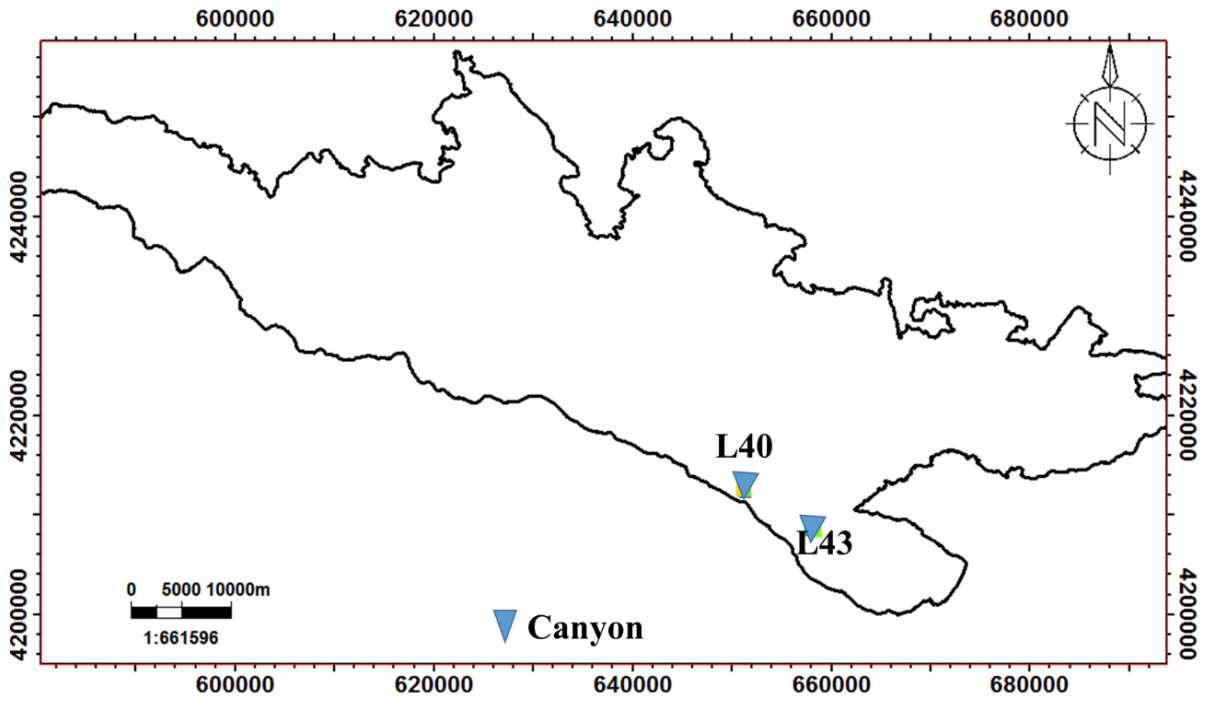

Figure 50 Boundary map of the GoC with mapped canyon locations observed in L40 and L43.

L44: located in the Alkyonides domain (Figure 51), it shows the basement is very shallow with a thin layer of Syn-rift and probably Early-rift. An east dipping normal fault was traced in the eastern section of the line.

L46: is located at the northern margin of the Central-East domain (Figure 52). The basement is at a shallow level along the whole section, especially in the eastern part of the line. A thin layer of Syn-rift sequence is interpreted. The Early-rift package is thinner than the Late-rift, but in the central section, it thickens in the form of growth strata toward the east dipping normal fault and then pinches out toward the east. The Late-rift sequence has a uniform thickness in the western part of the line, but it thickens in the central section and then pinches out toward the east. Two canyons were observed in the eastern section of the line, canyon1is ~500 m wide and ~400 m depth, and canyon 2 with the depth of ~300 and ~300 m wide.

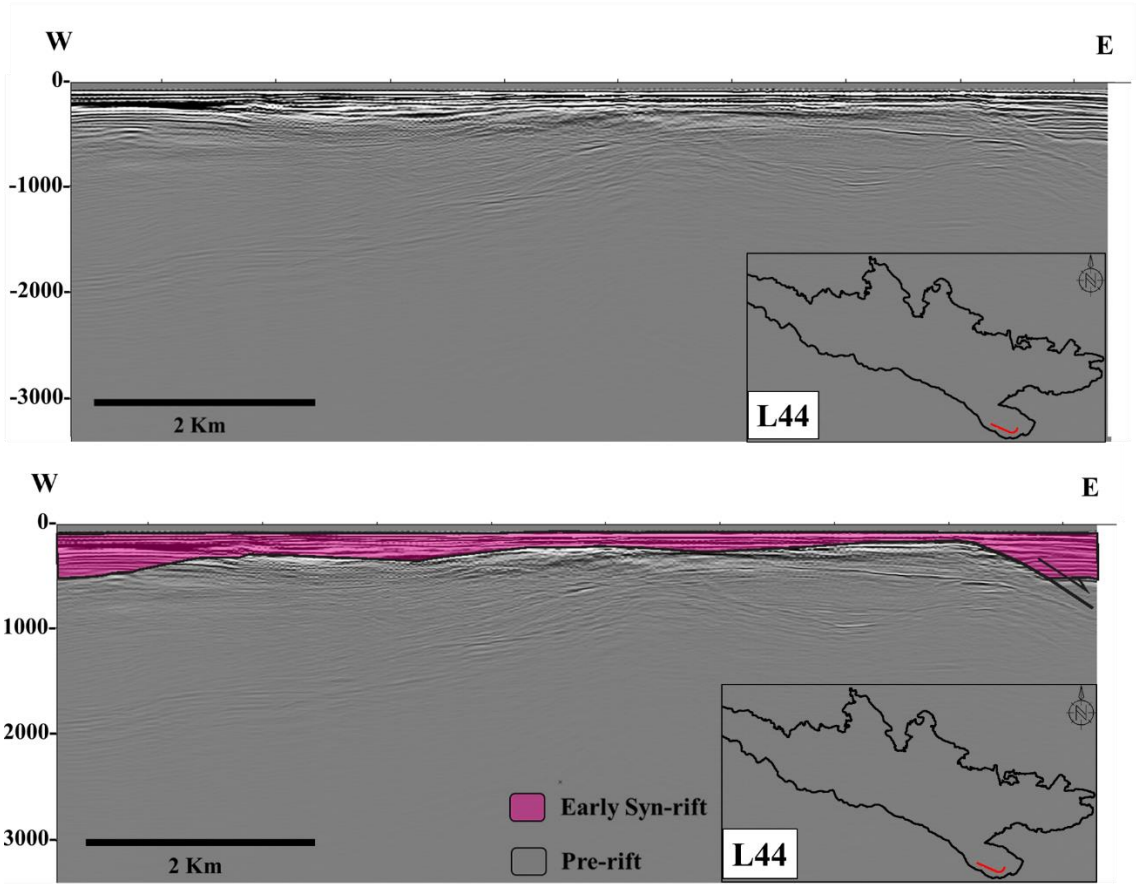

Figure 51 Non-interpreted and interpreted seismic profile L44.

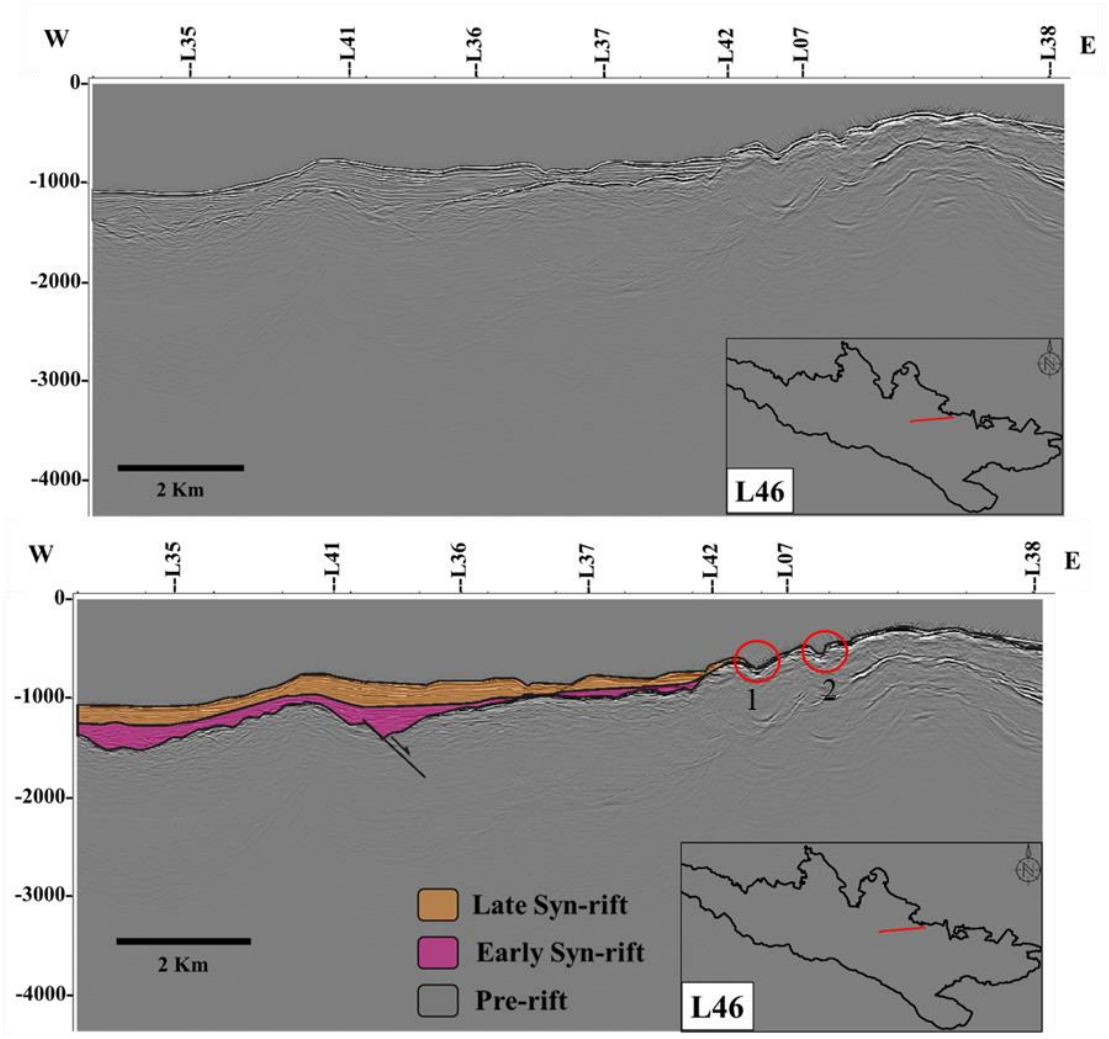

Figure 52 Non-interpreted and interpreted seismic profile L46 with marked two canyons in the eastern section of the line.

L47: is located on the flank of the southern margin of the Central-East domain (Figure 53). The seismic profile shows noise but also a sharp reflector which was interpreted as a basement. The basement reflector is almost a straight line in the eastern section before it drops dramatically and takes on an anticline shape. This change was interpreted as a fault that crosses both the basement and Early-rift sections with a displacement of ~1.9 km and dip angle of 43°. In comparison, the Late-rift section has a wavy upper boundary with approximately the same thickness along the western and central part of the seismic profile.

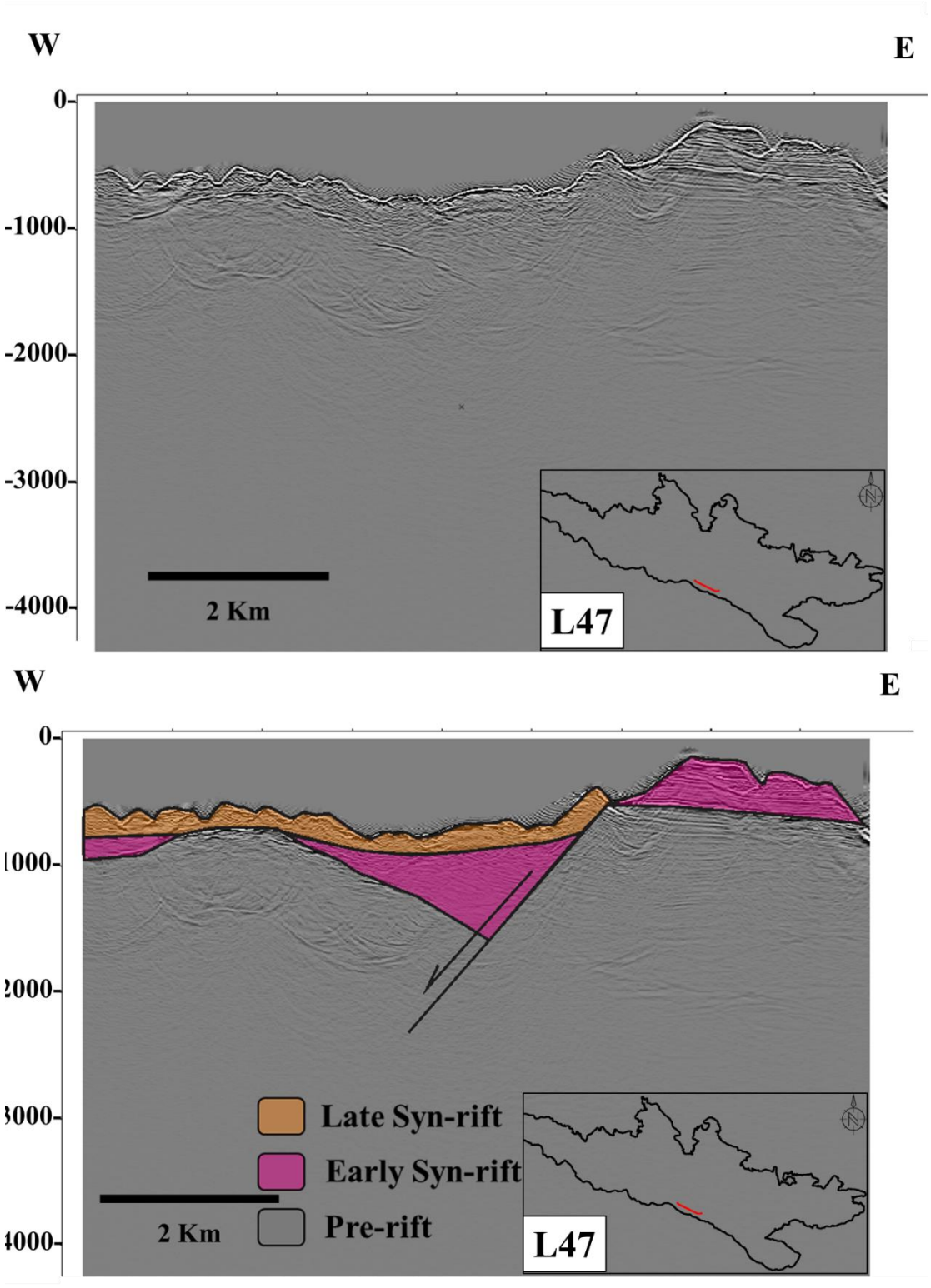

Figure 53 Non-interpreted and interpreted seismic profile L47.

The strike of the faults was difficult to derive as the dataset is 2D and the distance between each line is large. In this case study, the S-N direction was assumed as most of the seismic lines are W-E oriented.

All W-E lines were combined, in order of north to south, in Figure (54) to show the variation in structures and stratigraphy along the Gulf. A variation in thickness of the main packages was observed along the N-S direction. The thickest package of the Late Syn-rift is mostly located in the Central-East domain, while the thickest package of the Early-Syn-rift is located in the Central-West domain. Most of the interpreted N-S faults dip toward the east.

A map of the main basin and intra sub-basins was produced to gain a better overview of sediment geometry variation (Figure 55). Three intra sub-basins were observed in the Early Syn-rift, two located in the Central-West domain and one in the East domain. However, these three intra sub-basins are located in an elongated main basin in the Central and East domains, the other two sub-basins are located in the East and Alkyonides domains.

The Late Syn-rift basin distribution shows intra four sub-basins distributed along the elongated main basin and toward the southern margin. It seems that the majority of the Late Syn-rift sediments were mainly deposited in the Central-West and Central-East domains. In contrast, the intra sub-basins of the whole Syn-rift sequence are distributed along the entire main basin.

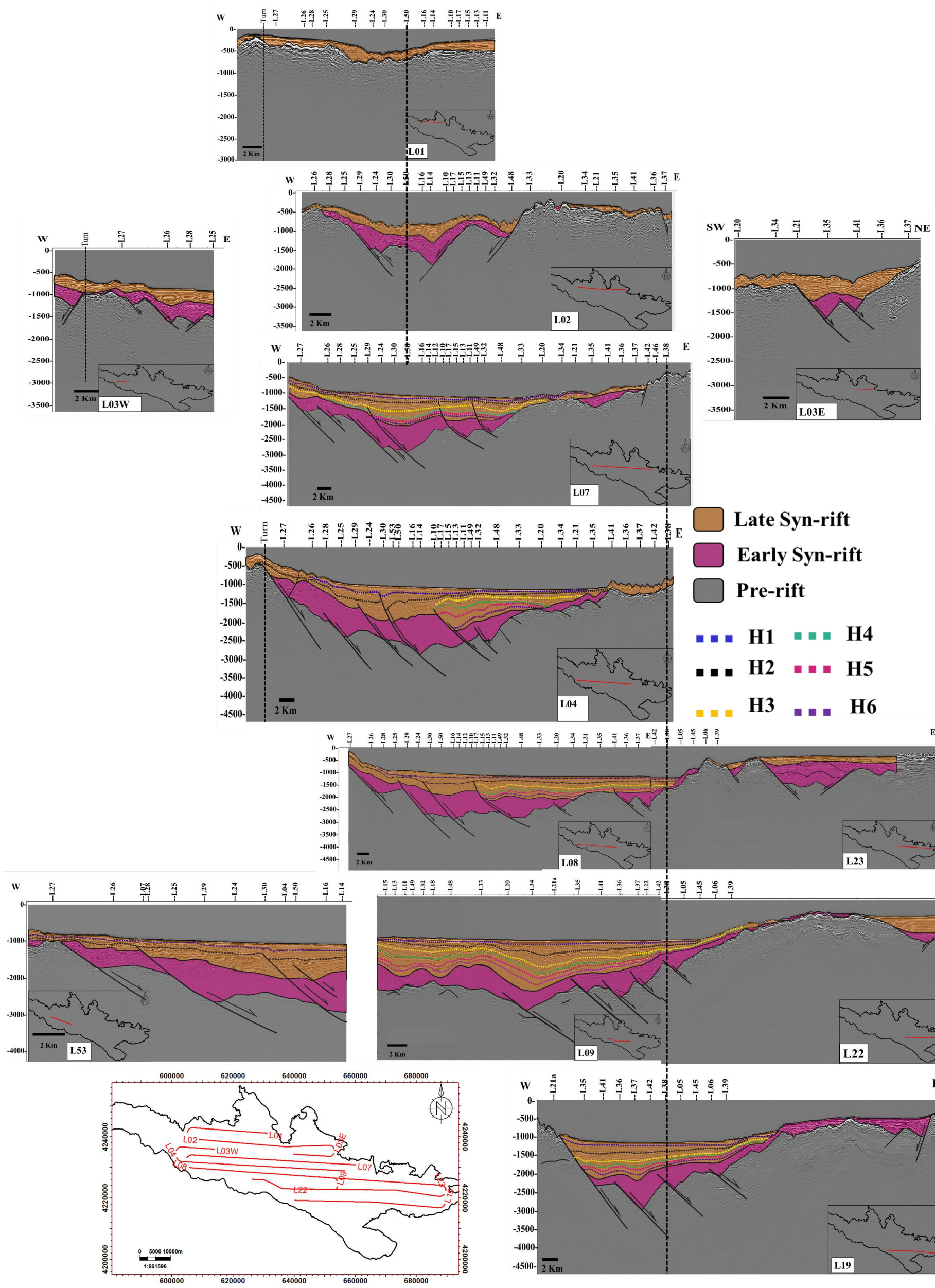

Figure 54 W-E seismic lines showing the structure variation from the southern margin to the northern margin of the Gulf, vertical scale unit is TWT(msec.)

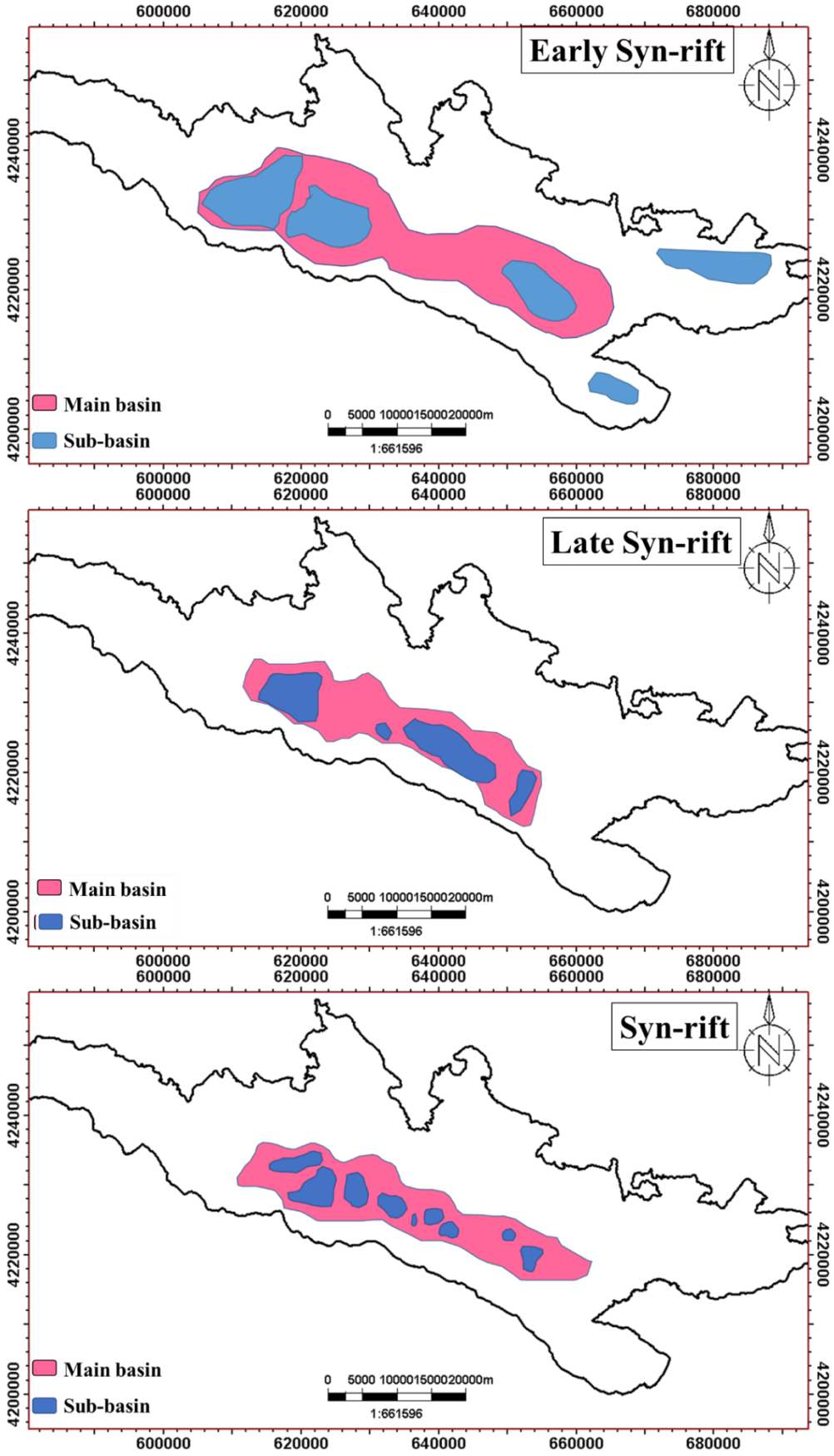

Figure 55 Map of the GoC with mapped main and intra sub-basins of the Early, Late, and whole Syn-rift sequences.

3.3 Structural and stratigraphic along S-N direction

All S-N seismic lines were interpreted (Appendix 1) and based on these observations, and interpretations variation in rift structures was noted along the Gulf domains: West, Central-West, Central-East, East and Alkyonides (Figure 56). Domain names were adapted after Nixon et al., (2016) to make the description of each line easier to achieve and navigate easily.

3.3.1 West Domain

The structures in the eastern part of West domain are controlled by south dipping normal faults forming a half-graben with basement at a shallow level and a small horst on the northern margin (Line 27). The thickest package of Syn-rift sediment is located where Line 07 cross-cuts, while the basement gets shallower toward the southern margin (due to less accommodation space).

Central Domain

In the Central domain, the structures are controlled by both north and south dipping faults forming a graben. In contrast, the basement structures vary laterally as in L48, in the Central-East domain, the basement has a half-graben structure with rotated hanging wall blocks, where the Syn-rift sequence has its maximum depth towards the south and pinches out towards the north.

3.3.2 Central- West

Line 28 shows the structure is controlled by three major faults, two south dipping normal faults and one north dipping normal fault. For Line 30, two normal north dipping faults control the structures. The late Syn-rift subdivision sequences were difficult to trace in the southern margin except for H1 and H2. The Early and Late Syn-rift sediments vary in thickness: they are thicker in the southern margin than the northern margin where the basement is higher.

3.3.3 East Domain

The structures in the eastern part of East domain are mainly controlled by north dipping faults at the southern margin. Lines 42, 38, 05 and 45 in the western part of East domain show two major south and north dipping faults that control the structures, together with the major north dipping faults at the southern margin of the Gulf. The basement is at the shallow level at the northern margin of the East domain.

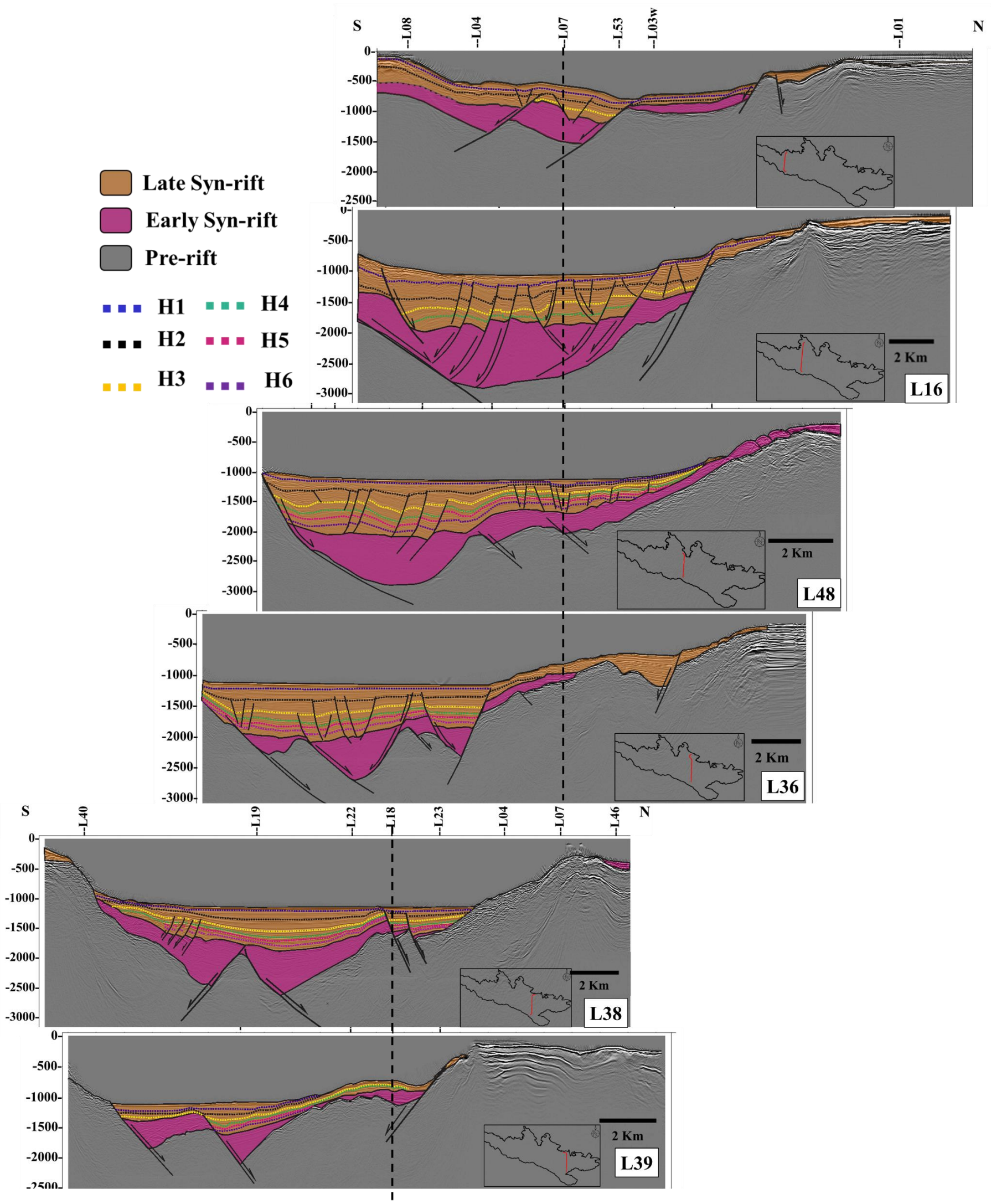

Figure 56 N-S seismic lines are showing the lateral variation along strike of N-S seismic lines. The vertical scale is TWT (msec).

3.4Time structure and thickness maps

The basement, Upper boundary of Early and Late Syn-rift horizons have been interpreted across the entire Gulf beside H1 and H2; those horizons were used to produce that time structure and thickness maps. In this sub-chapter, those maps are produced.

The time structure map of the basement (Figure 57) shows that the basement is shallow at the northern margin and in the Alkyonides section. It has its maximum depth in the Central and the East domains, forming a major depocenter most syn-rift sediments were deposited. Additionally, the Early Syn-rift time structure map (Figure 57) shows one main depocenter that is located in the Central-East and western part of the East domain with a depth of -1200 to -2500 ms, while its depth in the Central-West section is -1200 to -2000 ms and becomes shallower in the Alkyonides domain and the northern shore line. The H1 time structure map shows that the horizon is shallowest in the eastern part of West domain and a western and northern section of the Central-West domain and then gets deeper towards the East. The H2 surface map shows two depocenters located in the Central West and Central-East sections.

Thickness time maps of Early, Late, and whole Syn-rift package were generated in Figure 58:

Thickness time map of Early Syn-rift sediment: Shows that the thickest package of sediments is in the Central-West section, with a thickness of 600-100 ms, and gets shallower in the Central-East and the East sections of the Gulf.

Thickness time map of Late Syn-rift sediment: Shows that the maximum thickness of the Late Syn-rift package is located in the Central-East section with a thickness of 1200-1400 ms and gets shallower in the Central-West and East sections.

Thickness time map of the whole Syn-rift sediment: Shows that the thickest part is located towards the southern margin of the Central-West, Central-East and East domains and gets thinner towards the northern margin of the Gulf and in the Alkyonides section.

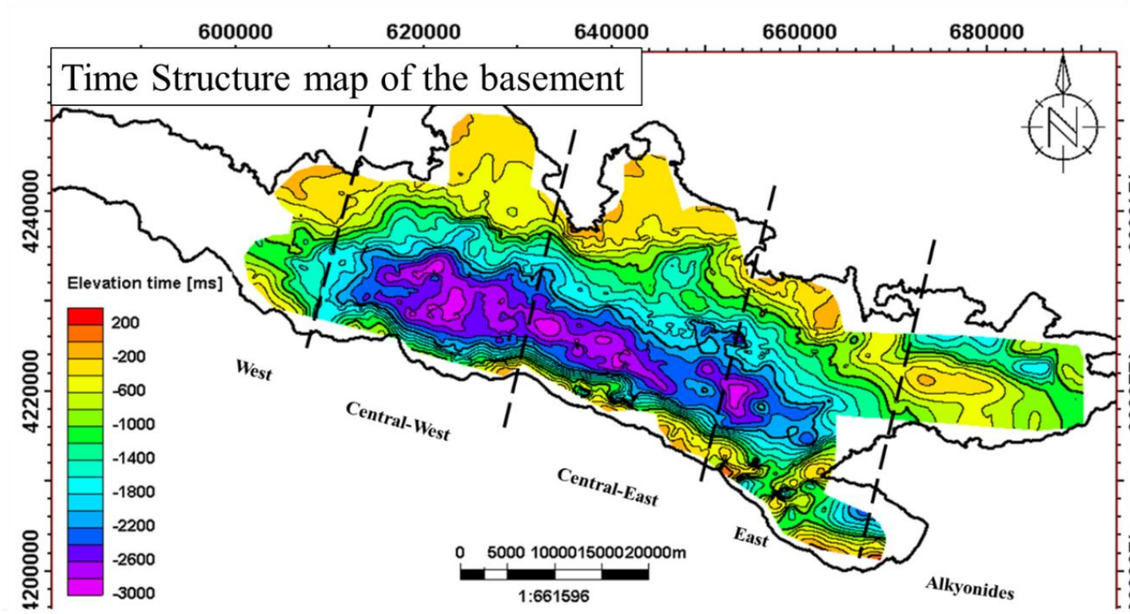

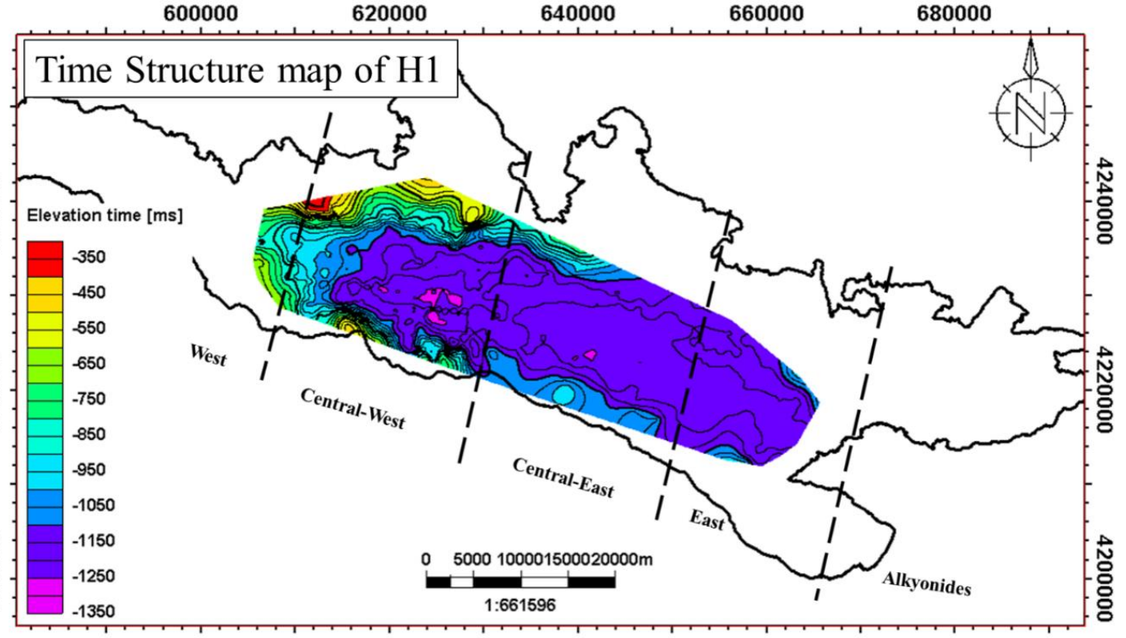

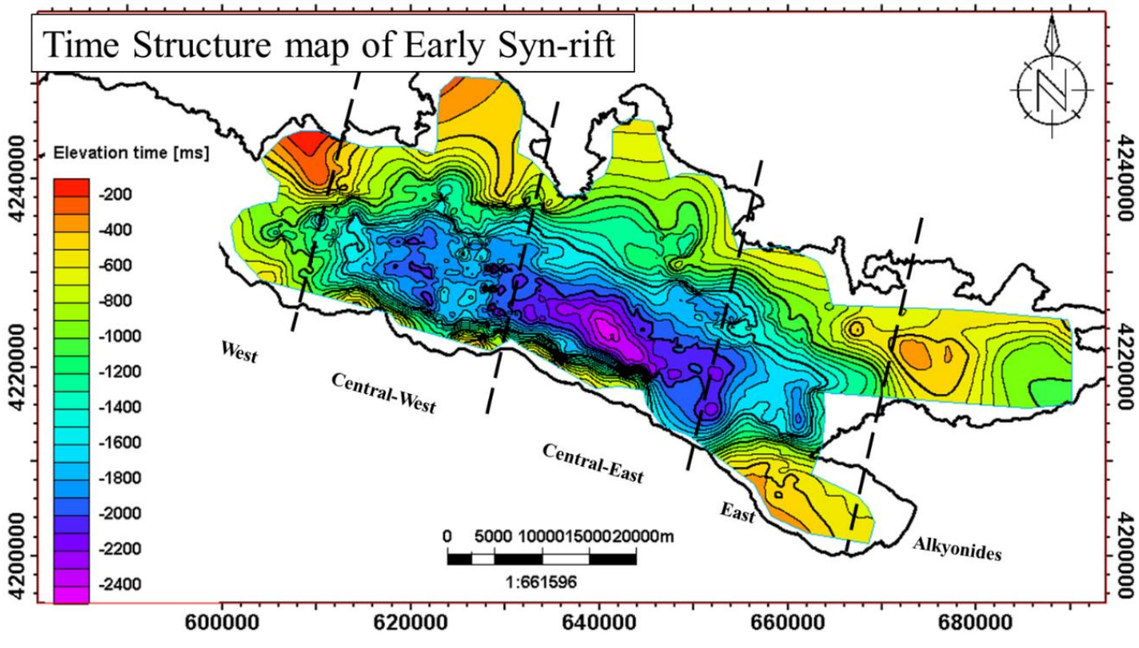

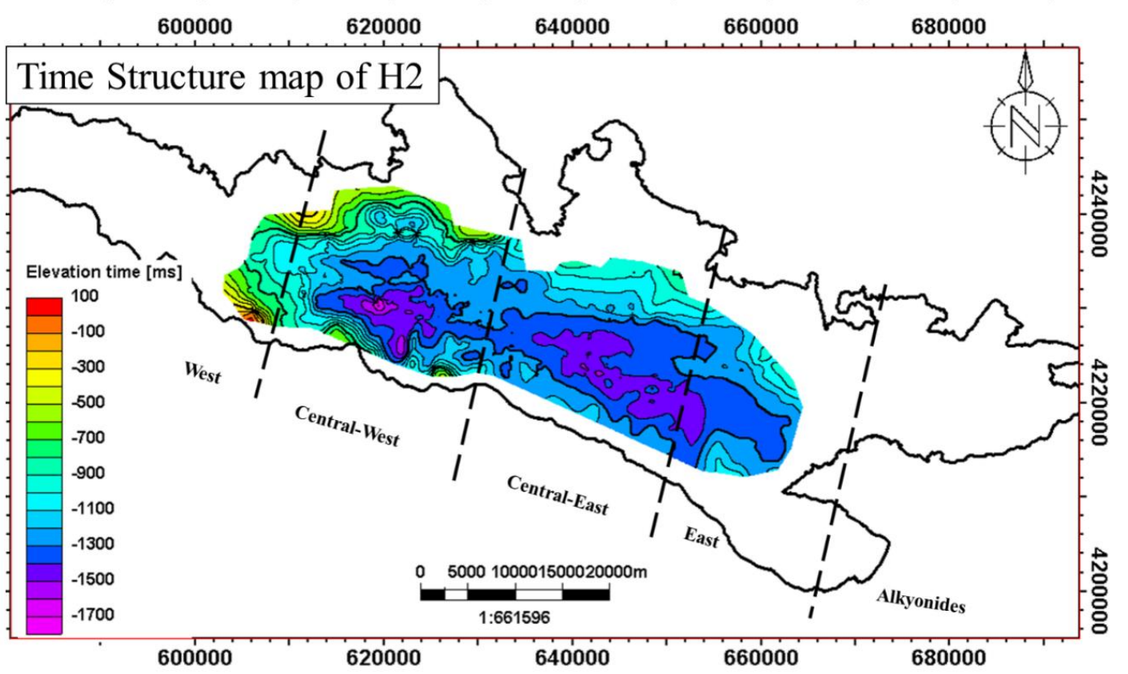

Figure 57 Time structure maps of the basement, Early syn-rift, H1 , and H2.Domains names are adopted after Nixon et al.(2016).

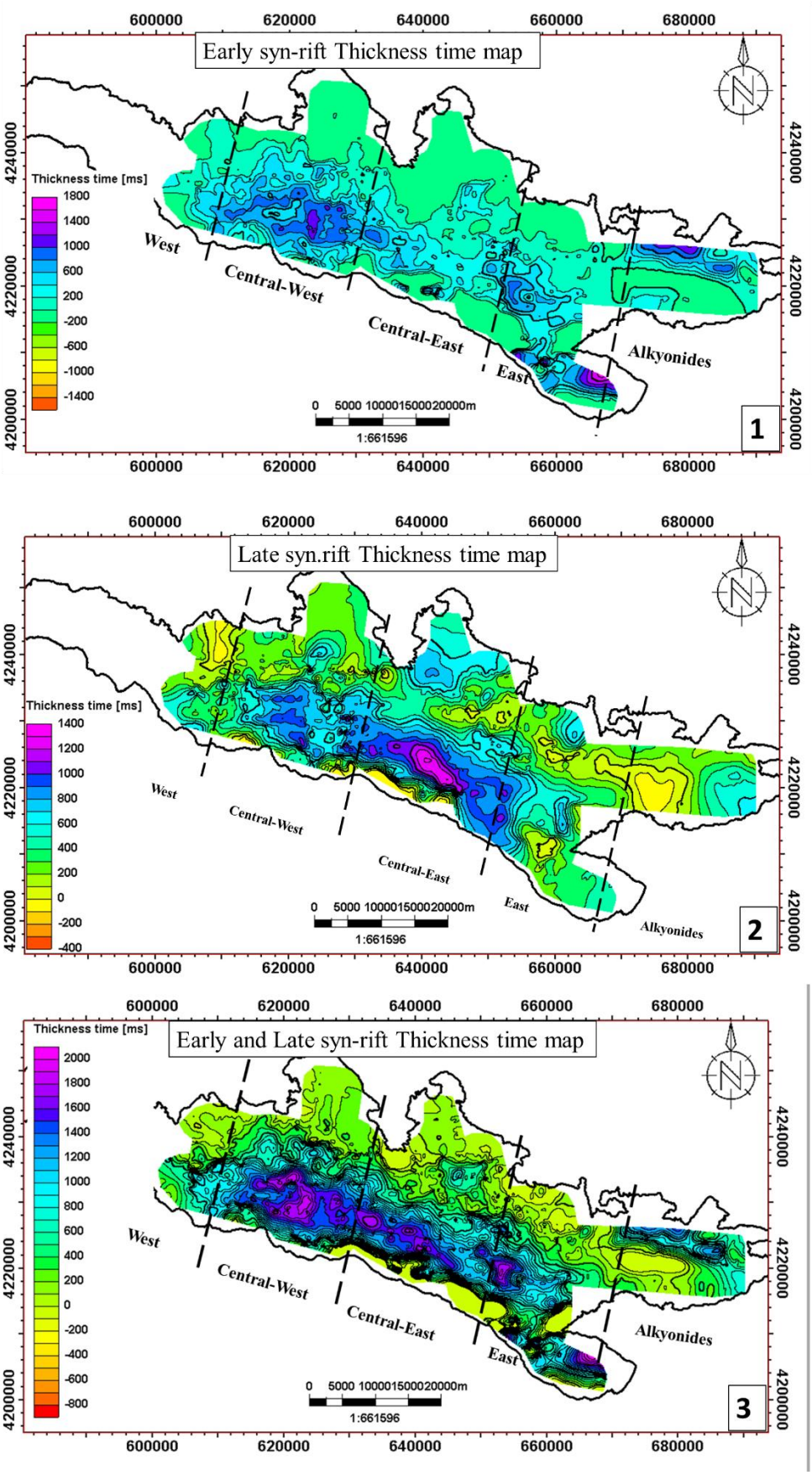

Figure 58 Time thickness maps: (1) Early Syn-rift, (2) Late Syn rift, and (3)whole Syn-rift package. Domains names are adopted after Nixon et al.(2016).

3.5 Along-strike variation of the basement structure

Seismic mapping indicated that structures vary along strike. Therefore, the aim of this sub-chapter is to investigate whether discrete zones or segments can be identified.

Most faults that mainly interact with the basement were mapped to better understand basement structure and architecture, the interpretation was carried out without extrapolation of faults in the area not covered by seismic data (Figure 59). Furthermore, the N-S faults which seem to be the same faults are connected (Figure 60). The final fault map shows possible N-S trending faults along the Gulf, in total 38 N-S faults are observed and named NS1 to NS38 (Figure 61).

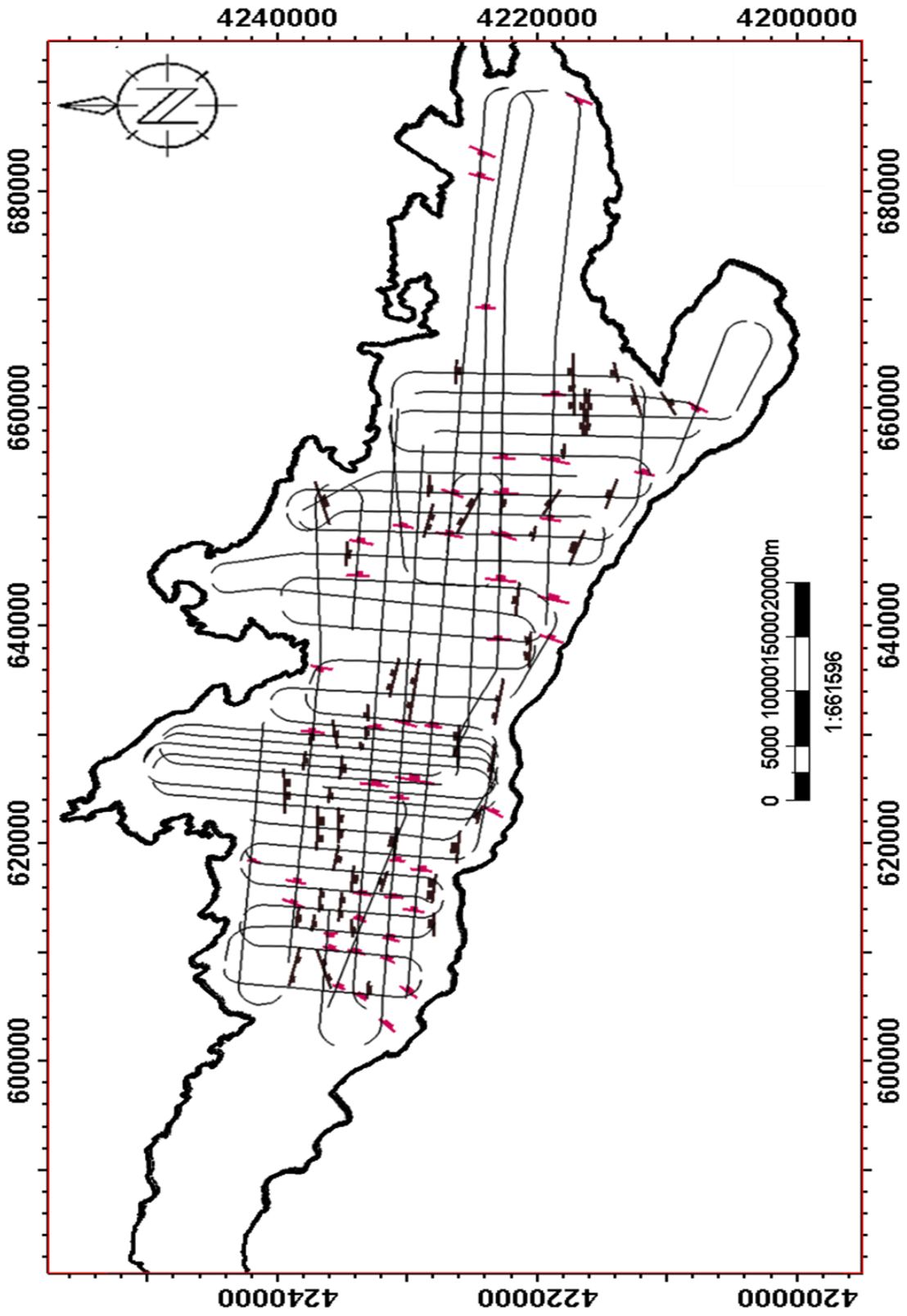

Figure 59 Structure map of GoC with interpreted N-S basement faults across the seismic lines, without extrapolation.

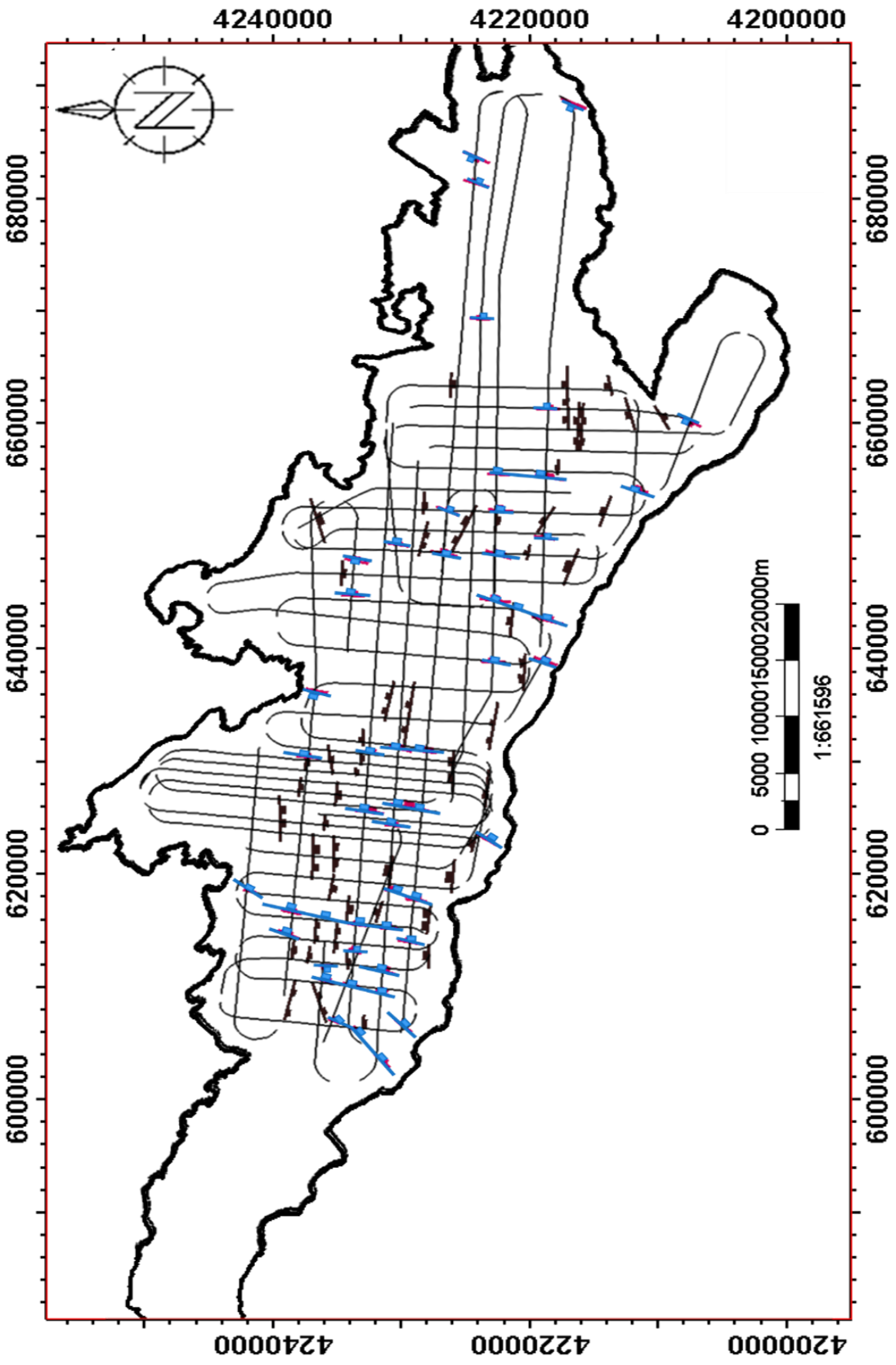

Figure 60 Structure map of the GoC with extrapolated N-S faults.

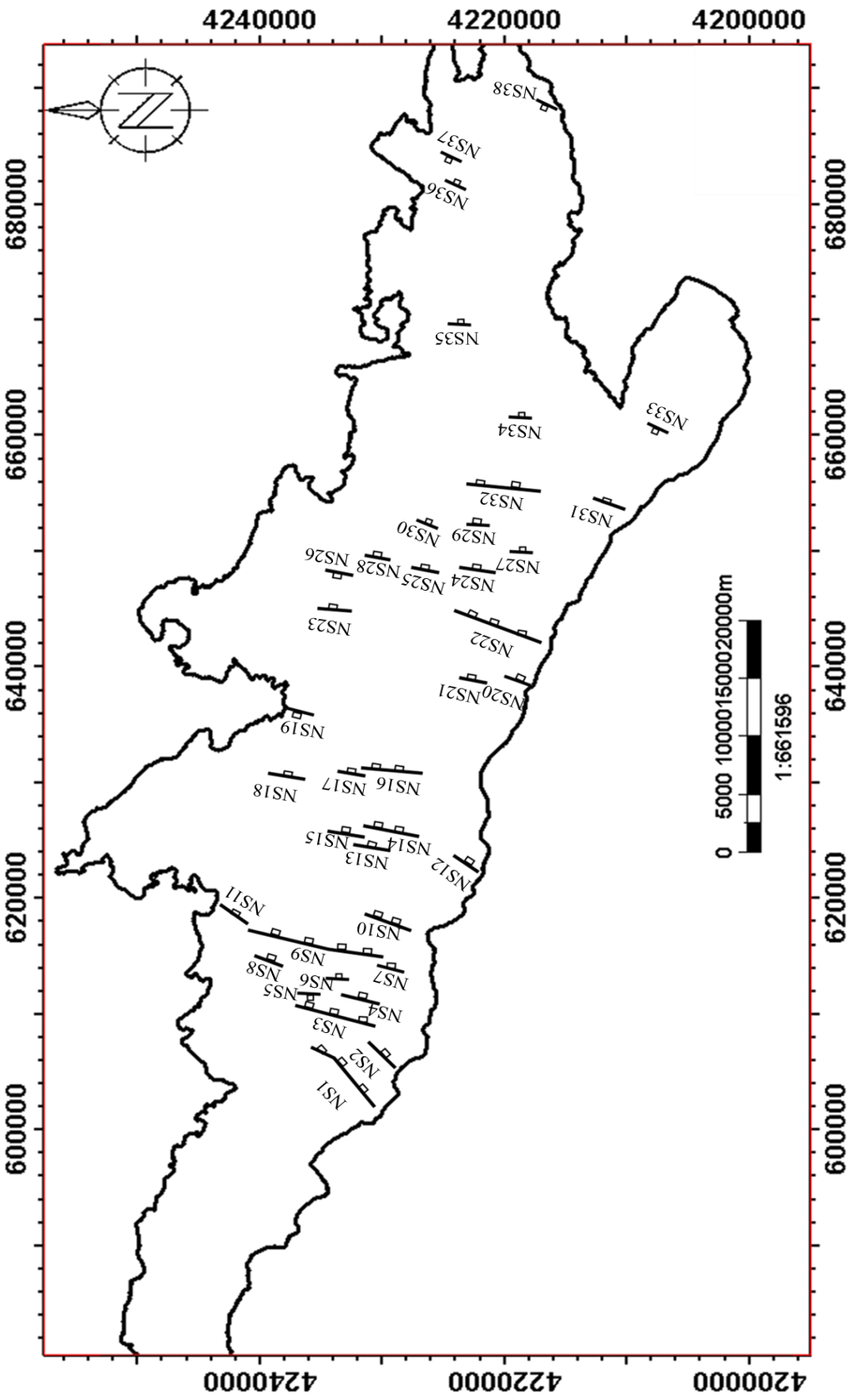

Figure 61 Gulf boundary with named N-S faults.

The basement structure changes from a S-dipping half graben in the eastern West domain to a graben in the Central-West domain, except in L30 where the structure becomes a N-dipping half graben. The same features are observed in the Central-East domain. Finally, the structure becomes a north dipping half-graben in the East domain (Figure 62).

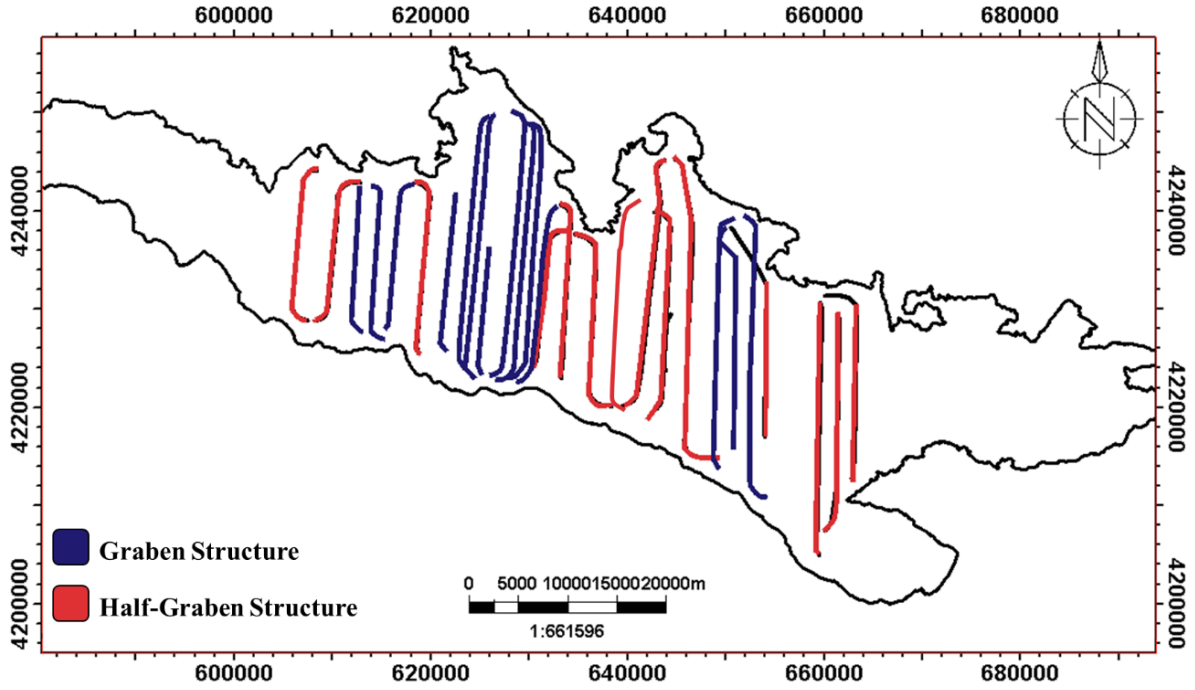

Figure 62 Map of GoC with N-S seismic lines, where their structures are defined by color.

Based on the structural geometry variation of the basement only shown in Figure (62), the structures are subdivided into segments and are named S1 to S8 in this study. A map with interpreted N-S faults and these eight segments is produced in Figure 63. Description of the segments is presented in the next section; all measurements are based on seismic line length as a more detailed study is needed to determine precise measurements.

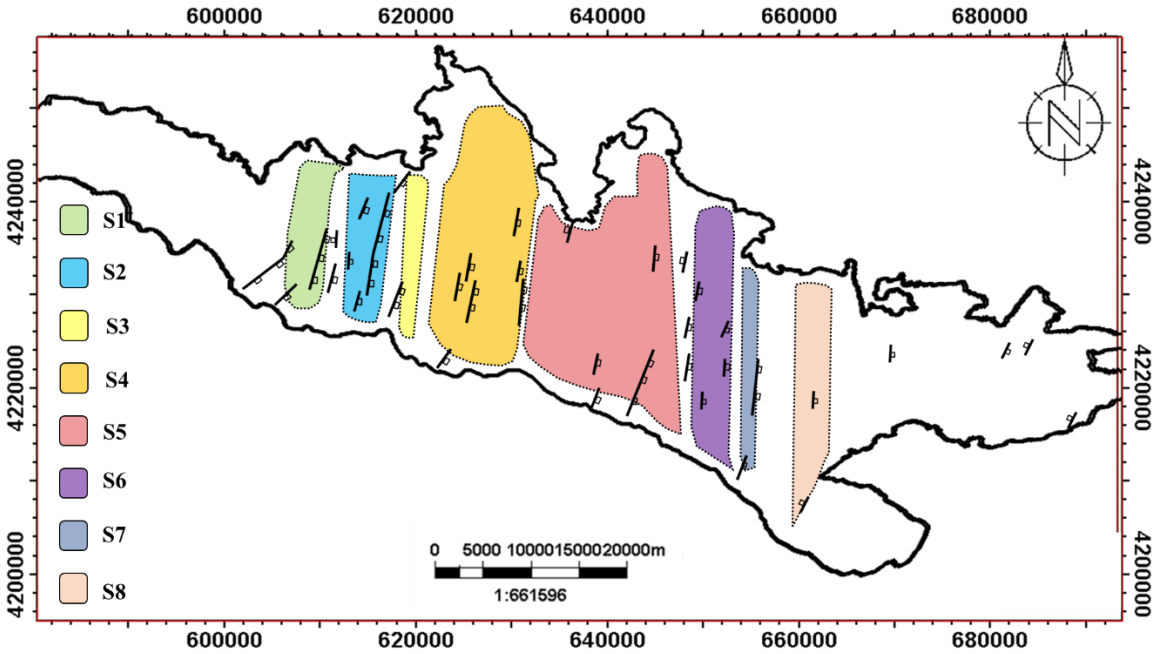

Figure 63 Map of GoC with interpreted segments based on the structural geometry of the basement.

3.5.1 Segment S1

Segment S1 is ~4.9 km wide and ~16 km long, it includes lines 27 (Figure 64) and 26 where both basement and Syn rift sediments have half-graben structures that dip towards the south. Three N-S oriented and east dipping faults are located along this segment: NS1, NS2, and NS3. NS1 is located on the western boundary, NS2 on the southern boundary and NS3 on the eastern boundary. Along the zone between S1 and S2, two N-S faults were traced: NS4 that dips toward the east, and NS5 that dips toward the west.

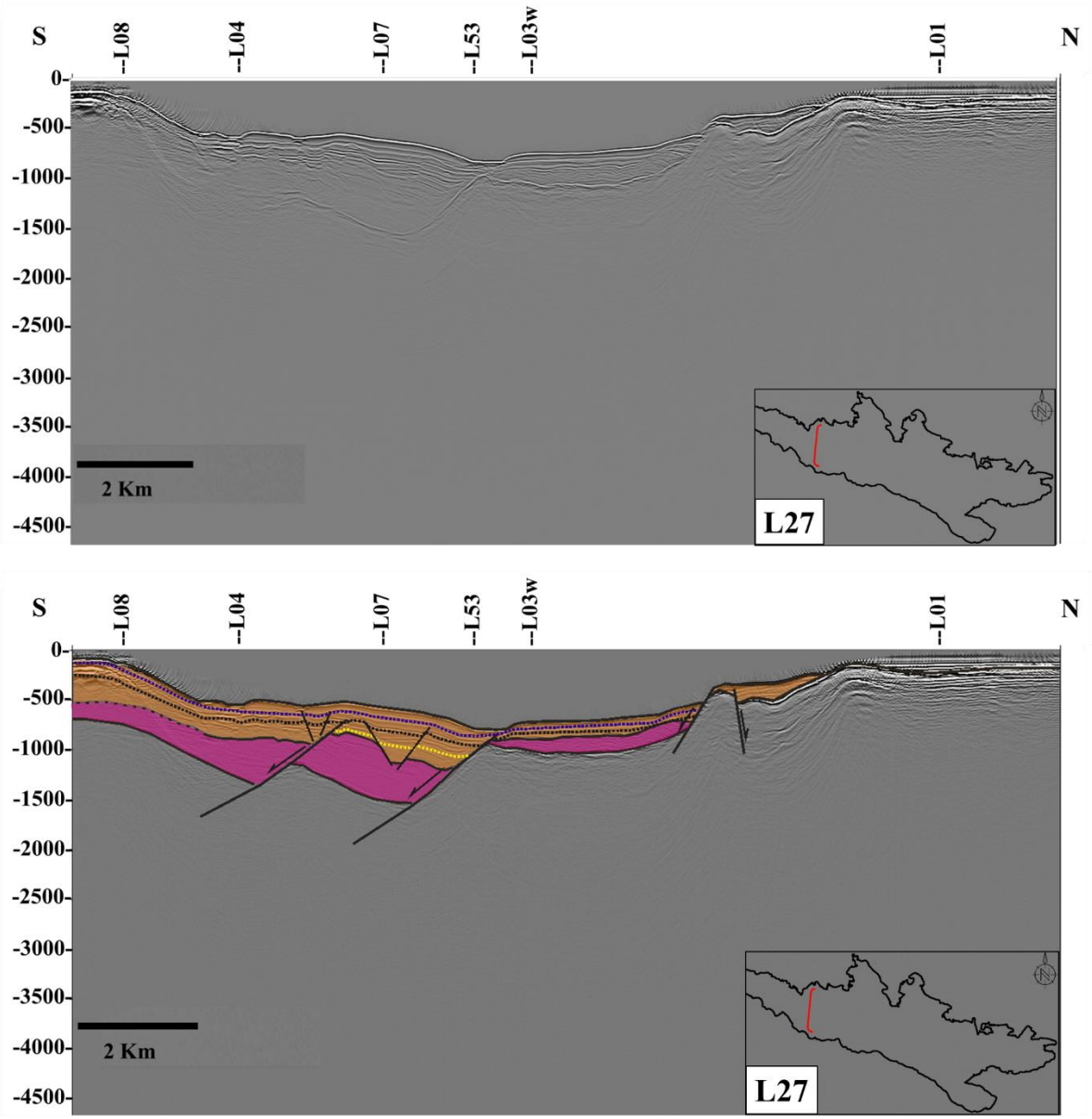

Figure 64 Non-interpreted and interpreted L27 presenting the structure in segment 1.

3.5.2 Segment S2

Segment S2 (Figure 65) is ~4.5 km wide and 15.9 km long; it includes lines 28, 25 and 29 where both basement and Syn rift sediments have a graben structures. Four N-S faults were traced in this segment: NS6 located on the western boundary, NS7, and NS8 located in the center of the segment and NS9 located toward the eastern boundary.

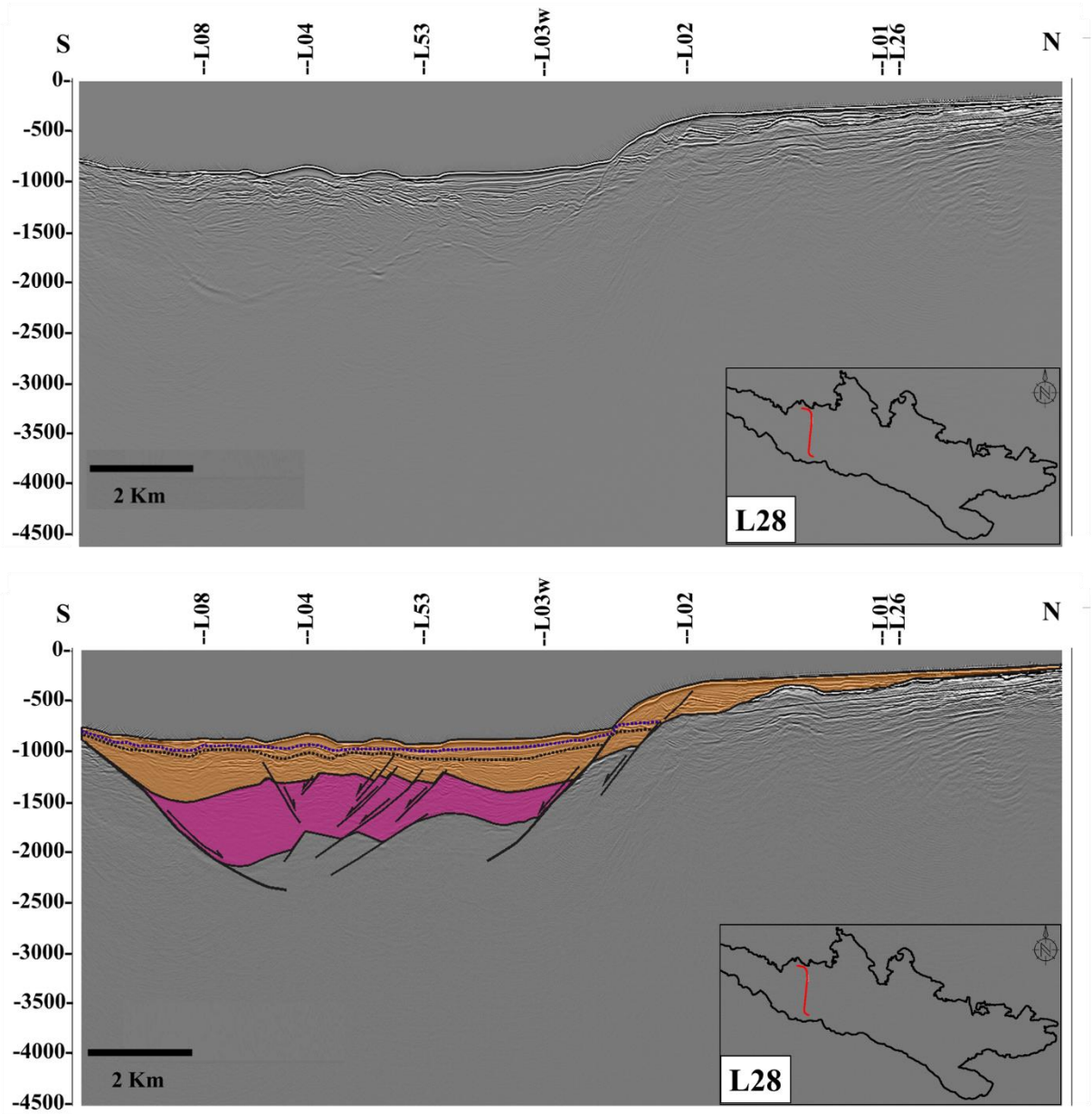

Figure 65 Non-interpreted and interpreted L28 presenting the structure in segment 2.

3.5.3 Segment S3

Segment S3 (Figure 66) is ~1.8 km wide and 17.7 km long; it includes line 30 where the basement structure is interpreted as a N-dipping half graben. Two N-S oriented and west dipping faults, NS10 and NS11, are located roughly on the western boundary.

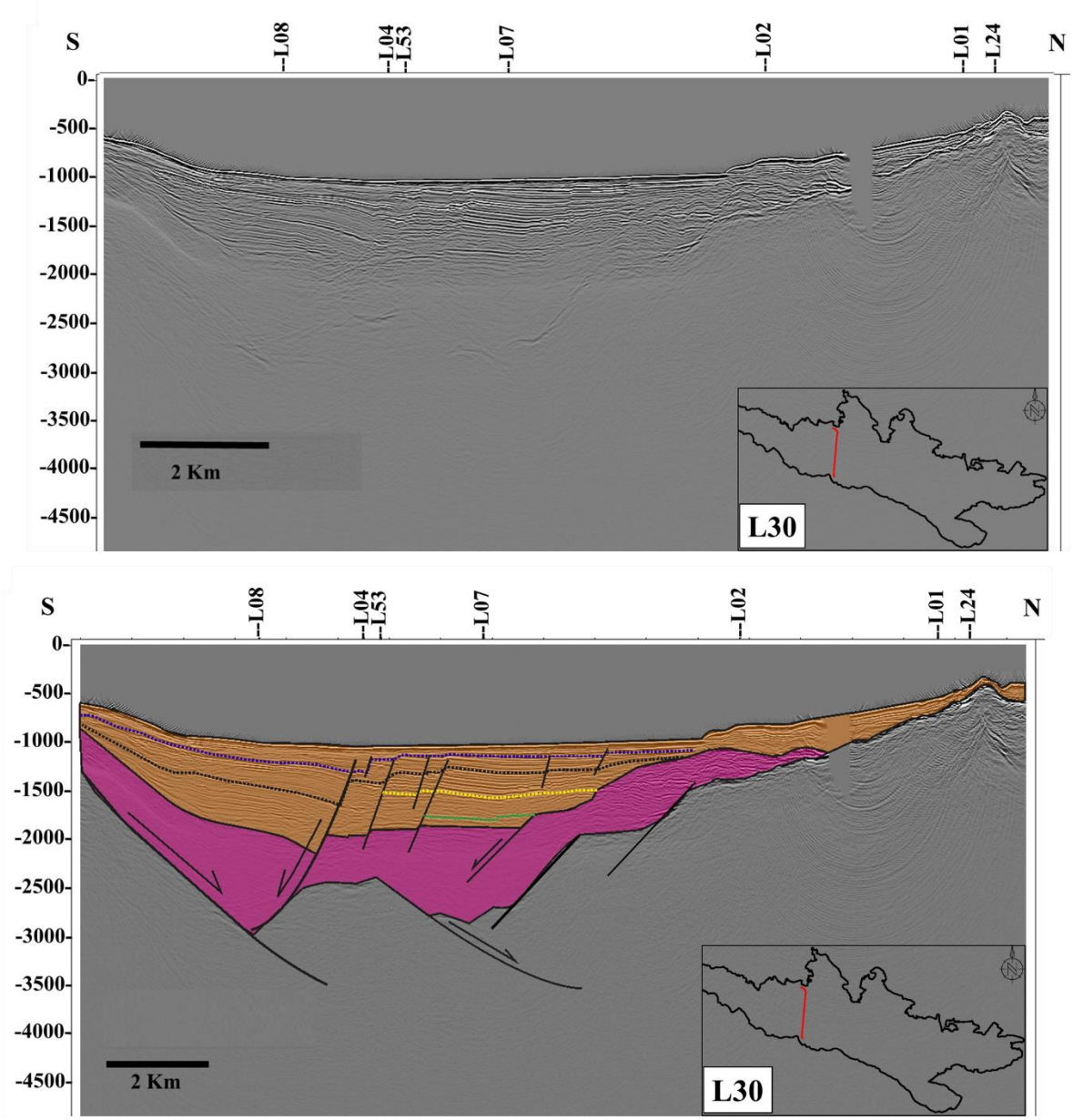

Figure 66 Non-interpreted and interpreted L30 presenting the structure in segment 3.

3.5.4 Segment S4

Segment S4 (Figure 67) is ~10 km wide and ~29.5 km long; it includes lines 50, 16, 14, 12, 11, 13, 15 and 49. The basement and Syn-rift sediments have a graben structure. In several lines for the syn-rift package, a roll-over anticline toward the south of the segment was observed (Figure 67). Seven N-S oriented and east dipping faults were traced along the segment: NS12 located in the southern boundary of the segment; NS13, NS14, and NS15 located in the western part of the segment; and NS16, NS17, and NS18 located toward the eastern boundary of the segment.

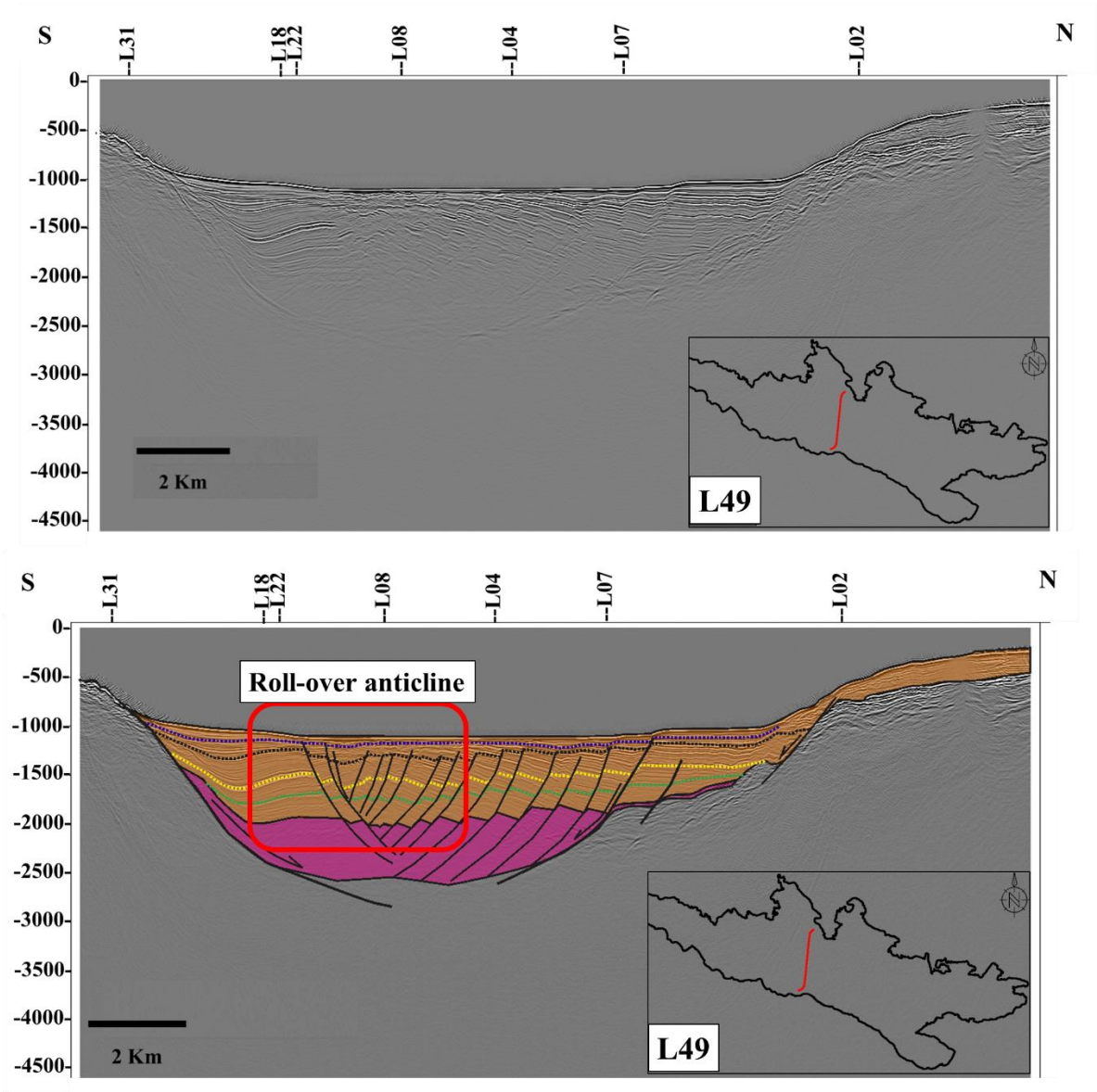

Figure 67 Non-interpreted and interpreted L49 presenting the structure in segment 4 with the roll-over anticline marked in the red box.

3.5.5 Segment S5

Segment S5 (Figure 68) is ~16 km wide with a length of ~16.8 km in the west and ~23.5 in the east, on average. It consists of seven seismic lines: 32, 48, 33, 20, 34, 21 and 35. The basement structure is a N-dipping half-graben, and the whole Syn-rift has a growth-strata geometry with the thickest package toward the south. Five N-S oriented faults were traced in this segment:

- NS19: dipping toward the west and located in the northern west section.
- NS20: dipping toward the east and located at the southern boundary of the segment.
- NS21: dipping toward the west and located in the middle of the southern section of the segment.

- NS22: dipping toward the east and located in the eastern part of the southern boundary.
- NS23: dipping toward the east and located at the eastern boundary, toward the north.

In the zone between S5 and S6 a N-S oriented fault NS26 is traced that dips toward the west.

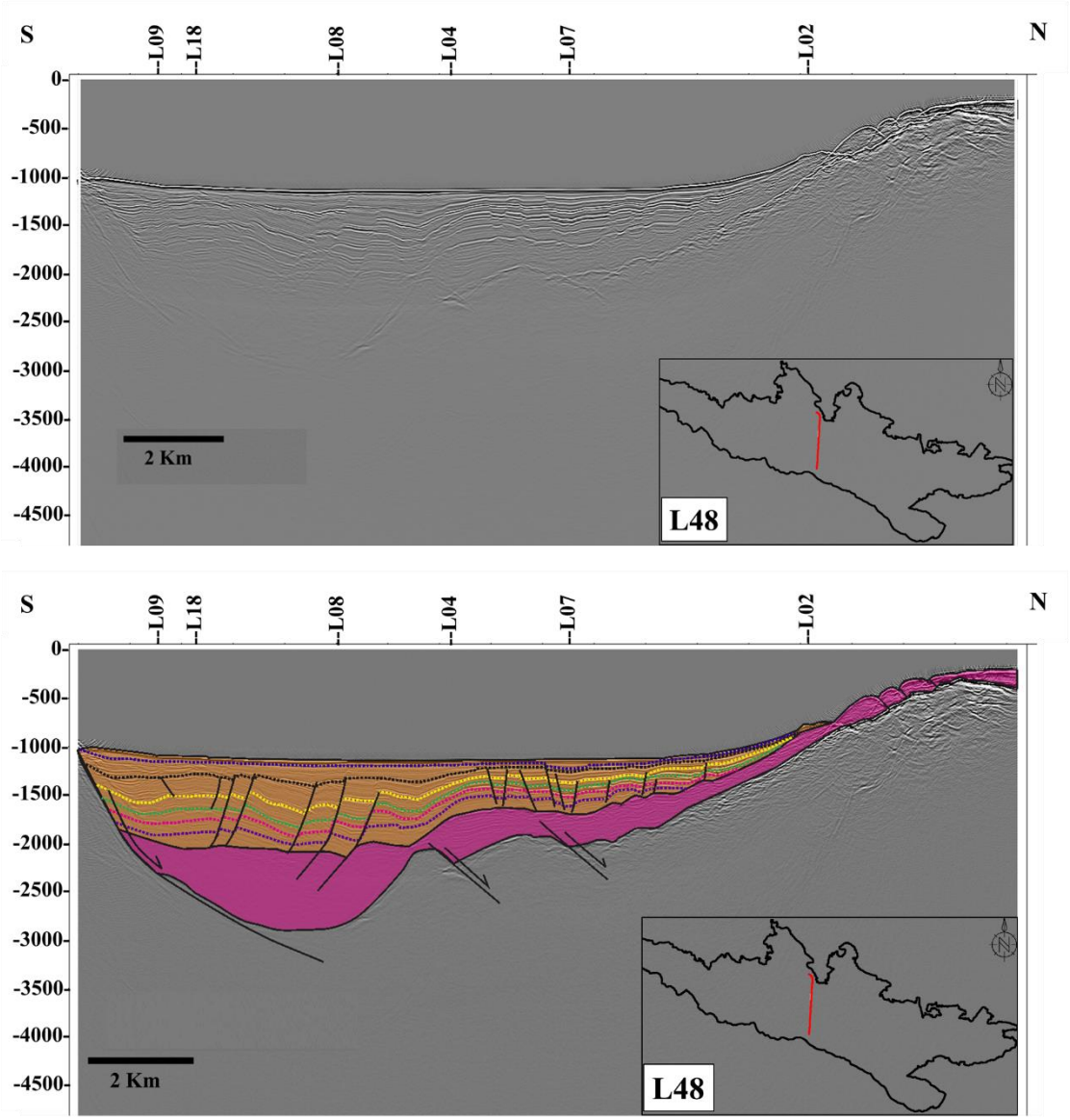

Figure 68 Non-interpreted and interpreted L48 presenting the structure in segment 5.

3.5.6 Segment S6

Segment S6 (Figure 69) is ~4.5 wide and ~26.8 long; it includes three lines: 41, 36, and 37. The basement structure is a graben including tilted blocks toward the north, and a horst structure was observed in line 37 (Figure 70). Seven N-S faults were traced along this segment and all of these dip toward the east: NS24, NS25, and NS28 are located on the western boundary, NS27 is located toward the western boundary in the south, and NS29 and NS30 are located in the middle of the eastern boundary.

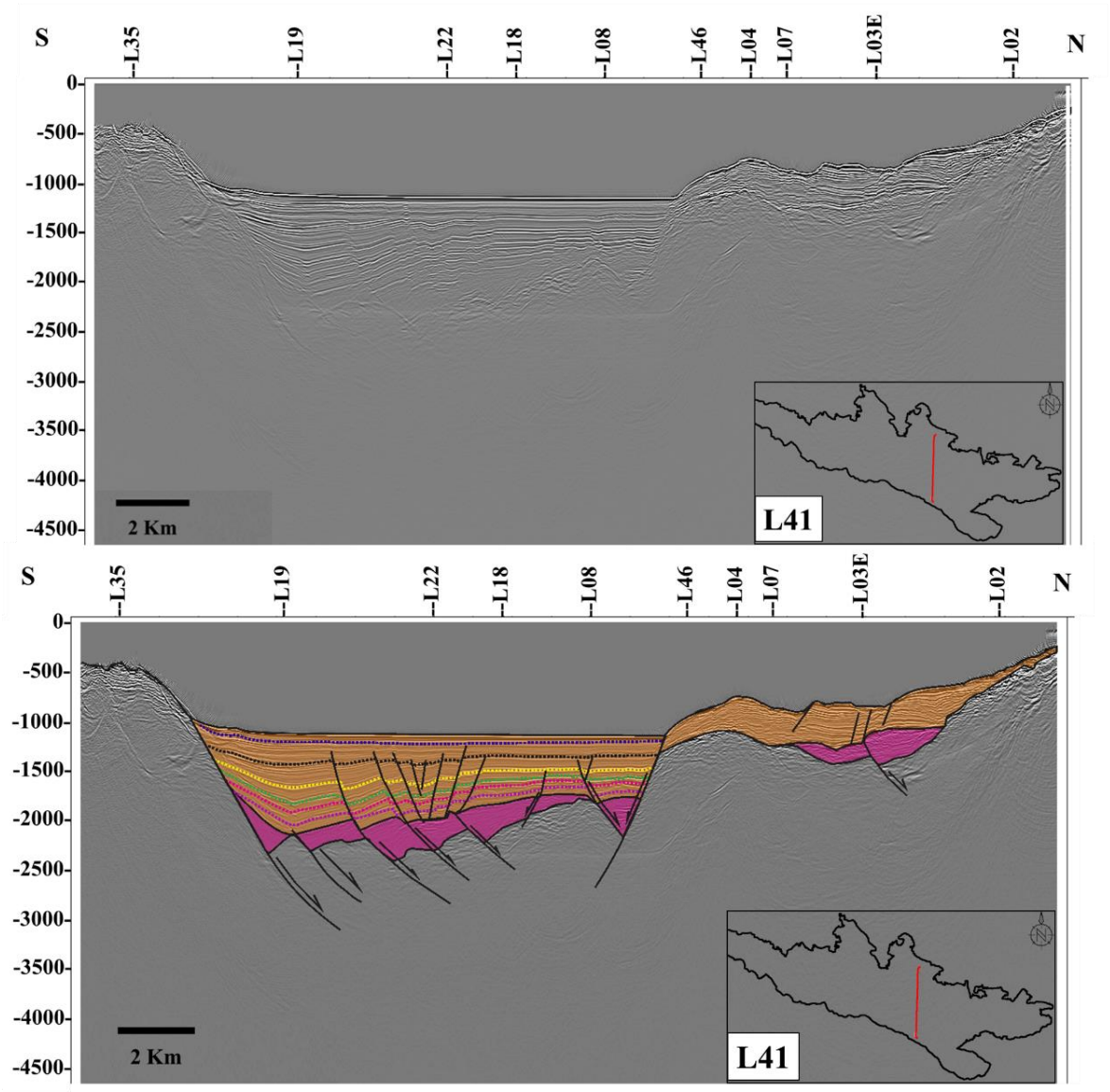

Figure 69 Non-interpreted and interpreted L41 presenting the structure in segment 6.

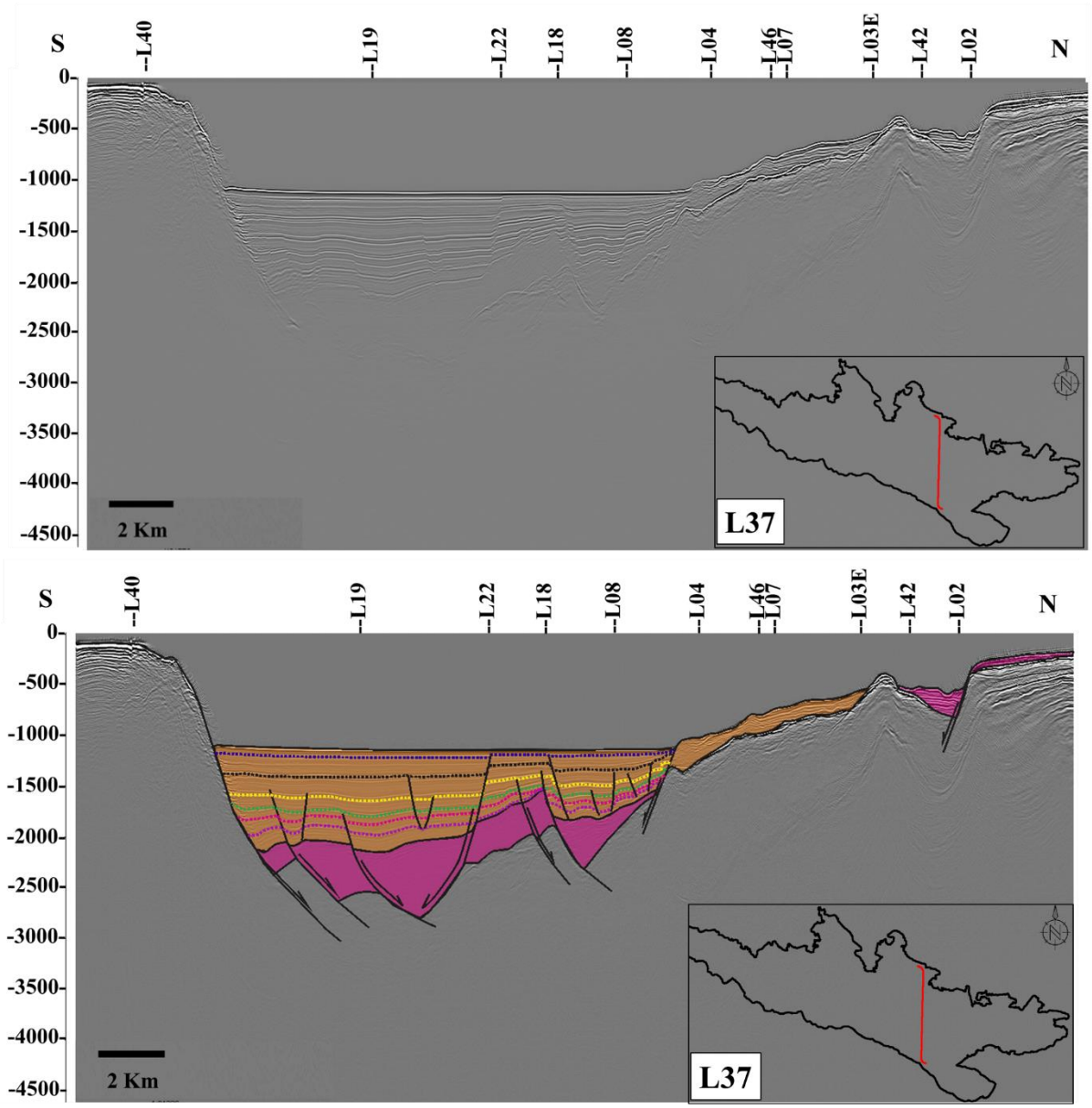

Figure 70 Non-interpreted and interpreted L37 introducing the structure in segment 6 with a horst structure.

3.5.7 Segment S7

Segment S7 is ~1.8 wide and ~22 km long and consists of one seismic line 42 (Figure 71). The seismic line length is shorter than other N-S seismic lines. Therefore, it is speculative to describe whether or not it forms a graben structure. However, from the available data, it seems to be two half grabens separated by a horst structure, where the Syn-rift sediment growth is toward the horst structure. Two N-S faults dipping toward the east were traced: NS32 on the eastern boundary and NS31 on the southern boundary.

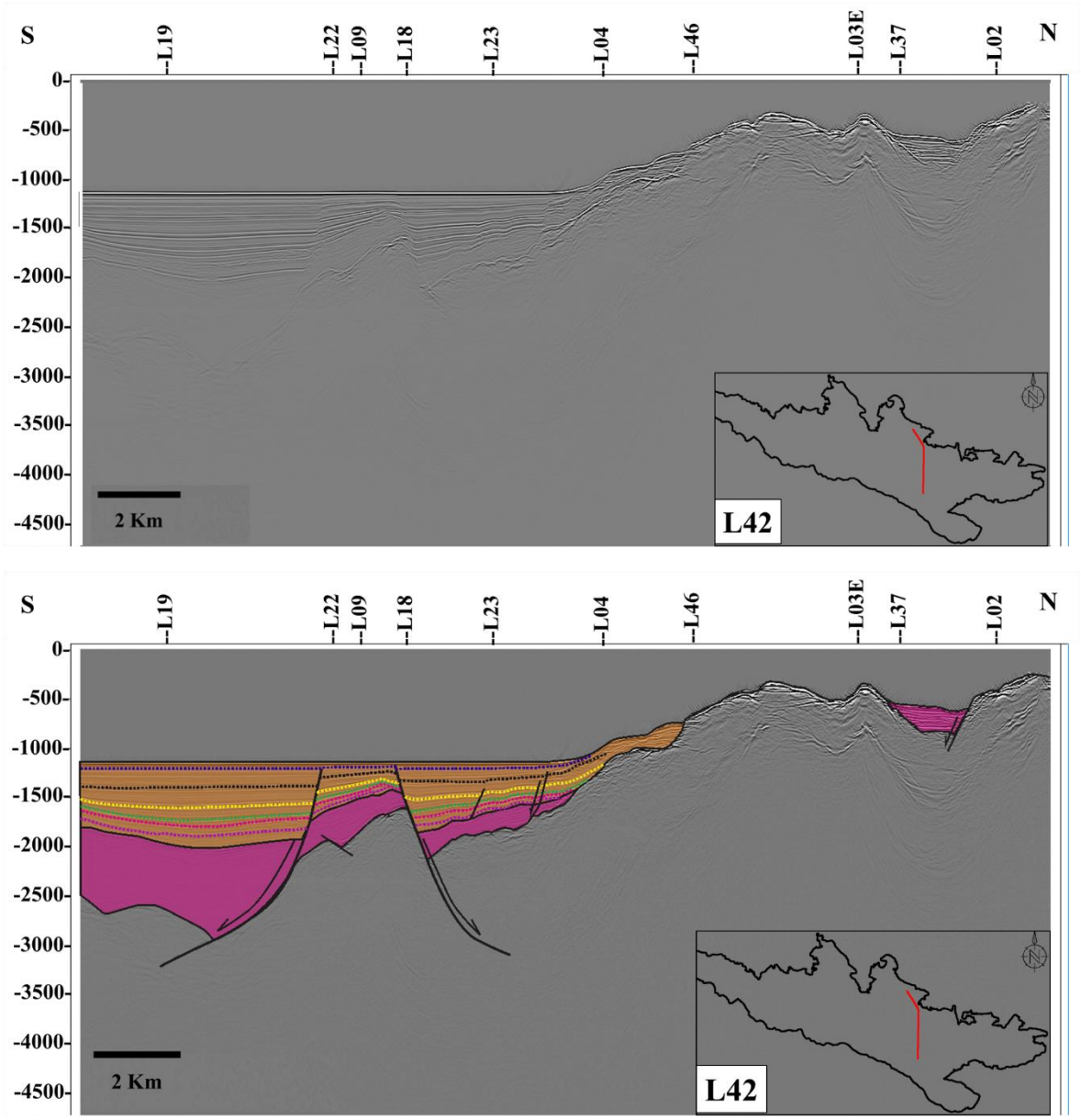

Figure 71 Non-interpreted and interpreted L42 presenting the structure in segment 7.

3.5.8 Segment S8

Segment 8 (Figure 72) is ~3.6 wide and ~25.9 km long and consists of three seismic lines: 39, 06 and 45. The basement structure is a S-dipping half graben, and the Syn-rift sediment growth is toward the south. Two N-S faults were traced: NS34 located in the middle of the segment dipping toward the east, and NS33 located at the southern boundary of the segment.

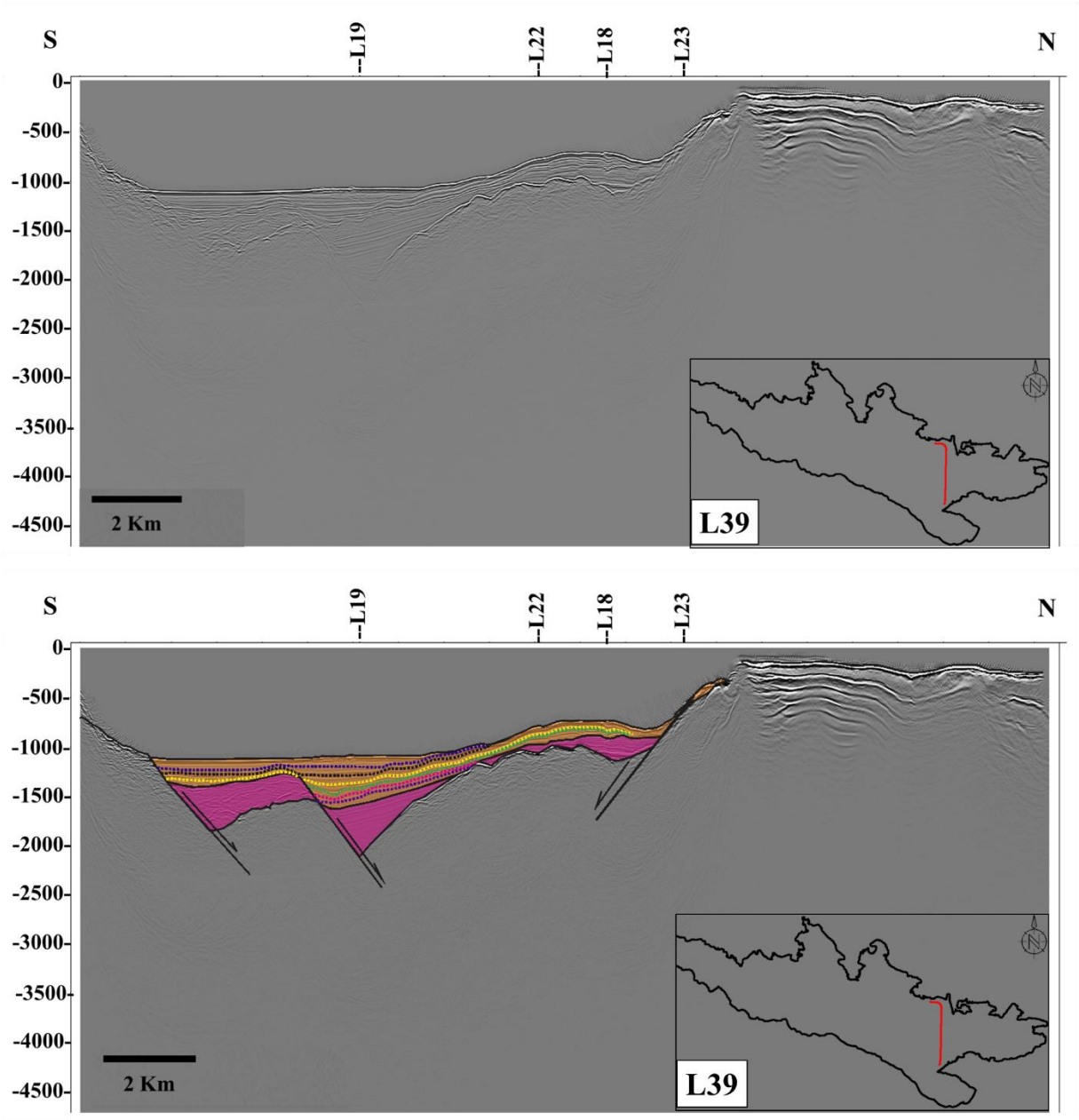

Figure 72 Non-interpreted and interpreted L39 presenting the structure in segment 8

A comparison of the basement segments with W-E lines 07, 08, 09, 22, and 53 was done. However, the purpose is to investigate the connection between N-S lateral change of basement structure against the W-E structures (Figures 73, 74, and 75). The observation is presented in the following section.

L53, L09, and L22: S1, S2, S4, S6, and S7 seem to cover footwalls and their growth strata of syn-rift in some places. S3 is located on a small anticline, while S5 appears to cover a part of a compressional feature. Furthermore, S8 seems to cover the most western part of a structural high (Figure 73).

L07: S1, S2, S3, S4, and S7 highlight faults components, while S5 covers a small structural high beside a hanging wall. S6 interval seems to highlight a small basin in the eastern section of the line (Figure 74).

L08&23: appears to have the same relation to the segments and the structures as in L07 (Figure 75).

Figure (76), shows a combined map of W-E faults together with basement segments to give a clear overview of the subdivision of basement into segments:

- Along S1 W-E faults seem to have the same length as the segment S1 width and bounded by N-S basement faults.
- S2: includes several W-E faults where they are mostly within the boundary of the segment, several W-E faults seem to be ended toward N-S faults.
- S3: W-E faults cover the segment and the zone between segment S3 and S4, in the southern part of S3 a W-E fault seem to be stopped toward an N-S fault.
- S4: includes several W-E faults mostly in the northern margin of the segment where most of the seem to be within the boundary of the segment.
- S5: the whole segment structure appears to be controlled by north dipping faults in the southern margin. In contrast, in the middle of a western section of the segment S5, the structures appear to be controlled by two more north dipping faults.
- S6: the structure is controlled by both south and north dipping faults and bounded by N-S faults.
- S7: north dipping faults control the structure in the southern margin of the segment.
- S8: the structures are controlled by north dipping faults and a horst structure in the middle of the segment.

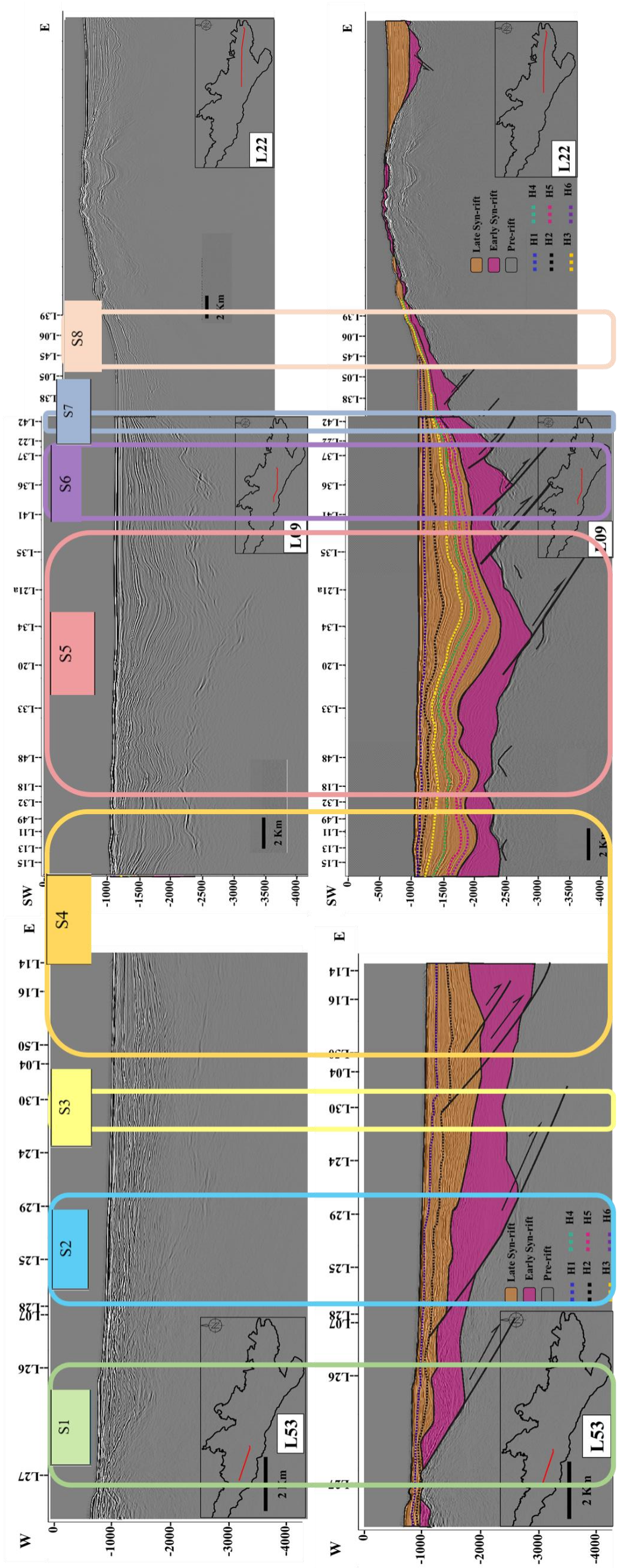

Figure 73 A comparison between W-E seismic lines (53,09, and 22) with observed basement segments.

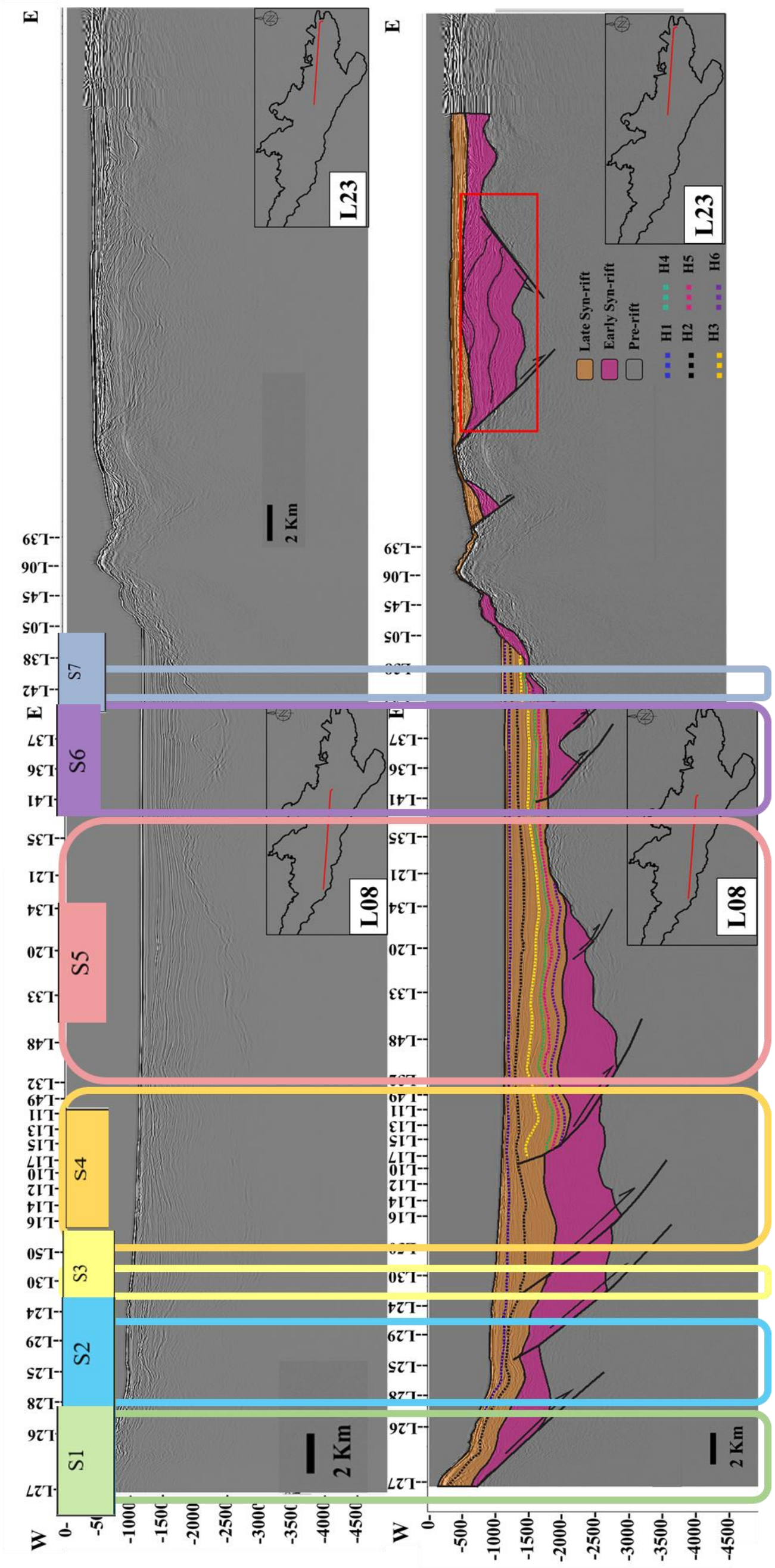

Figure 74 A comparison between W-E seismic lines L08 and L23 with observed basement segments.

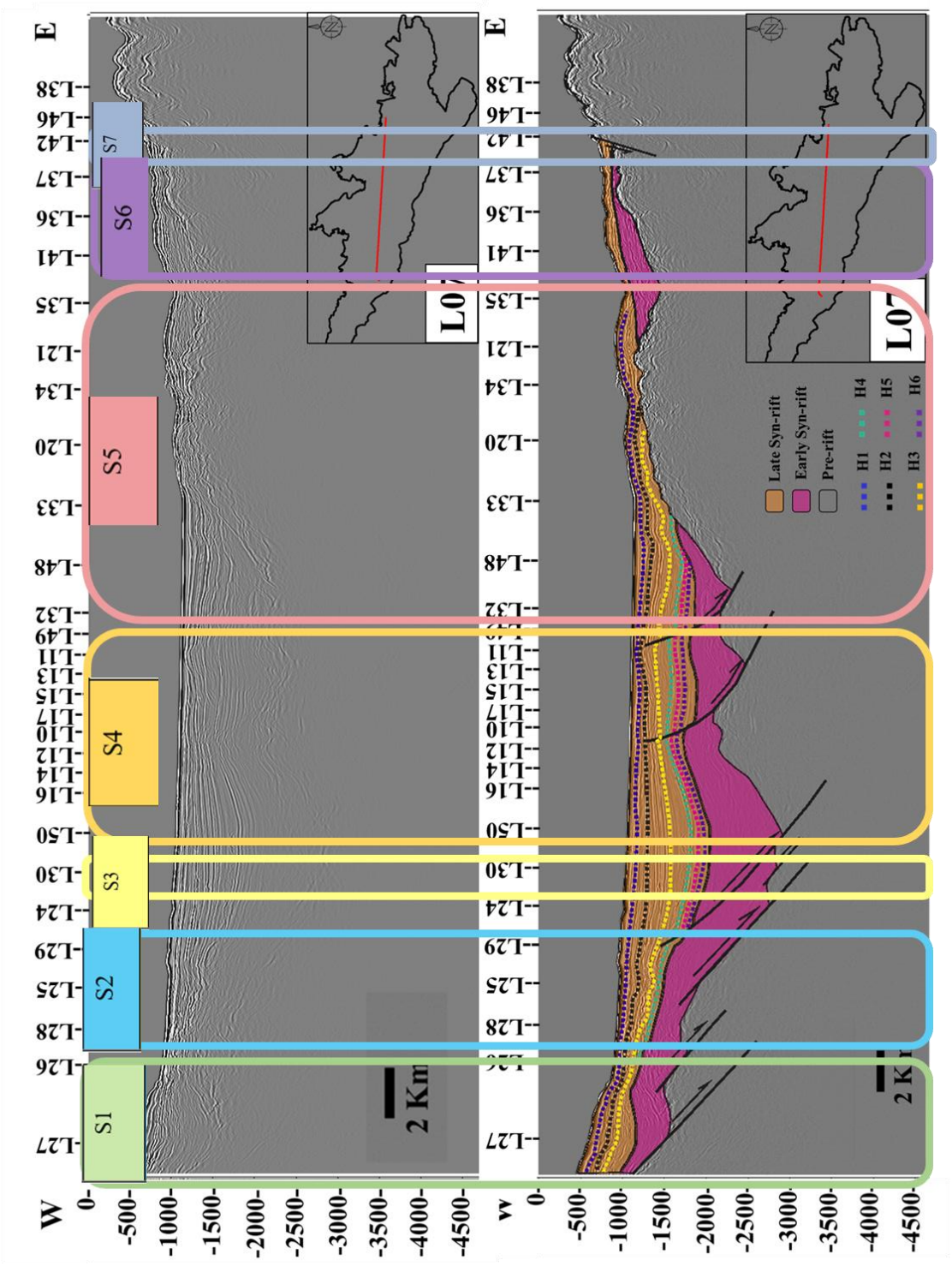

Figure 75 A comparison between W-E seismic line L07with observed basement segments.

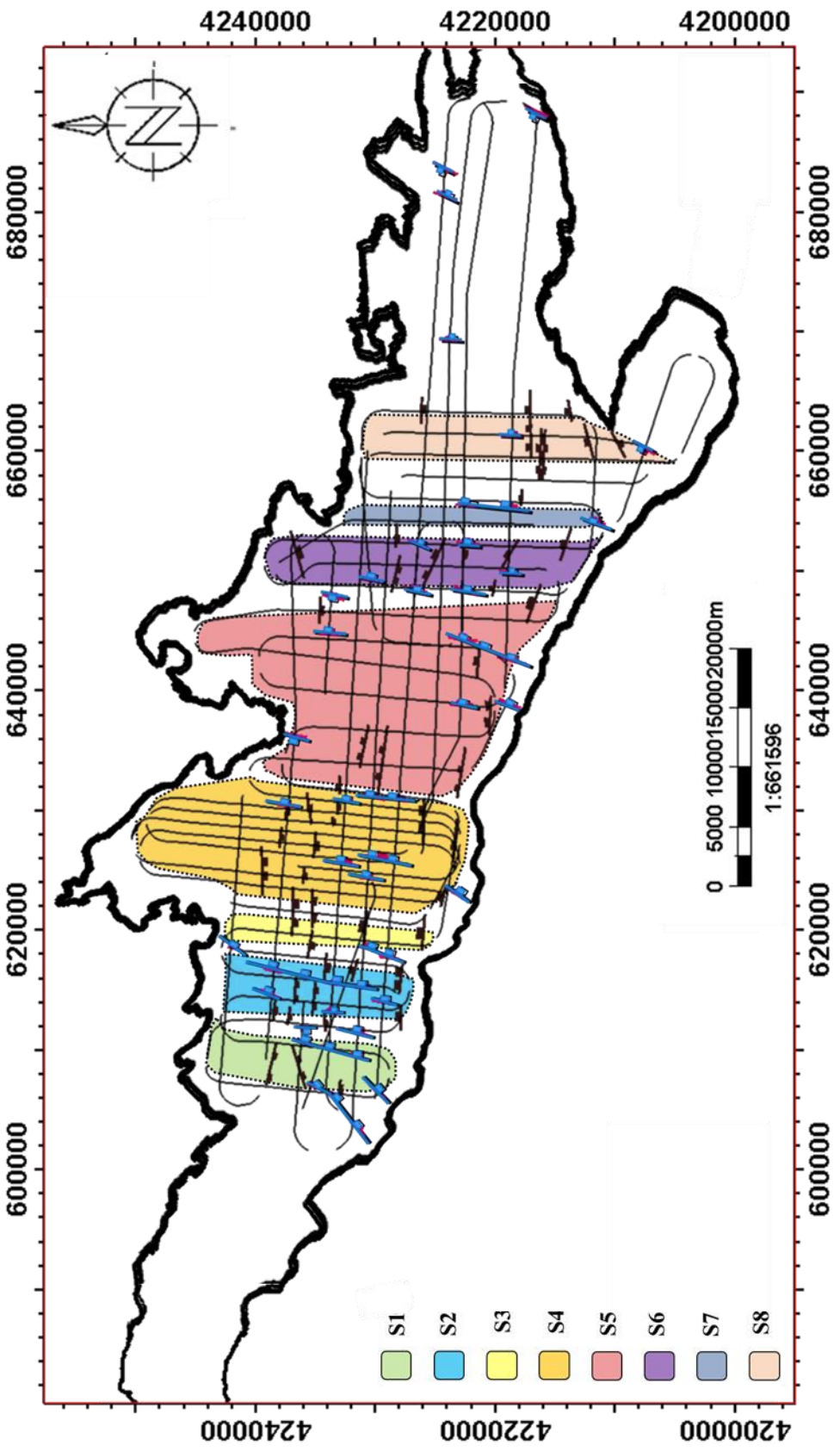

Figure 76 Structural map of GoC with interpreted faults that interact the basement and syn-rift package combined with segments and seismic lines used in this study.

3.6 Bathymetry data

In this study, the sea bottom horizon was combined with the bathymetry map of the western section of the GoC (McNeill *et al*., 2005) to produce an elevation time map covering the study area (Figure 77). The sea bottom is shallowest at the northern and southern margins as well as the West domain of the Gulf. The bathymetry map of the western Gulf shows SSW-NNE trending lineament structures (Figure 78), while in the Central and Eastern domains show no evidence of segmentation.

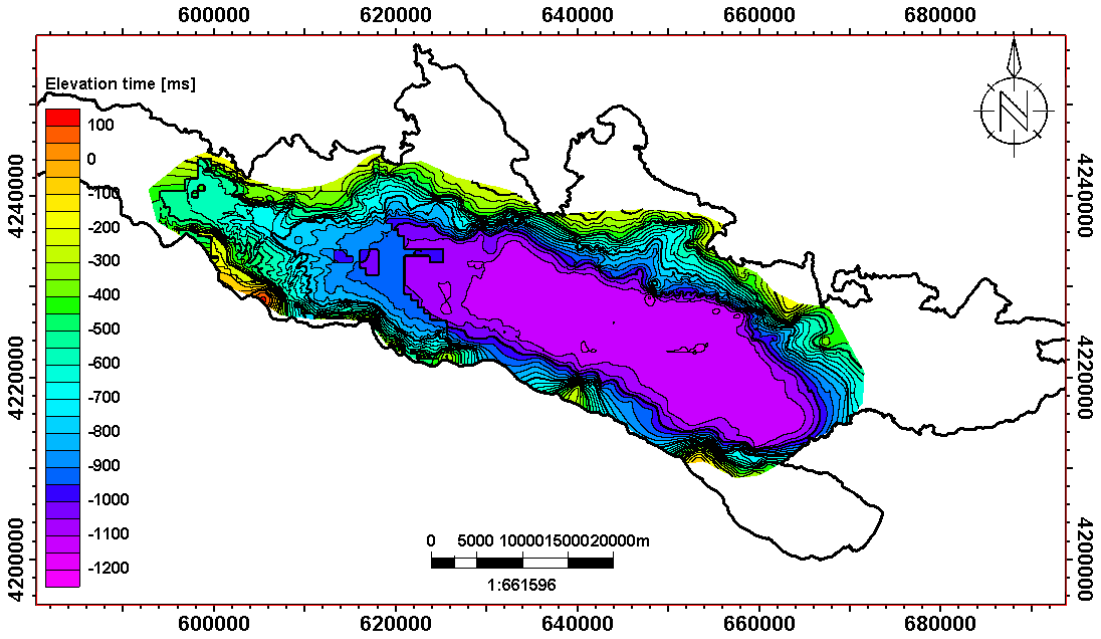

Figure 77 Combined bathymetry from the western section (McNeil et al., 2005) and sea bottom horizon interpretation.

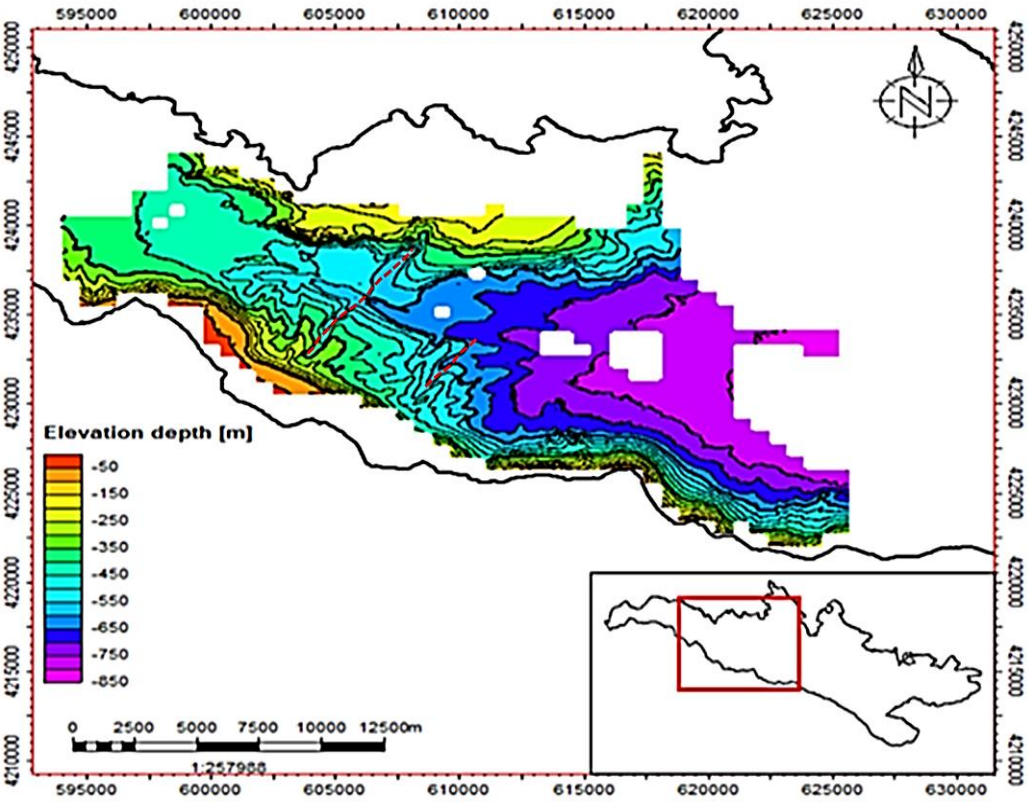

Figure 78 Bathymetry map of the western section (McNeil et al., 2005) showing SSW-NNE lineament features.

3.7 Earthquake data analysis

In this sub-chapter, a general study of earthquakes in the GoC is presented to understand their relationship with observed lateral variation along strike and to find out whether any lineament exists.

Earthquake data with a minimum magnitude of 2 in the period from July 1800 to July 2017 was used (Figure 79). Variation in earthquake activity and distribution patterns were observed along the Gulf and, subsequently, five zones were defined (Figure 80).

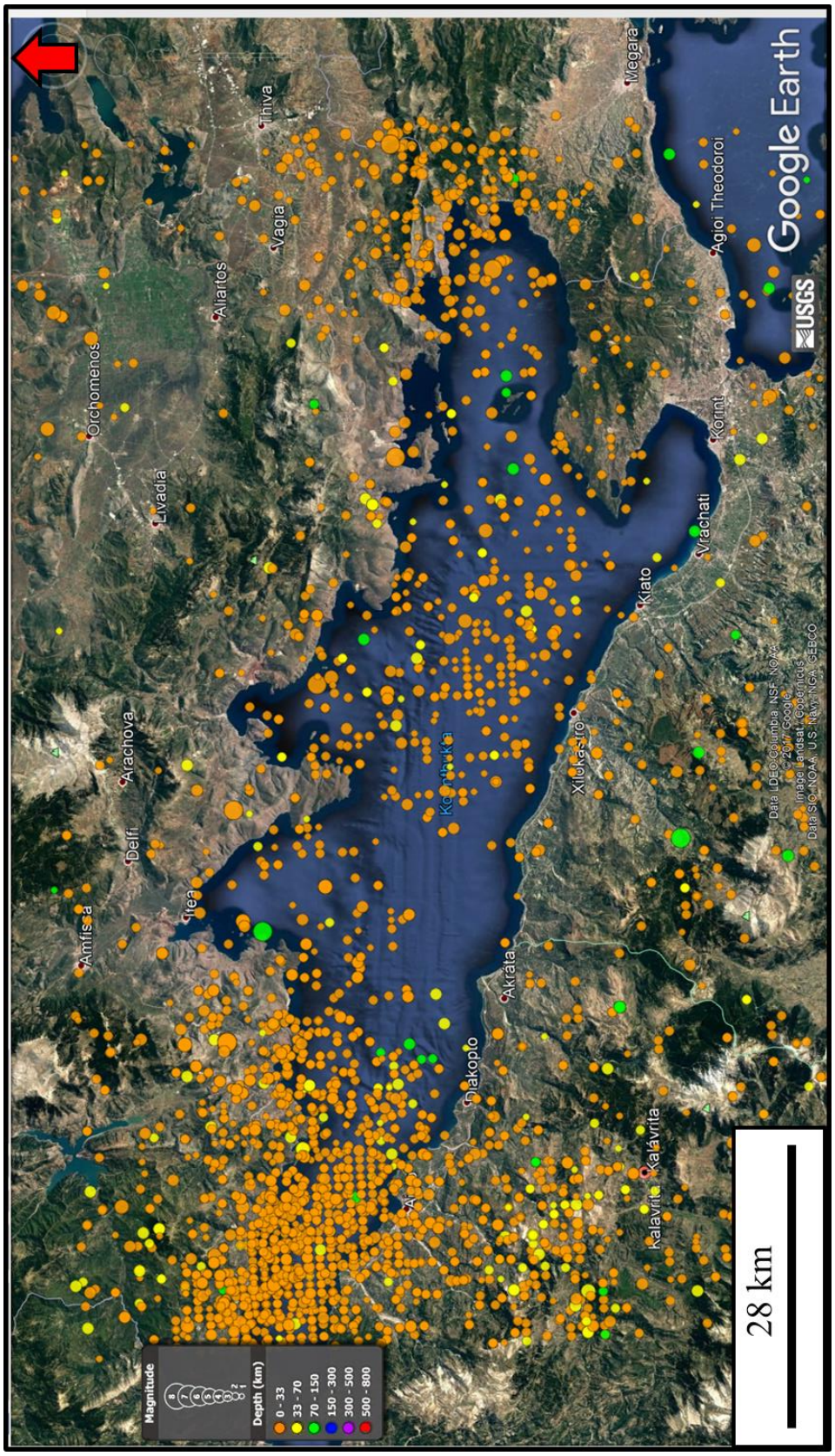

Figure 79 Map of the GoC with Earthquake data with magnitude >2.0 from 1800-2017 (Data from USGS).

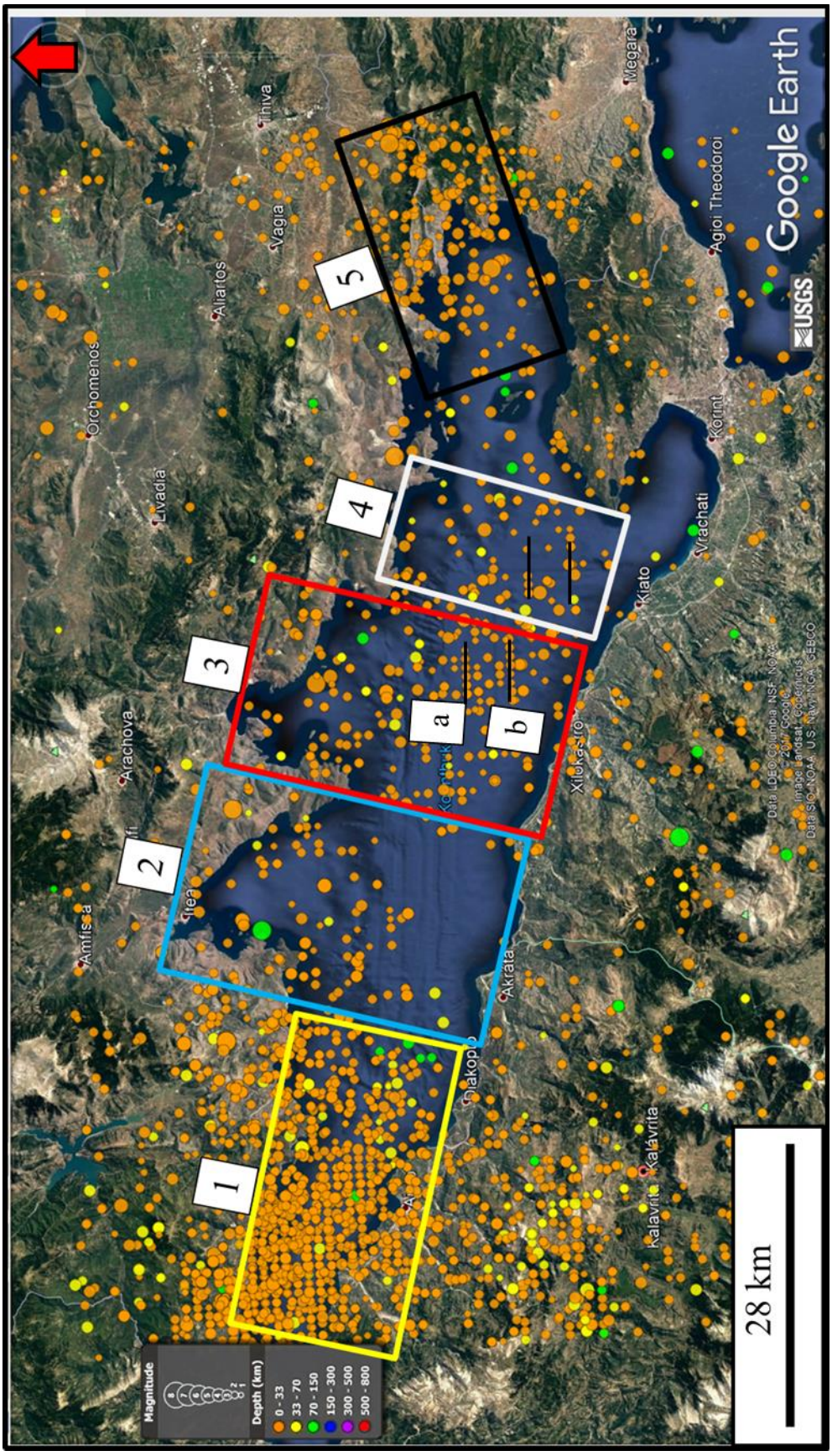

Figure 80 Map of the GoC with earthquake data with the magnitude of >2 from 1800-2017. Earthquake data are categorized into five zones based on their activity: zone1 is most active, zone 2 is less active, and zones 3, 4 and 5 are intermediate. W-E alignments a, b and c are marked in zone 3 and 4. (Data from USGS).

Zone 1: Covers the western section of the GoC, represent the most active zone along the Gulf as it contains the most of the earthquake data. The data in this zone is chaotic and difficult to find any orientation of the earthquakes, most of the data is located at a depth of 0-33 km. The amount of earthquake data at a depth of 33-70 km is less while very few at a depth of 70-150 km. The boundary between zone 1 and zone 2 characterized by a lineament trend where a transition from an active zone into almost inactive zone occurs.

Zone 2: the majority of earthquakes are located at a depth of 0-33 km, and most of them are located on the northern margin of the zone. Earthquakes at a depth of 33-70 km seem to be oriented NNE-SSE.

Zone 3: The boundary between zone 2 and zone 3 is lineament, the earthquake activity in zone 3 is greater than zone 2. Most of the earthquake data is located at a depth of 0-33 km with some of at a depth of 33-70 which are orienting NNE-SSW.

Zone 4: is less active than zone 3, the majority of the data is at a depth of 0-33 km. In the zone 3 and 4, 3 W-E alignments were observed: alignments a and b are located in zone 2, while alignment c is located in zone 4.

Chapter 4 Discussion

In this chapter, the result and the observation will be discussed as well compering the results with previous studies that were presented in the previous studies,

4.1 Rift Segmentation and lateral variation Hypothesis

Several authors have realized the lateral miscorrelation along the Corinth Rift and divided the rift based on that but have not focused on its boundaries or the reason of its appearance. In this sub-chapter the result of this study will be combined with the previous work for an analysis of the lateral variation along the GoC.

The sub-sequences of a Late rift were difficult to trace along strike, although horizons were clear and easy to trace only in the Central-East and East domains as well as the Alkyonides Gulf. The basement structural geometry constantly changed from graben to half-graben along the Gulf, resulting in different N-S blocks with different structures. Based on the variation in basement structures along strike, eight segments were identified. The present orientation of these segments is based on the orientation of the seismic lines including turns, which might not represent the original orientation of the segments.

By comparing the interpreted segments in this study and proposed zones of Ford et al. (2016), the border between C4 and C3 seems to correlate with the NS9 fault between S2 and S3 (Figure 81). Although the border between C1 and C2 seems to correlate with the border between S7 and S8, as mentioned before, the orientation of the proposed segments is based on the seismic line direction. The basis for zones proposed by Ford et al. (2016) was not given, which makes it difficult to draw comparisons here.

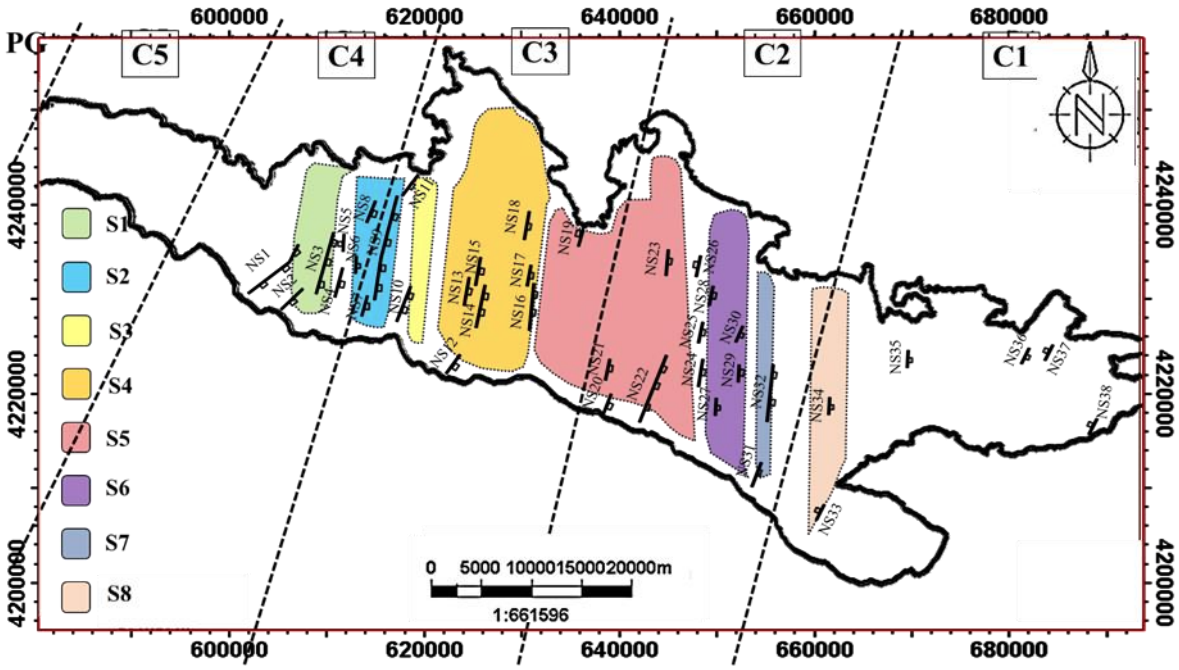

Figure 81 Map of the GoC with proposed segments and N-S faults; the zones C1 to C5, and PG are proposed by Ford et al. (2016).

Furthermore, it seems that zones proposed by Nixon *et al*., (2016) correlate with the proposed segments in three places (Figure 82):

1. The border between the West and Central-West domains correlates with the border between S1 and S2 and the interpreted NS3 fault.
2. The border between the Central-West and Central-East domains correlates with the border between S4 and S5 and the interpreted NS16 fault.
3. The border between the Central-East and East domains correlates with the border between S6 and S7.

As the proposed segments are based on the basement structure, I do agree with The last border between East domain and Alkyonides Gulf as the interpreted basement is at a shallow level in Alkyonides Gulf forming a structural high. In contrast, the basement is deeper in the East domain with Syn-rift packages forming two different structure characters from the basement. The difference in the number of zones could be because the main focus of this study was the N-S features concentrating on W-E lines, while Nixon *et al*. (2016) focused on the N-S seismic lines. The absence of interpreted W-E lines in Nixon *et al.* (2016) makes it challenging to discuss the difference; although the lateral variation along the strike was mentioned in, the boundaries were not emphasized by Nixon *et al.* (2016).

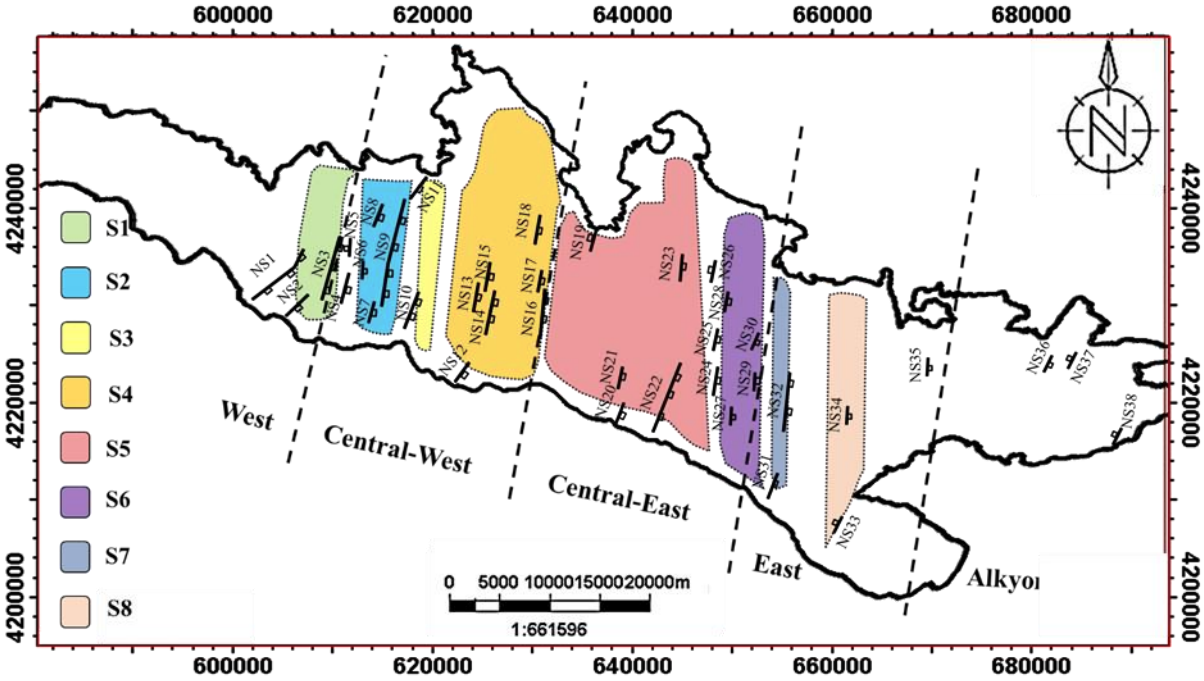

Figure 82 Map of the GoC with proposed segments and faults interpreted in this study and proposed domains by Nixon et al. (2016).

The proposed segments by Console *et al*. (2013), based on seismic activity data of the last 300 years and changes in Coulomb stress along the Gulf, correlate to observations in this study in several places (Figure 83):

1. The boundary of segment 3 correlates with the boundary of S3; segment 4 represents mostly the transition between S3 and S4 where the basement structure turns from graben (S1 and S3) into half-graben (S3) and then graben (S4) again.
2. The eastern boundary of segment 5 and western boundary of S6 correlates with the boundary between S5 and S6. The S6 segment could be wider, but due to the distance between the seismic lines (~2-3 km), it will be speculative to extrapolate segment S6.
3. The boundary between segments 6 and 7 matches the boundary between S8 and, as previously mentioned, the shallow basement in Alkyonides Gulf.
4. The eastern boundary of the proposed segment 3 seems to correlate with the segment 1 of the interpreted earthquakes (Figure 83). Moreover, the interpreted segment 2 of the earthquake data does not appear to correlate with proposed segments 4 and 5 by Console et al. (2013), but it does correlate with segment 4 proposed in this study.

It is difficult to correlate Segments 1, 2 and 8 due to the absence of the data in the mentioned area.

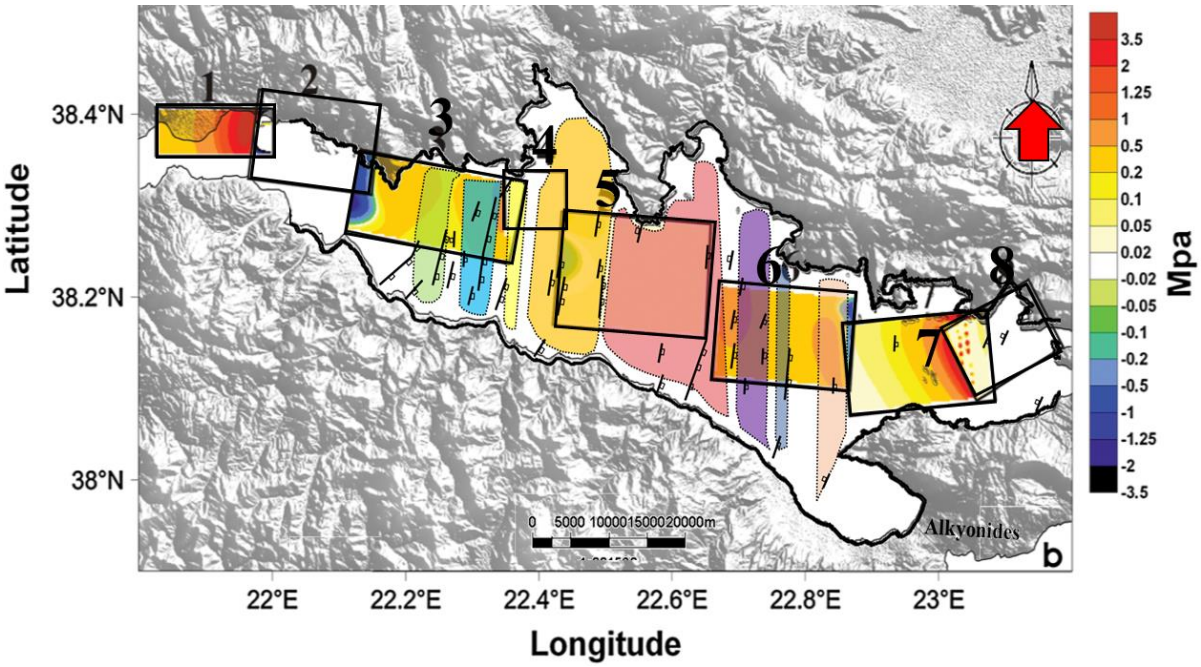

Figure 83 Map of the GoC with proposed segments based on Coulomb stress variation (Console et al., 2013) and interpreted segments and faults in this study.

The structural high proposed by Ghisetti & Vezzani (2004), based on the difference between the Aigion and Derveni-Corinth basins constructed after the discovery of a conductive layer by Pham (2000), seems correlatable with the NS9 Fault along S2 (Figure 84). Earthquake analysis, interpreted time structure and thickness maps all show evidence for faults NS9 and NS11 and the proposed structural high.

Time structure maps of the basement, Early and Late Syn-rift, H1, H2 and bathymetry (Figure 57) show that the elevation time along the proposed structural high by Ghisetti & Vezzani (2004), and proposed NS9 and NS11 faults in this study, changes depth abruptly from shallow in the west to deep toward the east .

Time thickness maps of Early, Late Syn-rift and whole Syn-rift packages (Figure 58) show the variation in the thickness on both sides of the proposed structural high, where the thickset package is located toward the east.

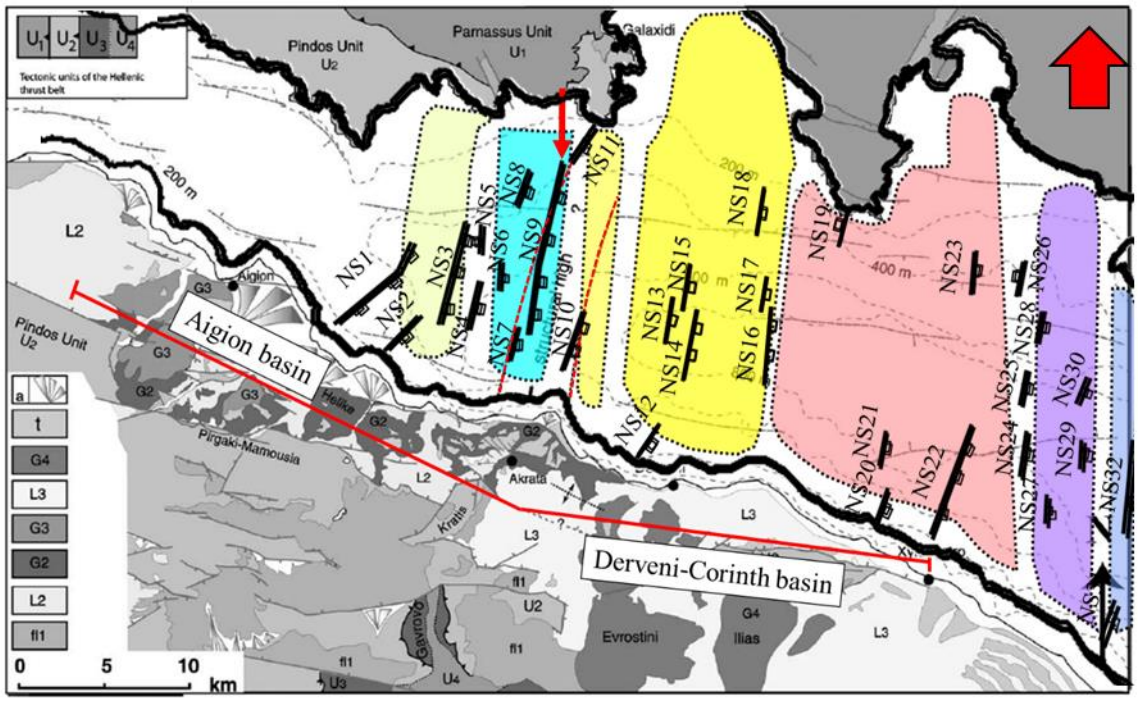

Figure 84 Geological map of the GoC with the suggested structural high by Ghisetti & Vezzani (2004) and interpreted segments and faults (modified after Ghisetti& Vezzani, 2004).

4.2 On- and offshore correlation

In this sub-chapter a correlation of previous onshore work will be correlated with the result of this study.

Mrlina (2014), proposed an N-S transfer fault onshore, where it aligns with the structural high proposed by Ghisetti & Vezzani (2004), due to gravity differences (Figure 85). The boundary between negative gravity and positive gravity is located on the same line as the boundary between segment S3 and S4.

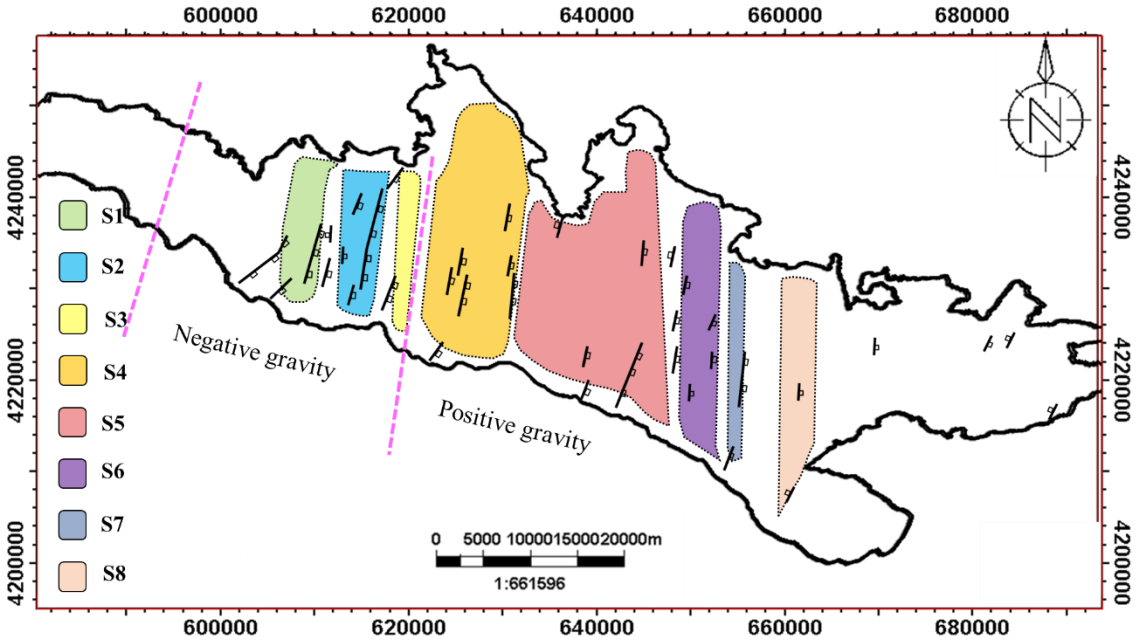

Figure 85 Map of the GoC with interpreted segments and faults; the pink dash lines show the location of the gravity change after Mrlina (2014).

By correlating the proposed Kerinities fault by Pacchiani & Lyon-Caen (2010) with interpreted N-S faults in the western section of the Gulf (Figure 86), a possible continuation of the Kerinities fault might translate offshore based on three suggested scenarios, as there are two interpreted N-S faults located at the Kerinitis River:

1. The NS1 fault may be a continuation of the Kerinitis fault offshore, associated with stepping (Figure 86a).
2. The NS1 fault may be interpreted as a curved fault or two different N-S faults, where the northern part of the fault can be aligned with the Kerinitis fault.
3. The NS2 fault might represent the Kerinities fault offshore, associated with stepping.

To highlight the stepping in scenarios 1 and 3, it assumed that there is stepping offshore, but it could be stepping onshore as well. Therefore, a more detailed study is necessary.

The bathymetry data from the western Gulf shows, as mentioned before, a lineament NNE-SSW trend. This trend aligns with the Kerinitis fault (Figure 86b). This observation supports the second scenario listed above.

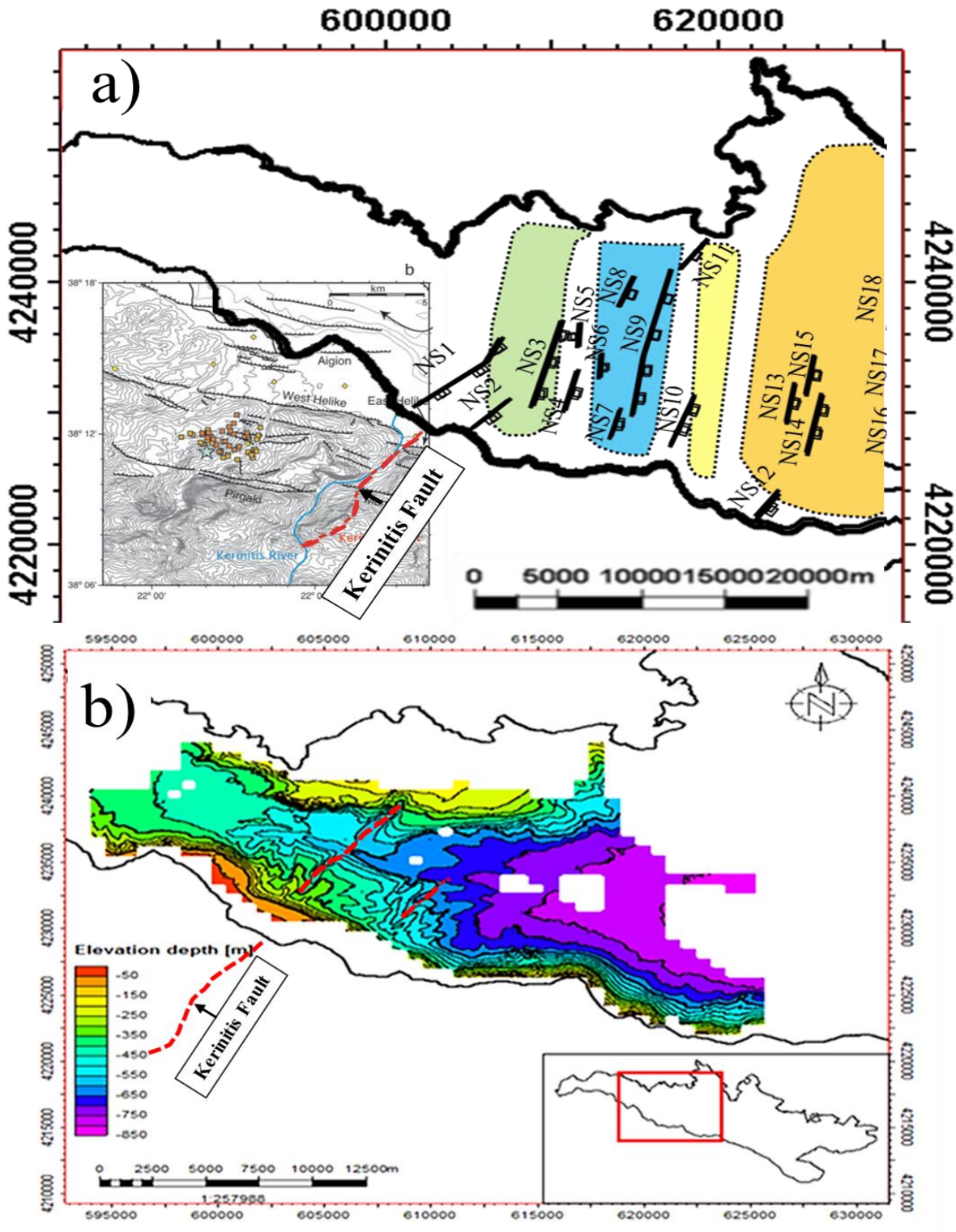

Figure 86 a) Proposed Kerinitis fault by Pacchiani & Lyon-Caen (2010) in the western sector of the Gulf combined with the interpretation of this study. b) Bathymetry of the western Gulf (McNeil et al., 2005.). The Kerinities fault (onshore) seems to correlate well with the NNE-SSW feature in the bathymetry.

Transfer faults which have been suggested by Dahman (2015) at the onshore margin in the western section of the Gulf, seem to be correlatable with the observed N-S faults in the offshore margin (Figure 87):

1. The transfer fault along the Kerinitis River correlates and aligns with the NS1 fault.
2. The transfer fault along the Vouraikos River aligns with the NS2 fault.
3. The transfer faults along the Ladhopotamos river points toward the zone between segment S1 and S2, where there are two N-S faults one dipping west and the other east. This could be a possible transfer zone.

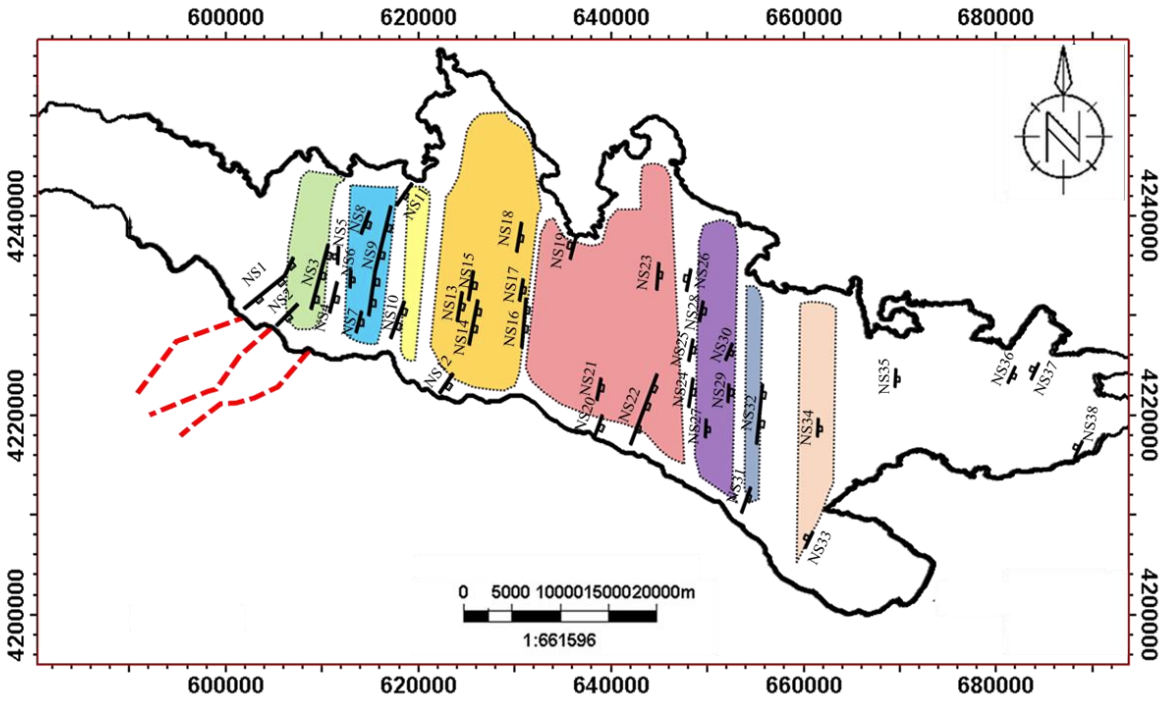

Figure 87 Structural map of the GoC with the transfer faults that were proposed by Dahman (2015) marked in red dash lines.

4.3 Correlation between earthquake zones and interpreted segments

In this sub-chapter the observed earthquake segments are compared to the interpreted segments (Figure 88). The earthquake study was not detailed since segment 1 of the earthquake analyses contains a huge amount of data making it difficult to distinguish interpreted segments 1, 2 and 3.

The eastern boundary of zone 1 aligns with the western boundary of segment 3, and the western boundary of zone 2 aligns with the eastern boundary of segment 3. Although it aligns with the structural high proposed by Ghisetti and Vezzani (2004). Furthermore, the earthquakes data has an NNE-SSW lineament trend between zone 1&2 and 2&3.

Zone 2 includes segment 4 and the western most section of segment 5, where the boundary aligns with NS19. Zone 3 includes the eastern boundary of segment 5 and segment 6, where the eastern boundary of zone 3 correlates with NS29 and NS30. Furthermore, zone 4 covers segment 7 and 8.

The earthquakes analysis could be done more scientifically to study the lineaments features and their relation of the segmentation of the Corinth Rift.

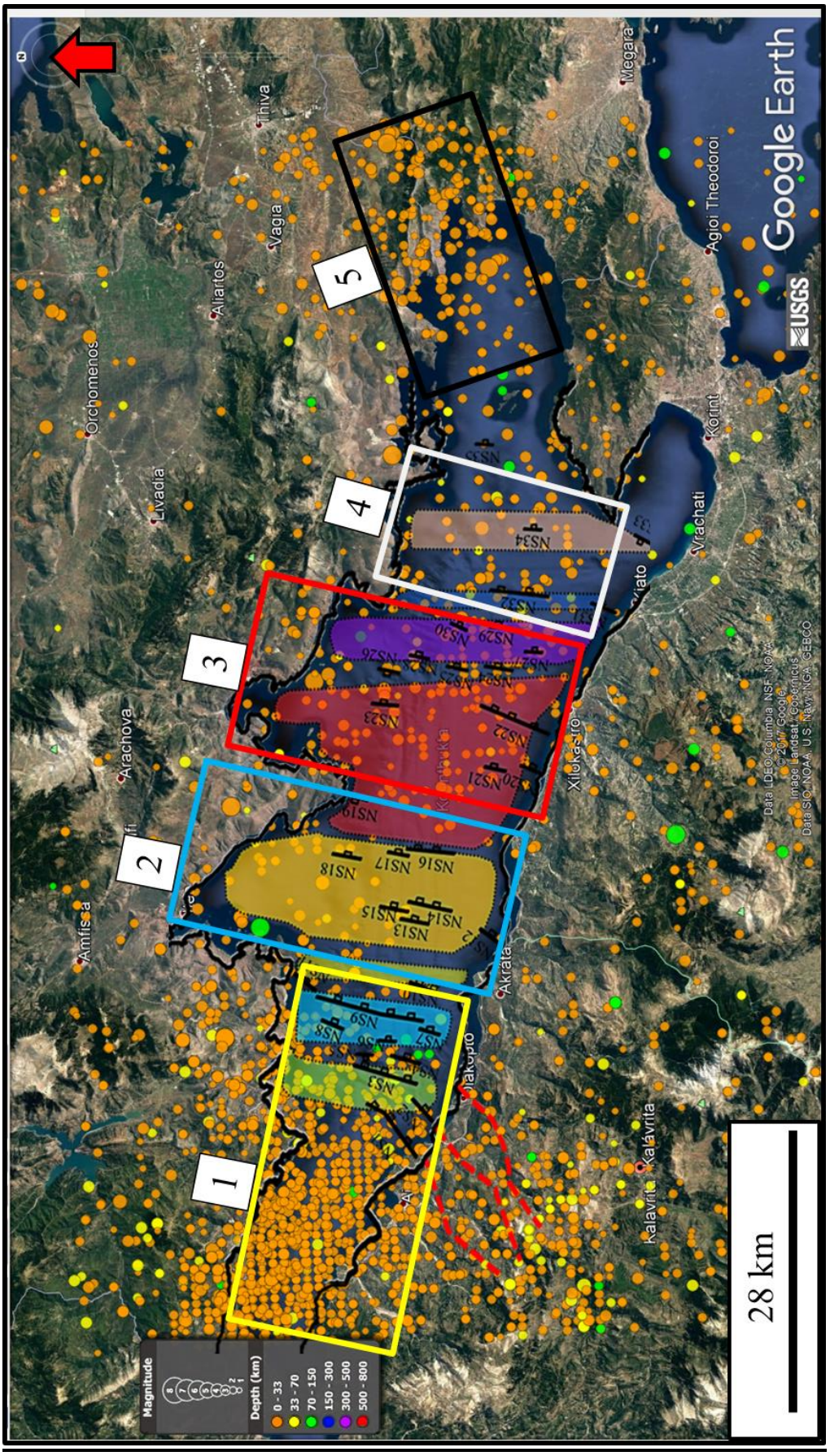

Figure 88 Map of the GoC with observed earthquake zones and interpreted segments (earthquake data from USGS).

4.4 Possible structural model of the GoC

The conceptual model by Lister et al. (1986) was used to investigate whether the basement structure variation along strike in the GoC can be used to confirm the presence of transfer faults (Figure 89).

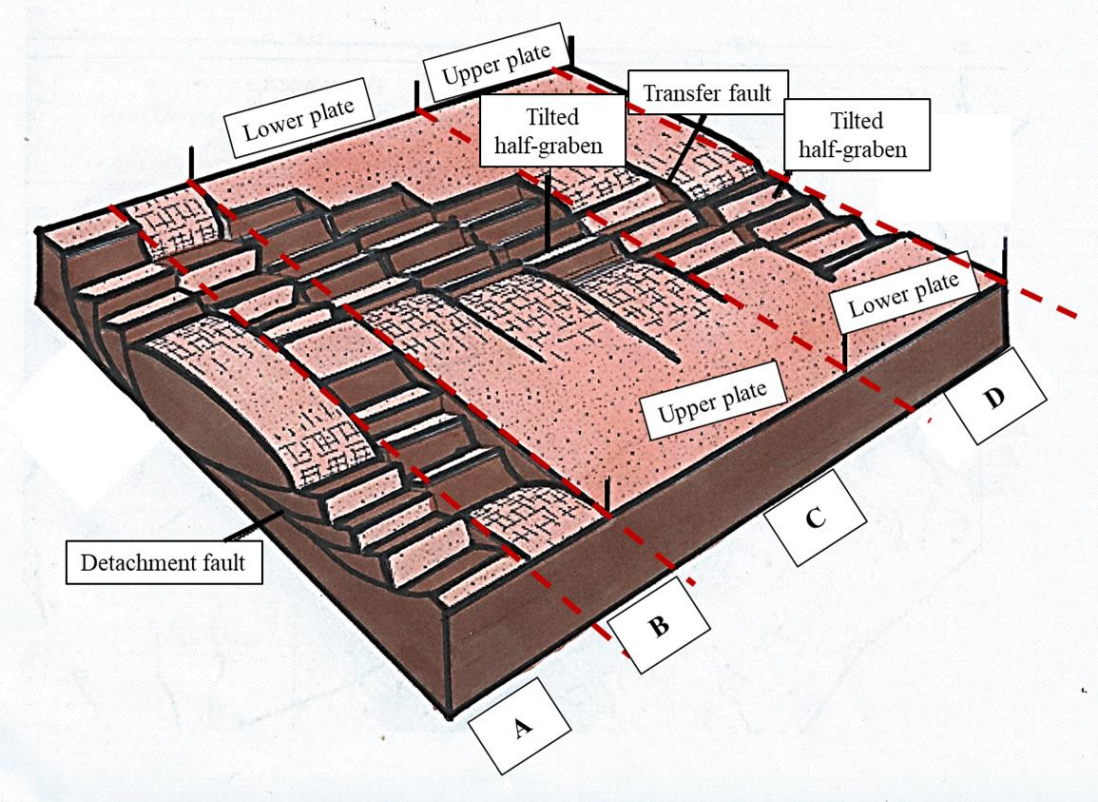

Figure 89 Conceptual 3D model proposed by Lister et al. (1986) showing the architecture of the extensional passive margin, including the change from upper to lower plate by transfer faults. The red dash lines represent the boundaries between each segment in this model. Modified after Lister et al. (1986).

The variation of the basement structure along strike in the GoC observed in this study, is similar to the proposed model based on the presence of all segments (A, B, C, D and E) in the Gulf:

- **Segment A:**

In segment S4 a large anticline and listric normal faults were observed in several N-S lines, an example is L49 (Figure 90).

- **Segment B:**

Line 37 in segment 6 (Figure 91) shows a horst structure in the basement, which represents a similar structure in Segment B (Figure 89).

- **Segment C:**

The basement has a north dipping half-graben structure in segment S5; Figure 92 shows L48 which represents segment C in the conceptual model in Figure 89.

- **Segment D:**

Is represented by L27 and L26 in the western section of the Gulf with a south dipping half-graben structure (Figure 93).

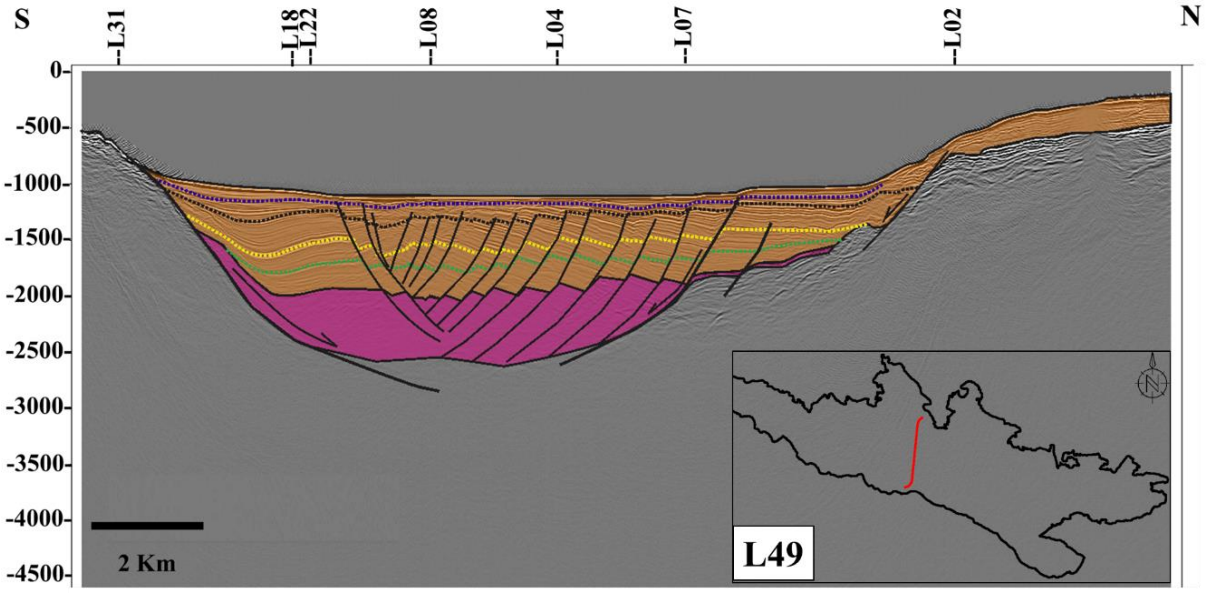

Figure 90 Interpreted N-S seismic line L49, showing the graben structure with a roll-over anticline towards the south in the syn-rift package. This section represents Segment A in Figure 82.

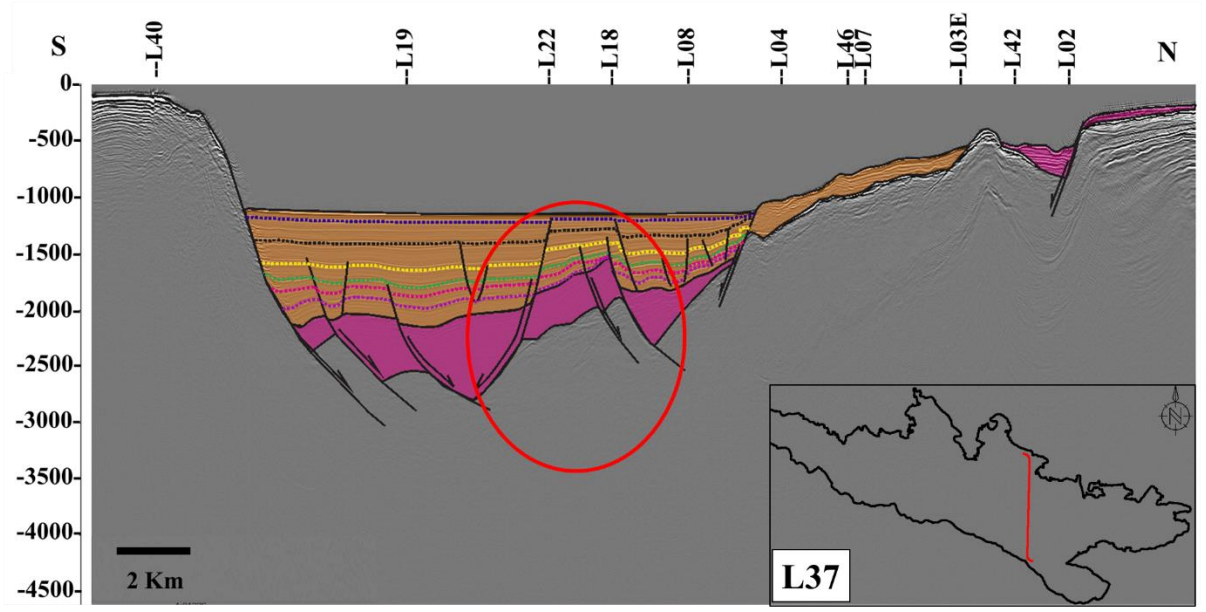

Figure 91 Interpreted N-S seismic line L37, showing the horst structure in the basement and syn-rift package marked with a red circle. This section is similar to Segment B in Figure 82.

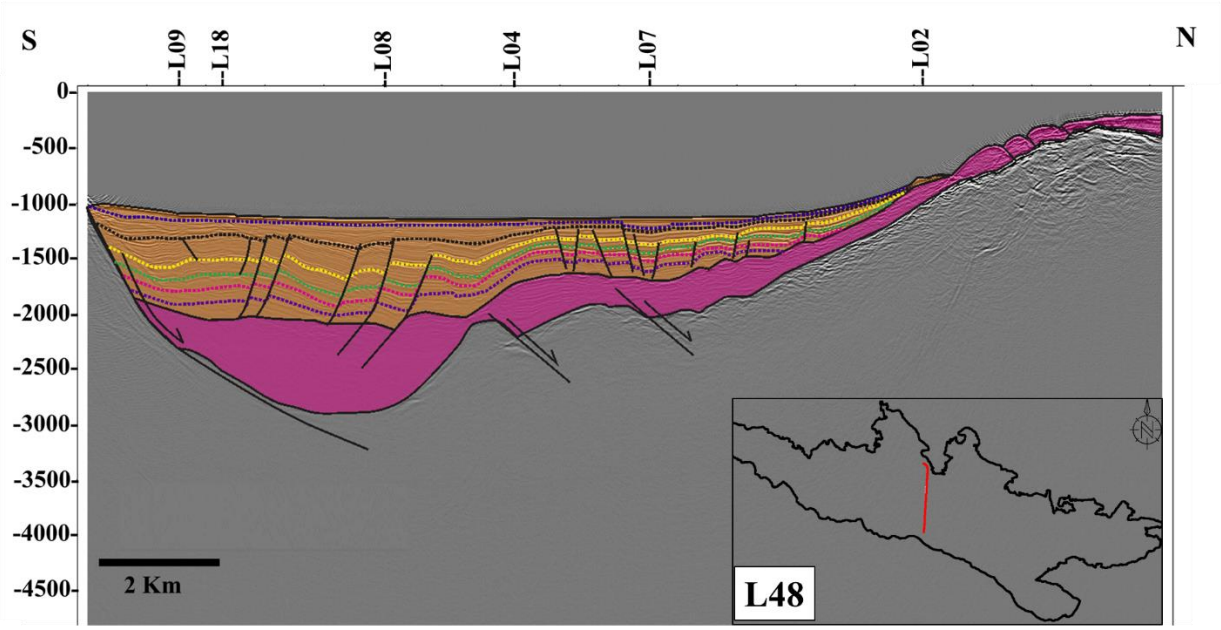

Figure 92 Interpreted N-S seismic line L48 showing N-dipping the half graben structure of the basement, bearing a similarity to segment C in Figure 82.

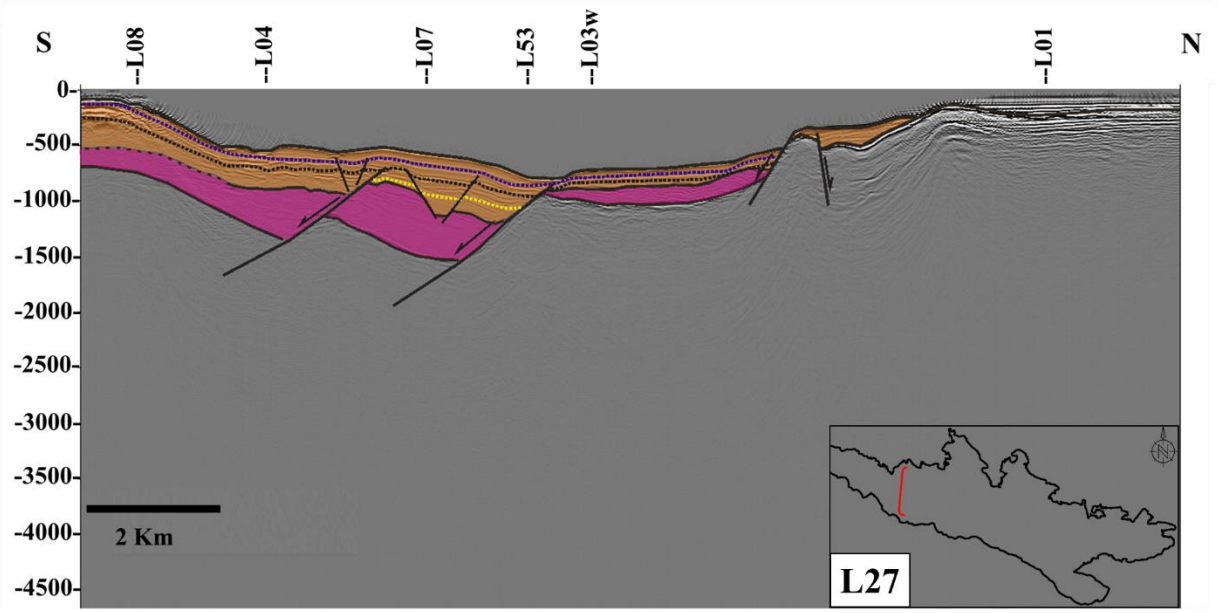

Figure 93 Interpreted N-S seismic line L27, showing the S-dipping half graben structure of the basement, similar to segment D in Figure 82.

Transfer model proposed by Lister et al. (1986) correlate with basement structure. In contrast, the comparison of W-E seismic lines with the subdivision segments of the basement shows several segments that are bounded by faults (Figure 72, 73, and 74). Furthermore, Early and Late syn-rift reflect a significant effect of observed basement's segments in the W-E seismic lines.

Regional Perspective

Segmentation of earthquake data was suggested by Papoulia et al. (2006) based on the variation of fault orientation and their connected seismicity. Furthermore, Papoulia *et al*. (2006) suggested that the deformation in those zones increase toward the south. In contrast, Palyvos *et al*. (2006) proposed transverse fault in the Northern Evia Island.

Those suggestions could have a relationship with interpreted basement structure in the GoC in this study.

Based on previous studies and observations in this study, a table was produced to summarize and present the similarity and evidence for interpreted N-S faults (Table 8).

In total seven transfer faults are proposed: four major, three minor and three sub-transfer faults (Figure 94). Almost all the proposed transfer faults are oriented NNE-SSW.

Table 8 Comparison of N-S structures proposed in previous studies and this study.

Fault	Evidences	
	This study	**Previous studies**
NS1	Seismic interpretation, time structures maps, earthquakes and bathymetry of western Gulf. Located on the western segment 1 boundary.	1. **Dahman (2015):** The transfer fault along Kerinitis river. 2. **Pacchiani&Lyon-Caen (2011):** The transfer fault along Kerinitis river
NS2	Seismic interpretation, time structures maps, and earthquakes data	1. **Dahman (2015):** The transfer fault along Vouraikos river.
NS3	Seismic interpretation, time structures maps, and earthquakes data. NS3 is located on the eastern boundary of segment 1	1. **Dahman (2015):** The transfer fault along Ladhopotamos river. 2. **Nixon et al. (2016):** NS3 is located on the boundary between West and Central-West domains
NS4		
NS7	Seismic interpretation, time structures maps, and earthquakes data. NS9 and NS11 align with the eastern boundary of segment 2	1. **Ghisetti& Vezzani (2004):** align with the proposed structural high. 2. **Console et al. (2013):** align with the western boundary of segment 4. 3. **Ford et al. (2016):** are located on the boundary between Zone C4 and C3.
NS9		
NS11		
NS16	Seismic interpretation, Time structures maps. Located on the eastern boundary of segment 4.	1. **Nixon et al. (2016):** align with the boundary between Central-West and Central-East domains.
NS17		
NS12	**NS13**	Seismic interpretation	1. **Console et al. (2013):** are located on the eastern boundary of segment 5.
NS14	**NS15**		
NS20 **NS21**	Seismic interpretation, time structures maps, and earthquakes data	1. **Ford et al. (2016):** located near by the boundary between zone C2 and C3
NS23 **NS22**	Seismic interpretation	1. **Console et al. (2013):** Show alignment with the boundary between segments 5& 6.
NS29 **NS30**	Seismic interpretation	1. **Nixon et al.(2016):** located on the boundary between Central-East and East domains.
NS33	Seismic interpretation Earthquakes	1. **Console et al. (2013):** Show alignment with the boundary between segment 6& 7.

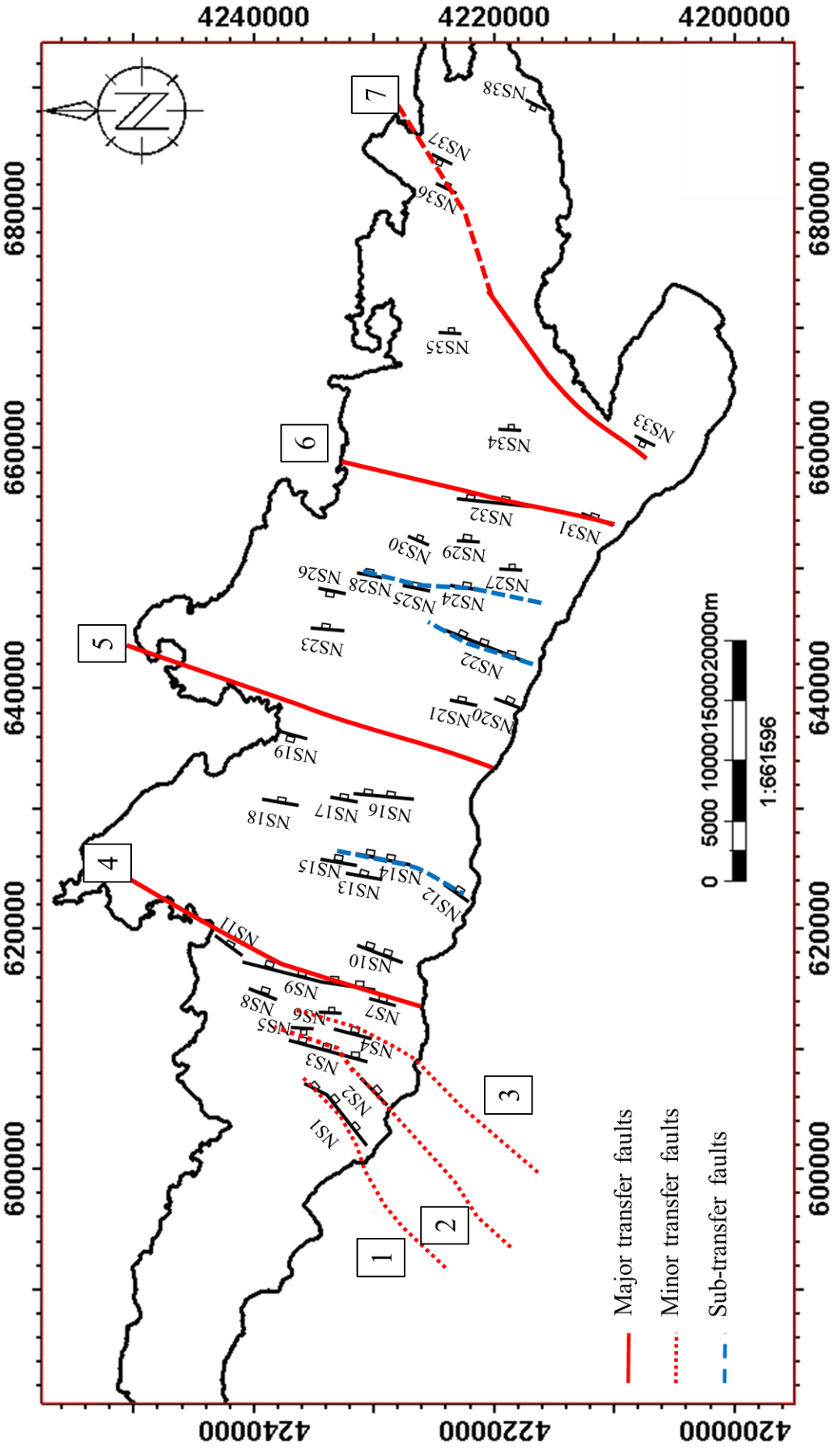

Figure 94 Structural map of the Gulf of the Corinth with proposed transfer faults.

Chapter 5 Conclusion

The offshore study of the GoC was key to understanding the Corinth Rift and several important insights were made in this thesis. Based on this study, the following conclusions were drawn:

- Evidence of segmentation of the GoC was substantial, as several NNE-SSW faults were traced along the Gulf, with dip angle range of 30° -40°.
- Eight segments were interpreted, based on the lateral variation of the basement structure along the strike.
- The boundaries between observed segments based on miscorrelation in previous studies seem to have been controlled by transfer faults.
- Ten transfer faults are proposed: four major, three minor and three sub-transfer faults, based on the interpretation and correlation of the previous studies.
- Onshore transfer faults proposed by Dahman (2015) continue offshore.
- Migration of the main basin occurred during deposition of the syn-rift sediments; the thickest package of the Early-rift sediment was deposited in the western section of the Central-West domain. In contrast, the thickest package of Late-rift was deposited in the Central-East domain.
- Early and Late-rift sequences have their maximum thickness toward the southern margin of the Gulf.
- The structural high that was proposed by Ghisetti & Vezzani (2004) seems to be fault bounded and related to the transfer fault structure.

References

Armijo, R., Meyer, B., King, G.C.P., Rigo, A., and Papanastassiou,D. (1996). "Quaternary evolution of the Corinth Rift and its implications for the Late Cenozoic evolution of the Aegean." Geophysical Journal International **126**: 11–53.

Athmer, W., Groenenberg, R., Luthi, S., & Willingshofer, E (2010). "Relay ramps as pathways for turbidity currents: A study combining analogue sandbox experiments and numerical flow simulations." Sedimentology **57**: 806-823.

Bell, R., E., McNeill, L, C., Timothy J. Henstock and Jonathan M. Bull (2011). "Comparing extension on multiple time and depth scales in the Corinth Rift, Central Greece." Geophysical Journal International **186**: 463-470.

Bell. R., E., Lisa C. McNeill, Jonathan M. Bull, Timothy J. Henstock (2008). "Evolution of the offshore western Gulf of Corinth." GSA Bulletin **120**: 156-178.

Bernad, P., et al. (2006). "Seismicity deformation and seismic hazard in the western rift of Corinth: New insihts from the Corinth Rift Laboratory (CRL)." Tectonophysics **426(1-2)**: 7-30.

Bintanja, R., and R. S. W. van de Wal (2008). "North American ice-sheet dynamics and the onset of 100,000-year glacial cycles." Nature **454**: 869-872.

Briole, P., A. Rigoe, H. Lyon-Caen, J . C. Ruegg, K. Papazissi , C. Mitsakaki, A. Balodimou, G. Veis, D. Hatzfeld, and A. Deschamps (2000). "Active deformation of the Corinth rift Greece: Results from repeated Global Positioning System surveys between 1990 and 1995." Journal of Geophysical Research **105**: 25,605-625,625.

Clarke, P. L., Davies, R.R., England, P.C., Parsons, B., Billiris, H., Paradissis, D., Veis, G., Cross, P.A., Denys, P.H., Ashkenazi, V., Bingley, R., Kahle, H., Muller, M., and Briole, P (1998). "Crustal strain in central Greece from repeated GPS measurements in the interval 1989–1997." Geophysical Journal International **135**: 195-214.

Collier, R., and Jones.G, (2004). Rift Sequences of the Southern Margin of the Gulf of Corinth (Greece) as Exploration / Production Analogues. AAPG International Conference. Barcelona, Spain.

Console, R., G. Falcone, V. Karakostas, M. Murru, E. Papadimitriou, and D. Rhoades (2013). "Renewal models and coseismic stress transfer in th8e Corinth Gulf, Greece, fault system." Journal of Geophysical Research Solid Earth **118**: 3655-3673.

Dahman, A. (2015). The Vouraikos Valley: an example of rift segmentation in the Corinth Graben, Greece. Faculty of Science and Technology, University of Stavanger. **Master**.

Degnan, P., J., and Robertson, A, H,F. (1998). "Mesozoic-early Tertiary passive margin evolution of the Pindos ocean (NW Peloponnese, Greece)." Sedimentary Geology **117**(1): 33-70.

Dercourt, J. (1964). Contribution a`le´tude ge´ologique du secteur du Pe´loponne`se septentrional. Universite´ de Paris, Paris.

Dewey, J. F., and C. Sengor (1979). "Aegean and surrounding regions: Complex multiplate and continuum tectonics in a convergent zone." Geological Society of America Bulletin. **90**: 84-92.

Dornsiepen, U., F., Manutsoglu, E., and Mertmann, D. (2001). "Permian-Triassic palaeography of the external Hellenides." Palaeography, Palaeoeclimatology, Palaeoecology **172**: 327-338.

Dornsiepen, U., Gerolymatos, E. and Jacobshagen, V. (1986). "Die Phyllit-Quartzit-Serie im fenster von Feneos (Nord- Peloponnes)." IGME Geological and Geophysical Research(Special Issue): 99-105.

Doutsos, T., and Piper, D. J. W. (1990). "Listric faulting, sedimentation, and morphological evolution of the Quaternary eastern Corinth rift, Greece: First stages of continental rifting." Geological Society of America Bulletin **102**: 812-829.

Doutsos, T., N. Kontopoulos, and G. Poulimenos (1988). "he Corinth-Patras rift as the initial stage of continental fragmentation behind an active island arc (Greece)." Basin Research **1(3)**: 177-190.

Fleury, J. (1980). Les zones de Gavrovo-Tripolitza et du Pindos (Gre`ce continentale et Pe´loponne`se du Nord). Evolution d'une plateforme et d'un bassin dans leur cadre alpin. Me´moire de la Socie´te´ ge´ologique du Nord. Lille**:** 651.

Ford, M., Hemelsdaël, R., Mancini, M., & Palyvos, N. (2016). "Rift migration and lateral propagation: evolution of normal faults and sediment-routing systems of the western Corinth rift (Greece)." The Geometry and Growth of Normal Faults **439**.

Ford, M., Rohais, S., Williams, E, A., Bourlange, S., Jousselin, D., Nicolas, B., and Malartre, F. (2012). "Tectono-sedimentary evolution of the western Corinth rift (Central Greece)." Basin Research **0**: 1-23.

Ford, M., S. Rohais, E. A. Williams, S. Bourlange, D. Jousselin, N. Backert, and F. Malartre (2013). "Tectono-sedimentary evolution of the western Corinth Rift (Central Greece)." Basin Research **25**: 3-25.

Fossen, H., and Rotevatn, A. (2016). "Fault linkage and relay structures in extensional settings—A review." Earth-Science Reviews **154**: 14-28.

Gawthorpe, R. L., and M. R. Leeder (2000). "Tectono-sedimentary evolution of active extensional basins." Basin Research **12**: 195-218.

Ghisetti, F., and Vezzani , L. (2004). "Plio–Pleistocene sedimentation and fault segmentation in the Gulf of Corinth (Greece) controlled by inherited structural fabric." Comptes rendus Geoscience **336**: 243-249.

Ghisetti, F., and Vezzani , L. (2005). "Inherited structural controls on normal fault architecture in the Gulf of Corinth (Greece)." Tectonics **24**: TC4016.

Gibbs, A., D., (1984). "Structural evolution of extensional basin margins." Journal of the Geological Society London **141**: 609-620.

Hemelsdael, R., and Ford, M. (2016). "Relay zone evolution: a historyof repeated fault propagation and linkage, central Corinth rift,Greece." Basin Research **28**: 34-56.

Horvath, F., and Berckhemer, H. (1982). "Mediterranean back-arc basins. In: Berckhemer H, Hsü KJ (eds) Alpine-Mediterranean geodynamics." Geodynamic Research **7**: 609-620.

Jackson, C. A., Gawthorpe, R.L., Leppard, C.W and Sharp, I.R (2006). "Rift-initiation development of normal fault blocks: insights from the Hammam Faraun fault block, Suez Rift, Egypt." Journal of the Geological Society London **163**: 165-184.

Jolivet, L. (2001). "A comparison of geodetic and finite strain pattern in the Aegean, geodynamic implications." Earth Planet. Sci. Lett. **187**: 95-104.

Jolivet, L., Labrousse, L., Agard, P., Lacombe, O., Bailly, V., Lecomte, E., Mouthereau, F. and Mehl, C. (2010). "Rifting and shallow-dipping detachments, clues from the Corinth Rift and the Aegean." Tectonophysics **483**: 287-304.

Larsen, P., H. (1988). "Relay structures in a Lower Permian basement-involved extension system, East Greenland." Journal of Structural Geology. **10**: 3-8.

Leeder, M. R., C. Portman, J. E. Andrews, R. E. L. Collier, E. Finch, R. L. Gawthorpe, L. C. McNeill, M. Perez-Arlucea, and P. Rowe (2005). "Normal faulting and crustal deformation, Alkyonides Gulf and Perachora peninsula, eastern Gulf of Corinth Rift, Greece." Journal of the Geological Society London **162**: 549-561.

Lekkas, S., and Papanikolaou, D. (1979). "On the Phyllite propblem in Peloponnesus." Annales Geologiques des Pays Helleniques **29**: 395-410.

Lister, G., S.,Etheridge,M,A, and Symonds, P,A (1986). "Detachment faulting and the evolution of passive continental margins." Geology **14**: 246-250.

McKenzie, D. (1978). "Active tectonics of the Mediterranean region." Geophysical Journal of the Royal Astronomical Society. **30**: 109-185.

McKenzie, D. P. (1972). "Active tectonics of the Mediterranean region." Geophysical Journal of the Royal Astronomical Society. **30**: 109-185.

McNeill, L. C., C.J. Cotterill, T.J. Henstock, J.M. Bull, A. Stefatos, R.E.Ll. Collier, G. Papatheoderou, G. Ferentinos, S.E. Hicks (2005). "Active faulting within the offshore western Gulf of Corinth, Greece: Implications for models of continental rift deformation." Geology **33**: 241-244.

Moretti, I., Sakellariou, D., Lykousis, V., and Micarelli, L. (2003). "The Gulf of Corinth: An active half graben?" Journal of Geodynamics **36**: 323-340.

Moustafa, A., R., and Khalil, S, M. (2017). "Control of compressional transfer zones on syntectonic and post-tectonic sedimentation: implications for hydrocarbon exploration." Journal of the Geological Society **174**: 336-352.

Mrlina, J. (2014). Do Active Transverse Faults Exist on the Southern Coast of Corinth Rift? 20th European Meeting of Environmental and Engineering Geophysics. Athens, Greece.

Nixon, C. W., et al. (2016). "Rapid spatiotemporal variations in rift structure during development of the Corinth Rift, central Greece." Tectonics **35**: 1225-1248.

Ori, G. G. (1989). "Geologic history of the extensional basin of the Gulf of Corinth (?Miocene-Pleistocene), Greece." Geology **17**: 918-921.

Pacchiani, F., and H, Lyon-Caen (2010). "Geometry and spatio-temporal evolution of the 2001 Agios Ioanis earthquake swarm (Corinth Rift, Greece)." Geophysical Journal International **180**: 59-72.

Pham, V., N., Bernad, P., Boyer, D., Chouliaras., Mouel, J, L, Le., and Stavrakakis, G, N. (2000). "Electrical conductivity and crustal structure beneath the central Hellenides around the Gulf of Corinth (Greece) and their relationship with the seismotectonics." Geophysical Journal International. **142**: 948-969.

Palyvos, N., Bantekas, I, and Kranis, H. (2006). "Transverse fault zones of subtle geomorphic signature in northern Evia island (central Greece extensional province): An introduction to the Quaternary Nileas graben." Geomorphology **76**: 363-374.

Papoulia, J., Markis, J., and Drakopoulou, V. (2006). "Local seismic array observations at north Evoikos, central Greece, delineate crustal deformation between the North Aegean Trough and Corinthiakos Rift." Tectonophysics **423**: 97-106.

Richter, D. (1976). "Das Flysch-Stadium der Helleniden-Ein Uberblick." Zeitschrift Dt. Geol. Ges. **127**: 96-128.

Roberts, S., and J. Jackson (1991). "Active normal faulting in central Greece: An overview." Journal of the Geological Society London Special Publication. **56(1)**: 125-142.

Rohais, S., and Moretti, I,. (2017). Structural and Stratigraphic Architecture of the Corinth Rift (Greece): An Integrated Onshore to Offshore Basin-Scale Synthesis. Lithosphere Dynamics and Sedimentary Basins of the Arabian Plate and Surrounding Areas. F. Roure, A. A. Amin, S. Khomsi, and M. A. M. Al Garni. Cham, Springer International Publishing**:** 89-120.

Rohais, S., and Moretti, I. (2016). Structural and Stratigraphic Architecture of the Corinth Rift (Greece): An Integrated Onshore to Offshore Basin-Scale Synthesis. Frontiers in Earth Sciences Springer International Publishing AG**:** 89-120.

Rohais, S., Eschard, R., Ford, M., Guillocheau, F. and Moretti, I. (2007a). "Stratigraphic architecture of the Plio-Pleistocene infill of the Corinth Rift: implications for its structural evolution." Tectonophysics **440**: 5-28.

Royden, L., H., and Papanikolaou, D, J. (2011). "Slab segmentation and late Cenozoic disruption of the Hellenic arc." Geochemistry Geophysics Geosystems **12**.

Sachpazi, M., C. Clément, M. Laigle, A. Hirn, and N. Roussos (2003). "Rift structure, evolution, and earthquakes in the Gulf of Corinth, from reflection seismic images." Earth Planet. Sci. Lett **216**: 243-257.

Sakellariou, D., Lykousis, V., Alexandri, S., Kaberi, H., Rousakis, G., Nomikou, P., Georgiou, P. & Ballas, D. (2007). "Faulting, seismicstratigraphic architecture and Late Quaternary evolution of the Gulf of Alkyonides Basin-East Gulf of Corinth, Central Greece." Basin Research **19**: 273-295.

Skourlis, K., and Doutsos, T. (2003). "The Pindos Fold-and-thrust belt (Greece): Inversion kinematics of a passive continental margin." International Journal of Earth Sciences **92**: 891-903.

Skourtsos, E., and H. Kranis (2009). "Structure and evolution of the western Corinth Rift, through new field data from the Northern Peloponnesus." Journal of the Geological Society London Special Publication **321**: 119-138.

Sorel.D (2000). "A Pleistocene and still-active detachment fault and the origin of the Corinth-Patras rift, Greece." Geology **28**: 83-86.

Tasrianto, R., and Escalona, A. (2015). "Rift architecture of the Lofoten-Vesterålen margin, offshore Norway." Marine and Petroleum Geology **64**: 1-16.

Taylor, B., Weiss,J, R., A. M. Goodliffe, M. Sachpazi, M. Laigle, and A.Hirn (2011). "The structures, stratigraphy and evolution of the Gulf of Corinth rift, Greece." Geophysical Journal International **185**: 1189-1219.

Taymaz, T., Jackson, J., & McKenzie, D (1991). "Active tectonics of the north and central Aegean Sea." Geophysical Journal International **106**: 433-490.

Wood, A., M. (2013). The influence of fault geometric uncertainty on hydrocarbon reservoir and simulation models. School of Earth and Environment, The university of Leeds. **Doctor of Philosophy:** 172-174.

Appendix 1

All interpreted and uninterpreted seismic lines are presented in the Appendix , the vertical axis is in TWT(msec) in the all lines.

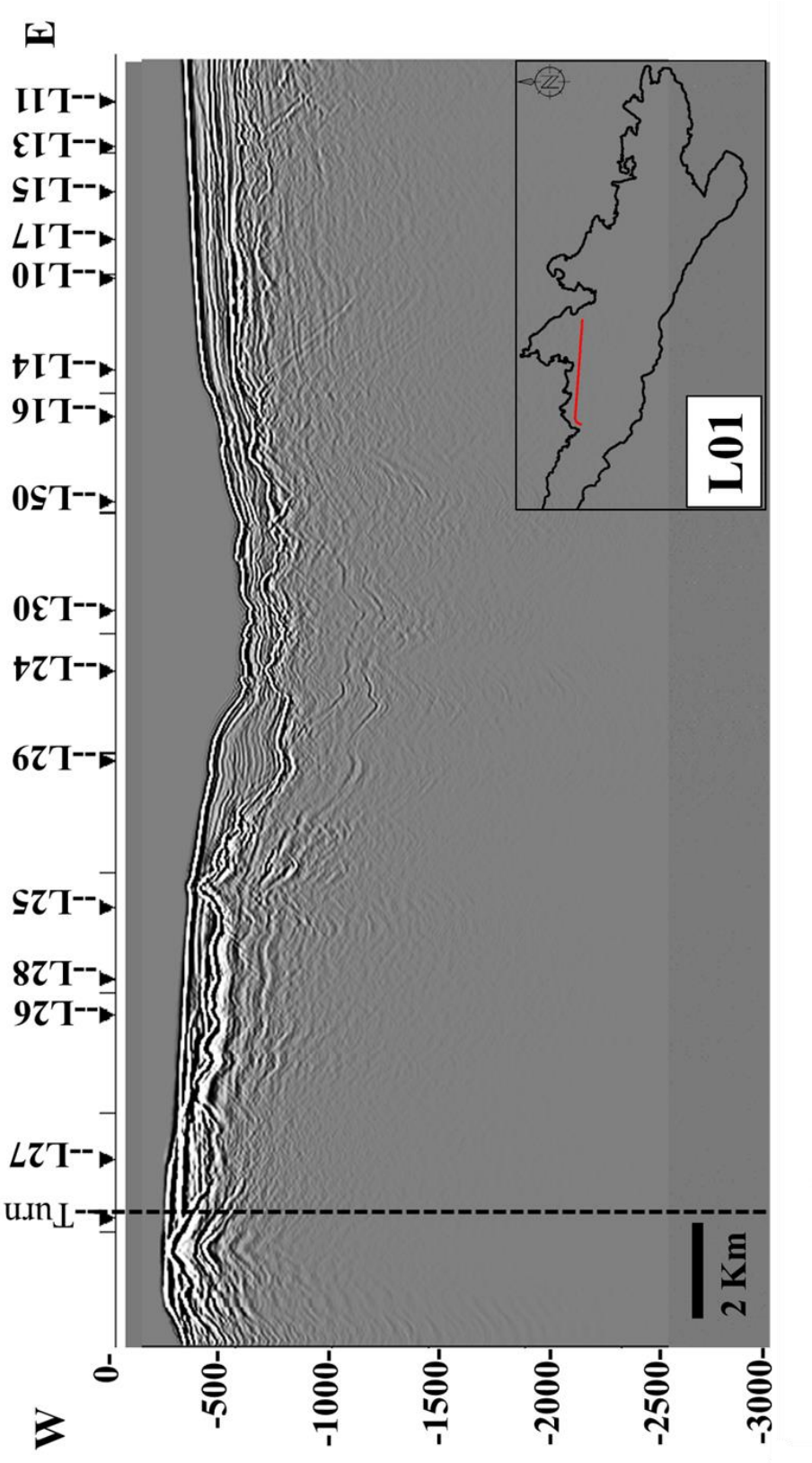

E
L11
L13
L15
L17
L10
L14
L16
L50
L30
L24
L29
L25
L28
L26
L27
Turn
W
0-
-500-
-1000-
-1500-
-2000-
-2500-
-3000-
2 Km
L01

E
L37
L36
L41
L35
L21
L34
L20
L33
L48
L32
L49
L11
L13
L15
L17
L10
L14
L16
L50
L30
L24
L29
L25
L28
L26
W
0
-500
-1000
-1500
-2000
-2500
-3000
-3500
L02
2 Km

E
L37
L36
L41
L35
L21
L34
L20
L33
L48
L32
L49
L11
L13
L15
L17
L10
L14
L16
L50
L30
L24
L29
L25
L28
L26
W
0
-500
-1000
-1500
-2000
-2500
-3000
-3500
L02
2 Km

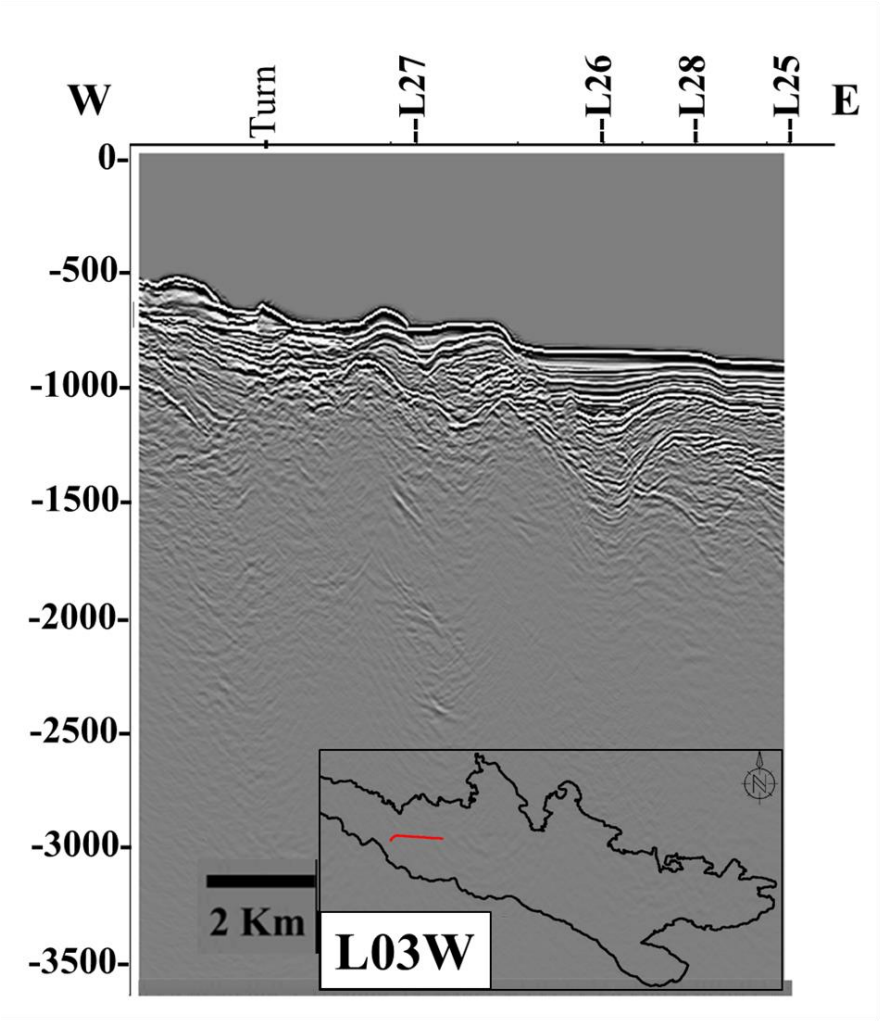
W
Turn
L27
L26
L28
L25
E
0
-500
-1000
-1500
-2000
-2500
-3000
-3500
2 Km
L03W

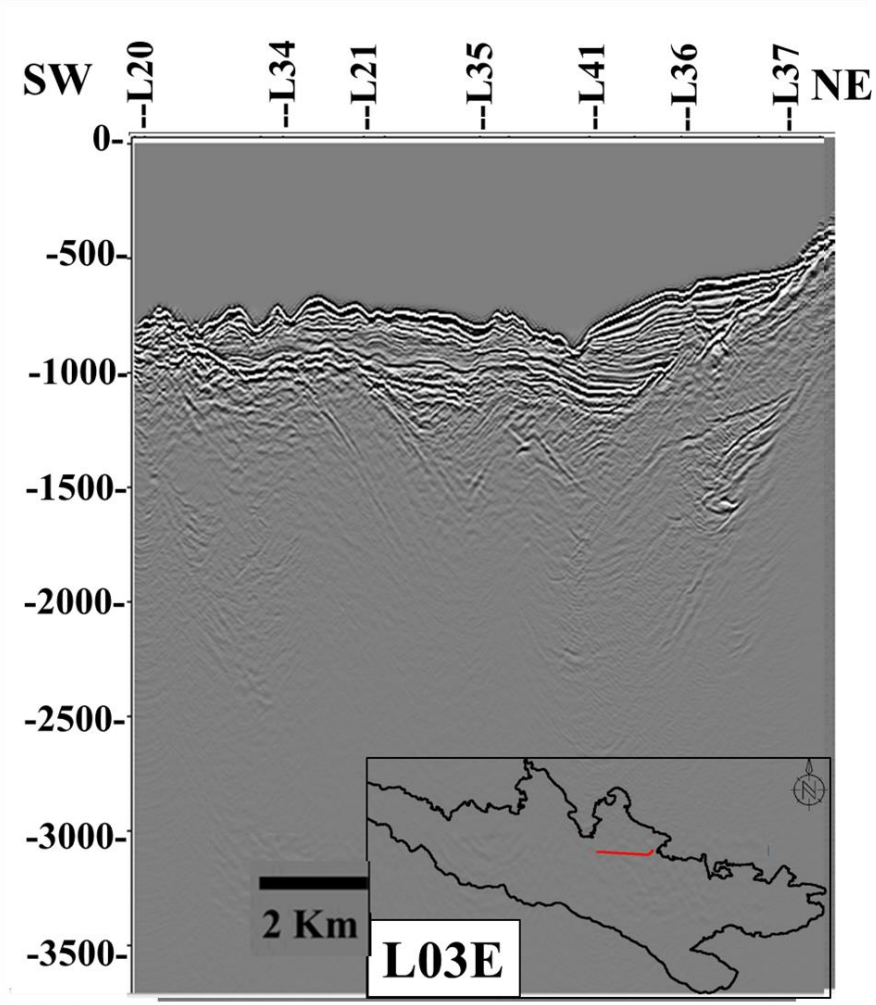
SW
L20
L34
L21
L35
L41
L36
L37
NE
0
-500
-1000
-1500
-2000
-2500
-3000
-3500
2 Km
L03E

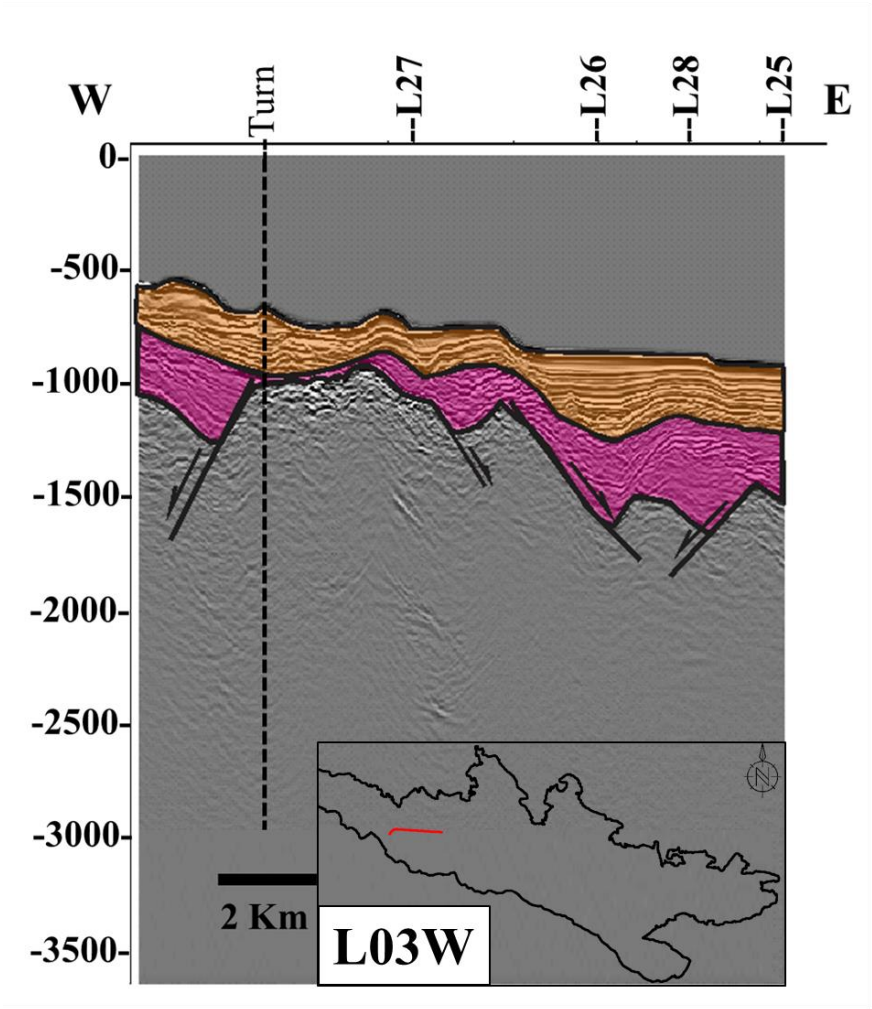
W
Turn
--L27
--L26
--L28
--L25
E
0-
-500-
-1000-
-1500-
-2000-
-2500-
-3000-
-3500-
2 Km
L03W

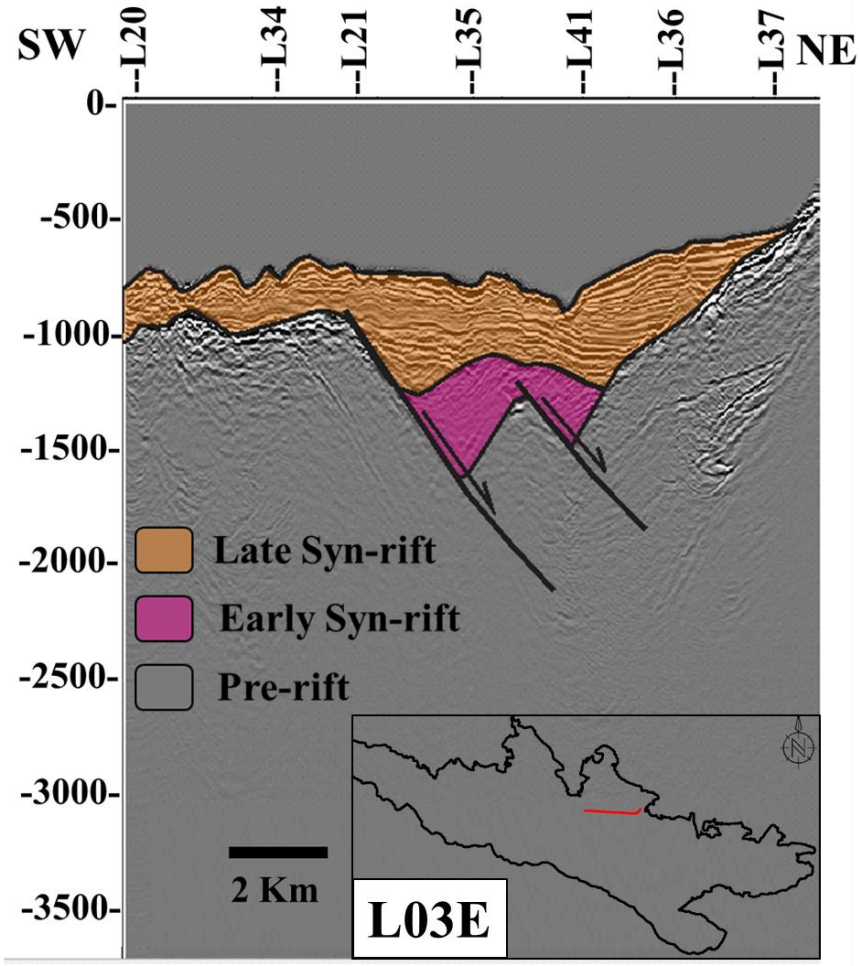
SW
--L20
--L34
--L21
--L35
--L41
--L36
--L37
NE
0-
-500-
-1000-
-1500-
-2000-
-2500-
-3000-
-3500-
Late Syn-rift
Early Syn-rift
Pre-rift
2 Km
L03E

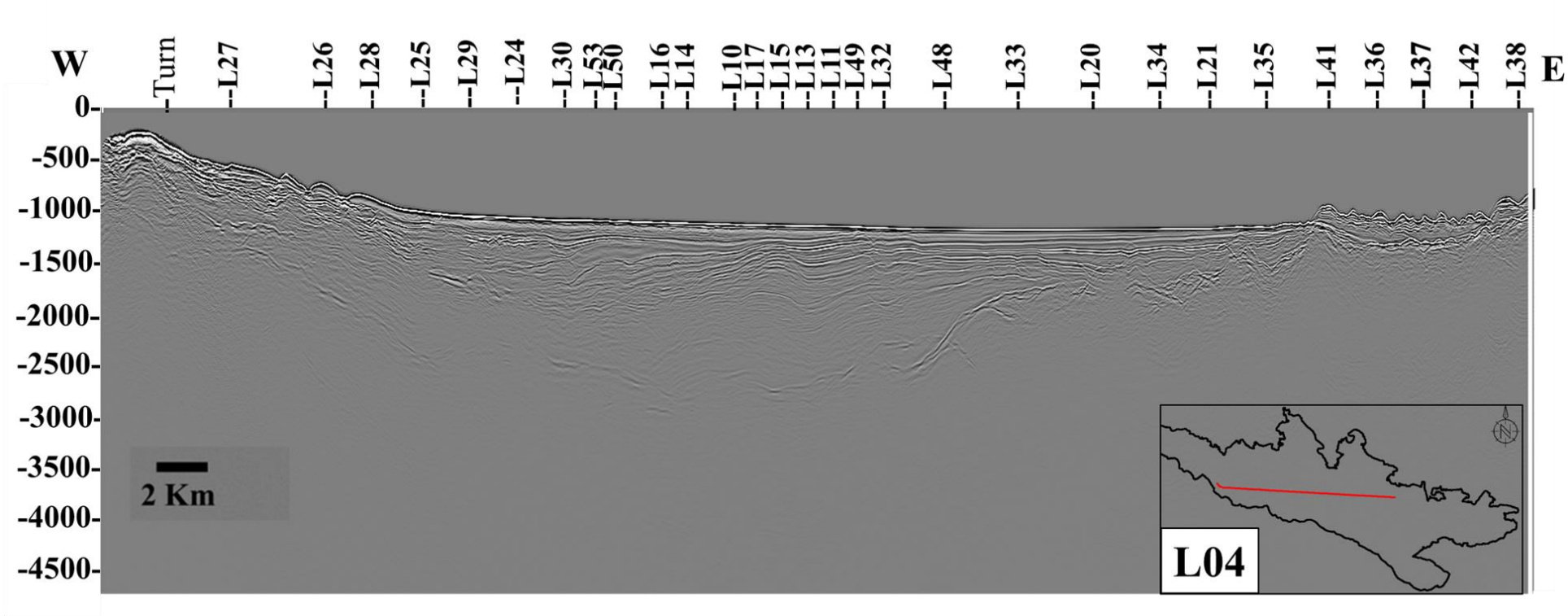
W
E
Turn
L27
L26
L28
L25
L29
L24
L30
L53
L50
L16
L14
L10
L17
L15
L13
L11
L49
L32
L48
L33
L20
L34
L21
L35
L41
L36
L37
L42
L38
0
-500
-1000
-1500
-2000
-2500
-3000
-3500
-4000
-4500
2 Km
L04

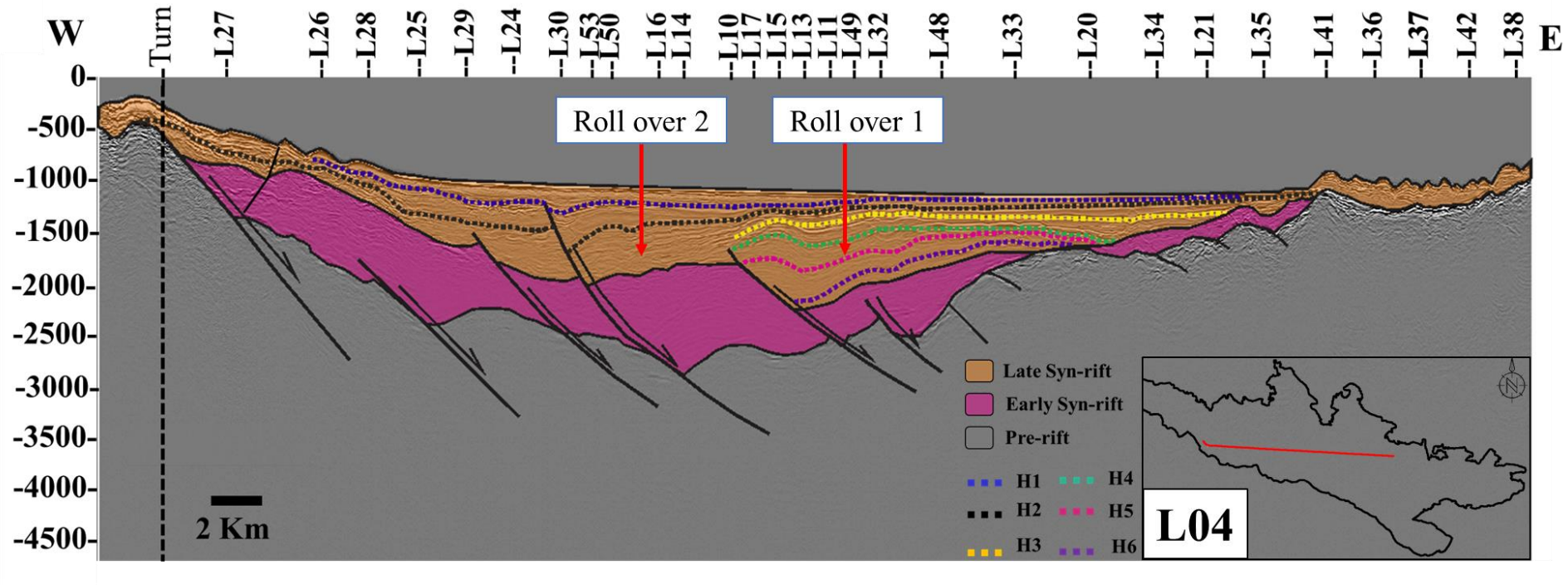
W
E
Turn
L27
L26
L28
L25
L29
L24
L30
L53
L50
L16
L14
L10
L17
L15
L13
L11
L49
L32
L48
L33
L20
L34
L21
L35
L41
L36
L37
L42
L38
0
-500
-1000
-1500
-2000
-2500
-3000
-3500
-4000
-4500
Roll over 2
Roll over 1
2 Km
Late Syn-rift
Early Syn-rift
Pre-rift
H1
H2
H3
H4
H5
H6
L04

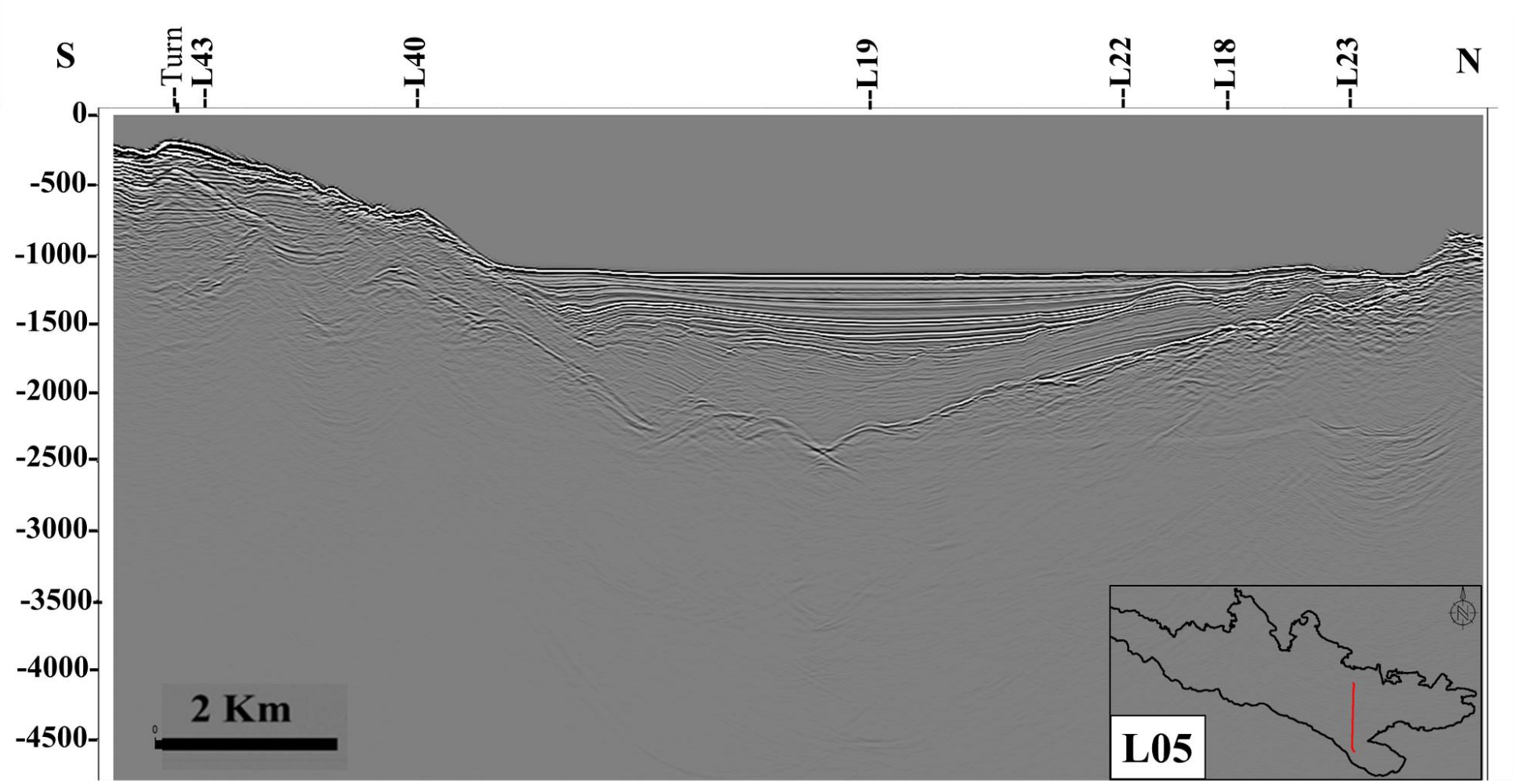
S
--Turn
--L43
--L40
--L19
--L22
--L18
--L23
N
0
-500
-1000
-1500
-2000
-2500
-3000
-3500
-4000
-4500
2 Km
0
L05

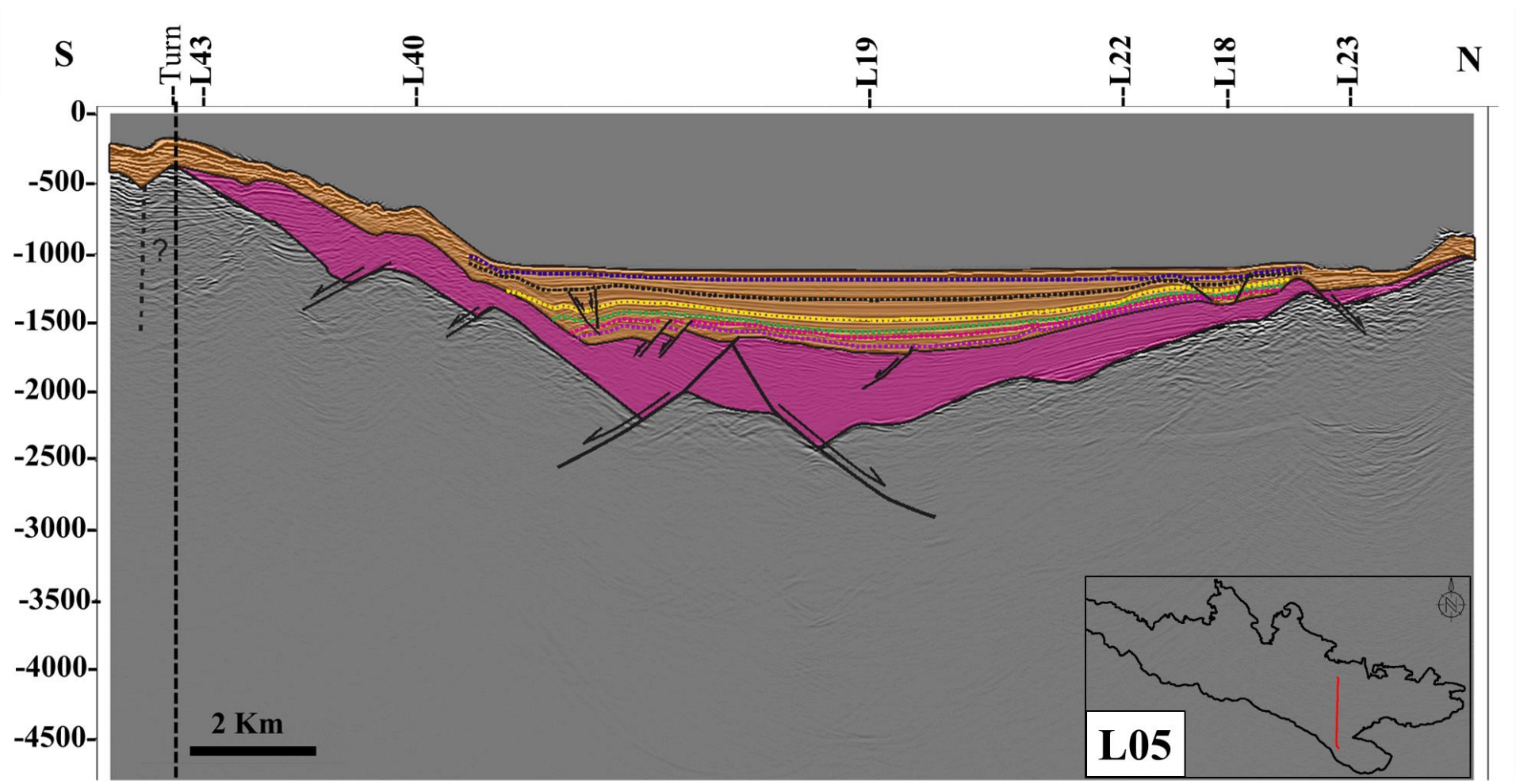
S
Turn
L43
L40
L19
L22
L18
L23
N
0
-500
-1000
-1500
-2000
-2500
-3000
-3500
-4000
-4500
?
2 Km
L05

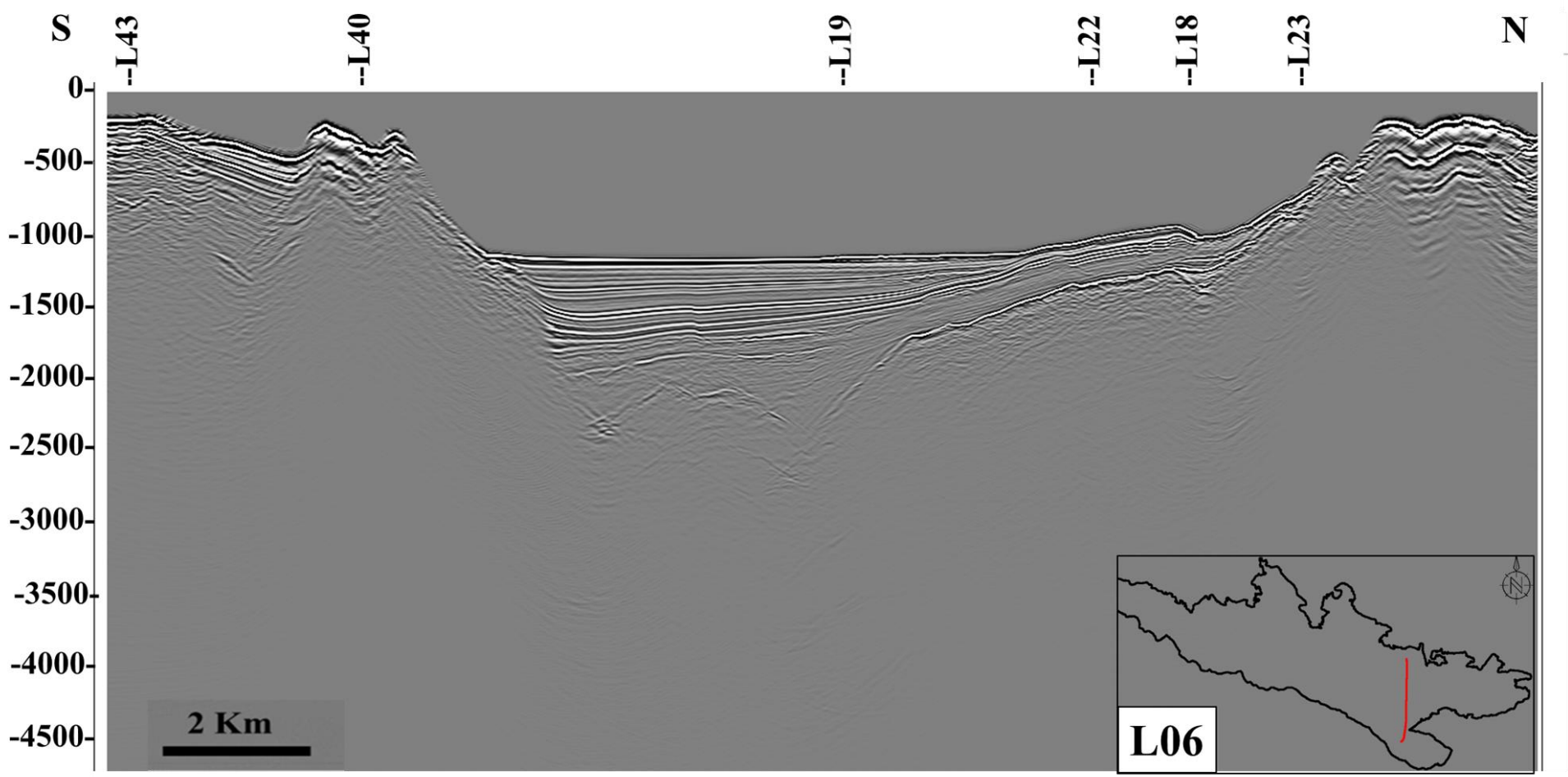
S
--L43
--L40
--L19
--L22
--L18
--L23
N
0
-500
-1000
-1500
-2000
-2500
-3000
-3500
-4000
-4500
2 Km
L06

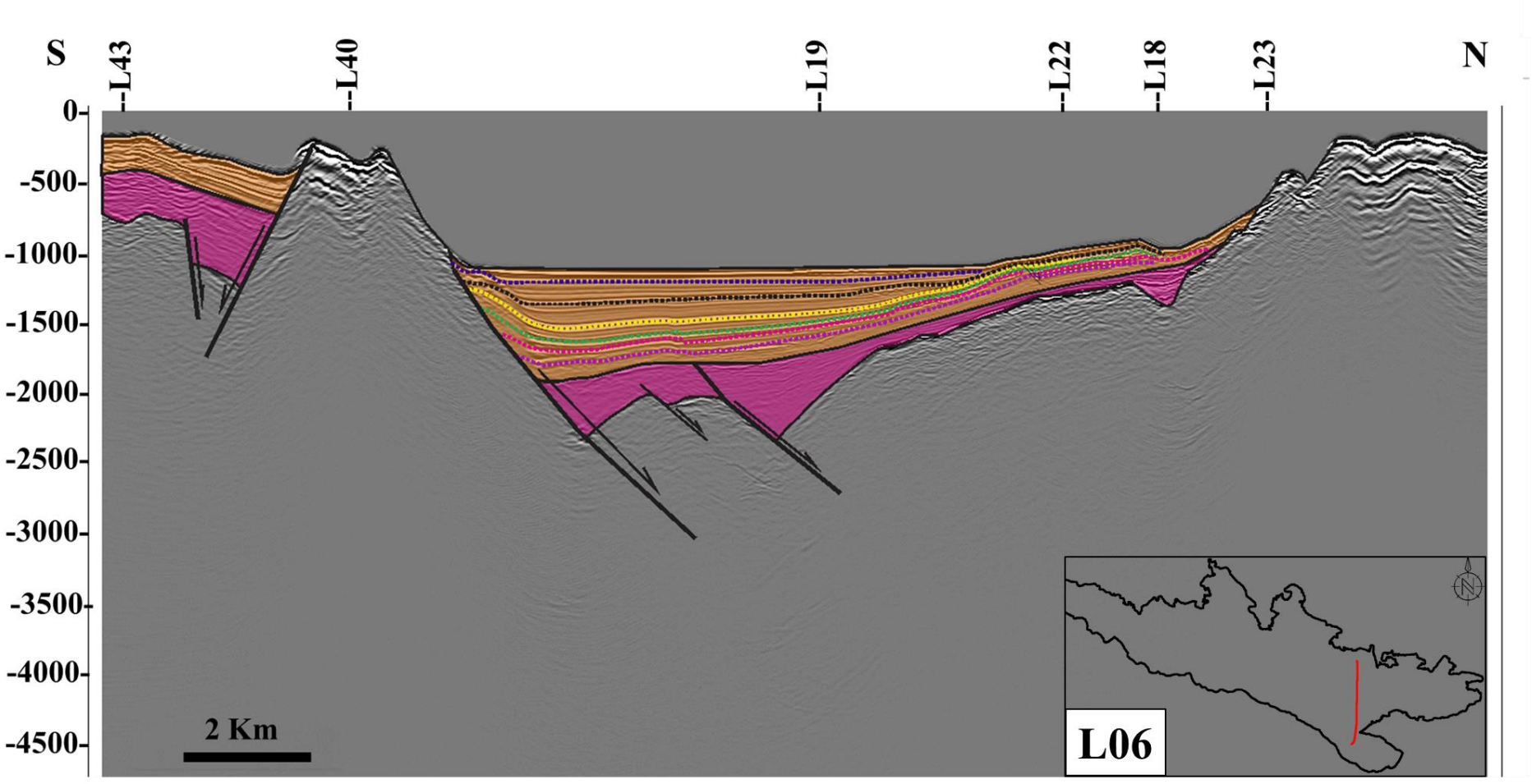
S
--L43
--L40
--L19
--L22
--L18
--L23
N
0
-500
-1000
-1500
-2000
-2500
-3000
-3500
-4000
-4500
2 Km
L06

E
--L38
--L46
--L42
--L37
--L36
--L41
--L35
--L21
--L34
--L20
--L33
--L48
--L32
--L49
--L11
--L13
--L15
--L17
--L10
--L12
--L14
--L16
--L50
--L30
--L24
--L29
--L25
--L28
--L26
--L27
W
0-
-500-
-1000-
-1500-
-2000-
-2500-
-3000-
-3500-
-4000-
-4500-
2 Km
L07

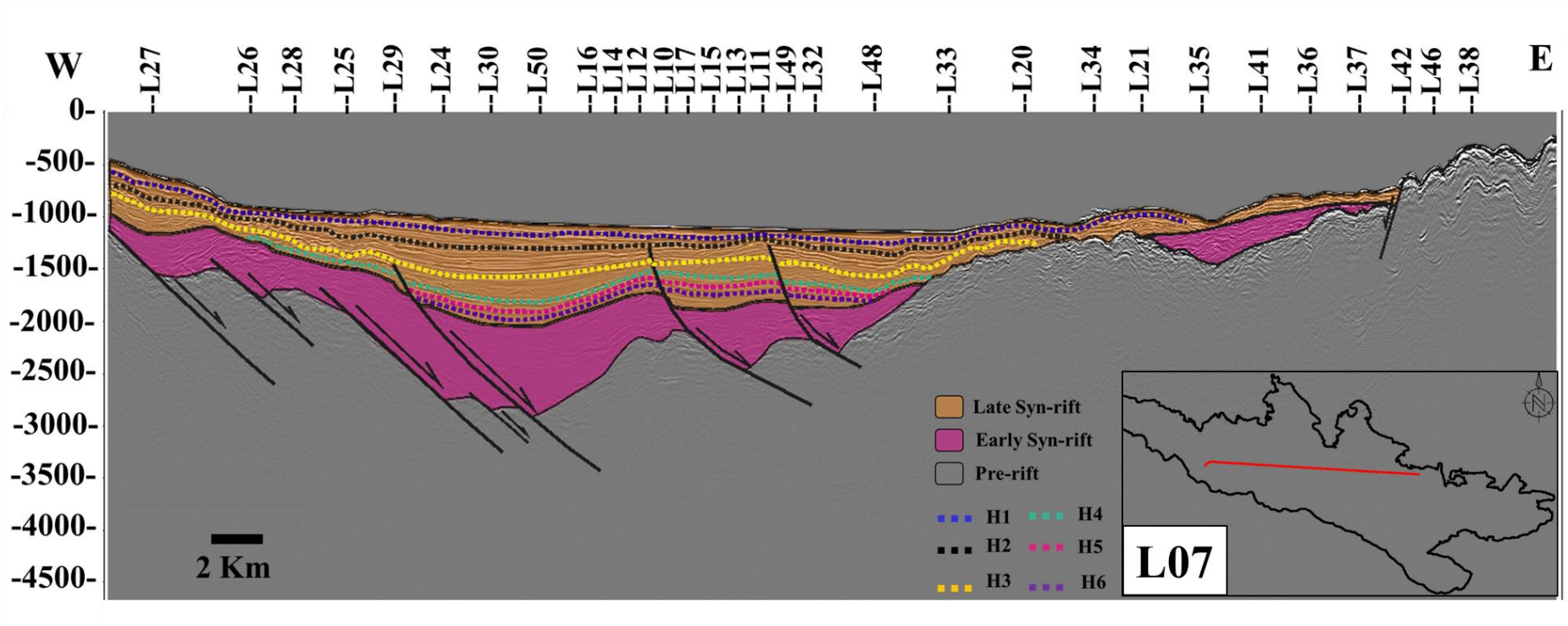
W
E
L27
L26
L28
L25
L29
L24
L30
L50
L16
L14
L12
L10
L17
L15
L13
L11
L49
L32
L48
L33
L20
L34
L21
L35
L41
L36
L37
L42
L46
L38
0-
-500-
-1000-
-1500-
-2000-
-2500-
-3000-
-3500-
-4000-
-4500-
2 Km
Late Syn-rift
Early Syn-rift
Pre-rift
H1
H2
H3
H4
H5
H6
L07

E
L37
L36
L41
L35
L21
L34
L20
L33
L48
L32
L49
L11
L13
L15
L17
L10
L12
L14
L16
L50
L30
L24
L29
L25
L28
L26
L27
W
0-
-500-
-1000-
-1500-
-2000-
-2500-
-300(
-350(
-4000-
-4500-
2 Km
L08

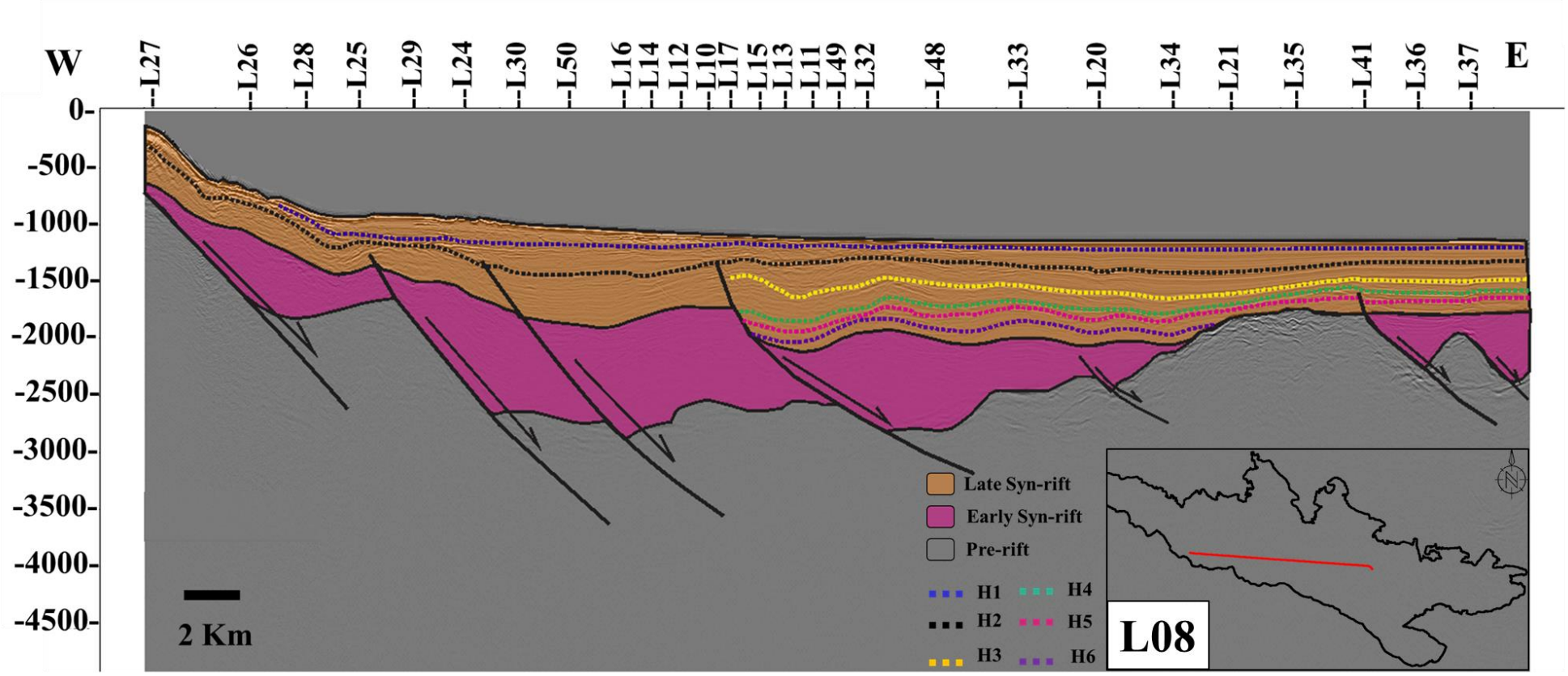
W
E
L27
L26
L28
L25
L29
L24
L30
L50
L16
L14
L12
L10
L17
L15
L13
L11
L49
L32
L48
L33
L20
L34
L21
L35
L41
L36
L37
0-
-500-
-1000-
-1500-
-2000-
-2500-
-3000-
-3500-
-4000-
-4500-
2 Km
Late Syn-rift
Early Syn-rift
Pre-rift
H1
H2
H3
H4
H5
H6
L08

SW
0
-500
-1000
-1500
-2000
-2500
-3000
-3500
-4000
L15
L13
L11
L49
L32
L18
L48
L33
L20
L34
L21a
L35
L41
L36
L37
L22
L42
2 Km
L09

SW
0
-500
-1000
-1500
-2000
-2500
-3000
-3500
-4000
L15
L13
L11
L49
L32
L18
L48
L33
L20
L34
L21a
L35
L41
L36
L37
L22
L42
2 Km
L09

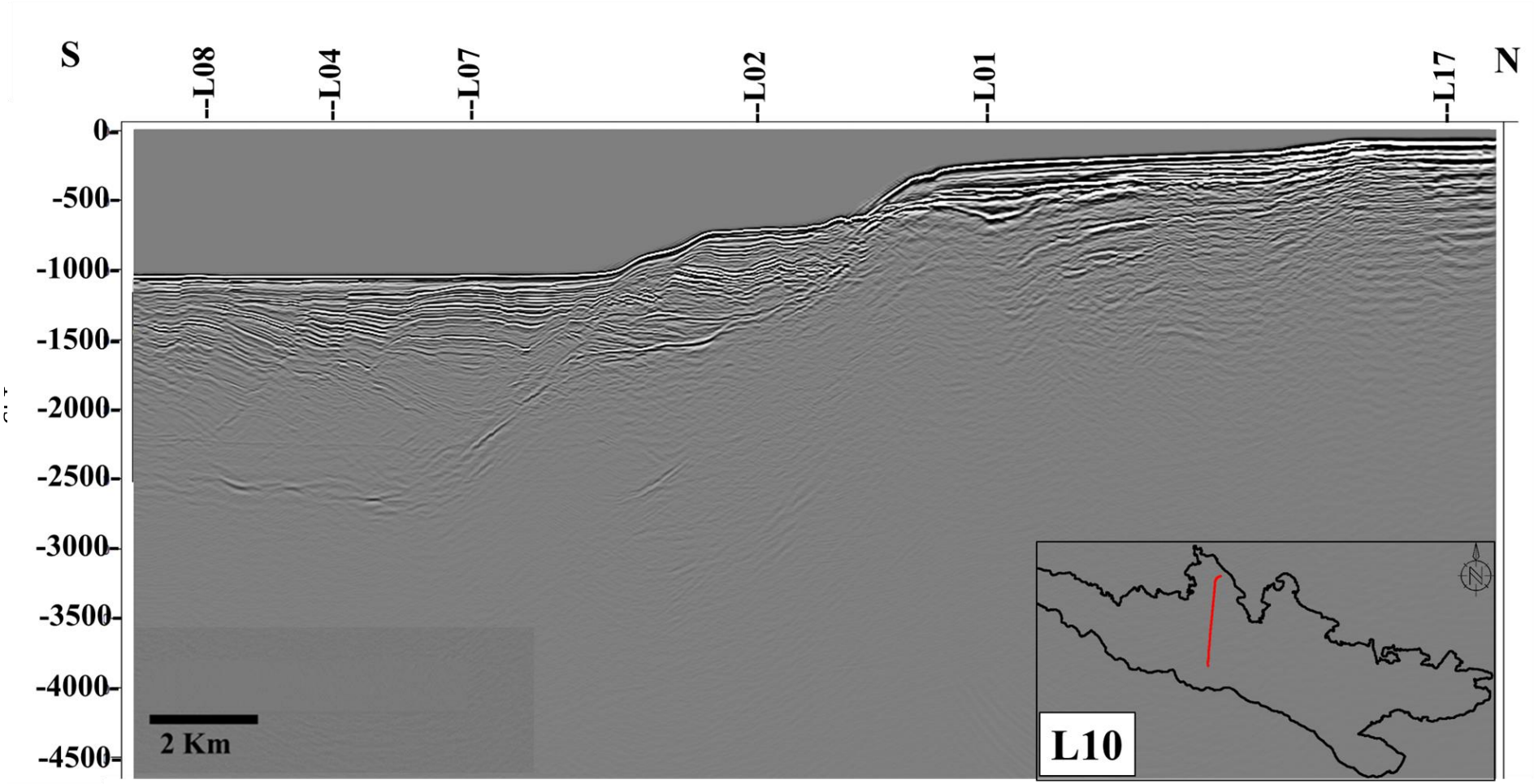
S
--L08
--L04
--L07
--L02
--L01
--L17
N
0
-500
-1000
-1500
-2000
-2500
-3000
-3500
-4000
-4500
2 Km
L10

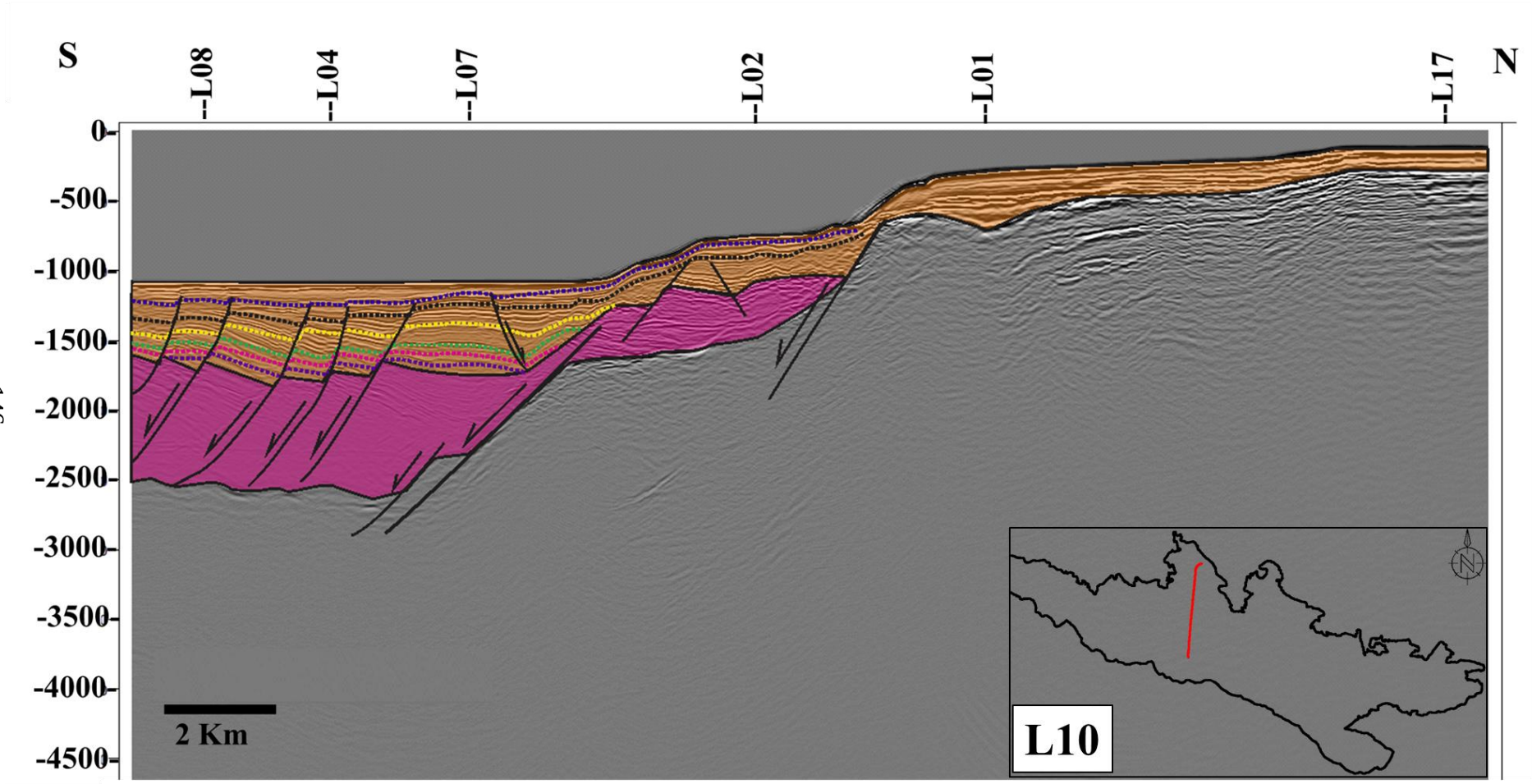
S
--L08
--L04
--L07
--L02
--L01
--L17
N
0
-500
-1000
-1500
-2000
-2500
-3000
-3500
-4000
-4500
2 Km
L10

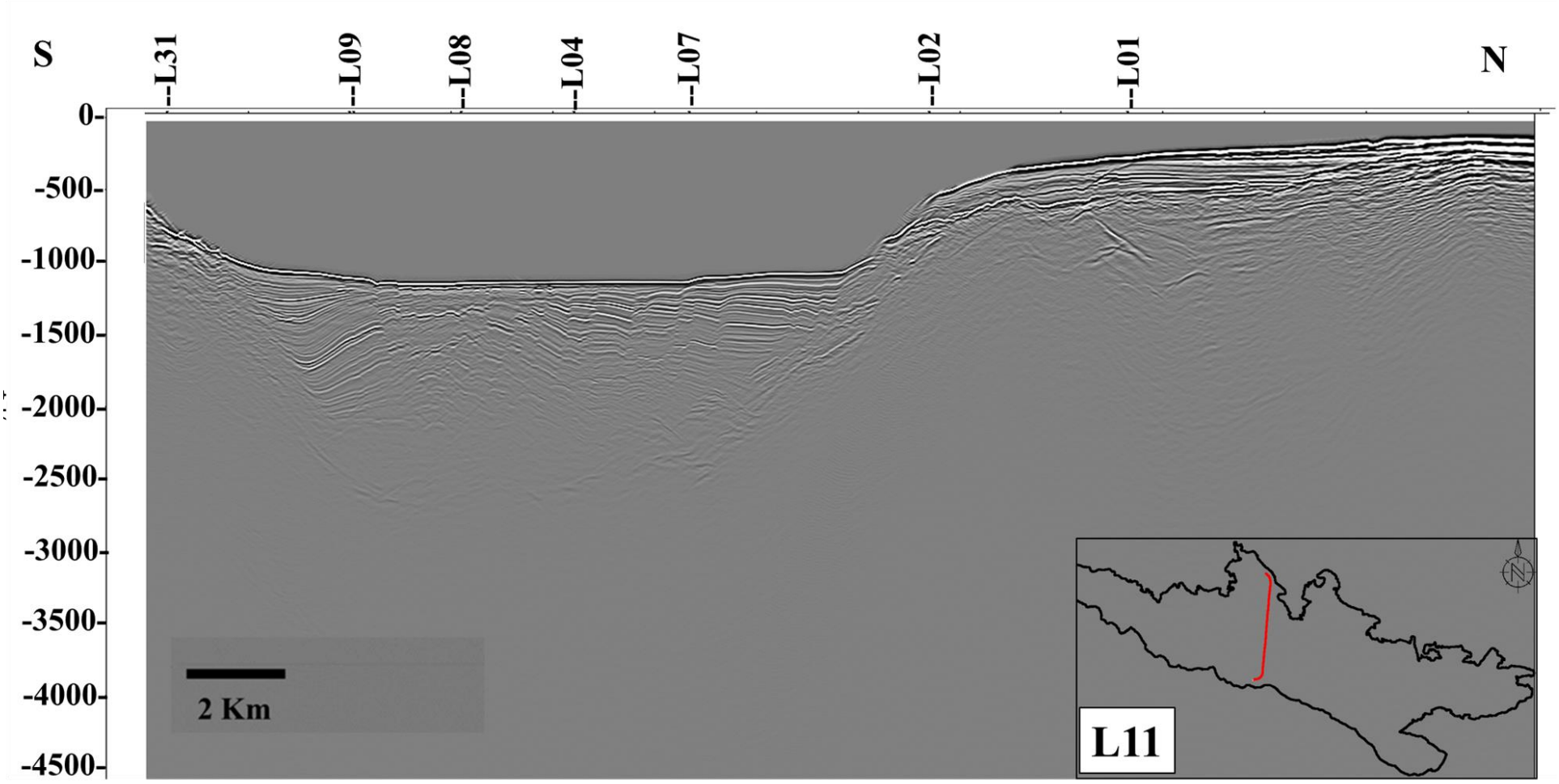
S
L31
L09
L08
L04
L07
L02
L01
N
0
-500
-1000
-1500
-2000
-2500
-3000
-3500
-4000
-4500
2 Km
L11

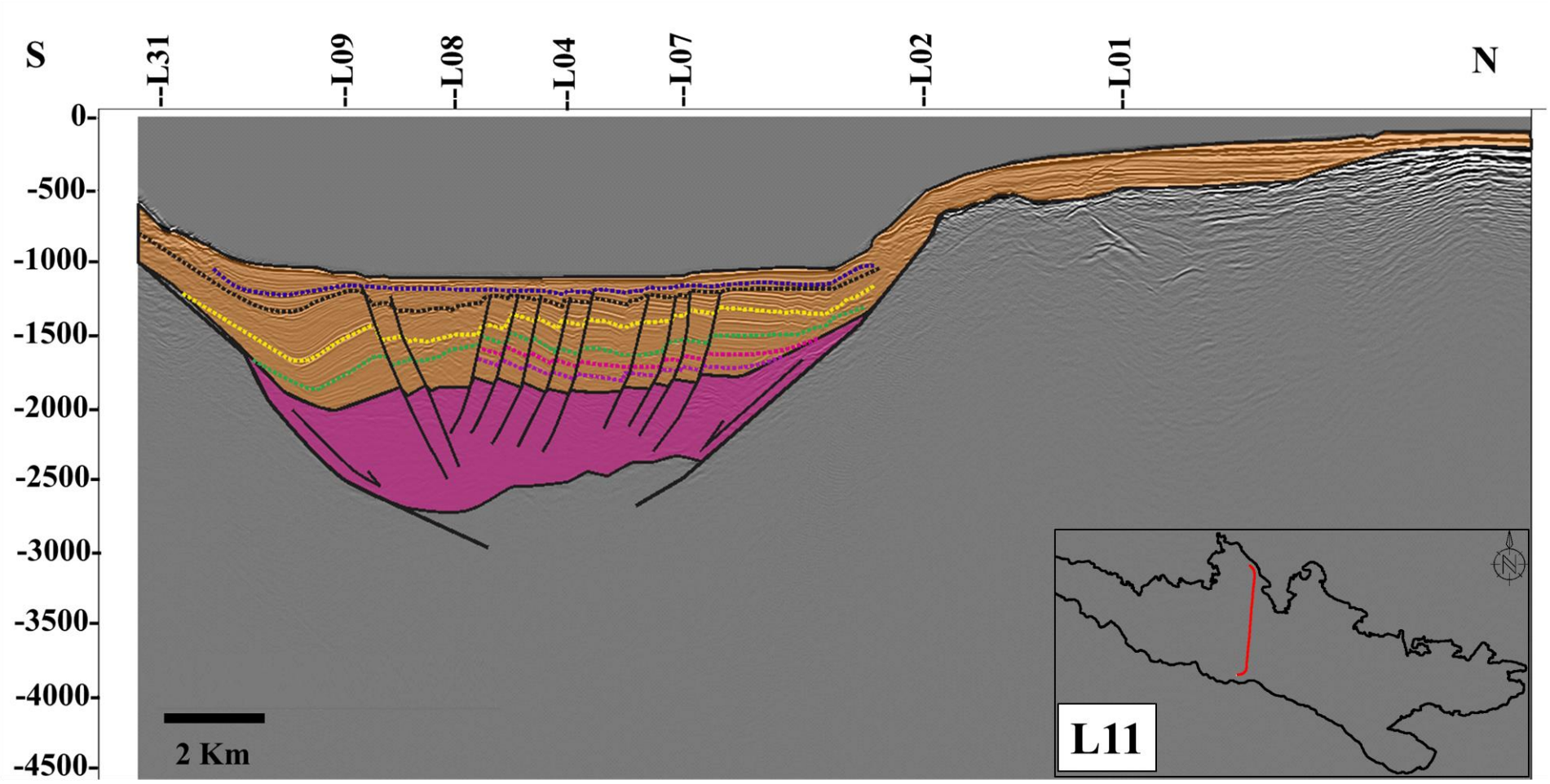
S
--L31
--L09
--L08
--L04
--L07
--L02
--L01
N
0-
-500-
-1000-
-1500-
-2000-
-2500-
-3000-
-3500-
-4000-
-4500-
2 Km
L11

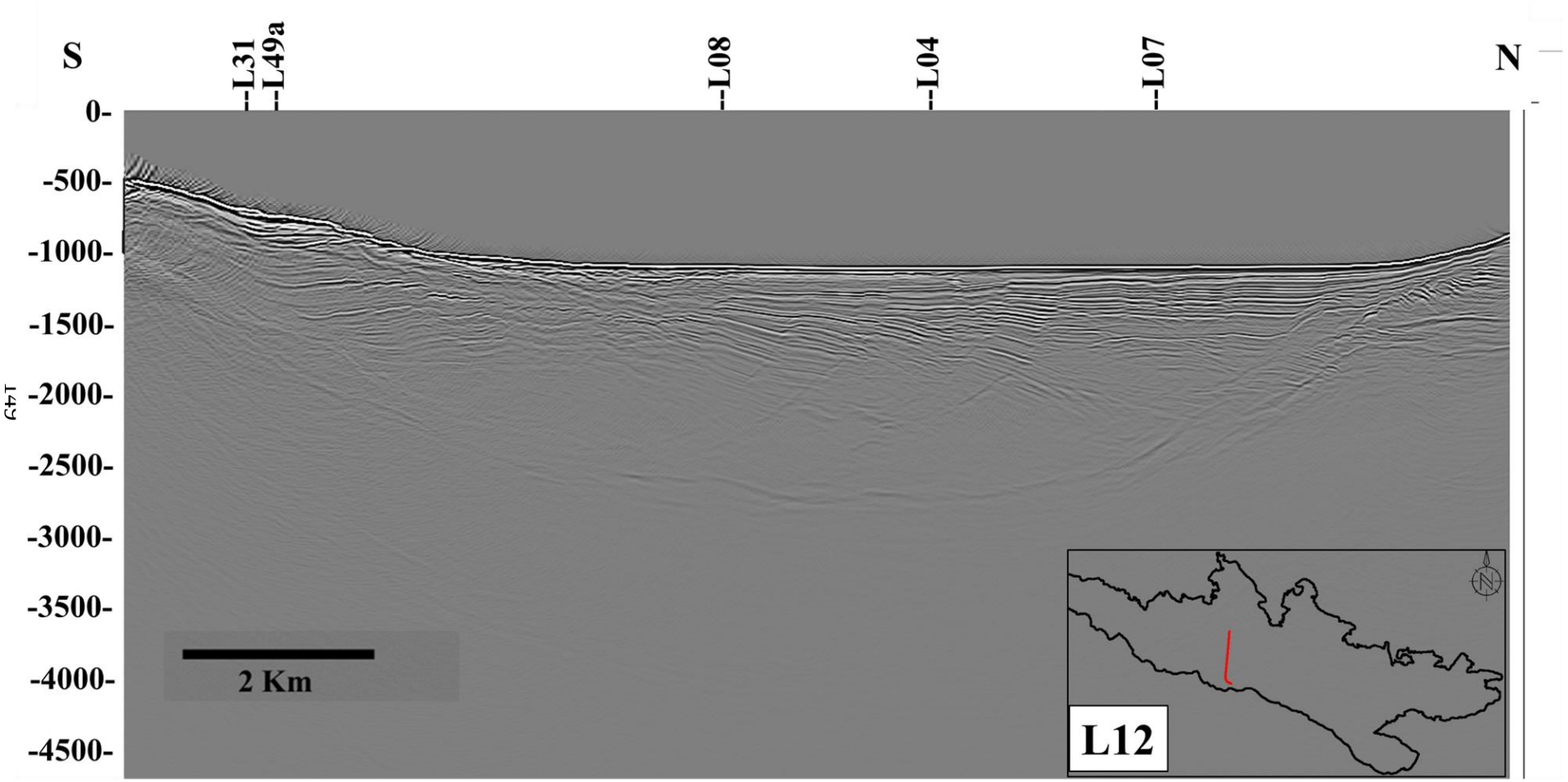
S
--L31
--L49a
--L08
--L04
--L07
N
0-
-500-
-1000-
-1500-
-2000-
-2500-
-3000-
-3500-
-4000-
-4500-
L49
2 Km
L12

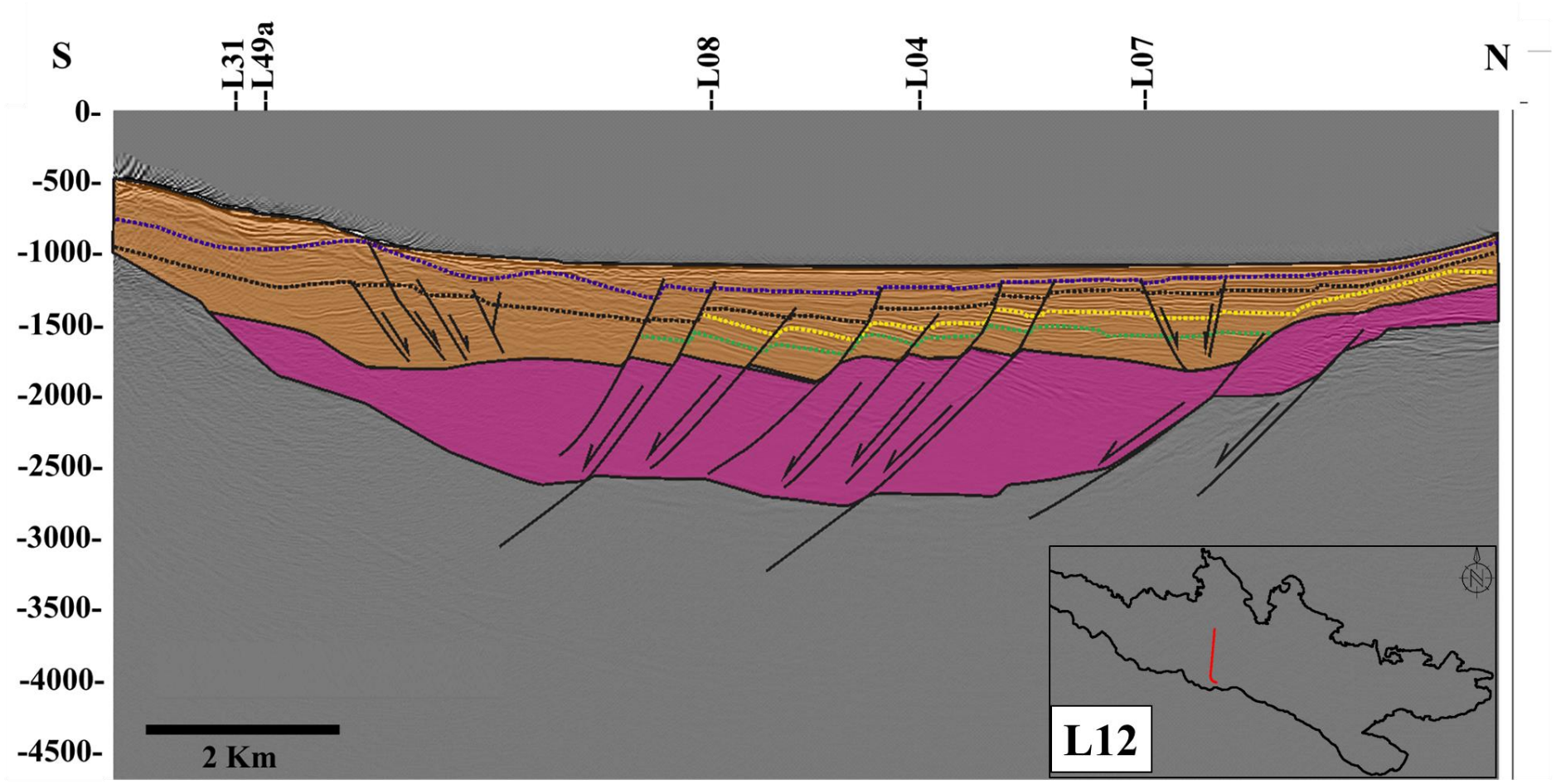
S
--L31
--L49a
--L08
--L04
--L07
N
0-
-500-
-1000-
-1500-
-2000-
-2500-
-3000-
-3500-
-4000-
-4500-
2 Km
L12

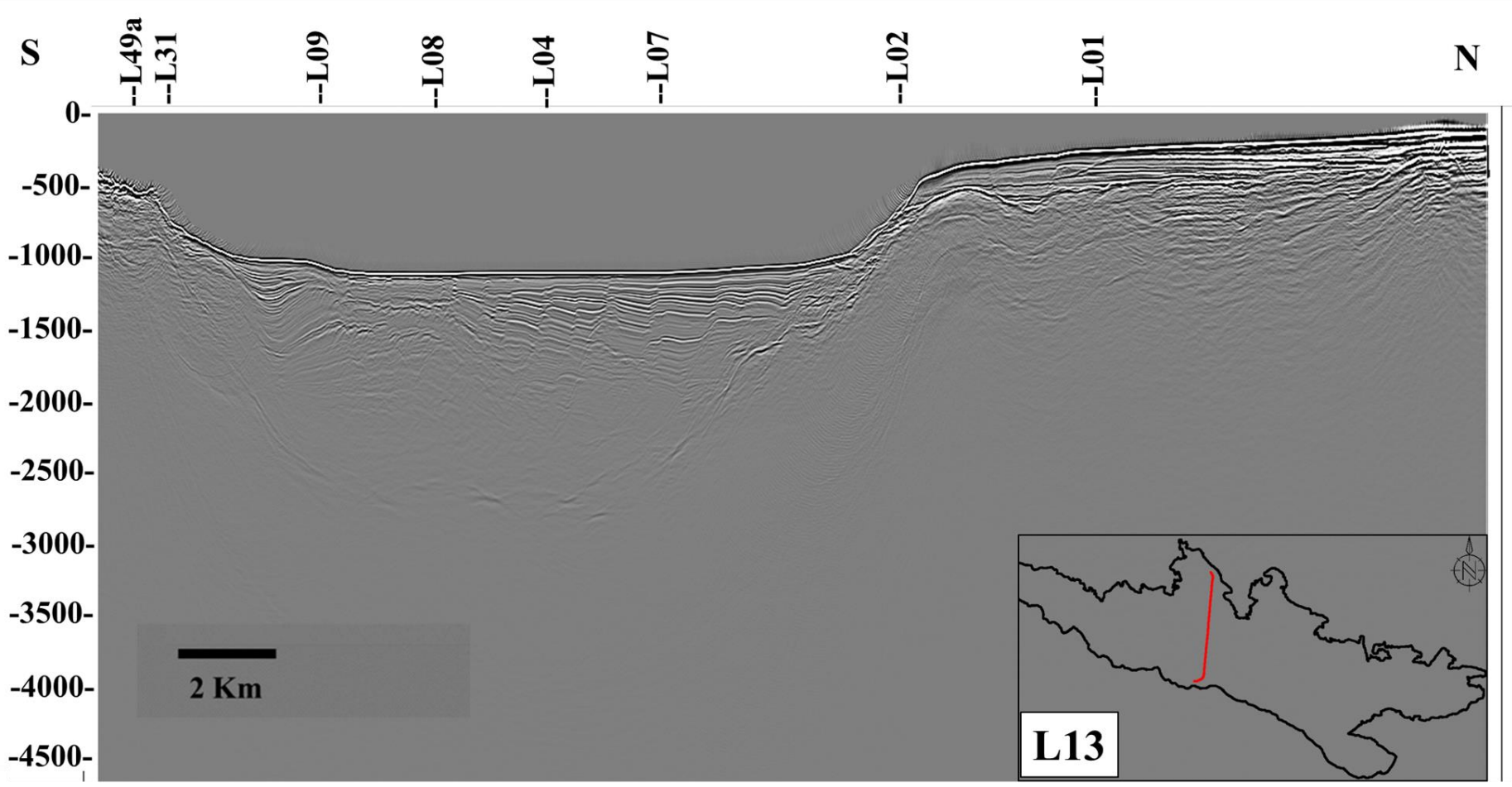
S
--L49a
--L31
--L09
--L08
--L04
--L07
--L02
--L01
N
0-
-500-
-1000-
-1500-
-2000-
-2500-
-3000-
-3500-
-4000-
-4500-
2 Km
L13

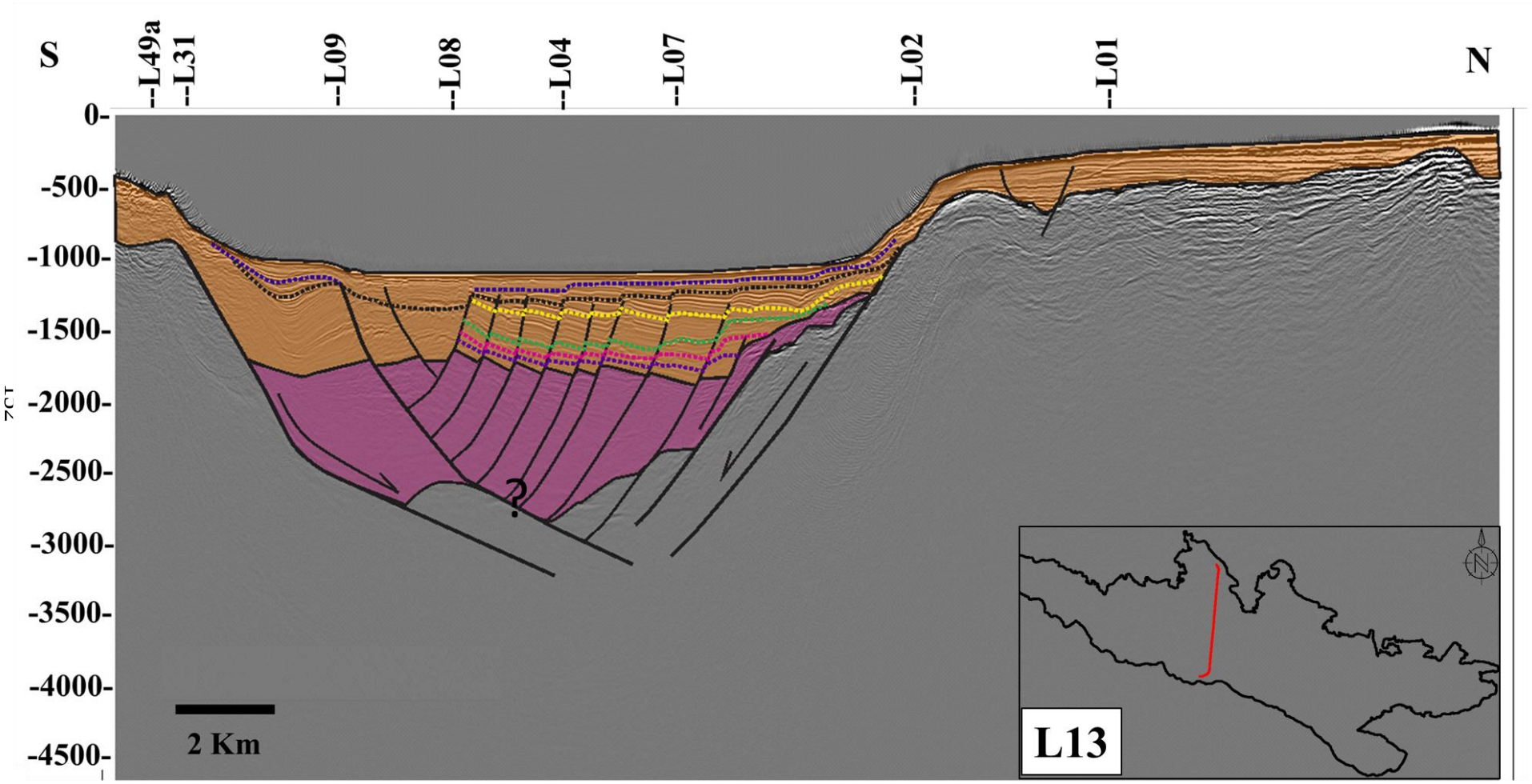
S
--L49a
--L31
--L09
--L08
--L04
--L07
--L02
--L01
N
0-
-500-
-1000-
-1500-
-2000-
-2500-
-3000-
-3500-
-4000-
-4500-
TCT
?
2 Km
L13

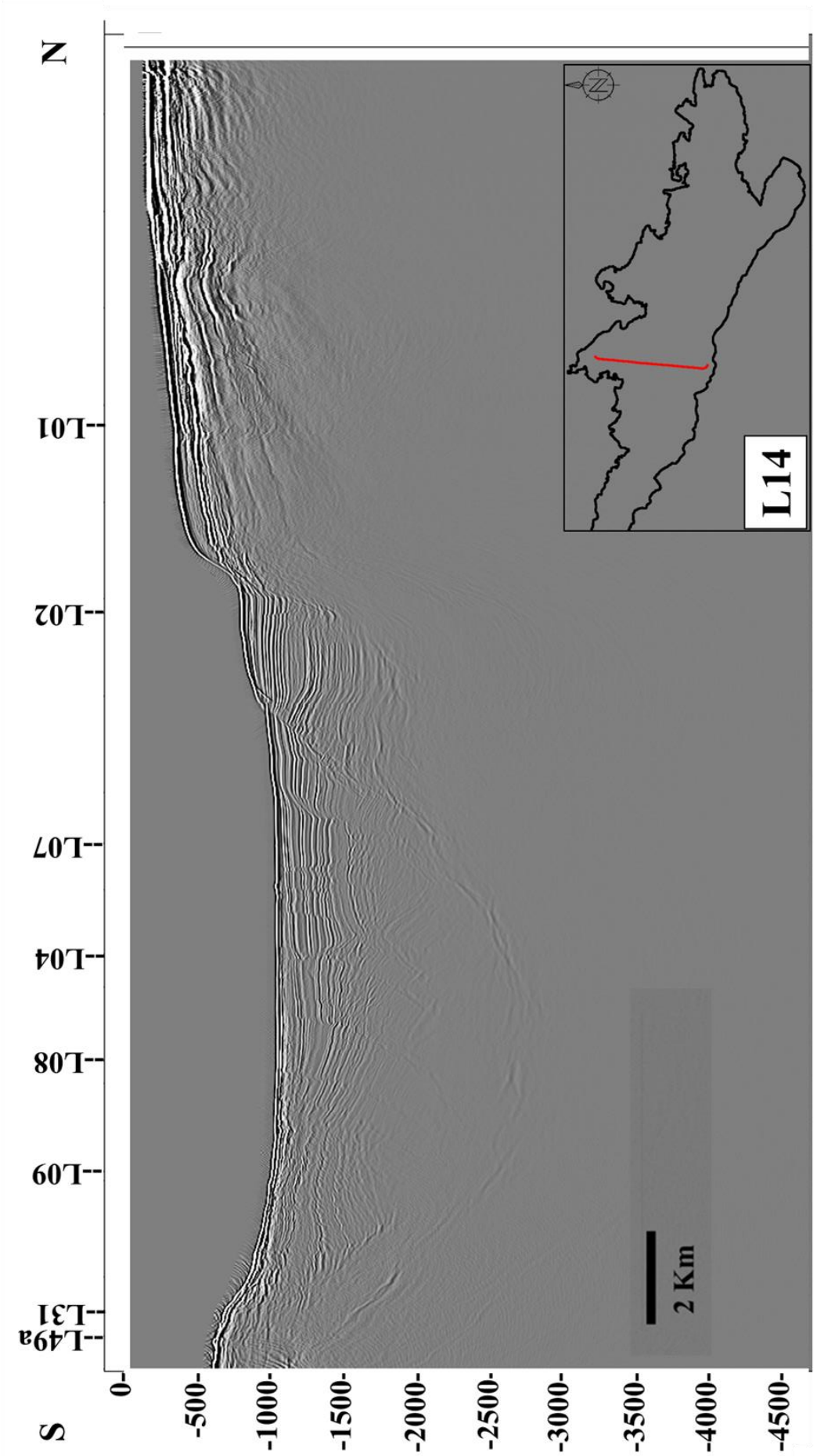
N
L01
L02
L07
L04
L08
L09
L31
L49a
S
0
-500
-1000
-1500
-2000
-2500
-3000
-3500
-4000
-4500
2 Km
L14

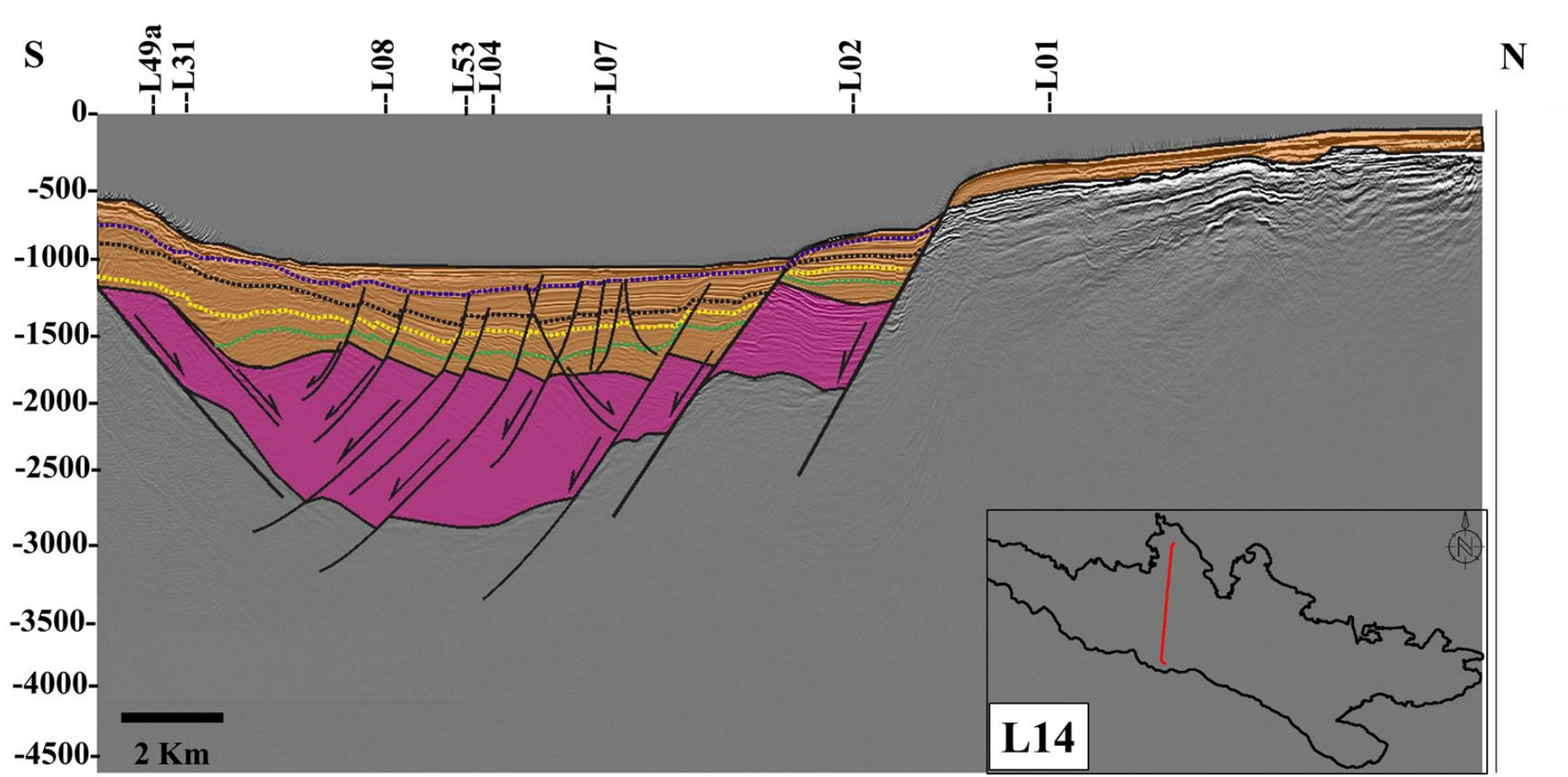
S
N
--L49a
--L31
--L08
--L53
--L04
--L07
--L02
--L01
0
-500
-1000
-1500
-2000
-2500
-3000
-3500
-4000
-4500
2 Km
L14

S
N
0-
-500-
-1000-
-1500-
-2000-
-2500-
-3000-
-3500-
-4000-
-4500-
L49a
L31
L09
L08
L04
L07
L02
L01
2 Km
L15

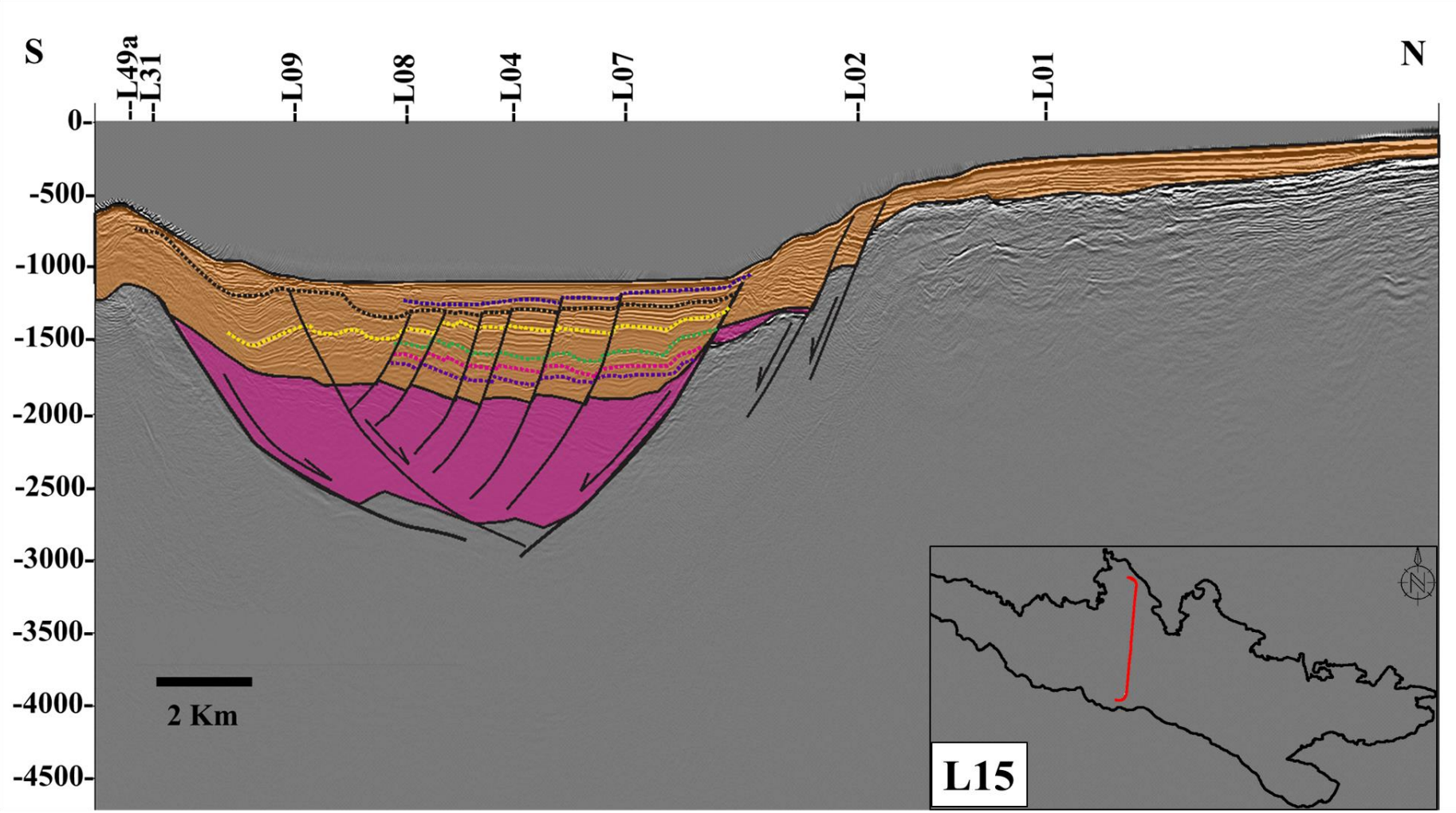
S
--L49a
--L31
--L09
--L08
--L04
--L07
--L02
--L01
N
0
-500
-1000
-1500
-2000
-2500
-3000
-3500
-4000
-4500
2 Km
L15

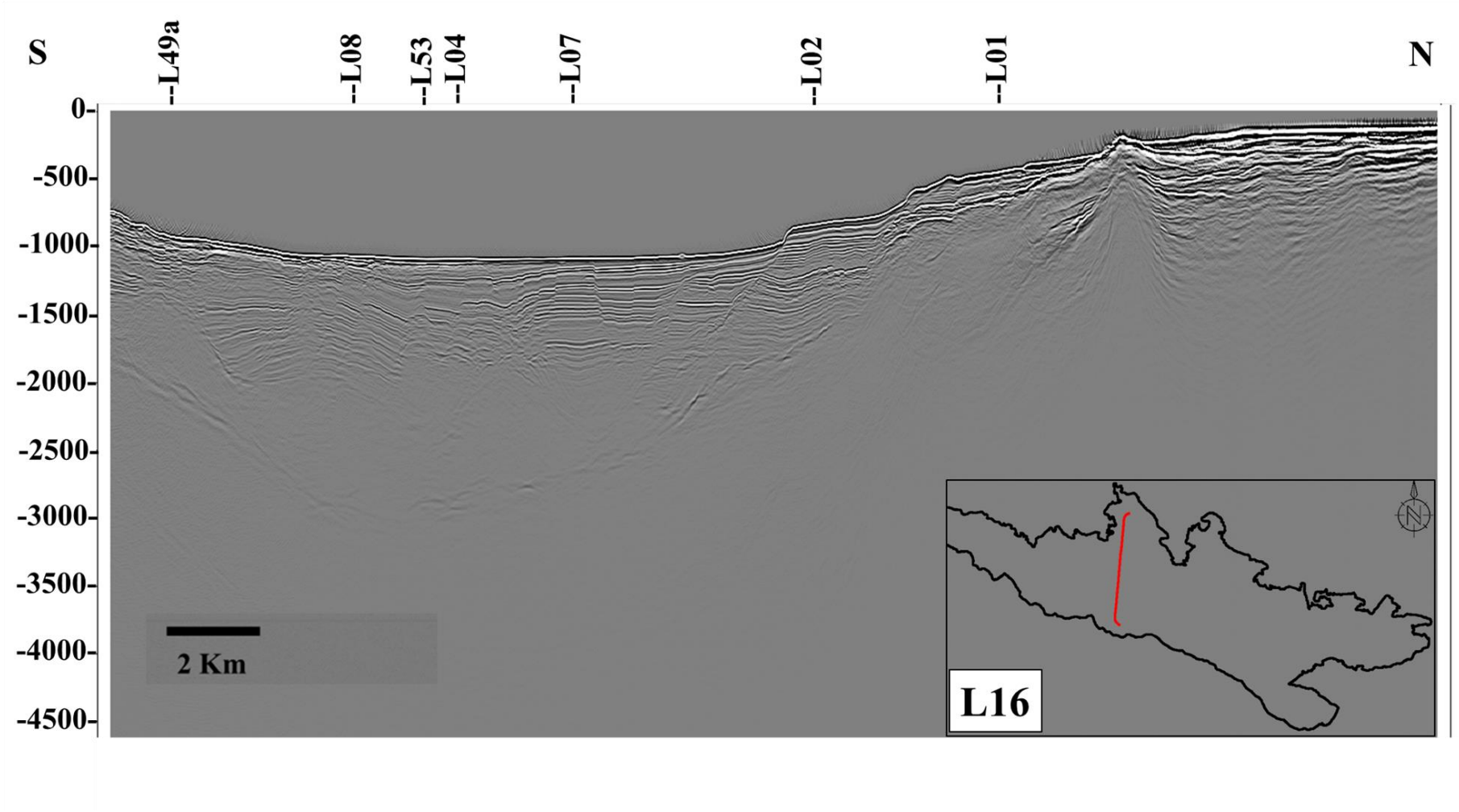
S
--L49a
--L08
--L53
--L04
--L07
--L02
--L01
N
0
-500
-1000
-1500
-2000
-2500
-3000
-3500
-4000
-4500
2 Km
L16

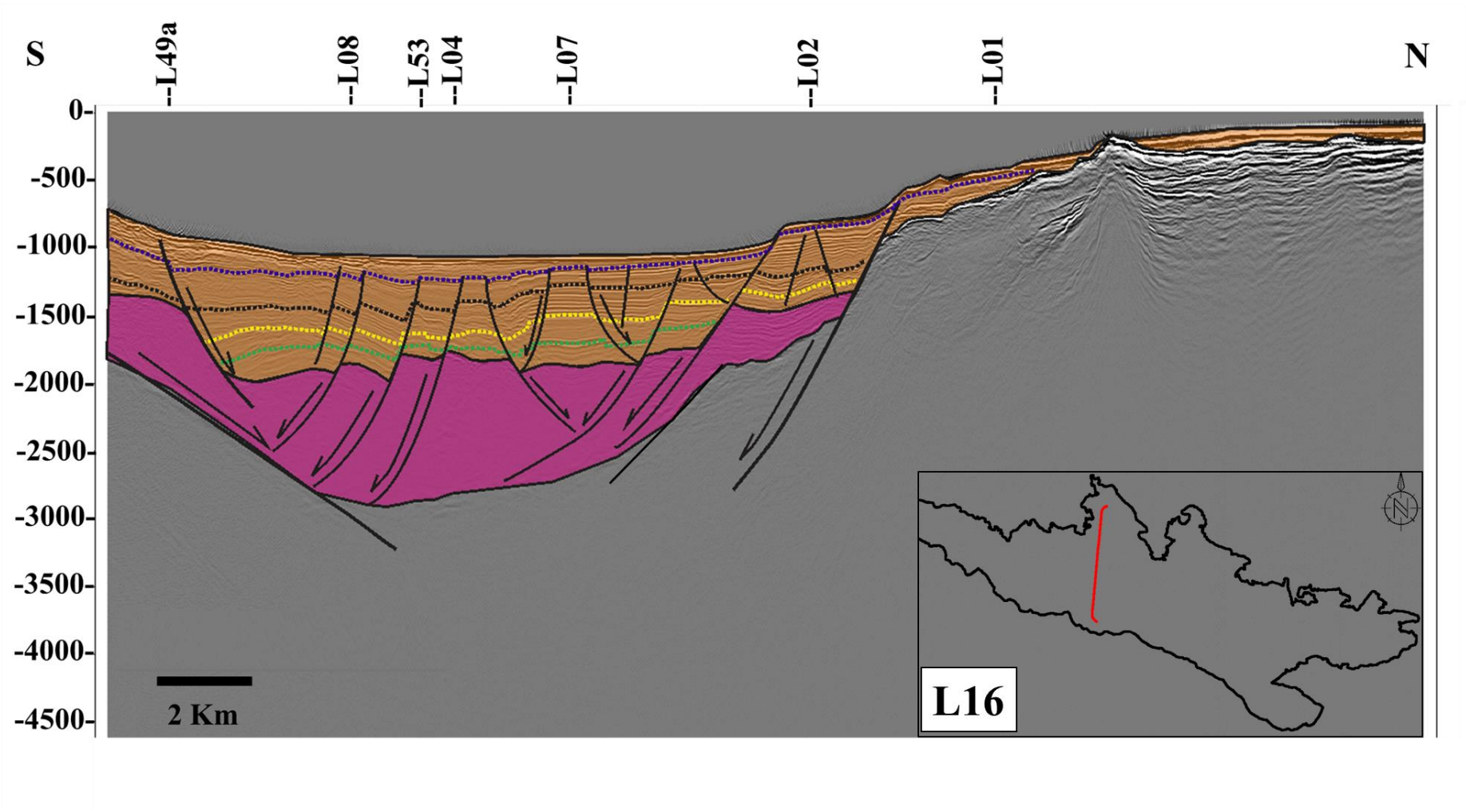
S
--L49a
--L08
--L53
--L04
--L07
--L02
--L01
N
0
-500
-1000
-1500
-2000
-2500
-3000
-3500
-4000
-4500
2 Km
L16

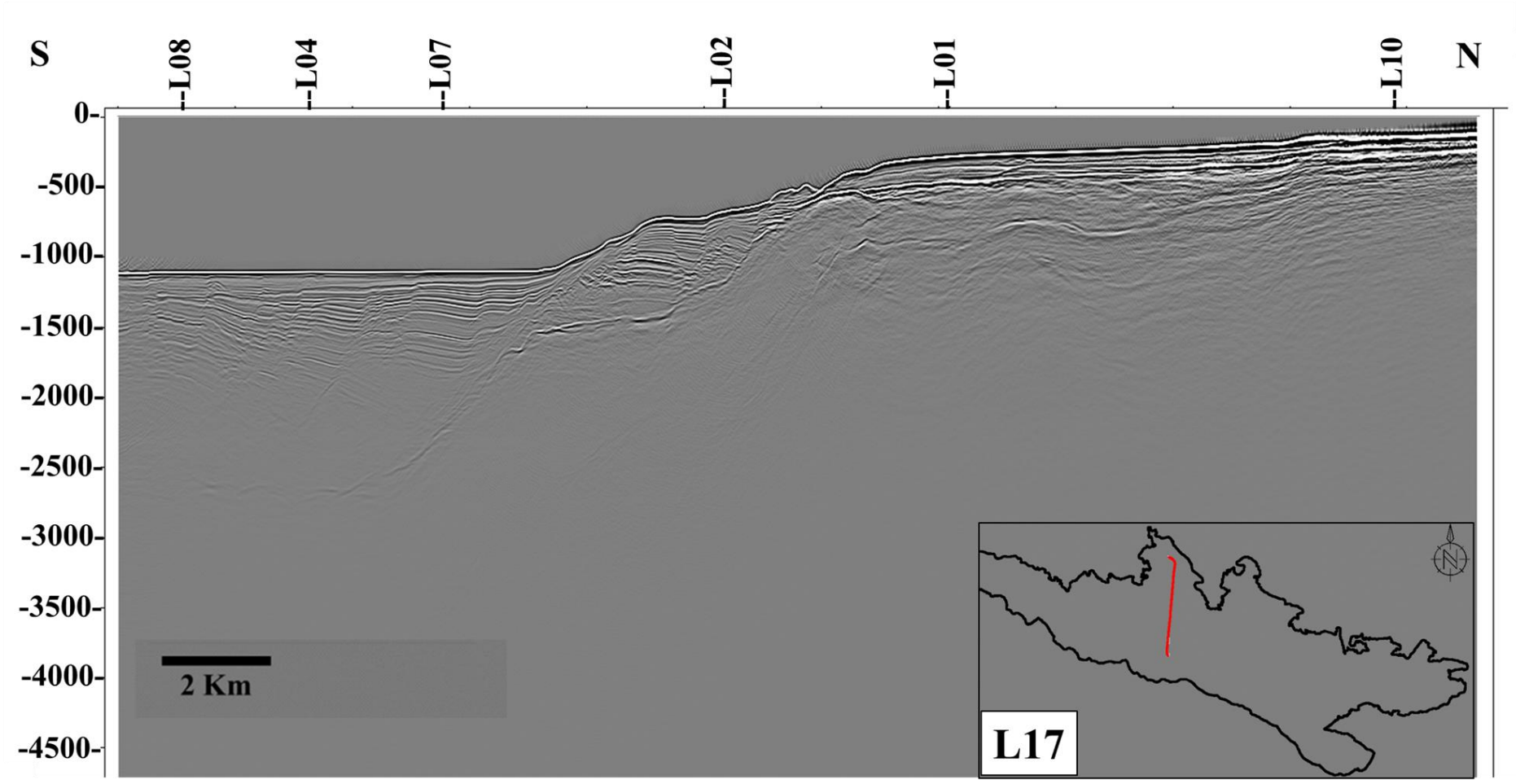
S
L08
L04
L07
L02
L01
L10
N
0
-500
-1000
-1500
-2000
-2500
-3000
-3500
-4000
-4500
2 Km
L17

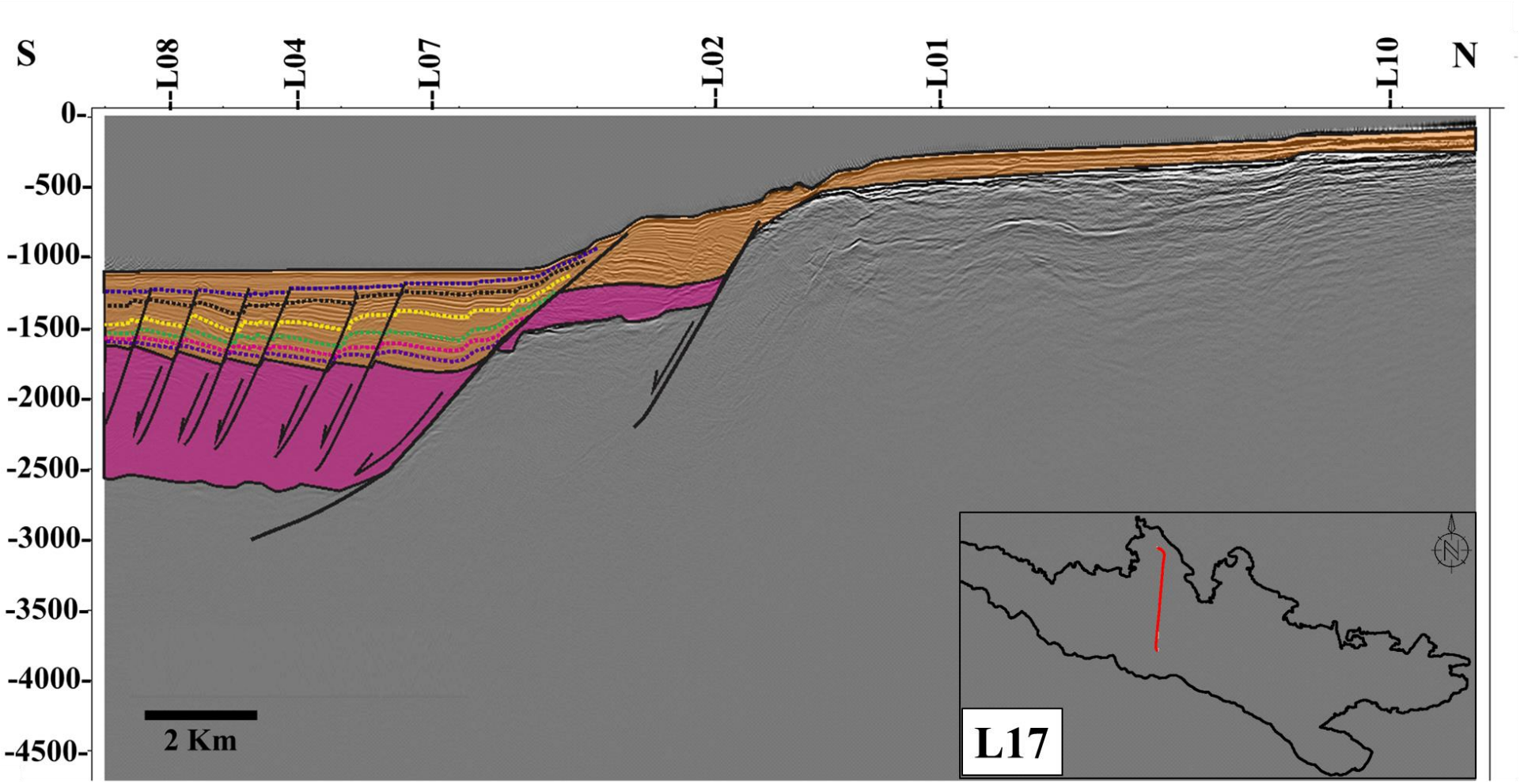
S
L08
L04
L07
L02
L01
L10
N
0
-500
-1000
-1500
-2000
-2500
-3000
-3500
-4000
-4500
2 Km
L17

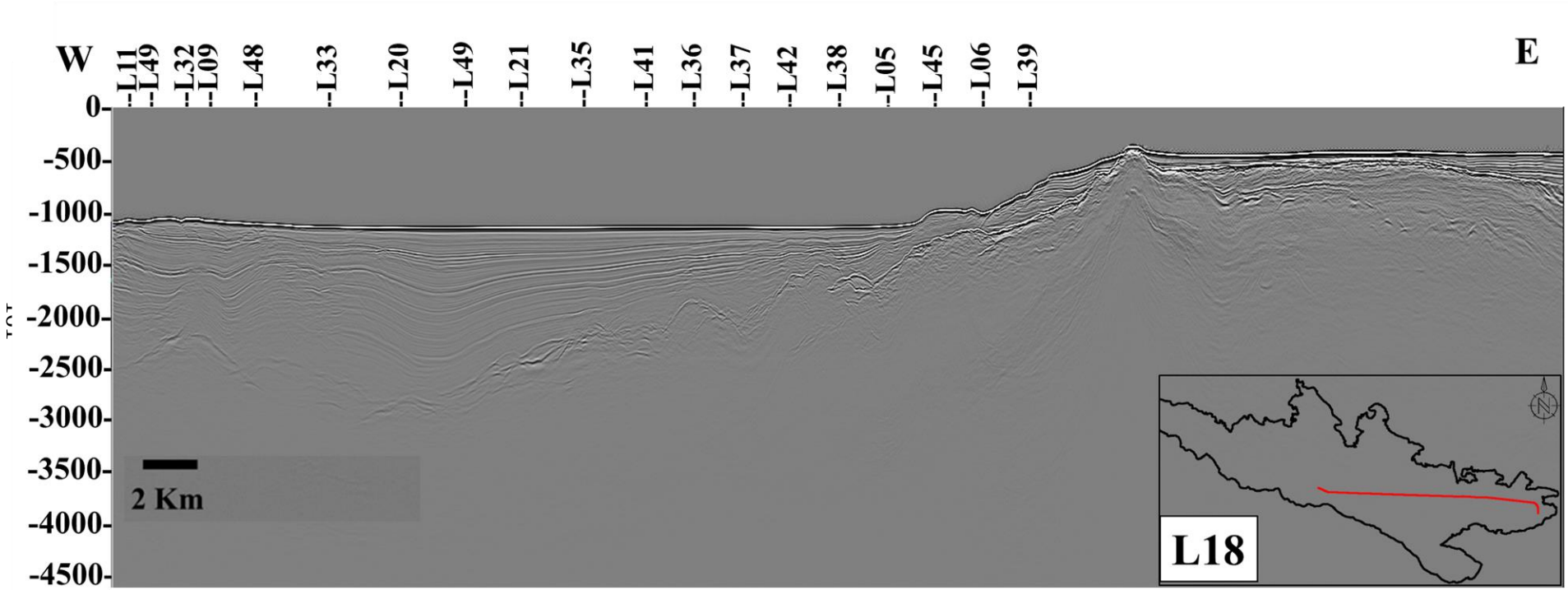
W
E
--L11
--L49
--L32
--L09
--L48
--L33
--L20
--L49
--L21
--L35
--L41
--L36
--L37
--L42
--L38
--L05
--L45
--L06
--L39
0
-500
-1000
-1500
-2000
-2500
-3000
-3500
-4000
-4500
2 Km
L18

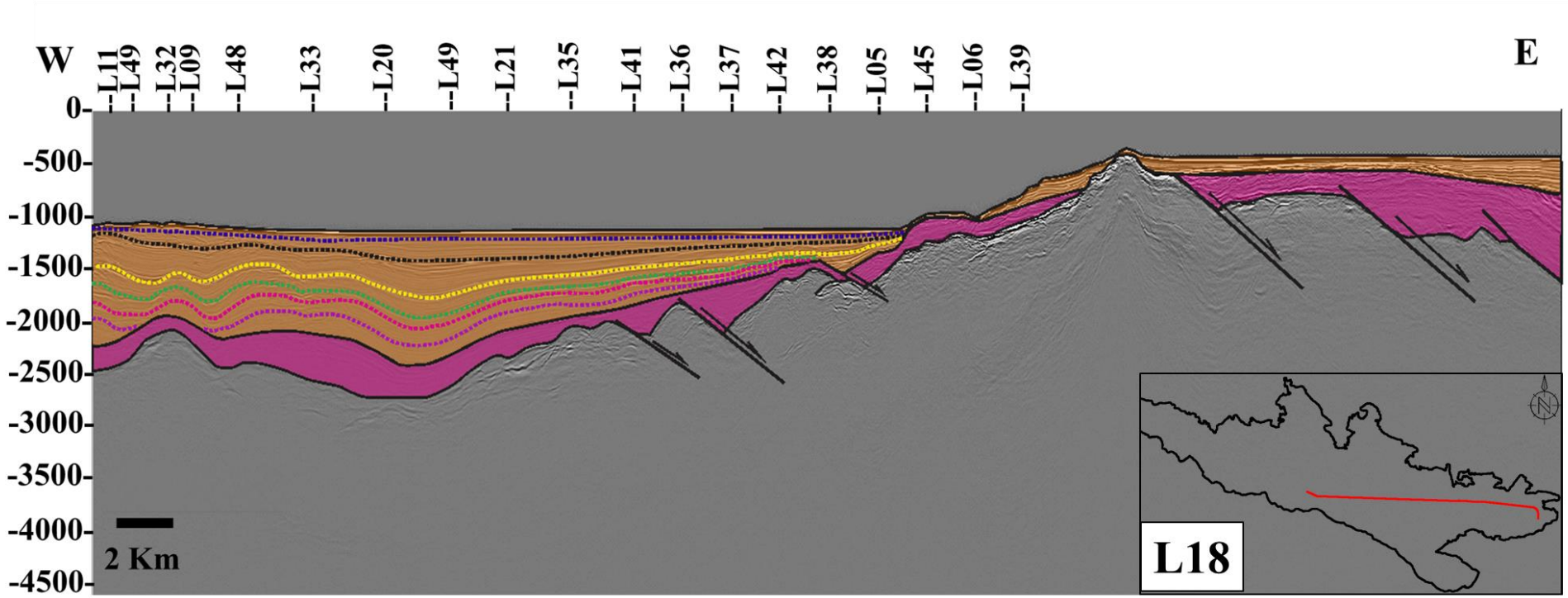
W
E
L11
L49
L32
L09
L48
L33
L20
L49
L21
L35
L41
L36
L37
L42
L38
L05
L45
L06
L39
0
-500
-1000
-1500
-2000
-2500
-3000
-3500
-4000
-4500
2 Km
L18

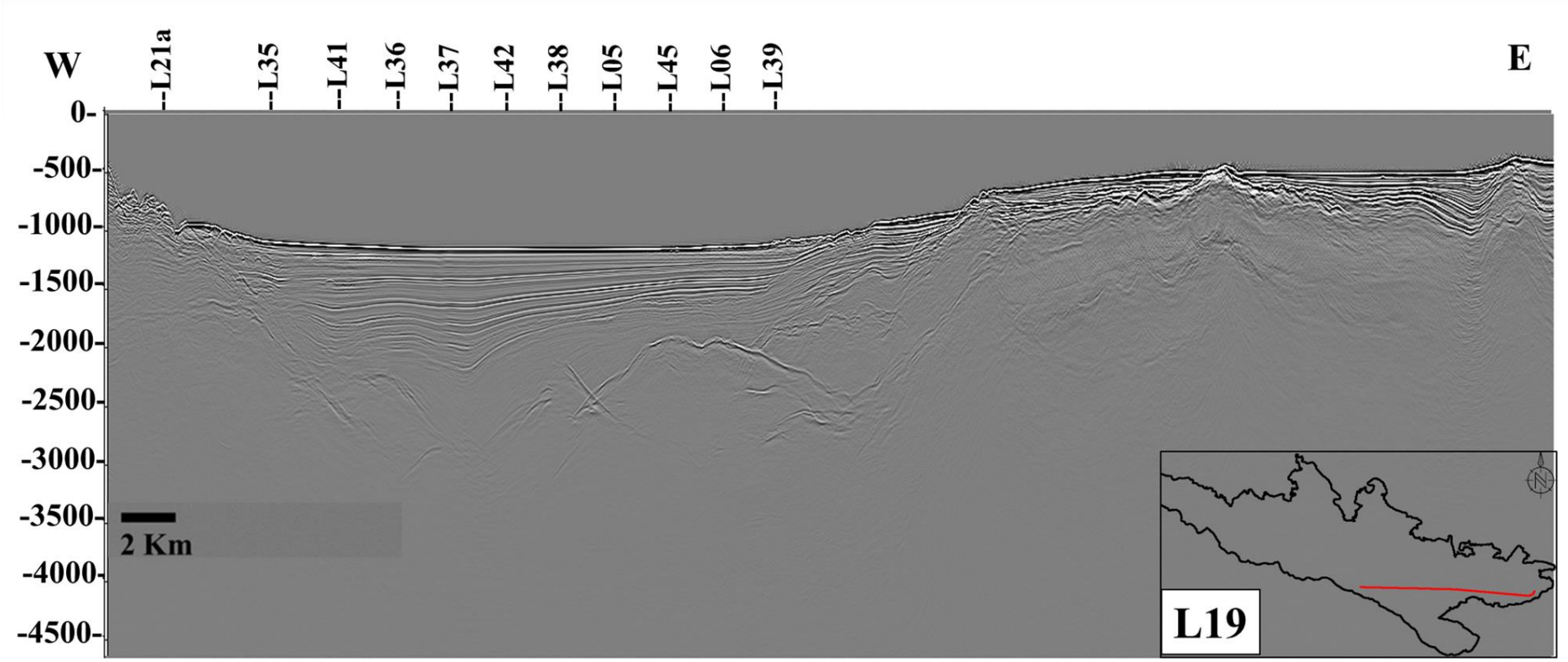
W
E
--L21a
--L35
--L41
--L36
--L37
--L42
--L38
--L05
--L45
--L06
--L39
0-
-500-
-1000-
-1500-
-2000-
-2500-
-3000-
-3500-
-4000-
-4500-
2 Km
L19

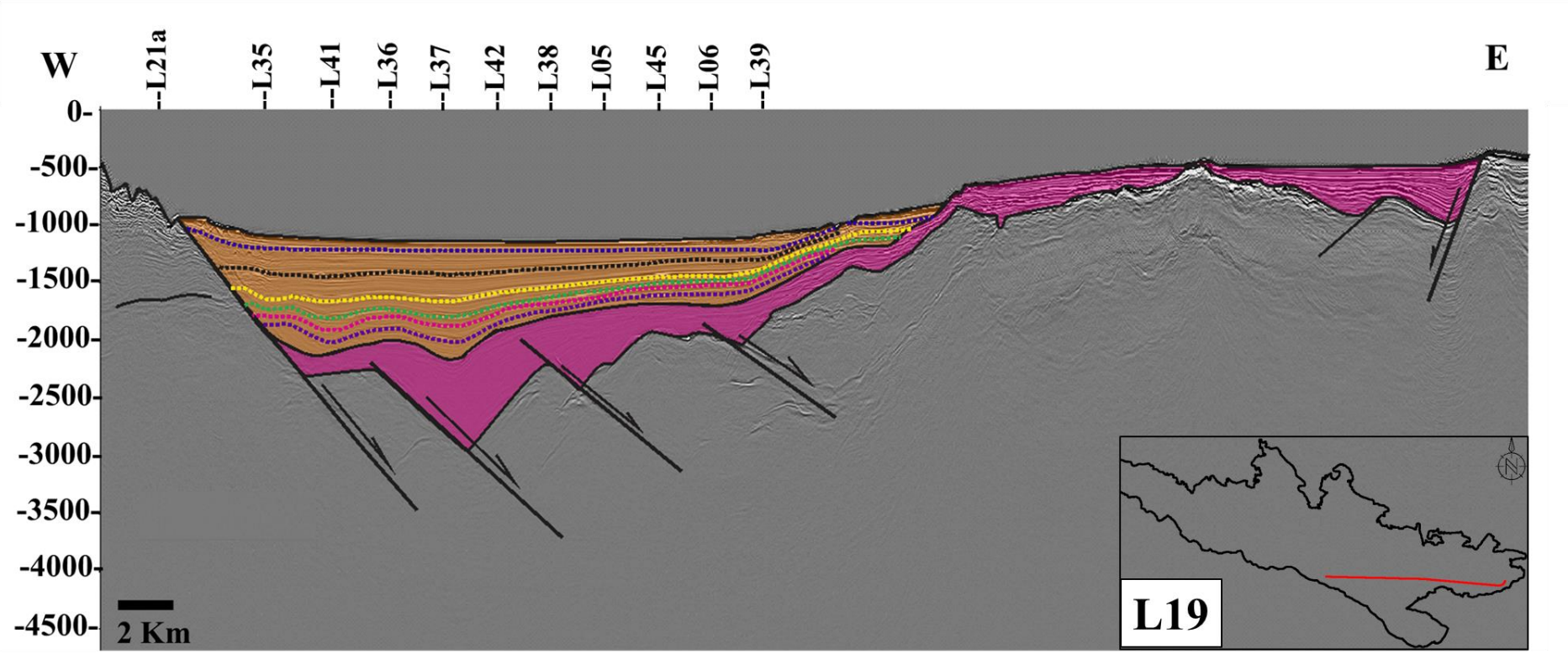
W
E
--L21a
--L35
--L41
--L36
--L37
--L42
--L38
--L05
--L45
--L06
--L39
0-
-500-
-1000-
-1500-
-2000-
-2500-
-3000-
-3500-
-4000-
-4500-
2 Km
L19

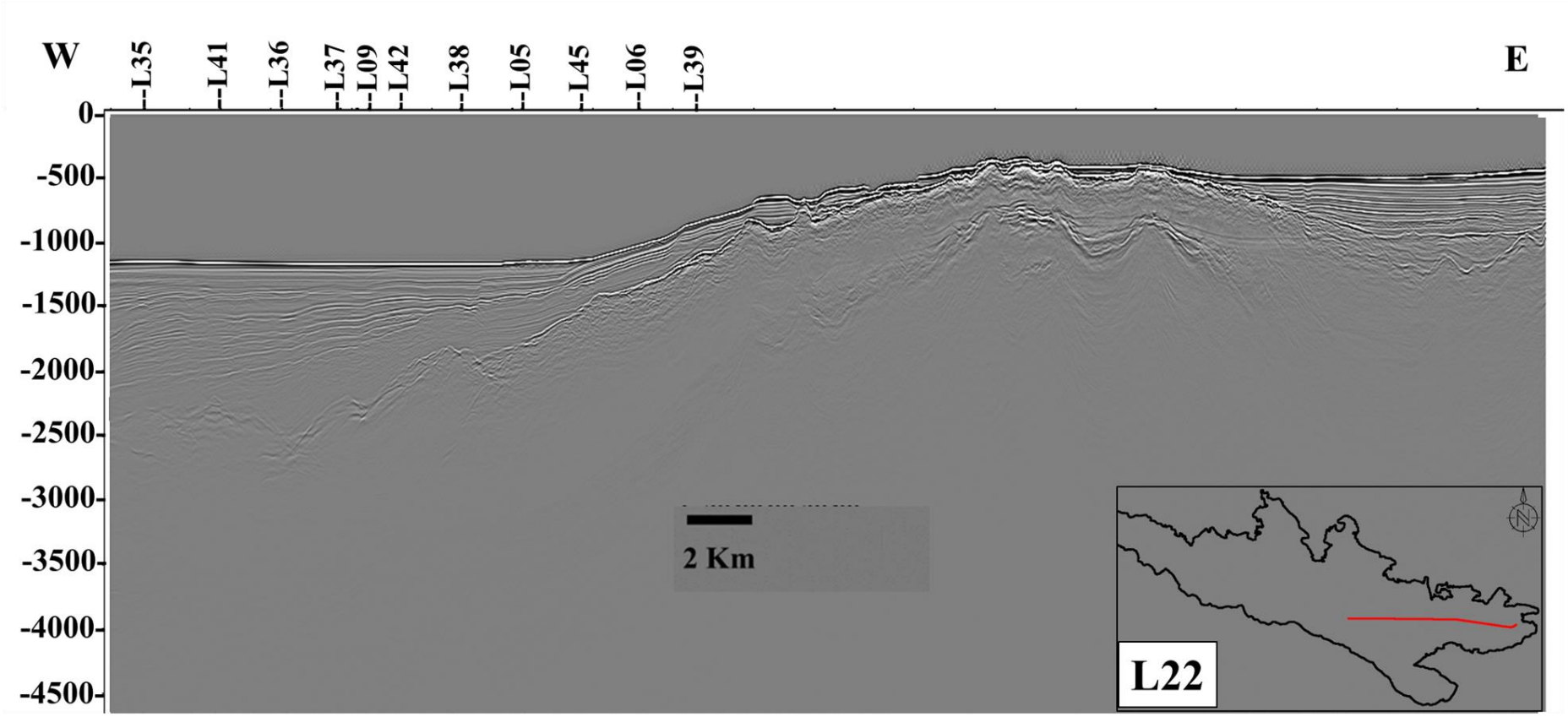
W
E
--L35
--L41
--L36
--L37
--L09
--L42
--L38
--L05
--L45
--L06
--L39
0
-500
-1000
-1500
-2000
-2500
-3000
-3500
-4000
-4500
2 Km
L22

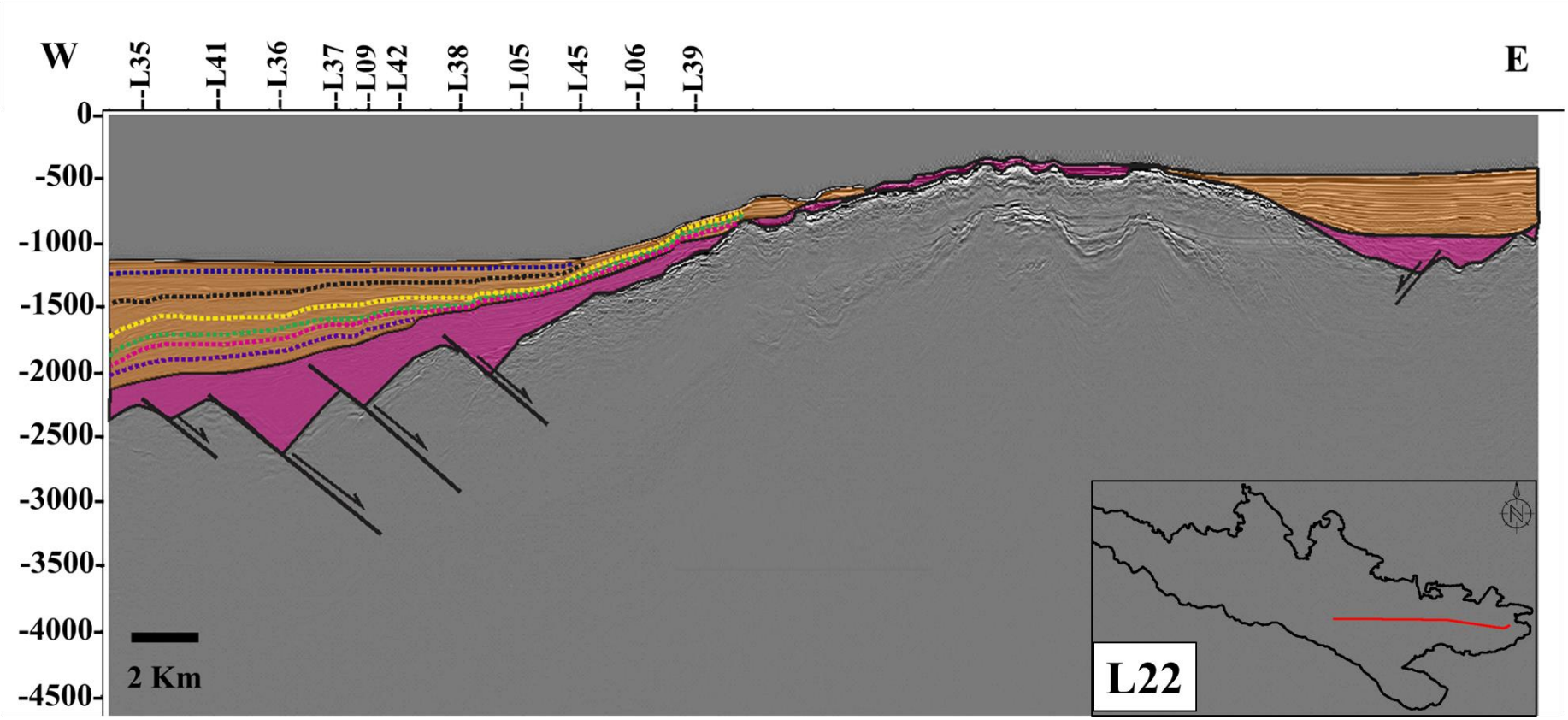
W
E
L35
L41
L36
L37
L09
L42
L38
L05
L45
L06
L39
0
-500
-1000
-1500
-2000
-2500
-3000
-3500
-4000
-4500
2 Km
L22

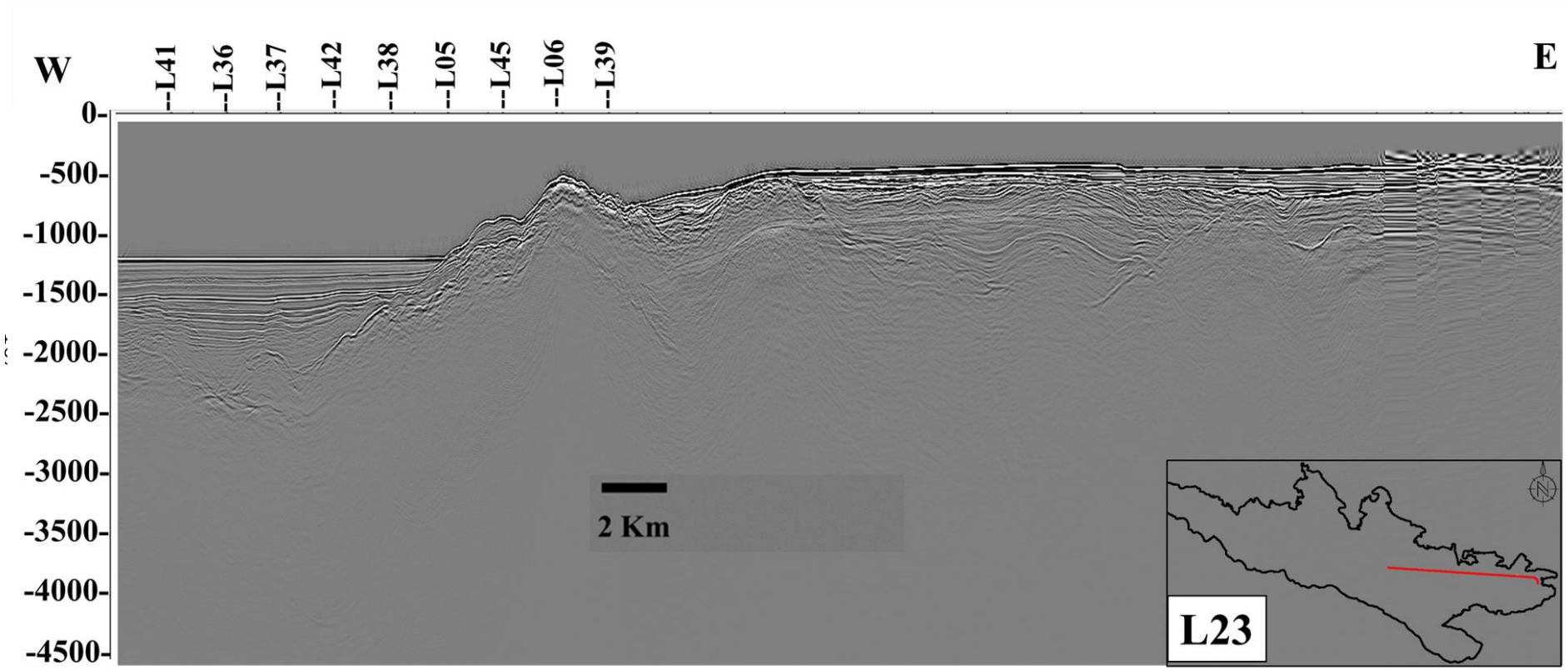
W
E
--L41
--L36
--L37
--L42
--L38
--L05
--L45
--L06
--L39
0-
-500-
-1000-
-1500-
-2000-
-2500-
-3000-
-3500-
-4000-
-4500-
2 Km
L23

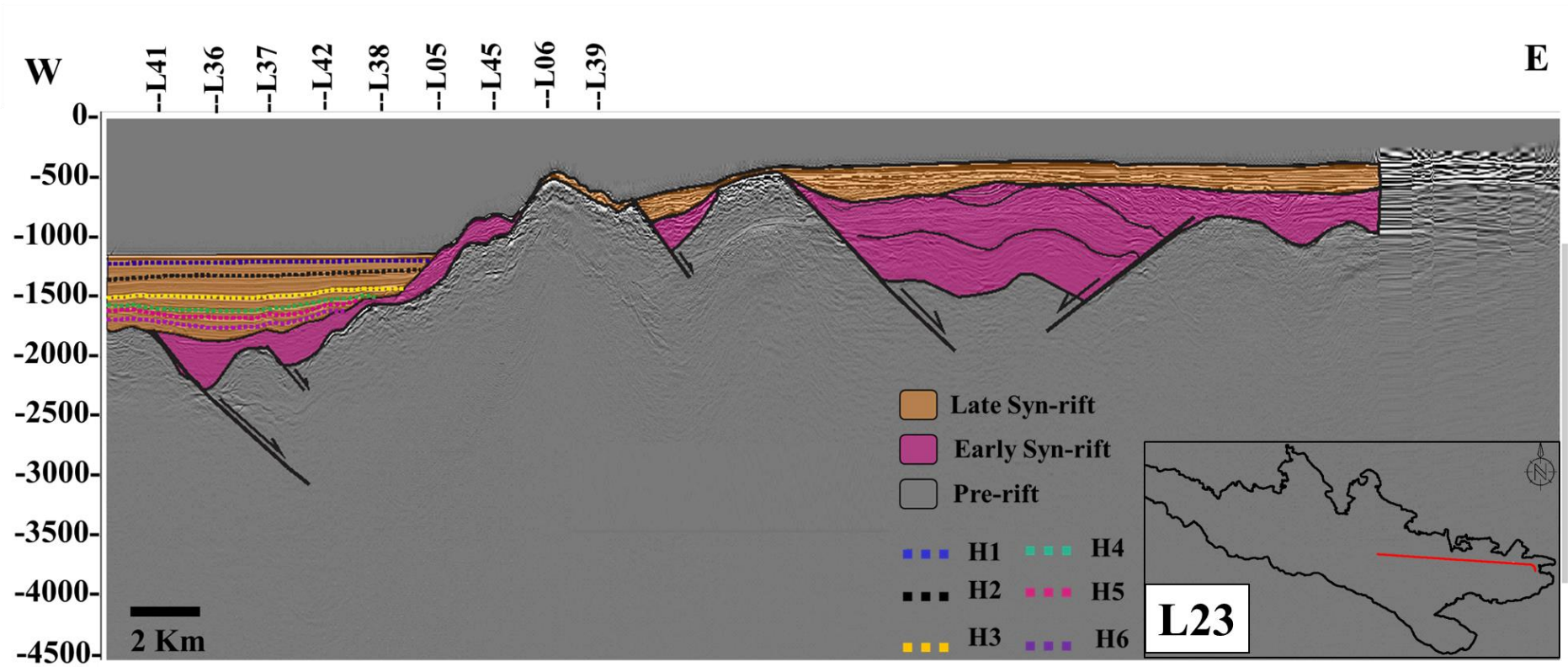
W
E
--L41
--L36
--L37
--L42
--L38
--L05
--L45
--L06
--L39
0-
-500-
-1000-
-1500-
-2000-
-2500-
-3000-
-3500-
-4000-
-4500-
2 Km
Late Syn-rift
Early Syn-rift
Pre-rift
H1
H2
H3
H4
H5
H6
L23

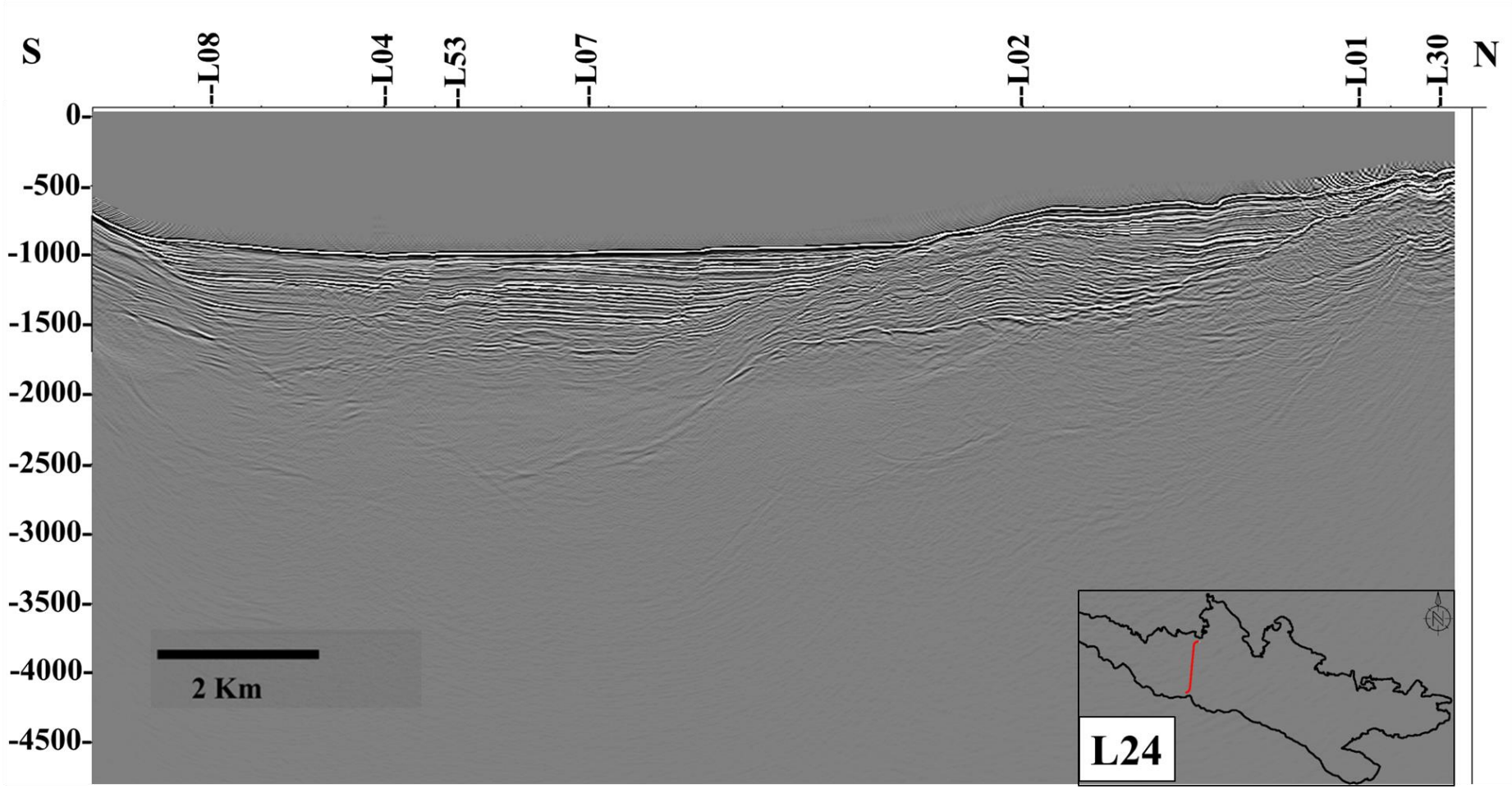
S
L08
L04
L53
L07
L02
L01
L30
N
0
-500
-1000
-1500
-2000
-2500
-3000
-3500
-4000
-4500
2 Km
L24

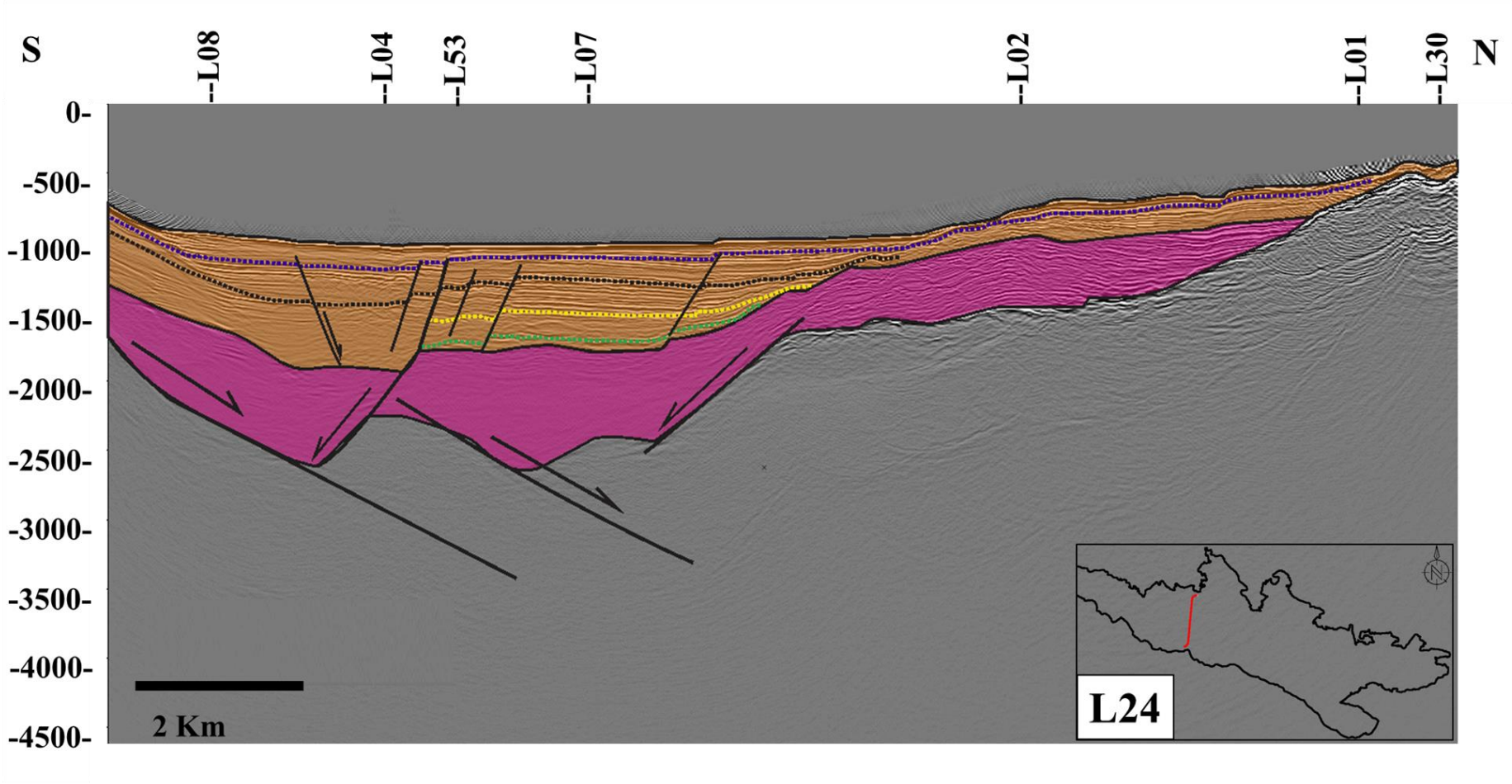
S
--L08
--L04
--L53
--L07
--L02
--L01
--L30
N
0-
-500-
-1000-
-1500-
-2000-
-2500-
-3000-
-3500-
-4000-
-4500-
2 Km
L24

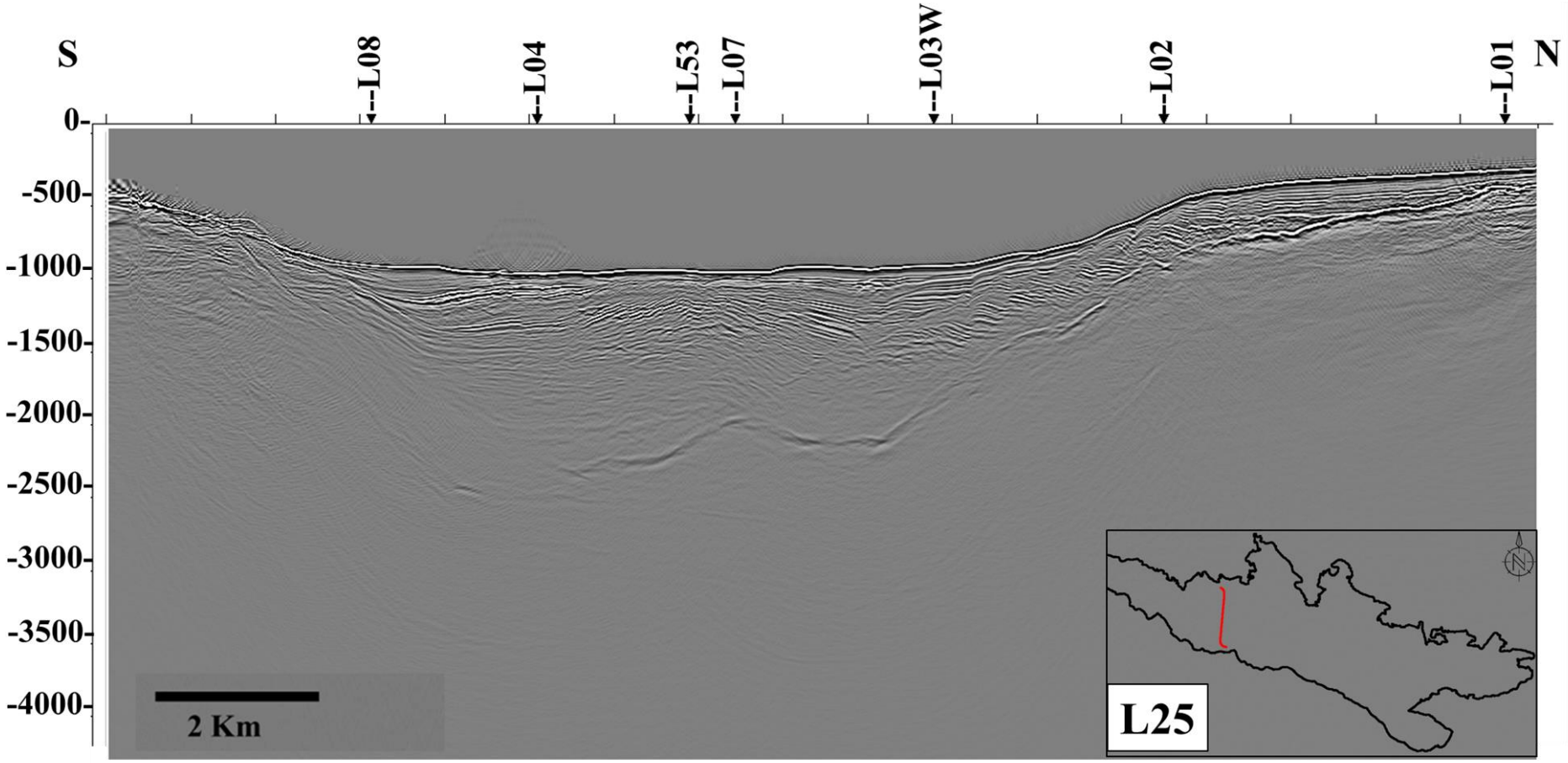
S
L08
L04
L53
L07
L03W
L02
L01
N
0
-500
-1000
-1500
-2000
-2500
-3000
-3500
-4000
2 Km
L25

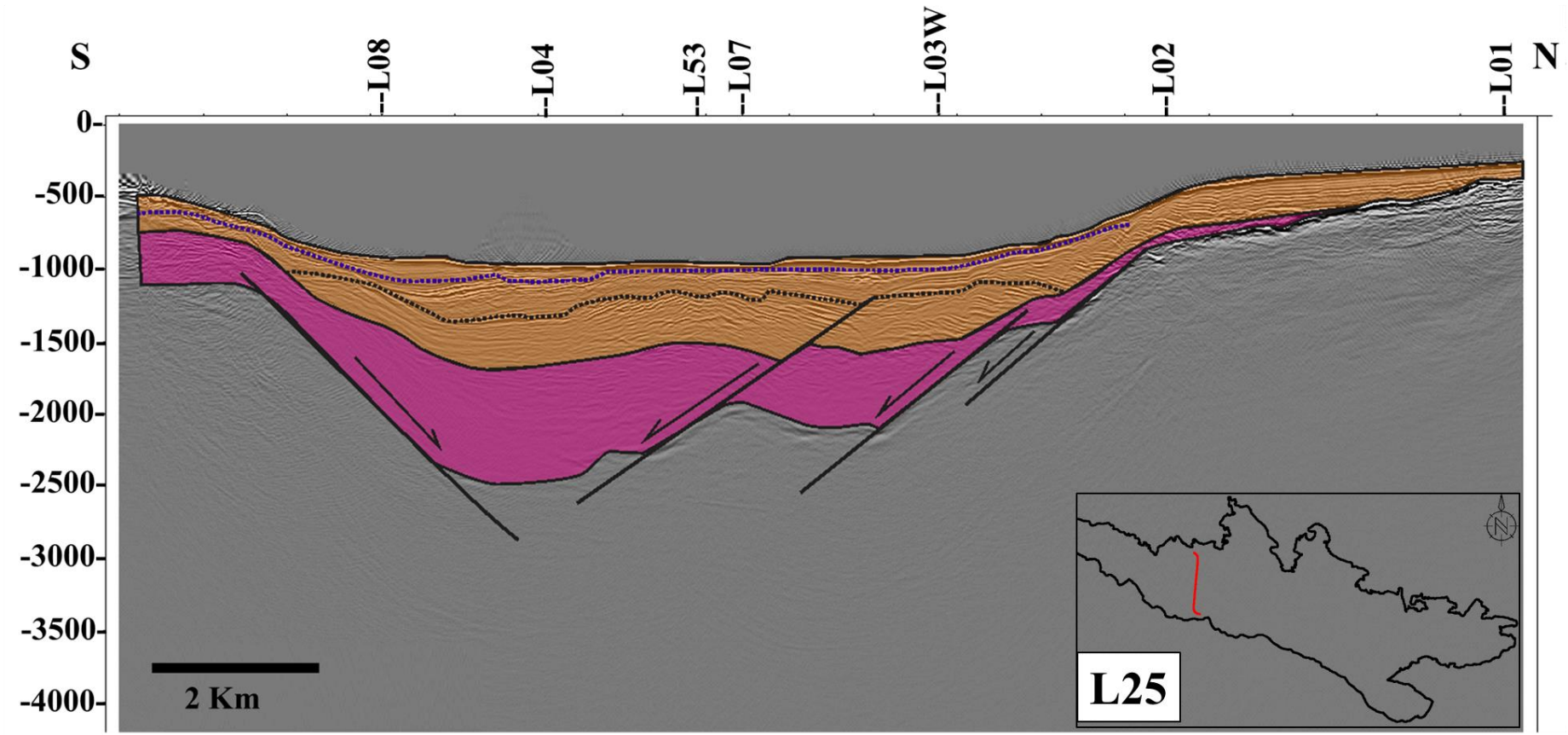
S
--L08
--L04
--L53
--L07
--L03W
--L02
--L01
N
0
-500
-1000
-1500
-2000
-2500
-3000
-3500
-4000
2 Km
L25

N
L28
L01
L02
L03w
L07
L04
L08
S
0
-500
-1000
-1500
-2000
-2500
-3000
-3500
-4000
L26
2 Km

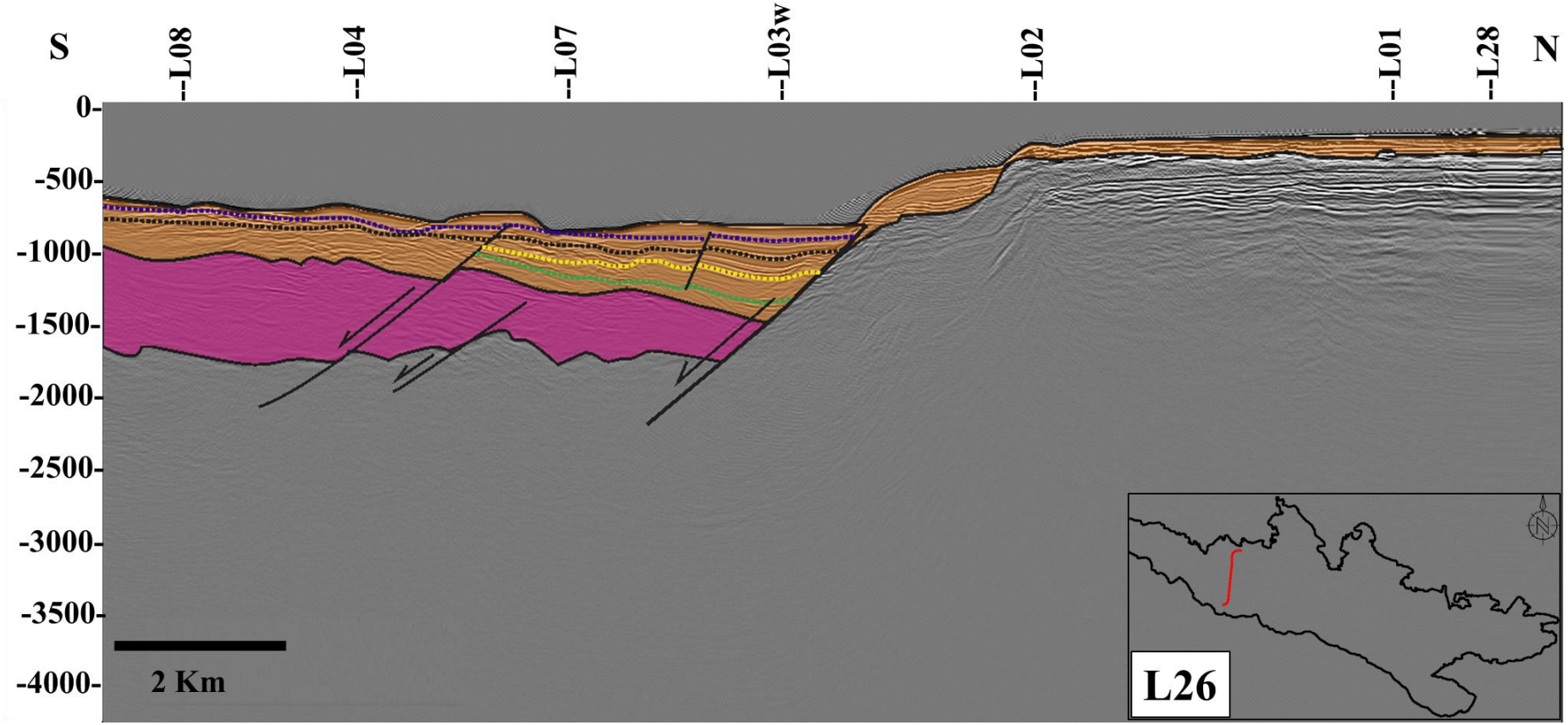
S
--L08
--L04
--L07
--L03w
--L02
--L01
--L28
N
0
-500
-1000
-1500
-2000
-2500
-3000
-3500
-4000
2 Km
L26

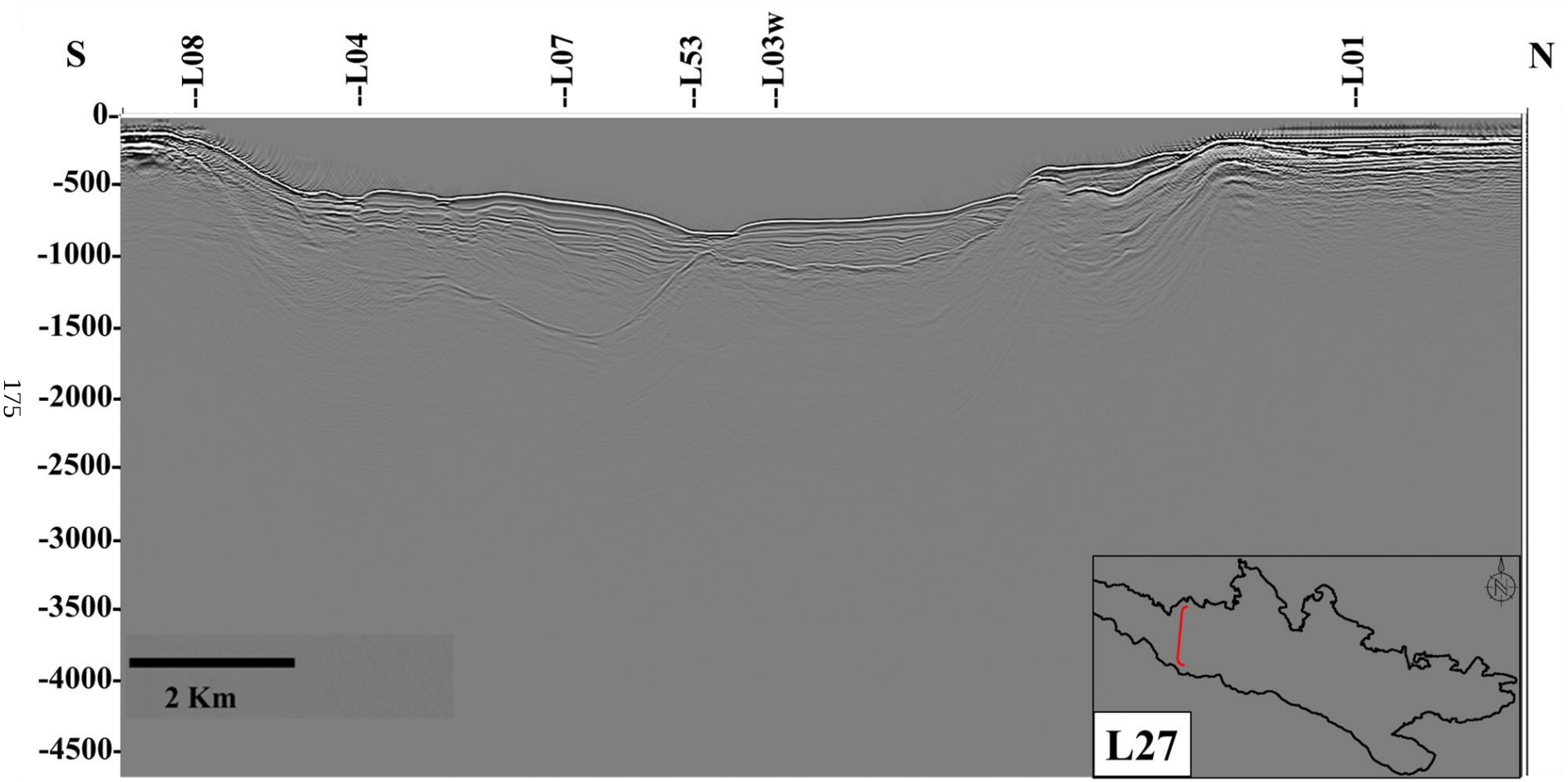
S
--L08
--L04
--L07
--L53
--L03w
--L01
N
0
-500
-1000
-1500
-2000
-2500
-3000
-3500
-4000
-4500
2 Km
L27

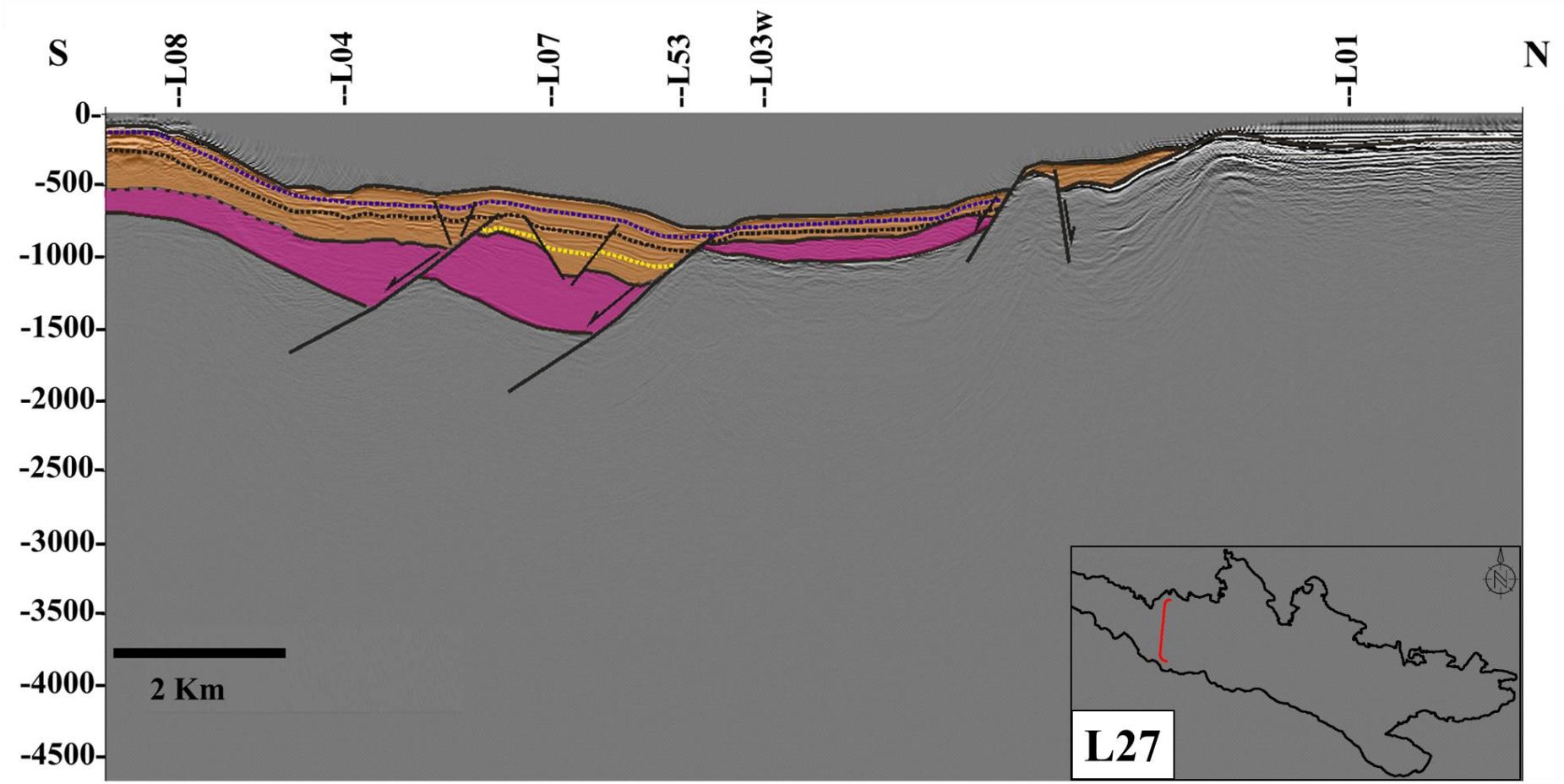
S
--L08
--L04
--L07
--L53
--L03w
--L01
N
0
-500
-1000
-1500
-2000
-2500
-3000
-3500
-4000
-4500
2 Km
L27

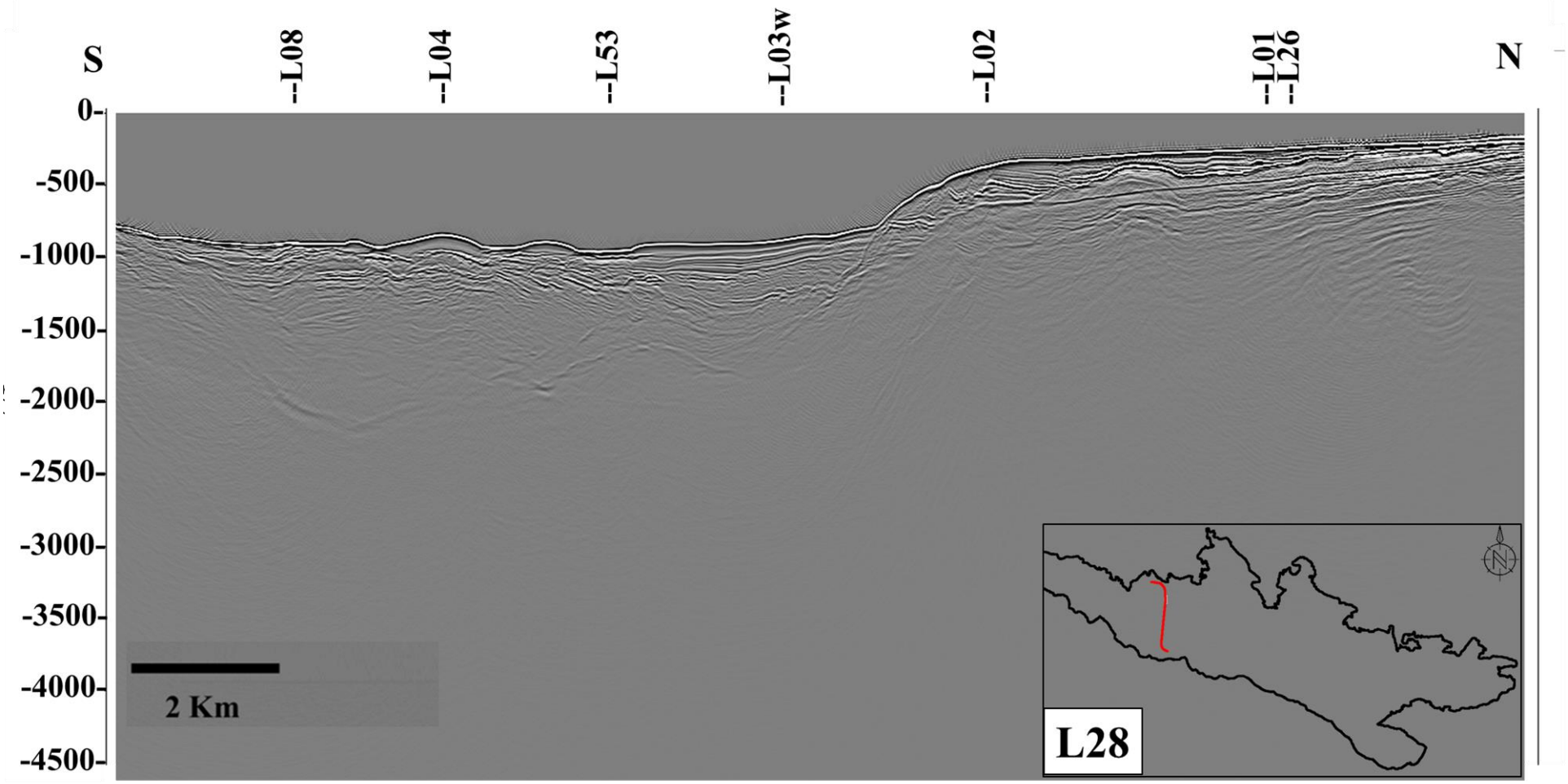
S
--L08
--L04
--L53
--L03w
--L02
--L01
--L26
N
0
-500
-1000
-1500
-2000
-2500
-3000
-3500
-4000
-4500
2 Km
L28

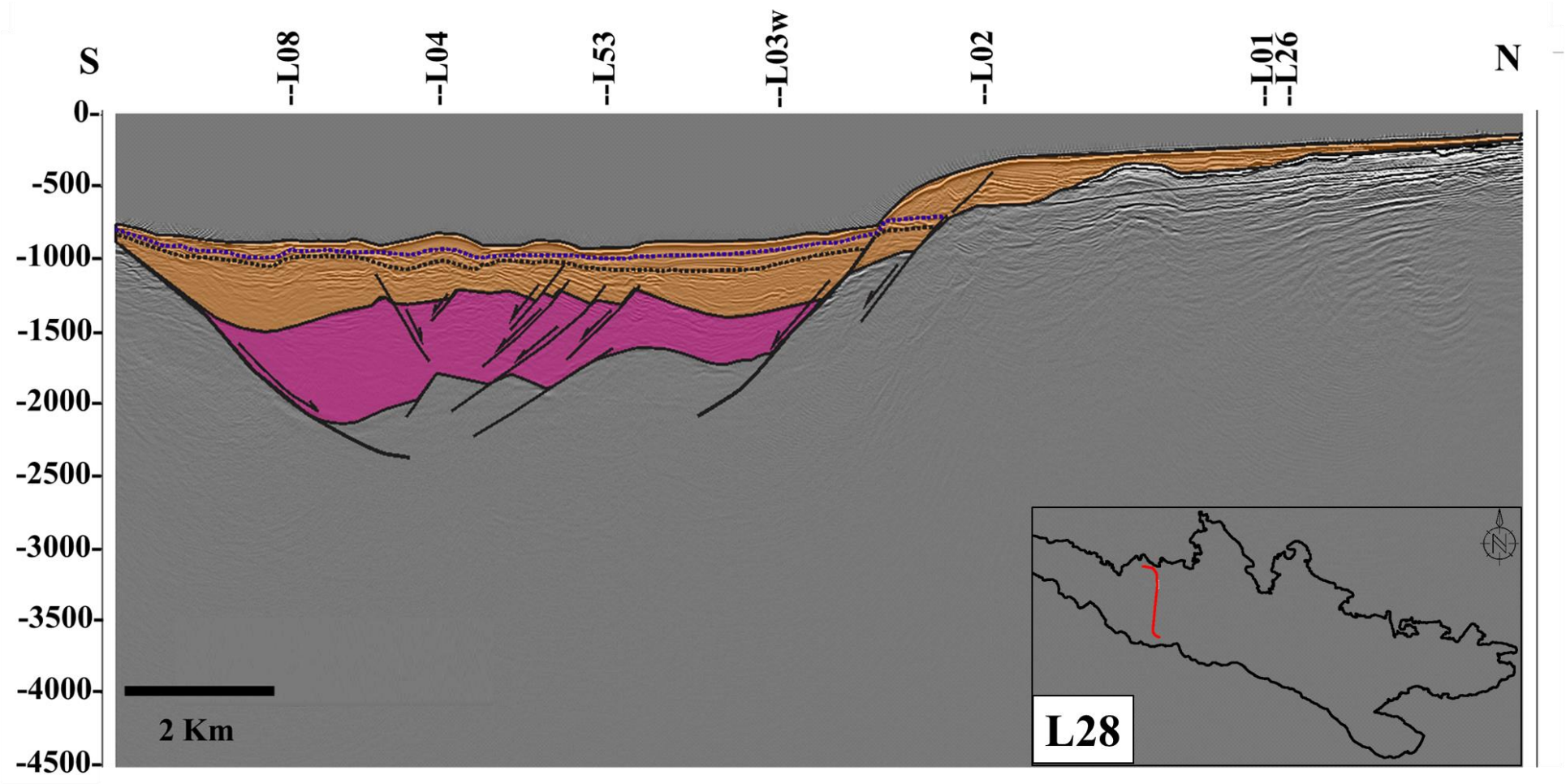
S
--L08
--L04
--L53
--L03w
--L02
--L01
--L26
N
0
-500
-1000
-1500
-2000
-2500
-3000
-3500
-4000
-4500
2 Km
L28

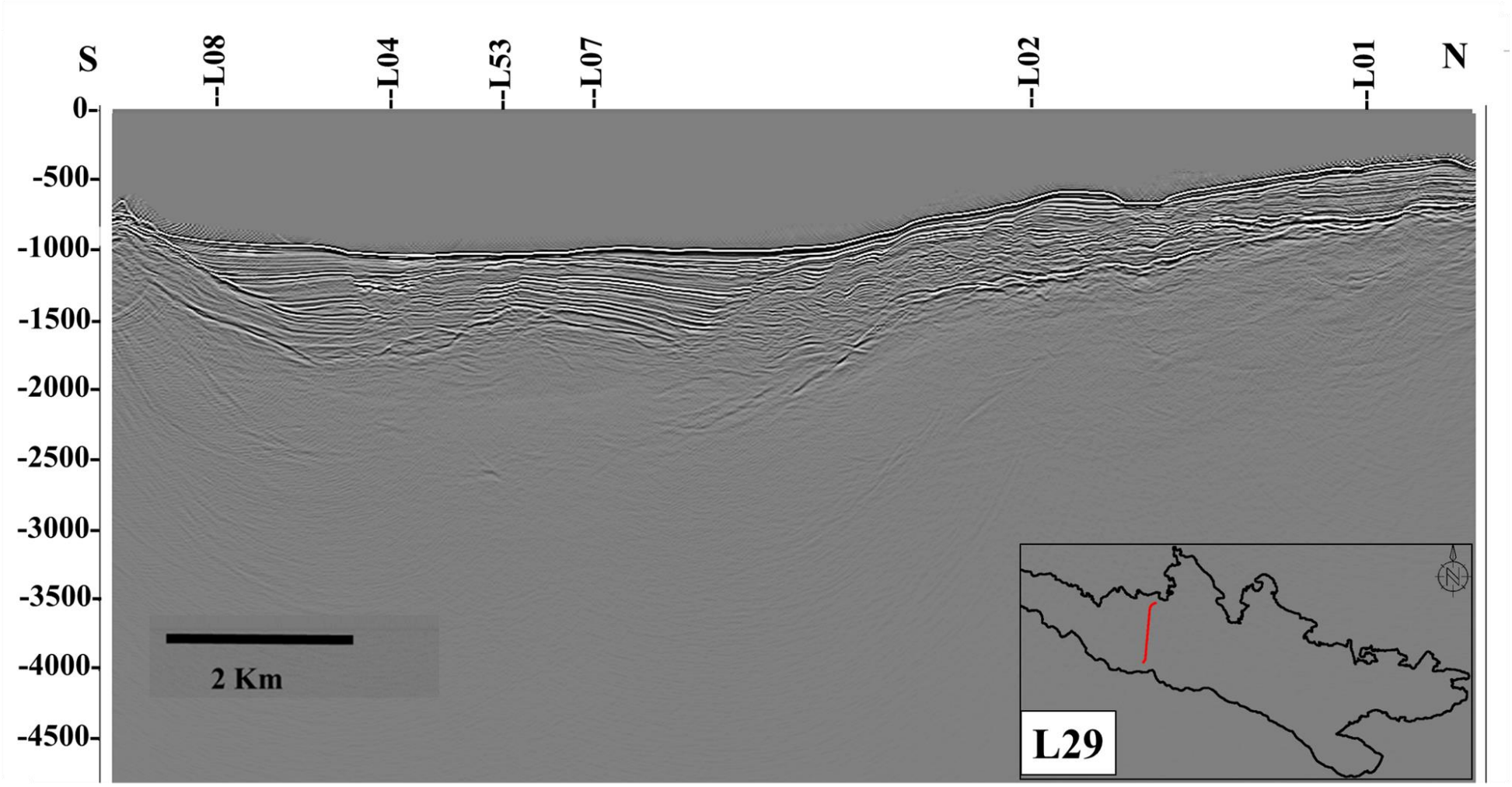
S
--L08
--L04
--L53
--L07
--L02
--L01
N
0
-500
-1000
-1500
-2000
-2500
-3000
-3500
-4000
-4500
2 Km
L29

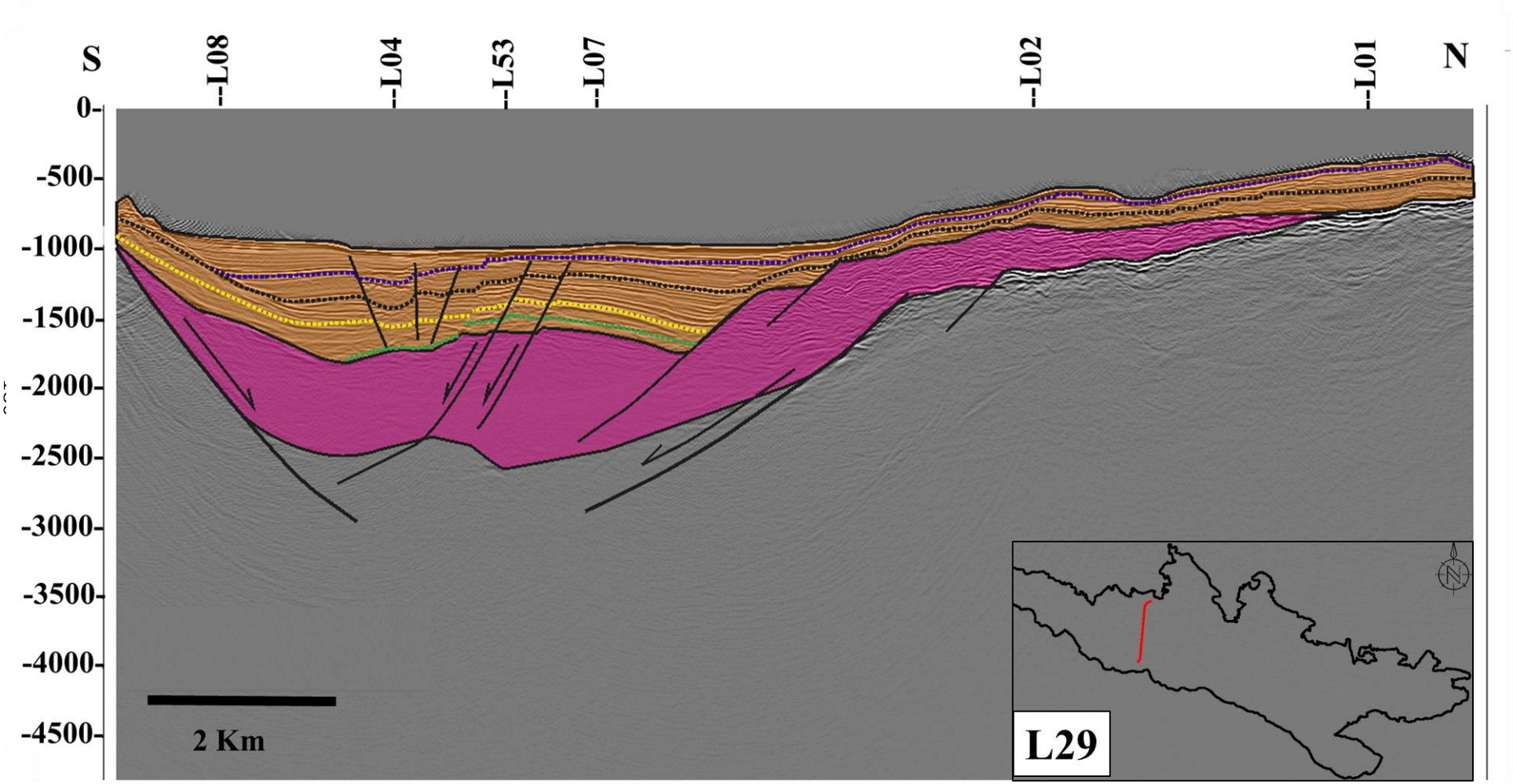
S
--L08
--L04
--L53
--L07
--L02
--L01
N
0
-500
-1000
-1500
-2000
-2500
-3000
-3500
-4000
-4500
2 Km
L29

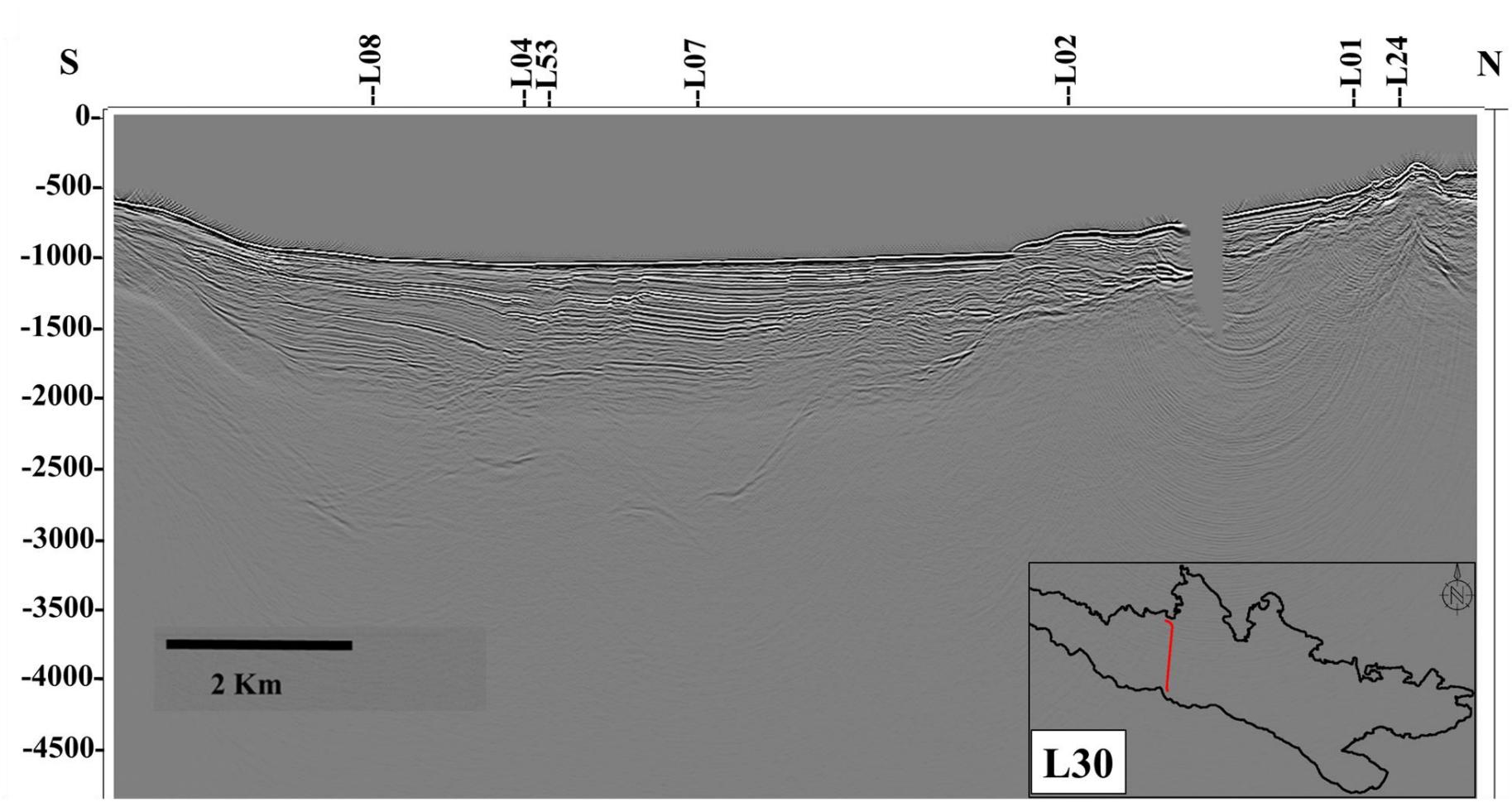
S
--L08
--L04
--L53
--L07
--L02
--L01
--L24
N
0
-500
-1000
-1500
-2000
-2500
-3000
-3500
-4000
-4500
2 Km
L30

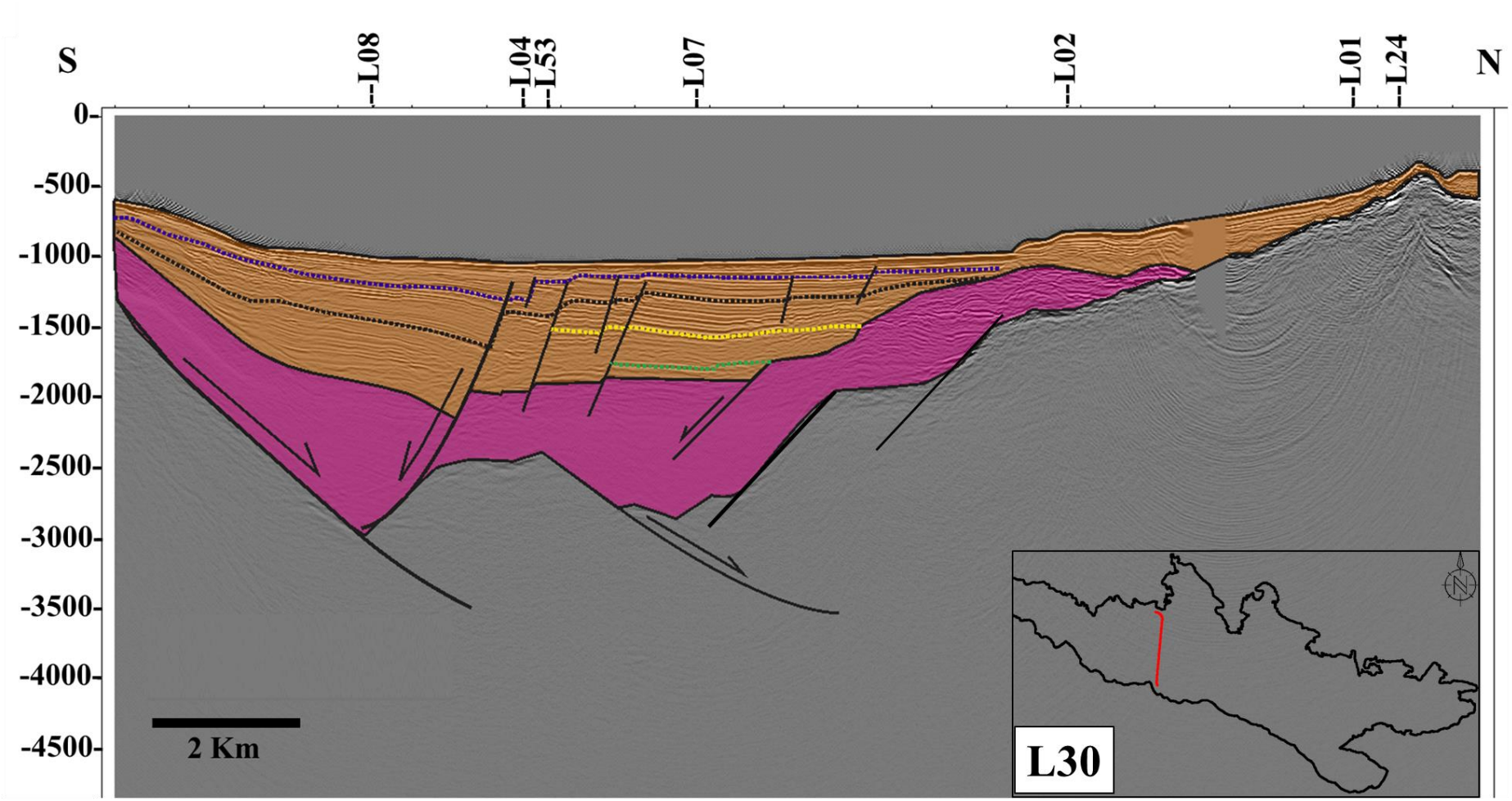
S
N
L08
L04
L53
L07
L02
L01
L24
0
-500
-1000
-1500
-2000
-2500
-3000
-3500
-4000
-4500
2 Km
L30

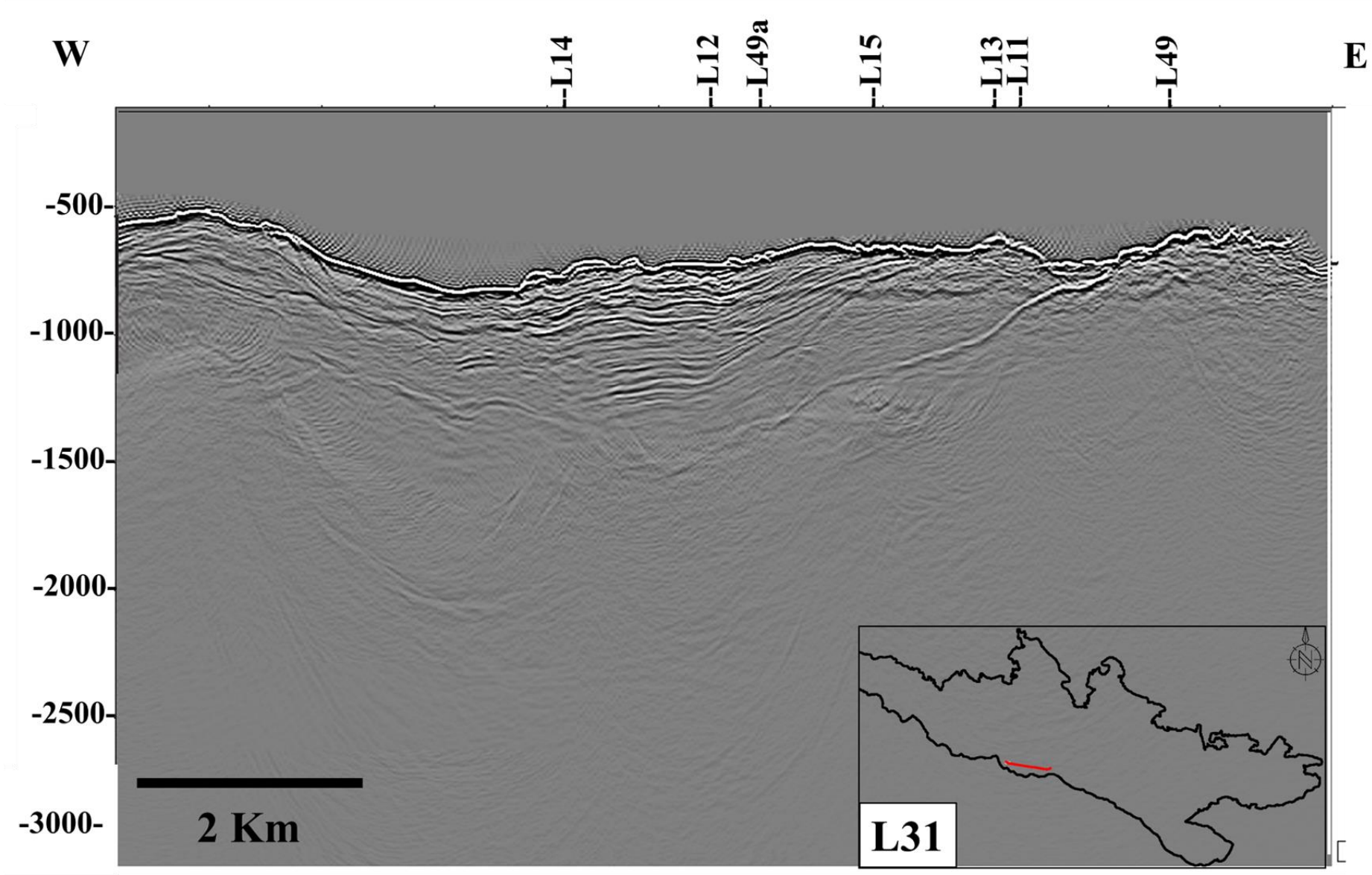
W
L14
L12
L49a
L15
L13
L11
L49
E
-500-
-1000-
-1500-
-2000-
-2500-
-3000-
2 Km
L31

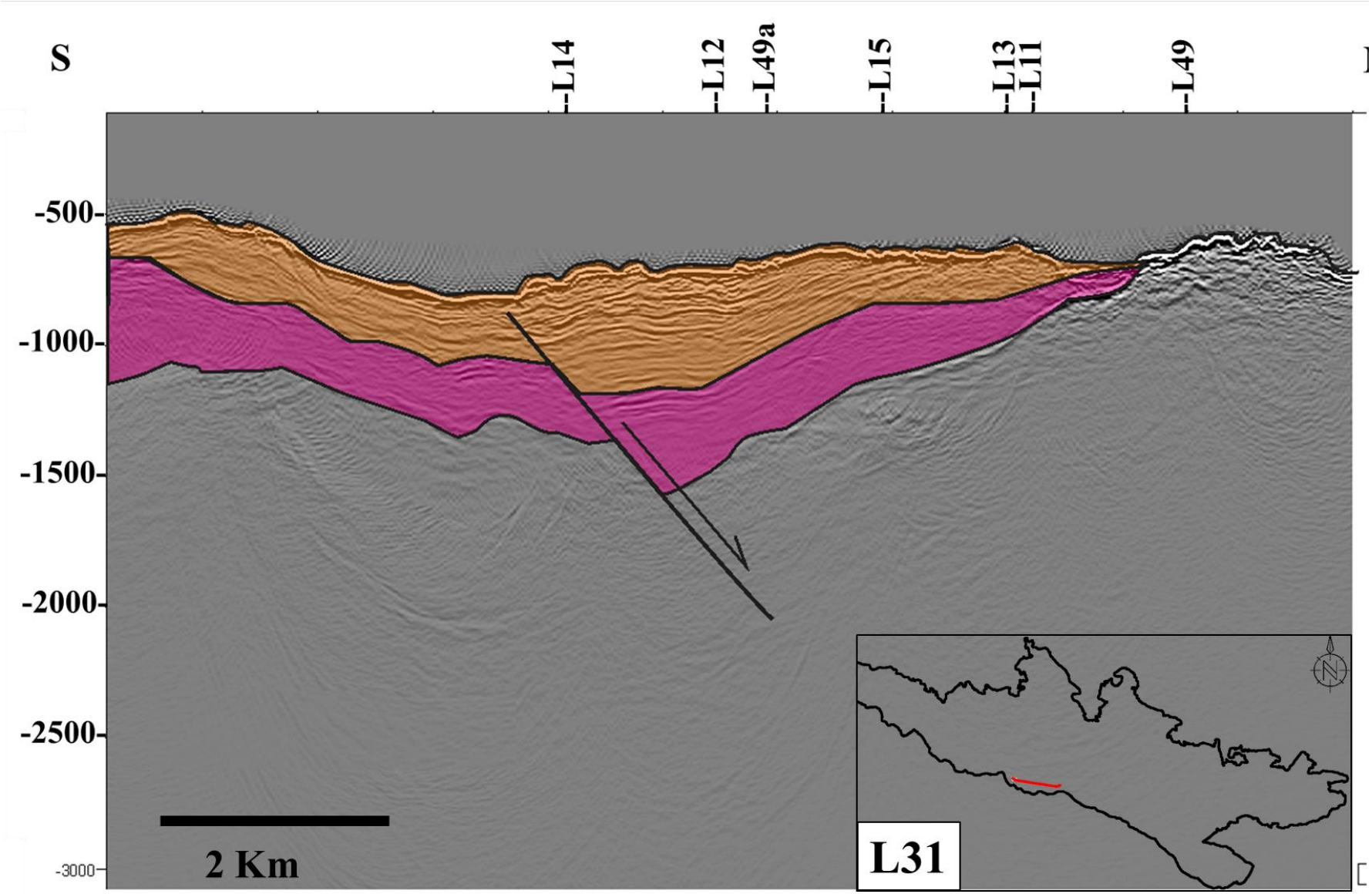
S
L14
L12
L49a
L15
L13
L11
L49
-500
-1000
-1500
-2000
-2500
-3000
2 Km
L31

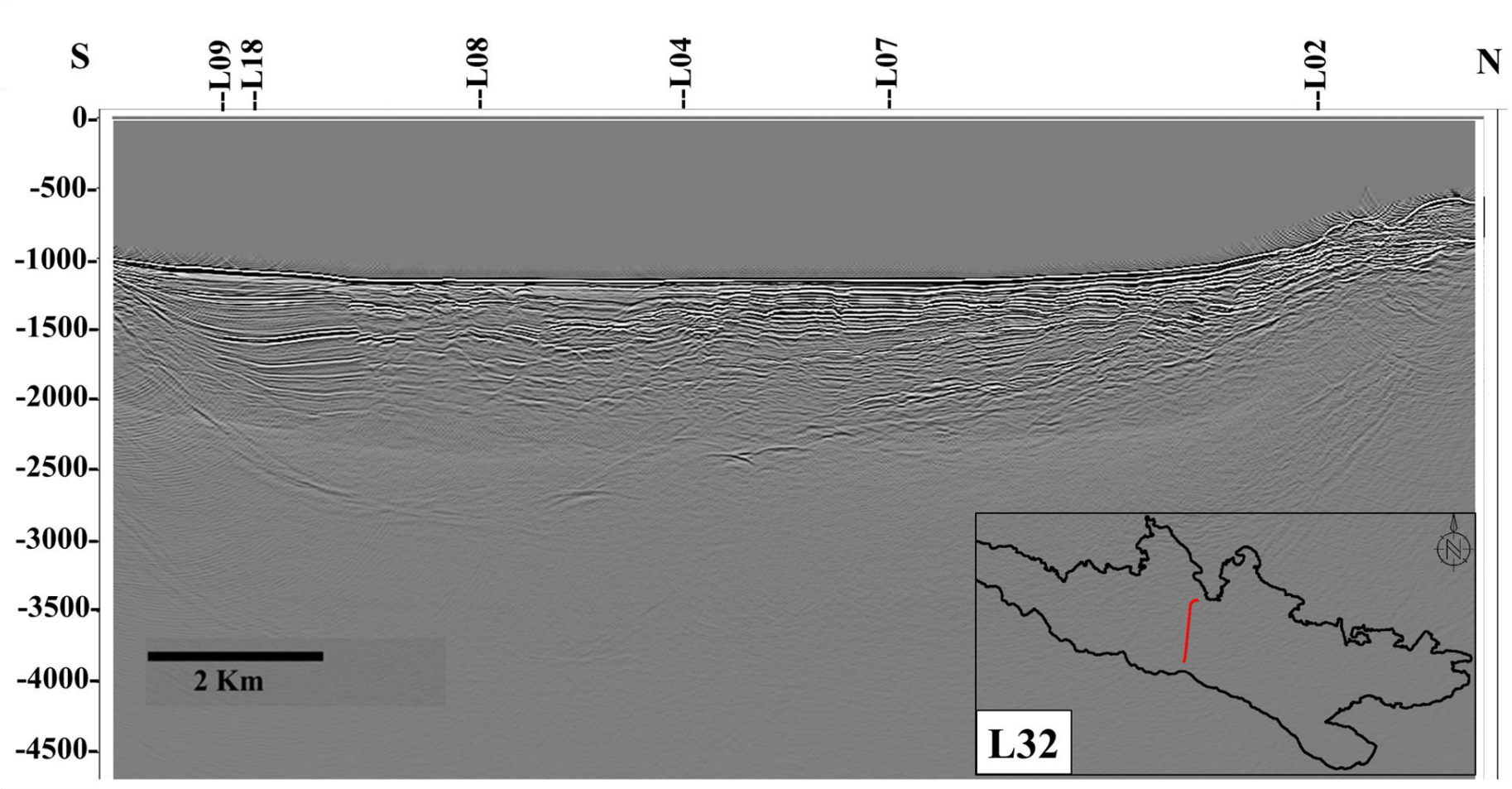
S
--L09
--L18
--L08
--L04
--L07
--L02
N
0-
-500-
-1000-
-1500-
-2000-
-2500-
-3000-
-3500-
-4000-
-4500-
2 Km
L32

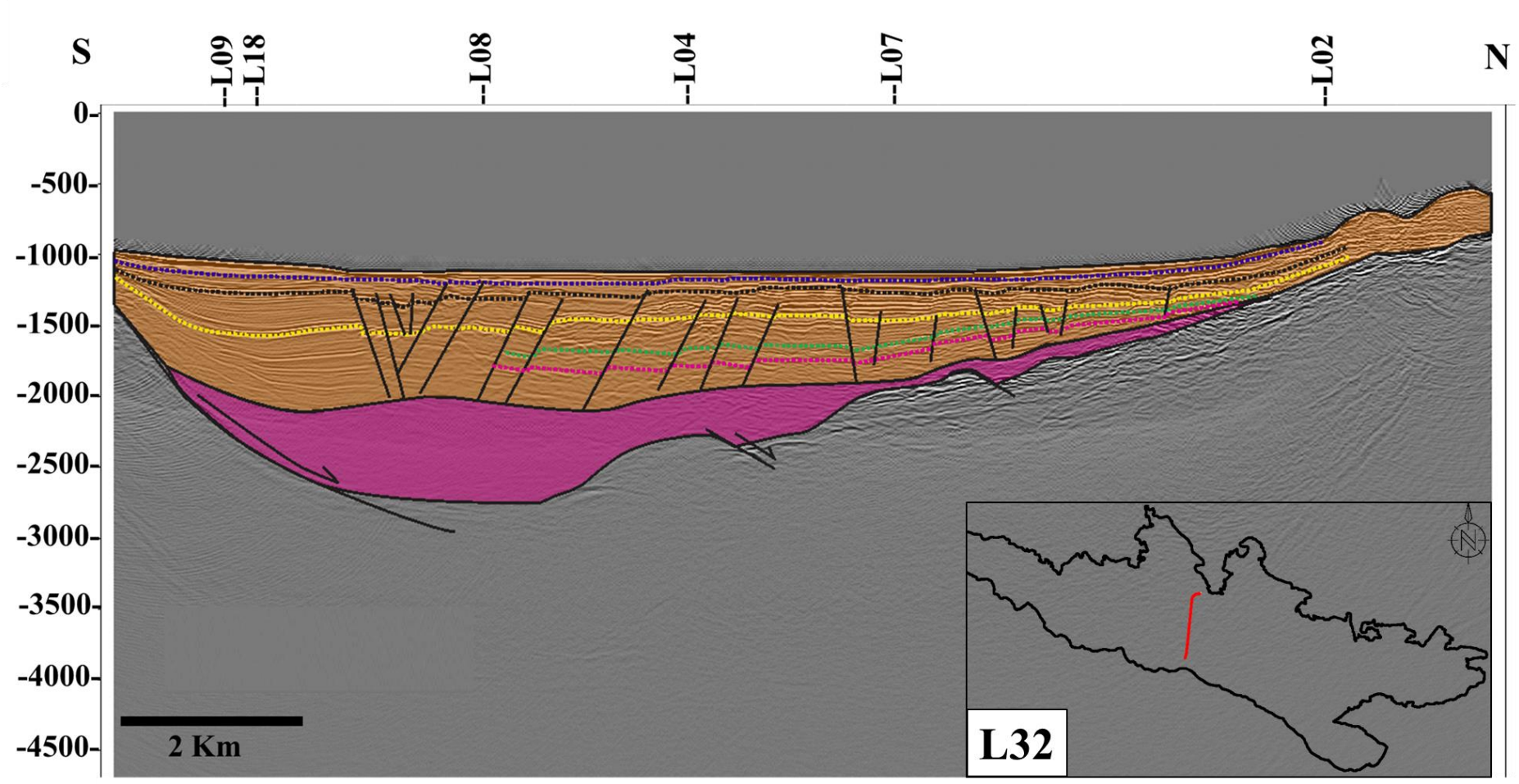
S
L09
L18
L08
L04
L07
L02
N
0
-500
-1000
-1500
-2000
-2500
-3000
-3500
-4000
-4500
2 Km
L32

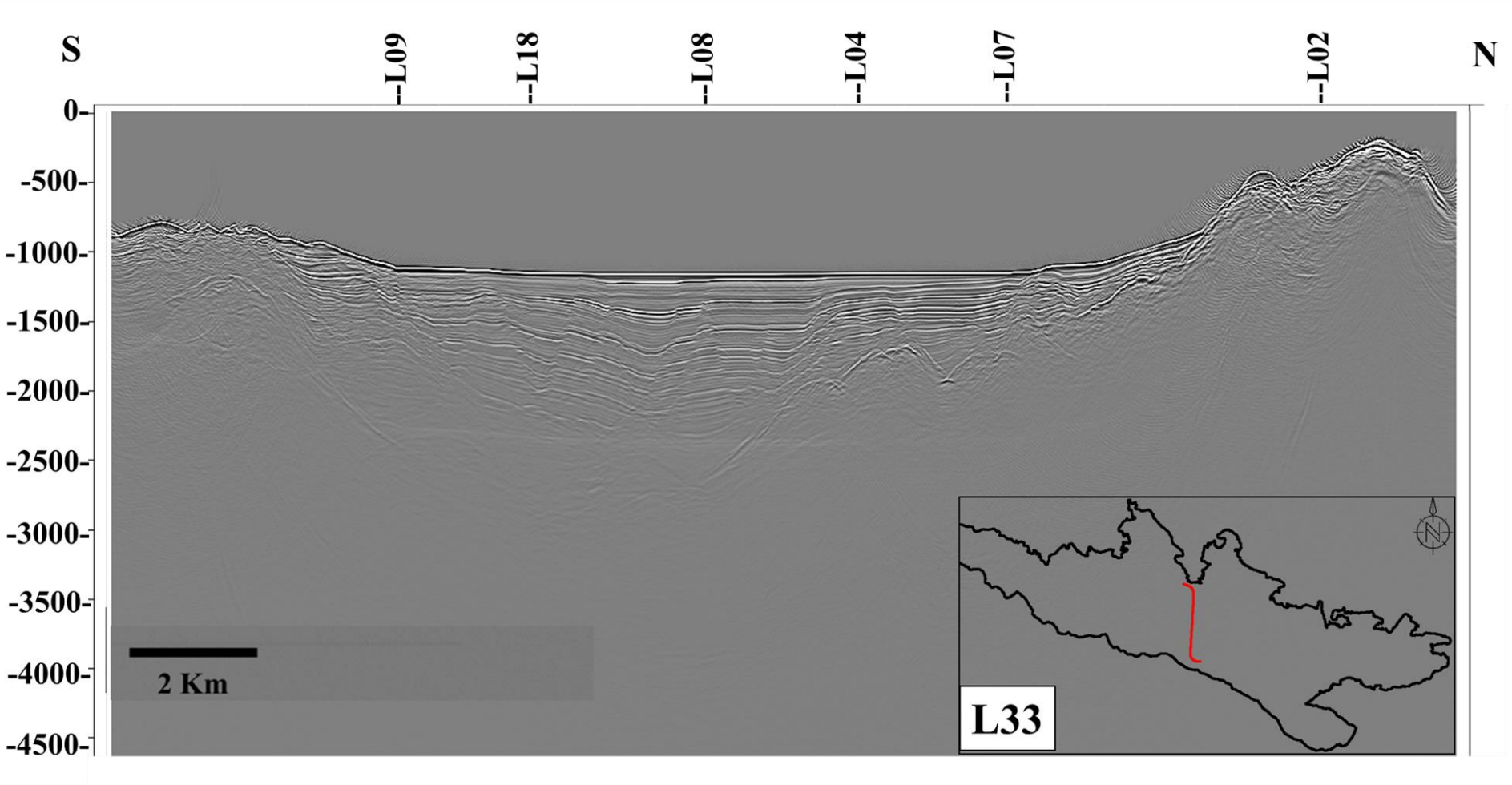
S
L09
L18
L08
L04
L07
L02
N
0
-500
-1000
-1500
-2000
-2500
-3000
-3500
-4000
-4500
2 Km
L33

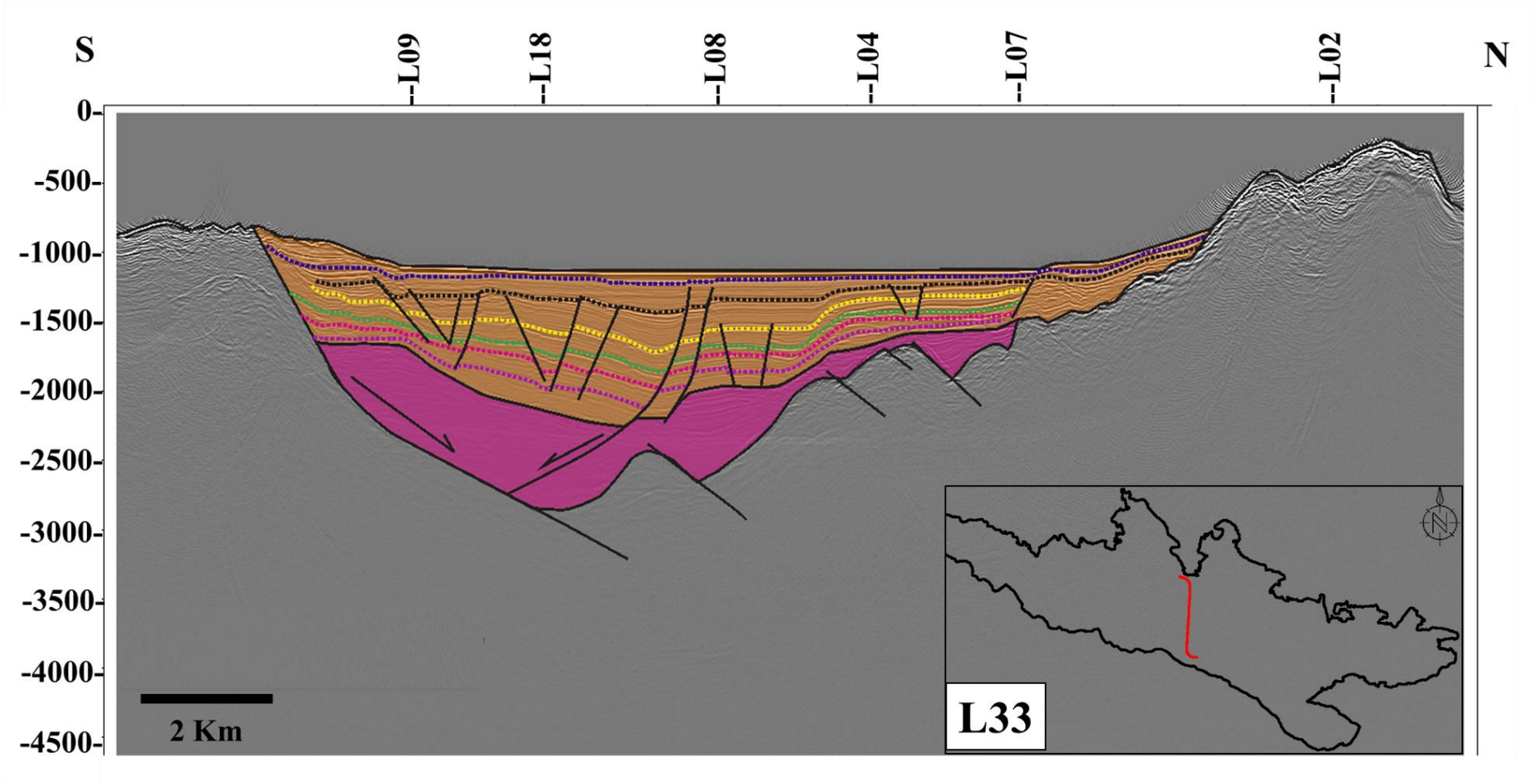
S
L09
L18
L08
L04
L07
L02
N
0
-500
-1000
-1500
-2000
-2500
-3000
-3500
-4000
-4500
2 Km
L33

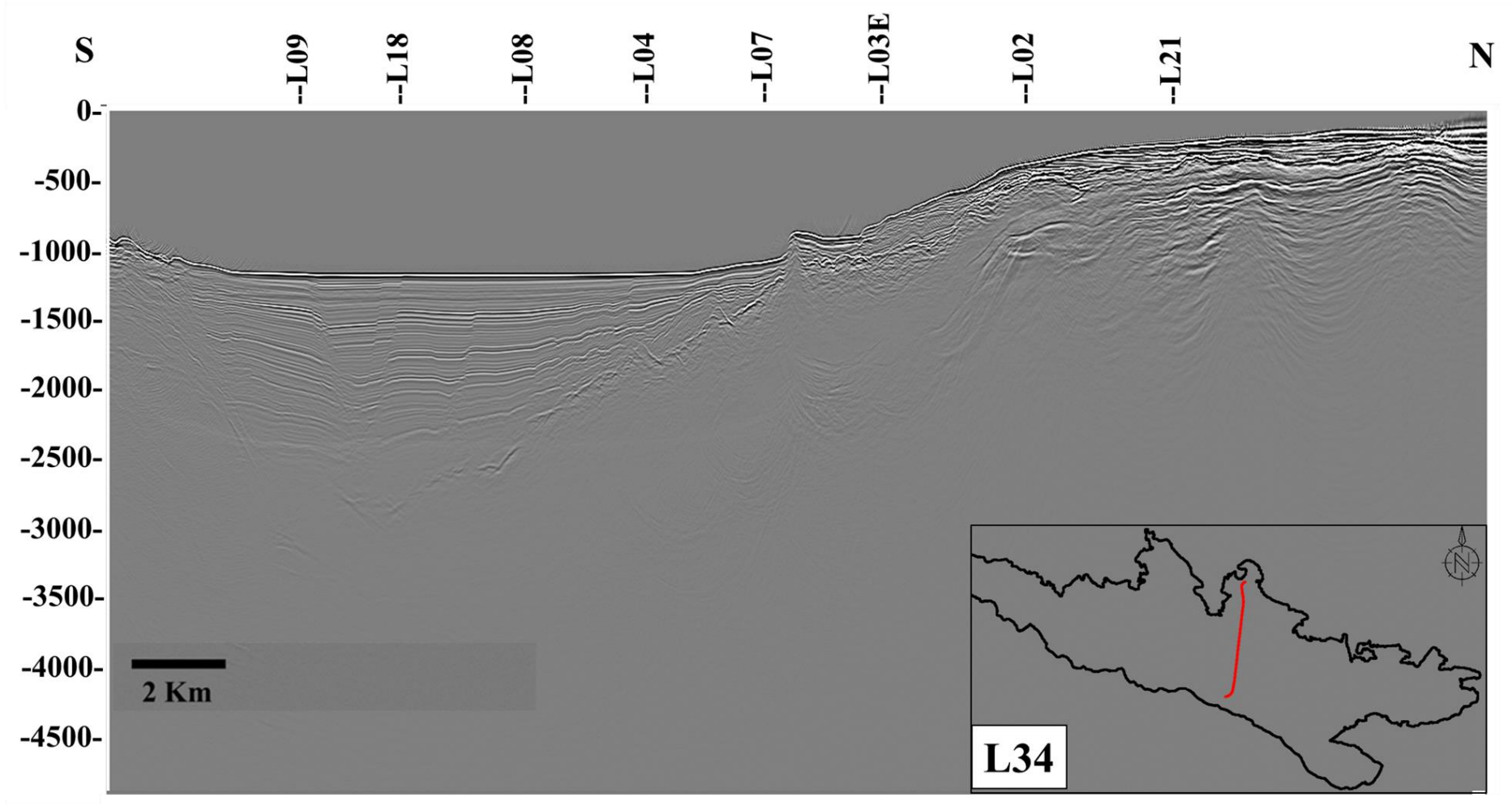
S
--L09
--L18
--L08
--L04
--L07
--L03E
--L02
--L21
N
0-
-500-
-1000-
-1500-
-2000-
-2500-
-3000-
-3500-
-4000-
-4500-
2 Km
L34

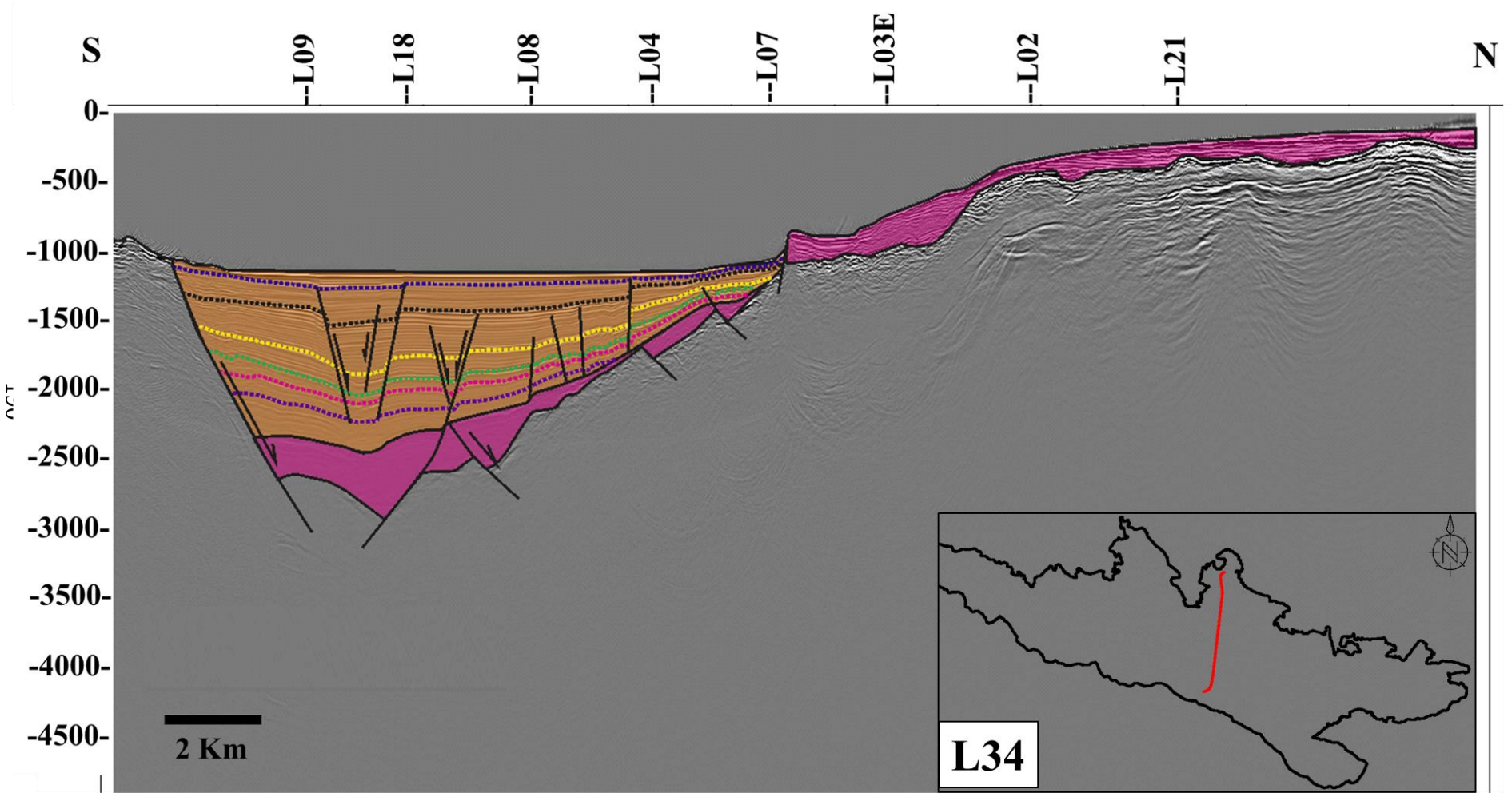
S
L09
L18
L08
L04
L07
L03E
L02
L21
N
0
-500
-1000
-1500
-2000
-2500
-3000
-3500
-4000
-4500
2 Km
L34

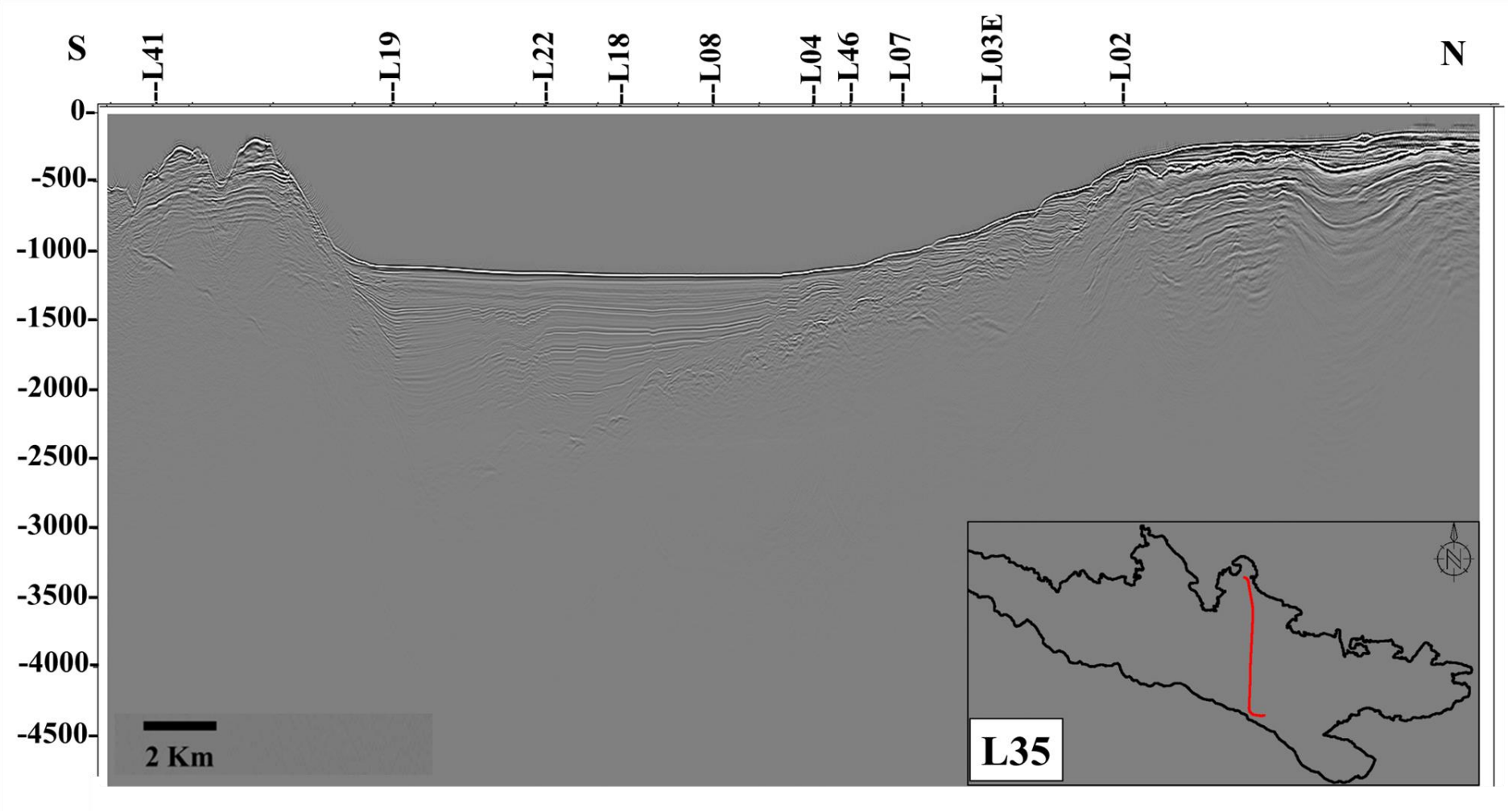
S
L41
L19
L22
L18
L08
L04
L46
L07
L03E
L02
N
0
-500
-1000
-1500
-2000
-2500
-3000
-3500
-4000
-4500
2 Km
L35

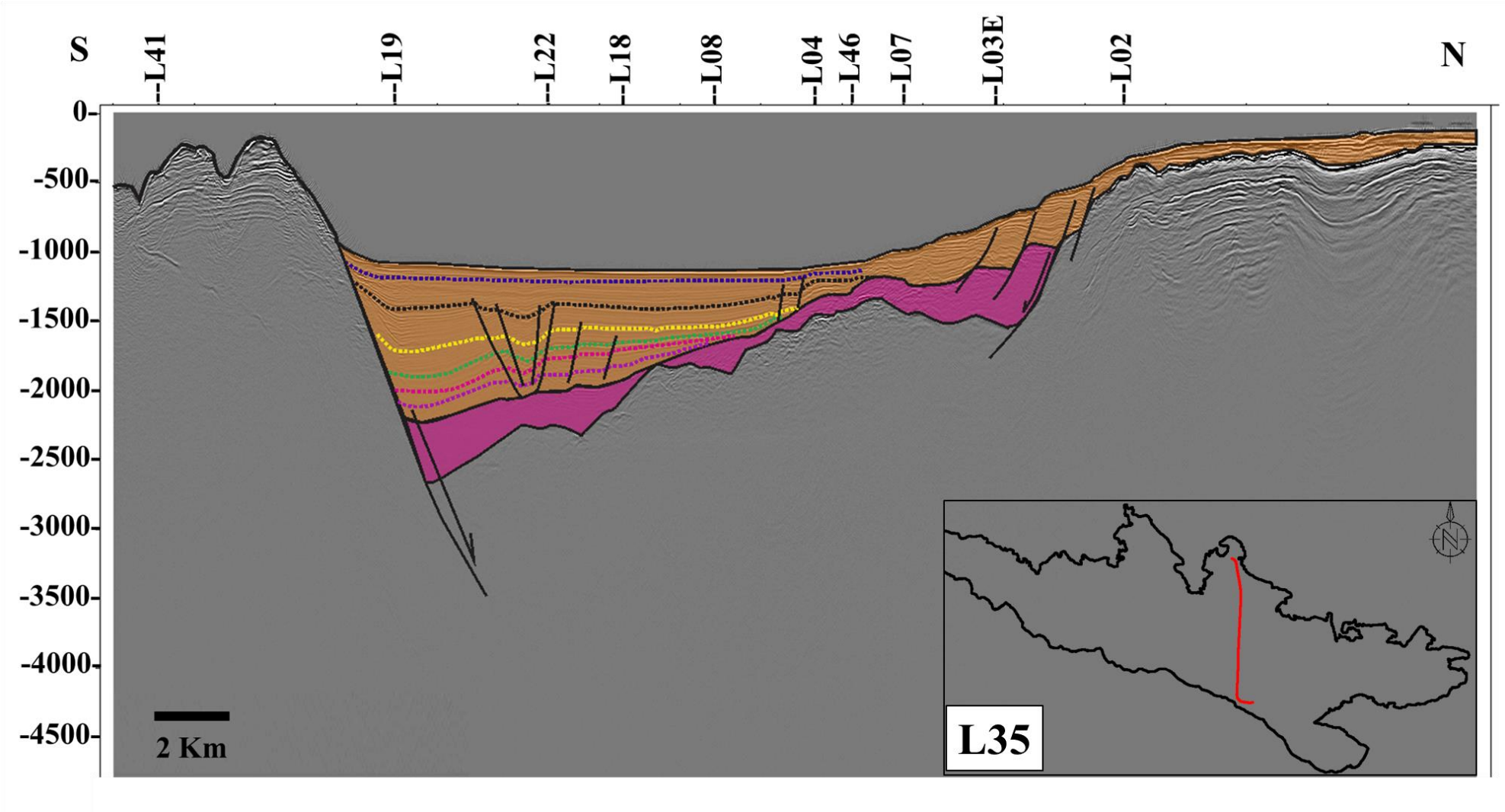
S
--L41
--L19
--L22
--L18
--L08
--L04
--L46
--L07
--L03E
--L02
N
0
-500
-1000
-1500
-2000
-2500
-3000
-3500
-4000
-4500
2 Km
L35

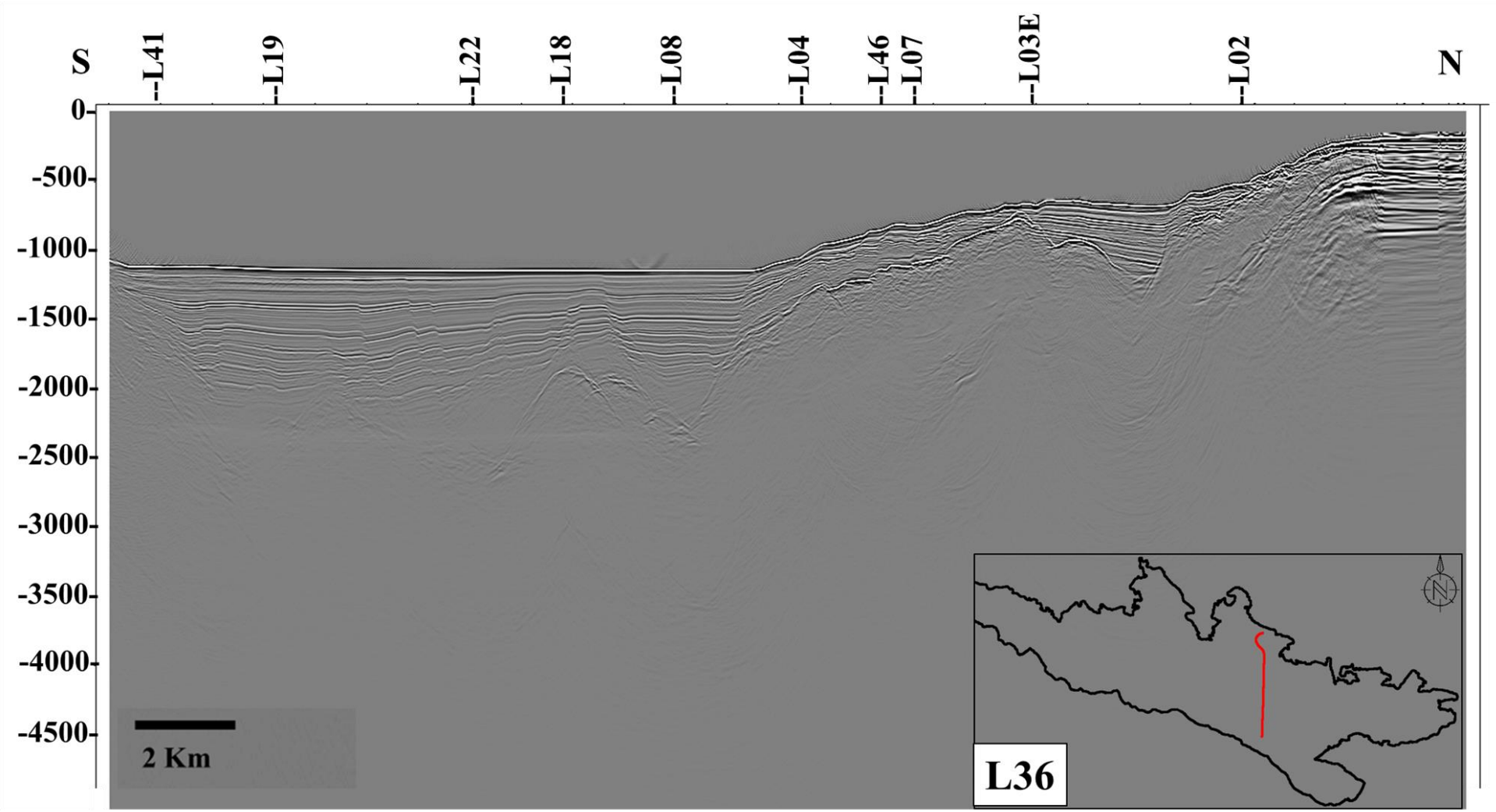
S
--L41
--L19
--L22
--L18
--L08
--L04
--L46
--L07
--L03E
--L02
N
0
-500
-1000
-1500
-2000
-2500
-3000
-3500
-4000
-4500
2 Km
L36

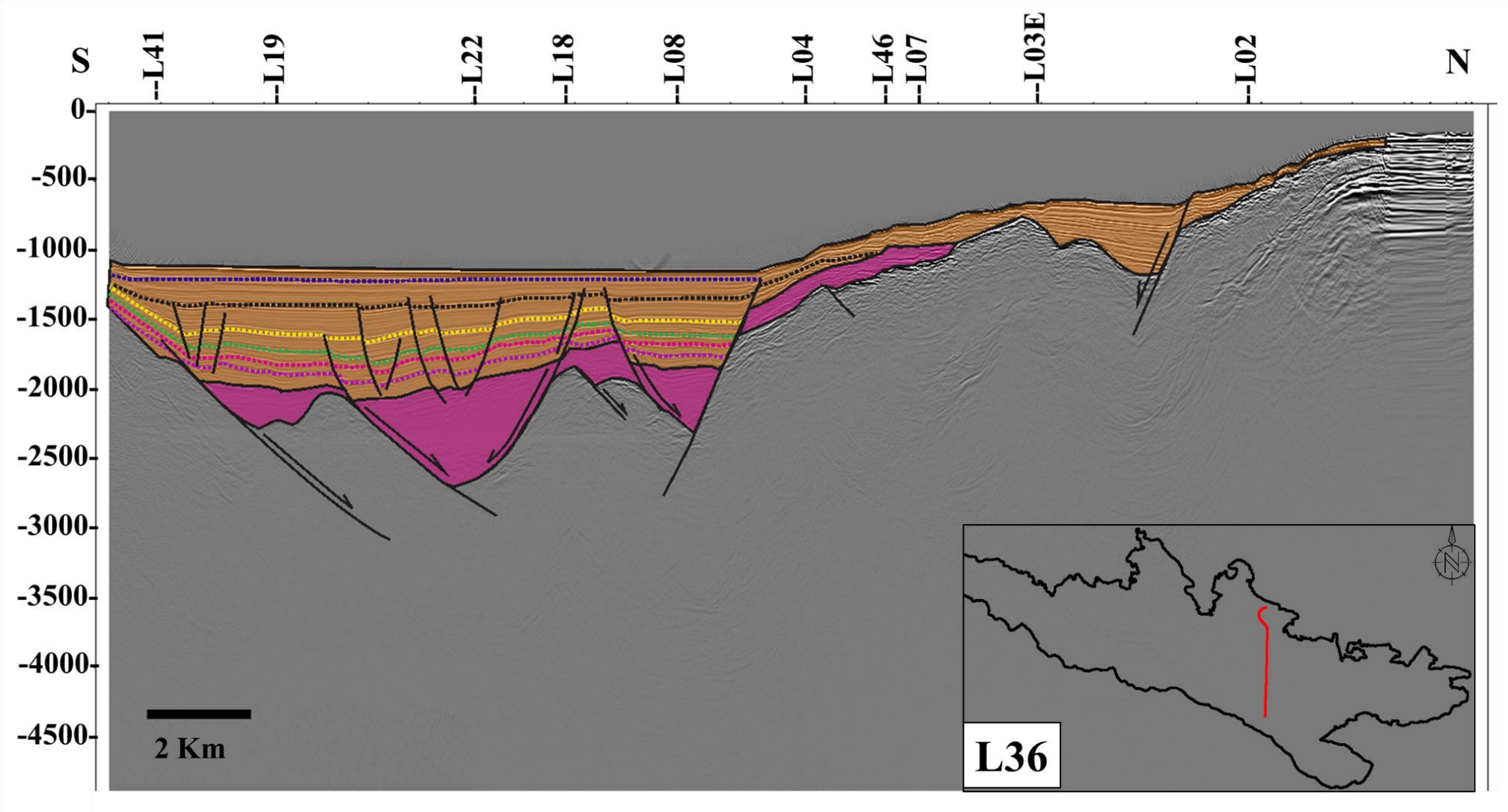
S
--L41
--L19
--L22
--L18
--L08
--L04
--L46
--L07
--L03E
--L02
N
0
-500
-1000
-1500
-2000
-2500
-3000
-3500
-4000
-4500
2 Km
L36

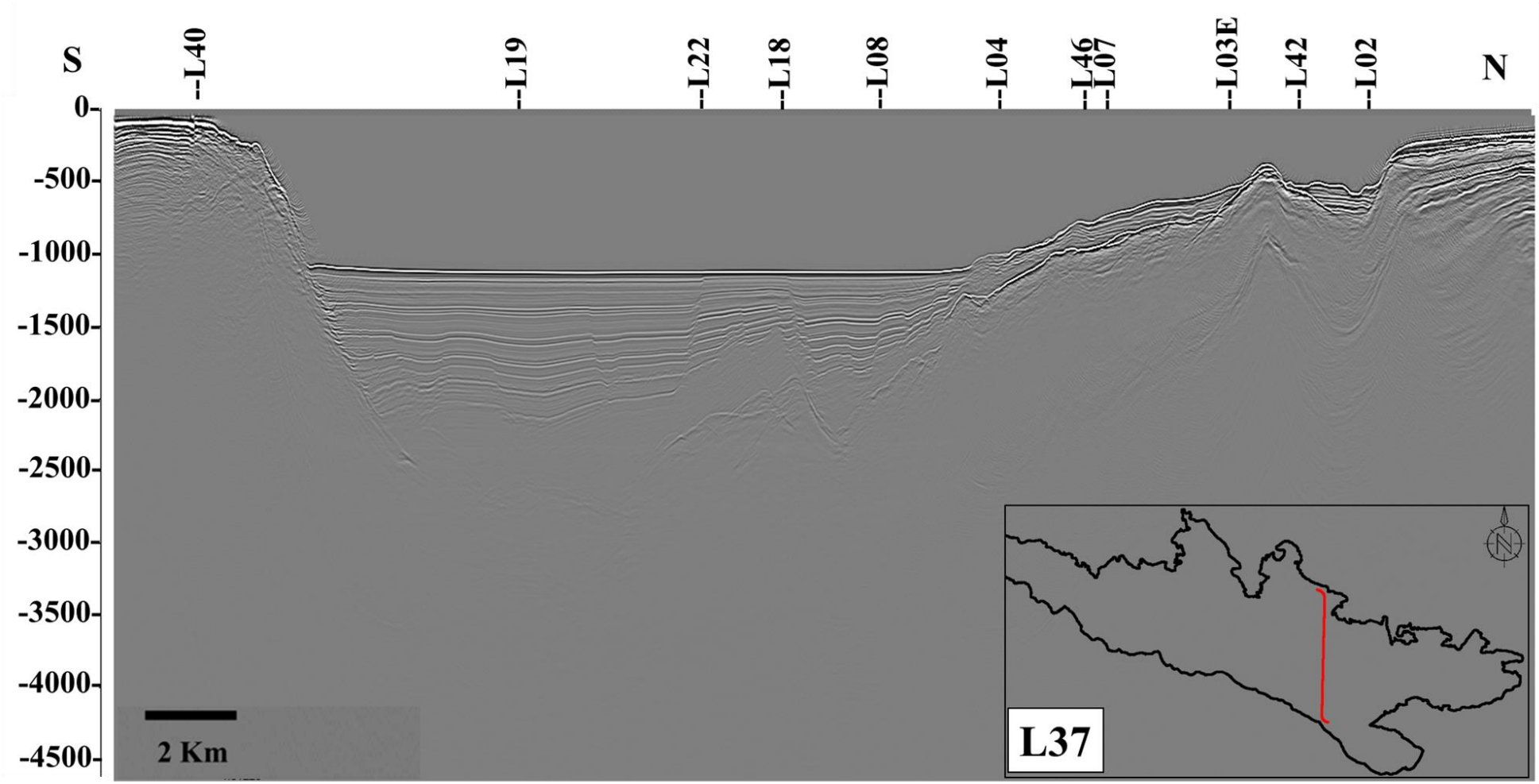
S
N
L40
L19
L22
L18
L08
L04
L46
L07
L03E
L42
L02
0
-500
-1000
-1500
-2000
-2500
-3000
-3500
-4000
-4500
2 Km
L37

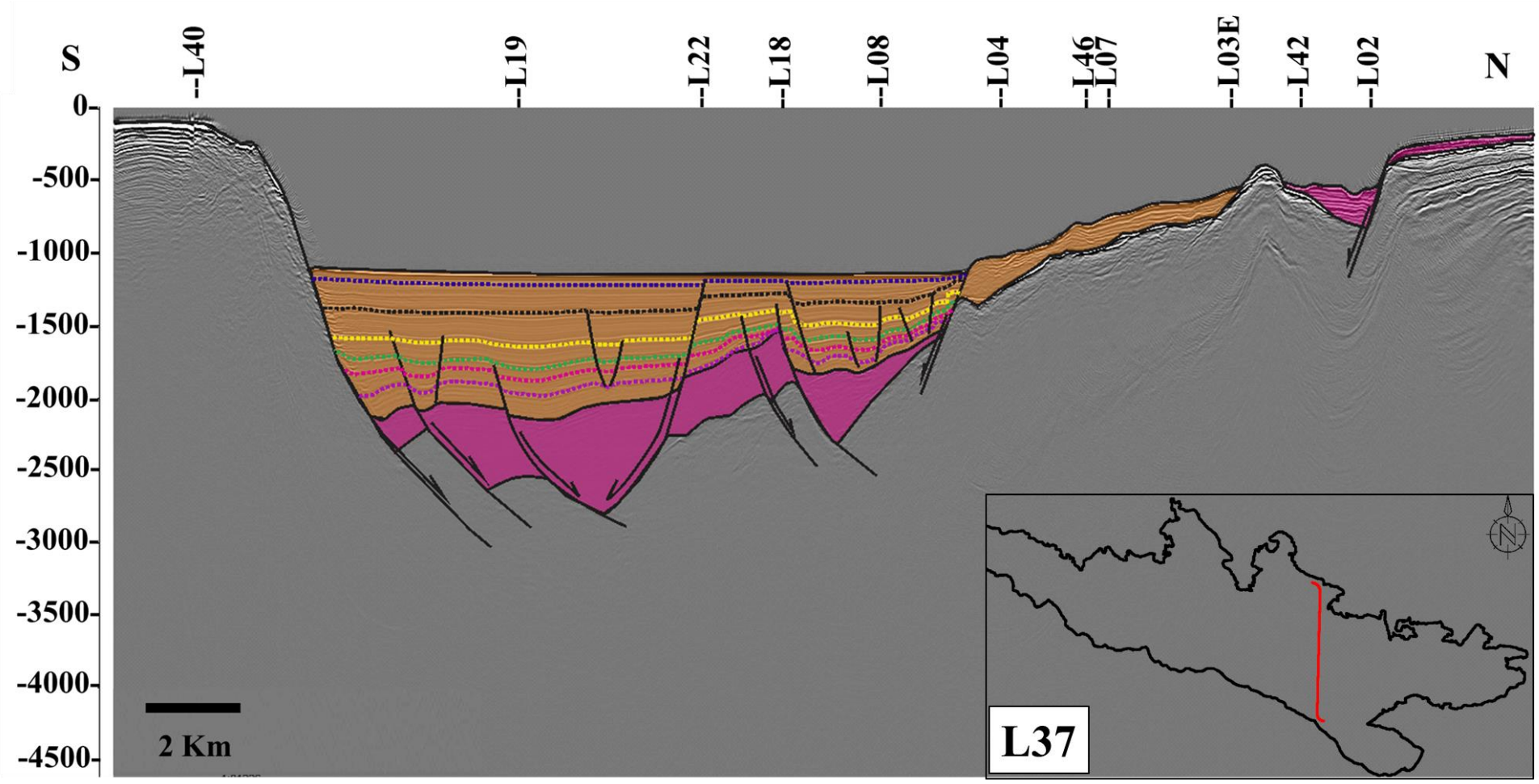
S
--L40
--L19
--L22
--L18
--L08
--L04
--L46
--L07
--L03E
--L42
--L02
N
0
-500
-1000
-1500
-2000
-2500
-3000
-3500
-4000
-4500
2 Km
L37

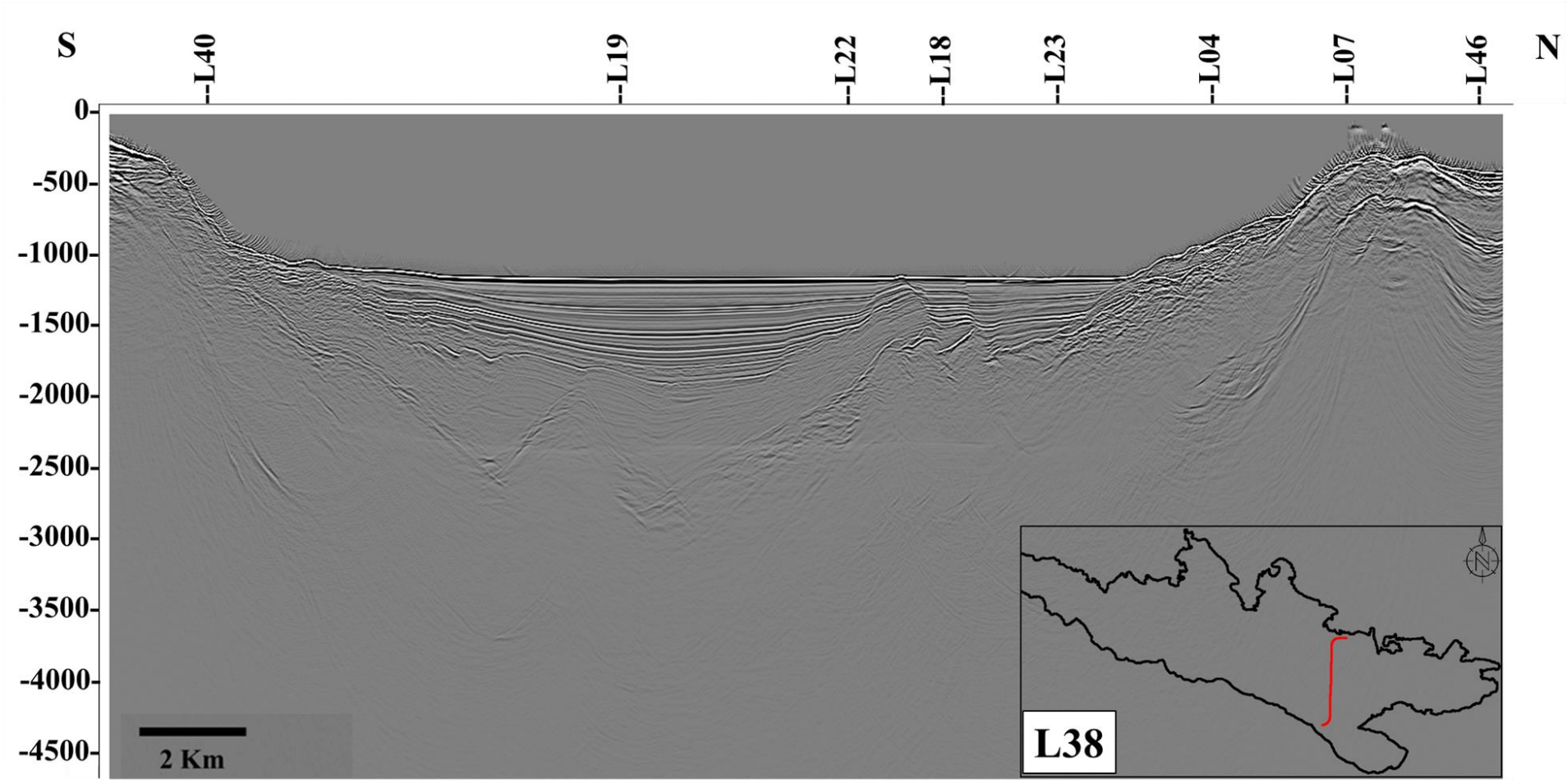
S
L40
L19
L22
L18
L23
L04
L07
L46
N
0
-500
-1000
-1500
-2000
-2500
-3000
-3500
-4000
-4500
2 Km
L38

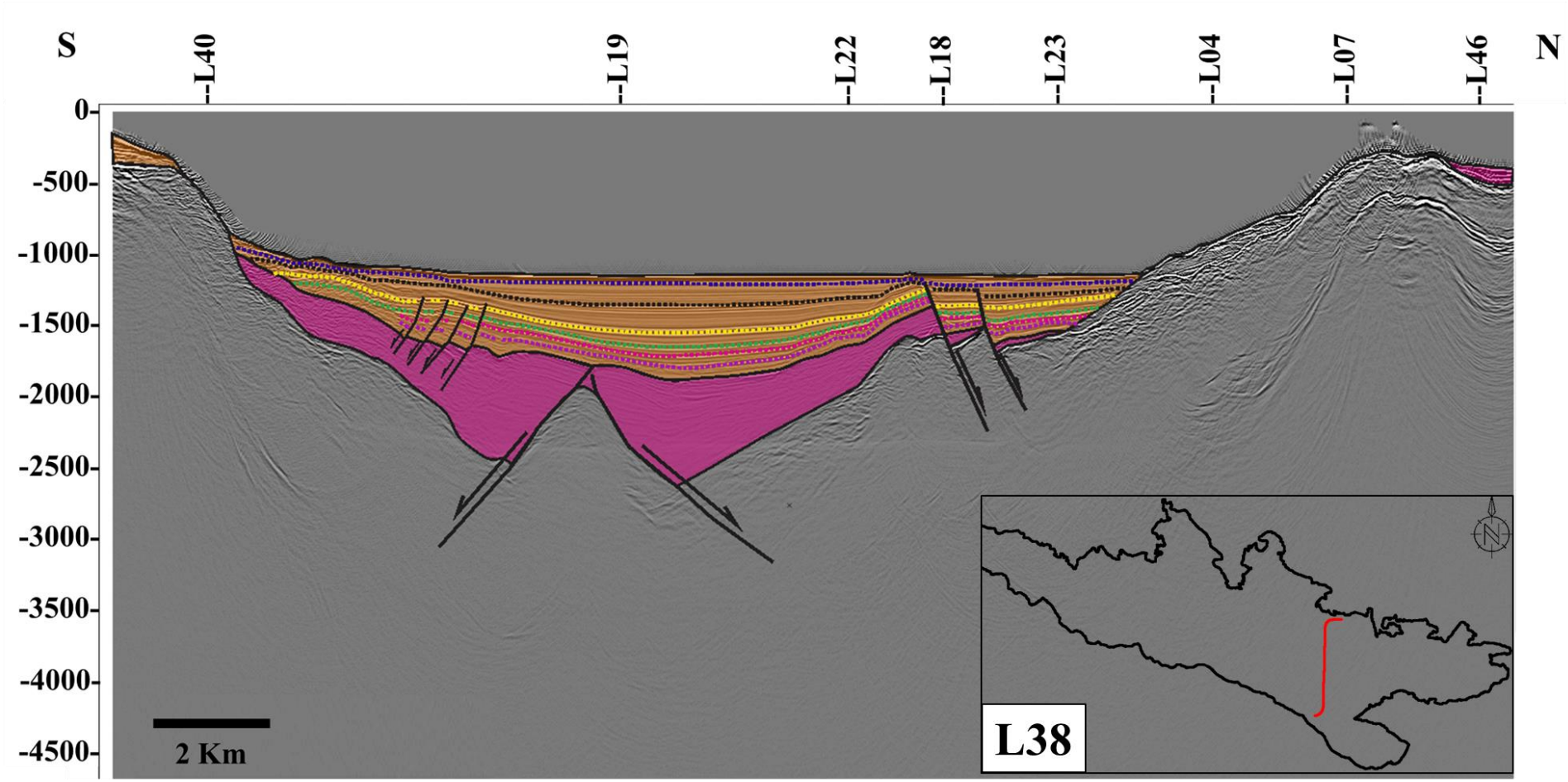
S
--L40
--L19
--L22
--L18
--L23
--L04
--L07
--L46
N
0
-500
-1000
-1500
-2000
-2500
-3000
-3500
-4000
-4500
2 Km
L38

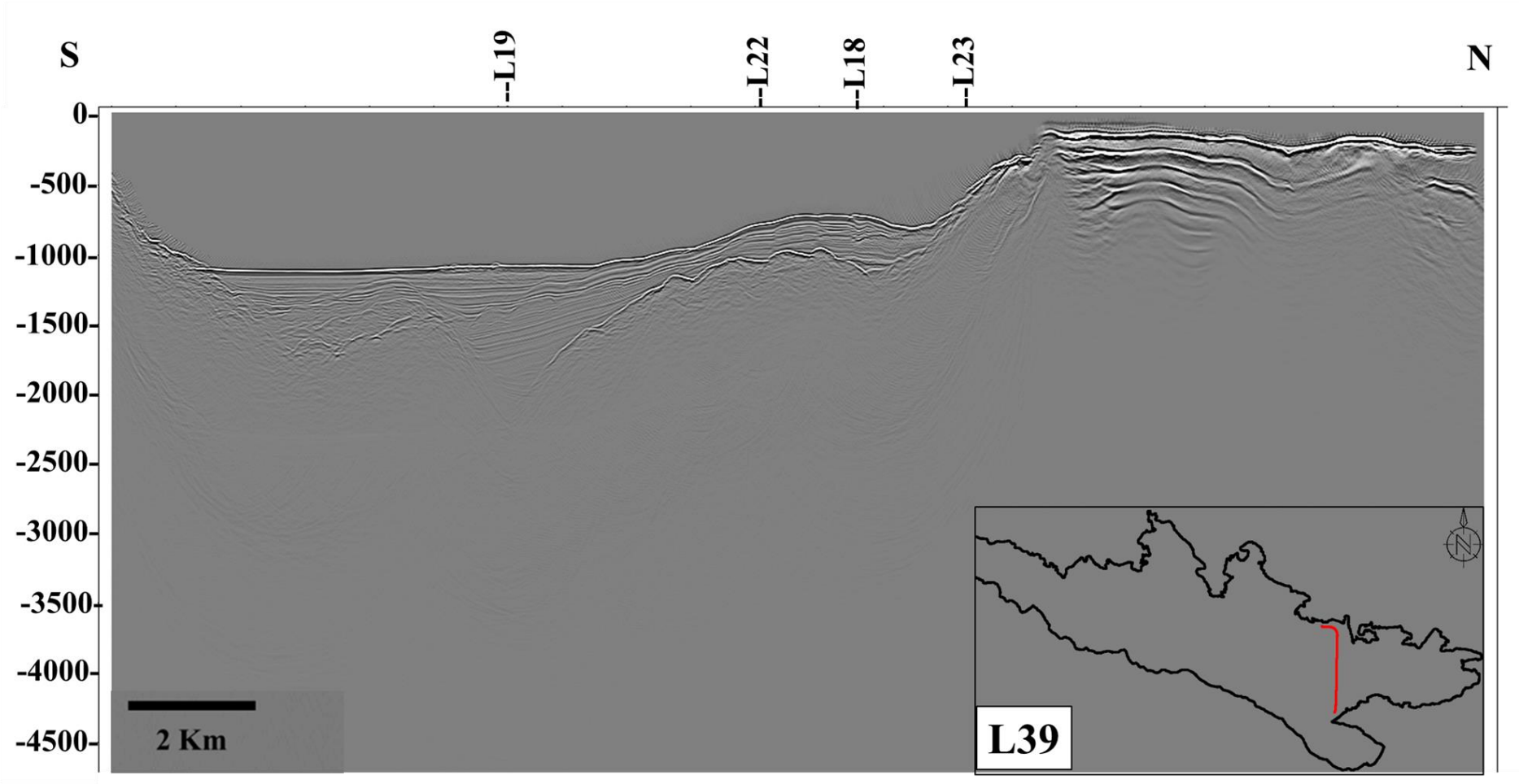
S
--L19
--L22
--L18
--L23
N
0
-500
-1000
-1500
-2000
-2500
-3000
-3500
-4000
-4500
2 Km
L39

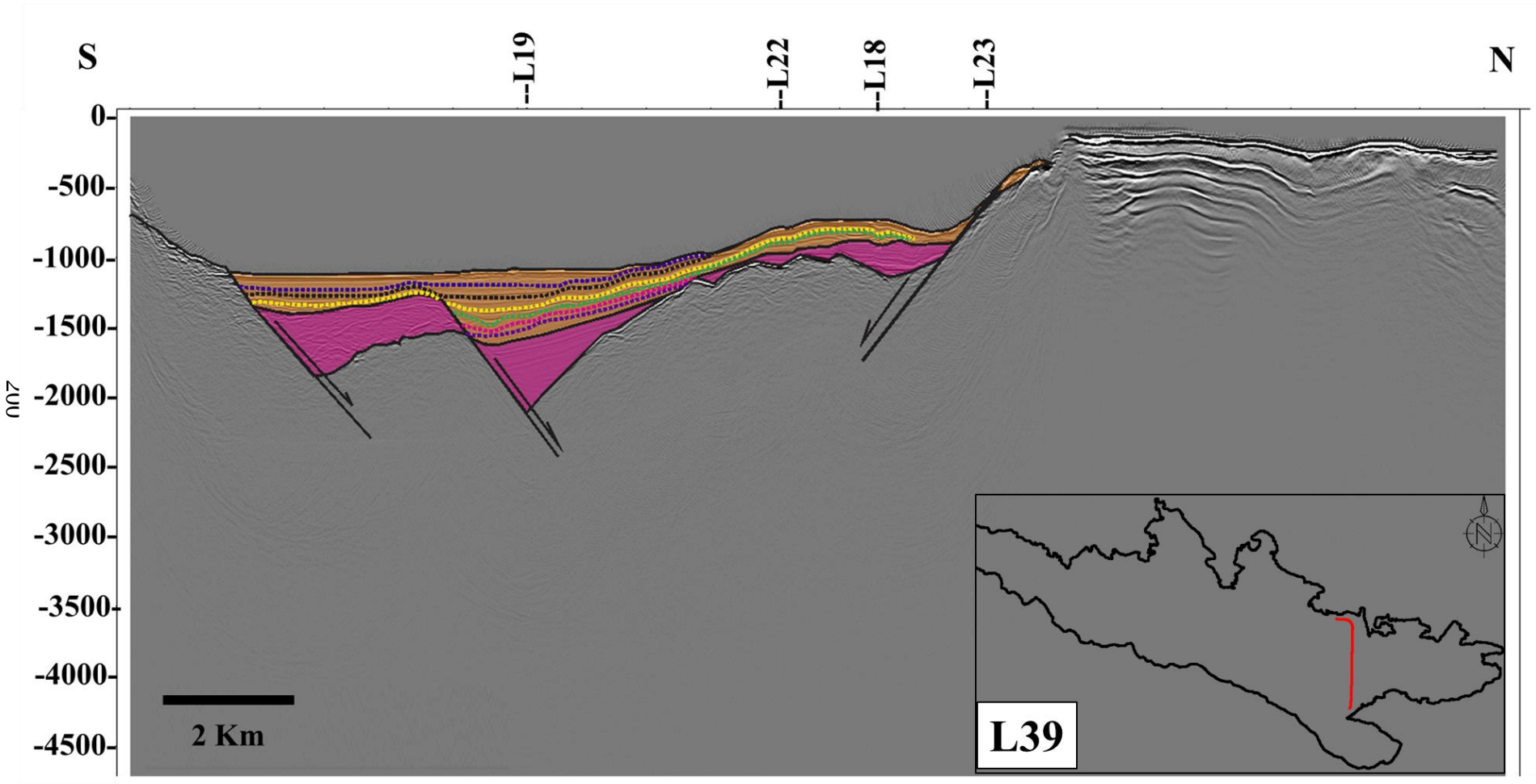
S
--L19
--L22
--L18
--L23
N
0
-500
-1000
-1500
-2000
-2500
-3000
-3500
-4000
-4500
2 Km
L39

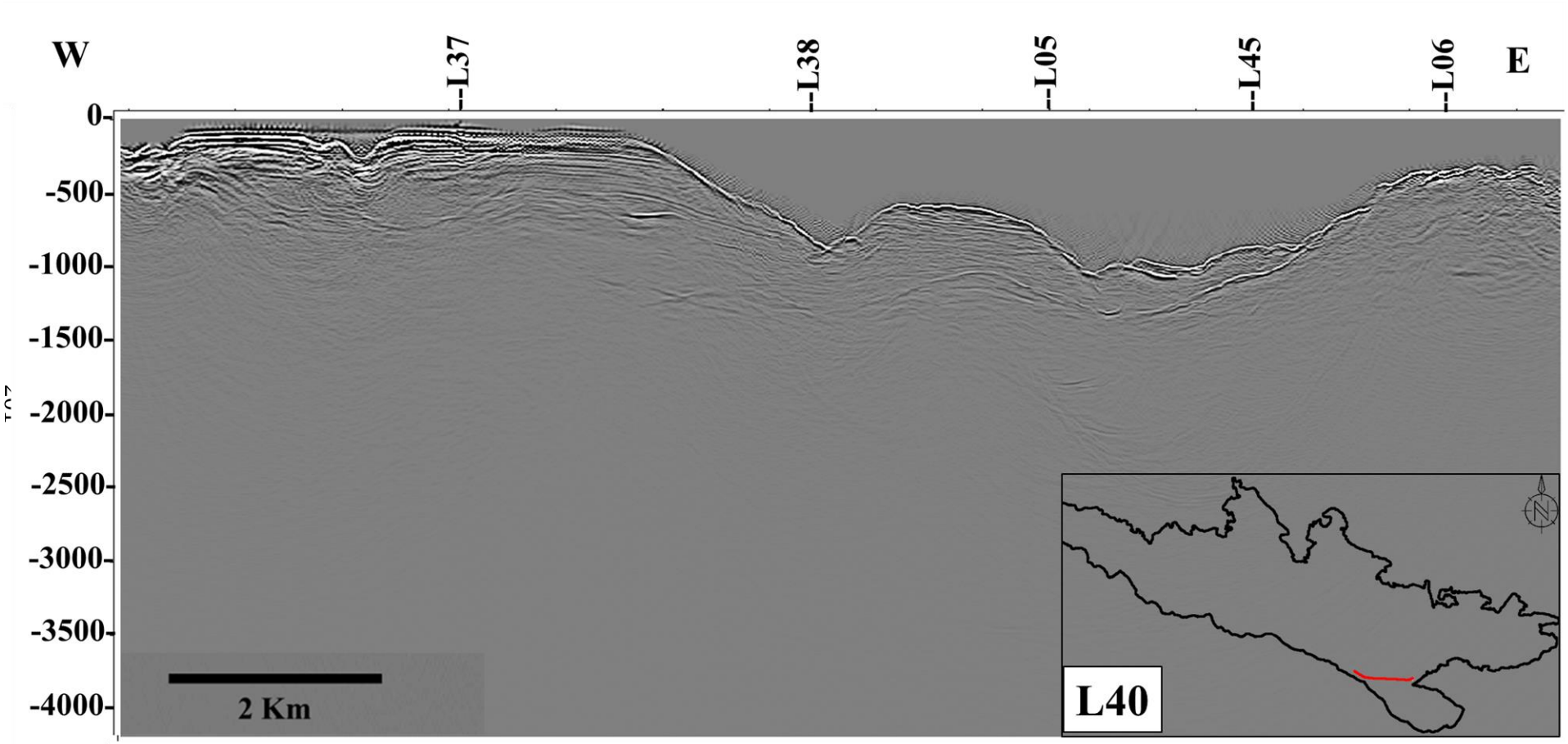
W
--L37
--L38
--L05
--L45
--L06
E
0
-500
-1000
-1500
-2000
-2500
-3000
-3500
-4000
2 Km
L40

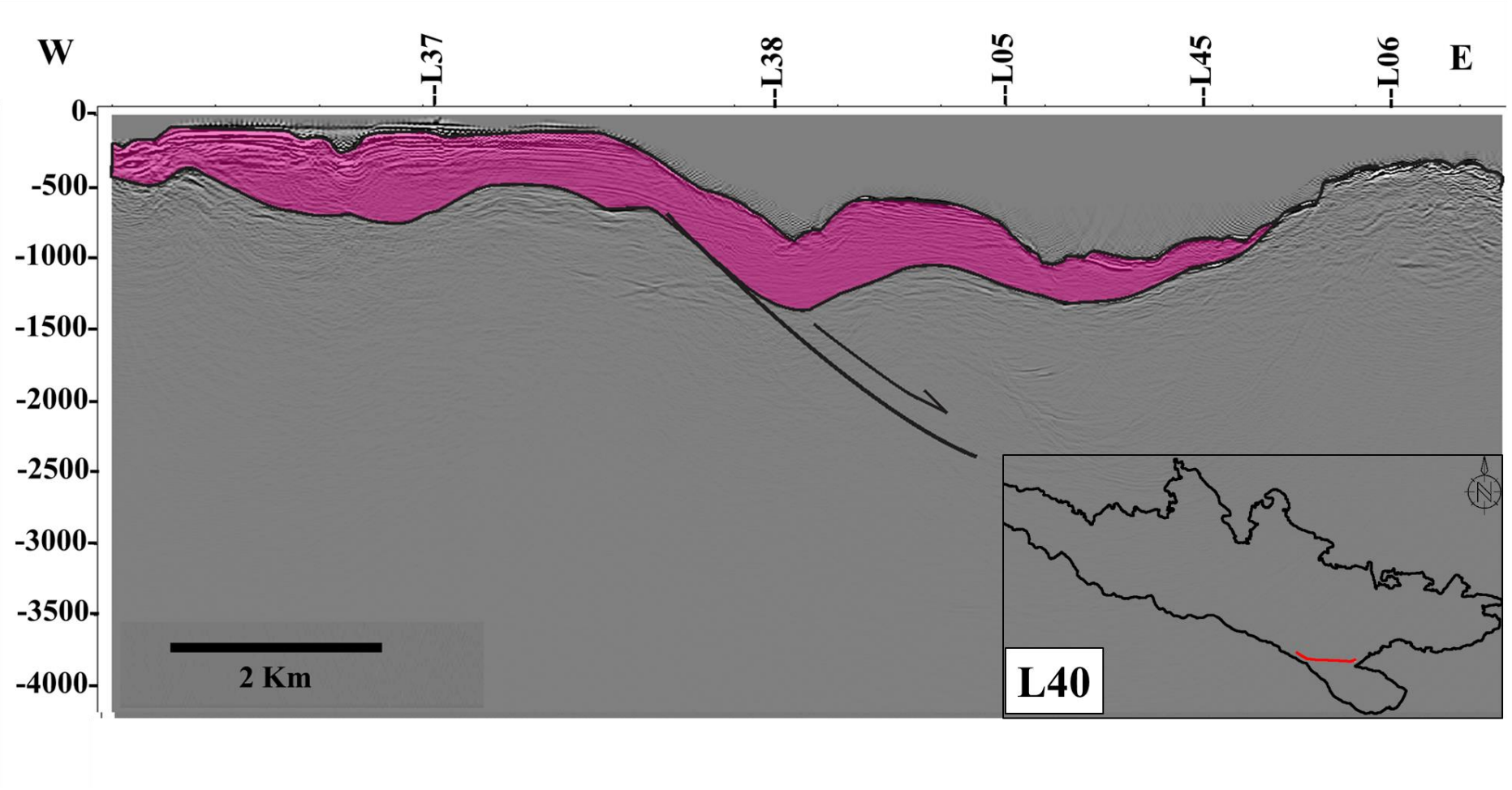
W
--L37
--L38
--L05
--L45
--L06
E
0
-500
-1000
-1500
-2000
-2500
-3000
-3500
-4000
2 Km
L40

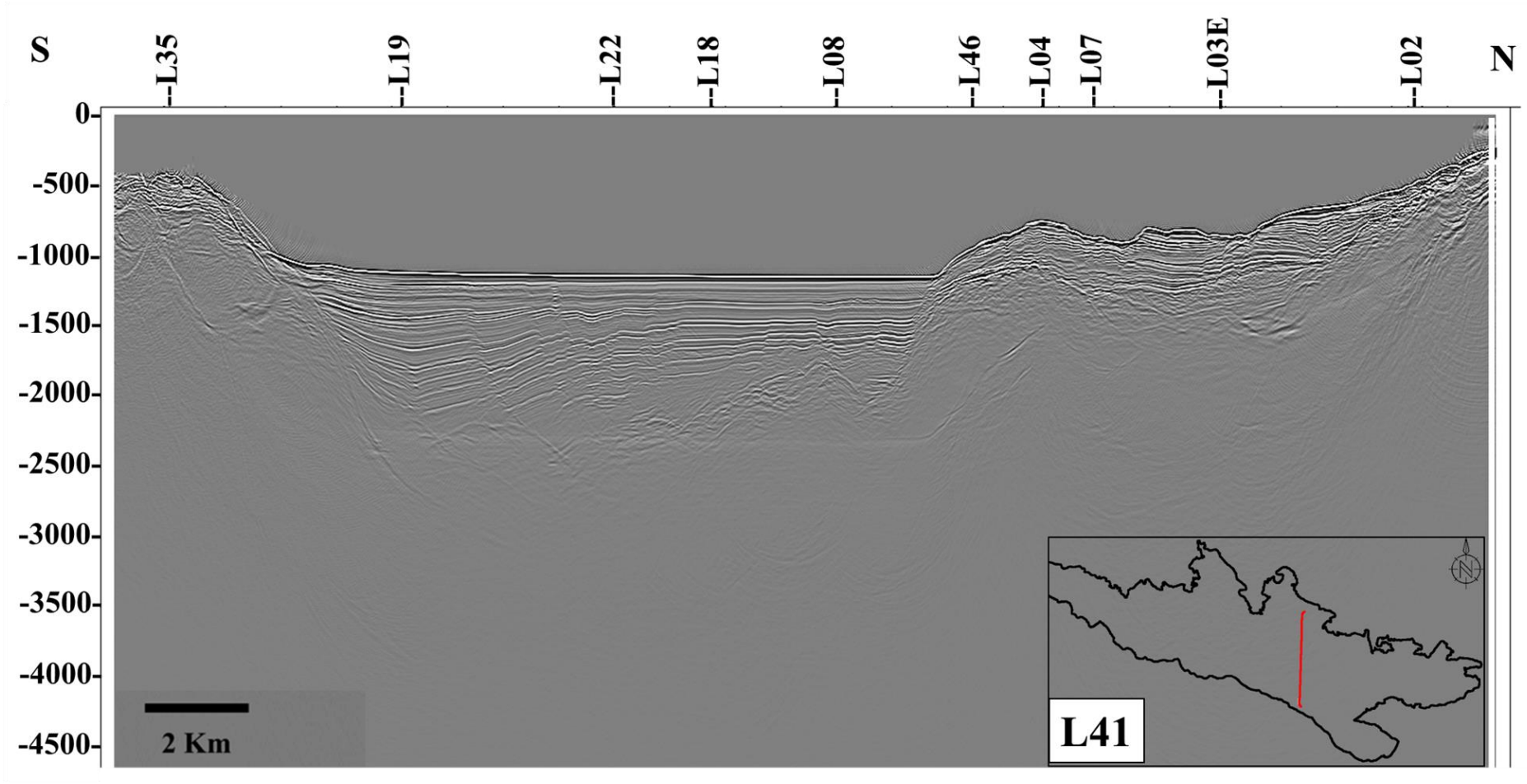
S
L35
L19
L22
L18
L08
L46
L04
L07
L03E
L02
N
0
-500
-1000
-1500
-2000
-2500
-3000
-3500
-4000
-4500
2 Km
L41

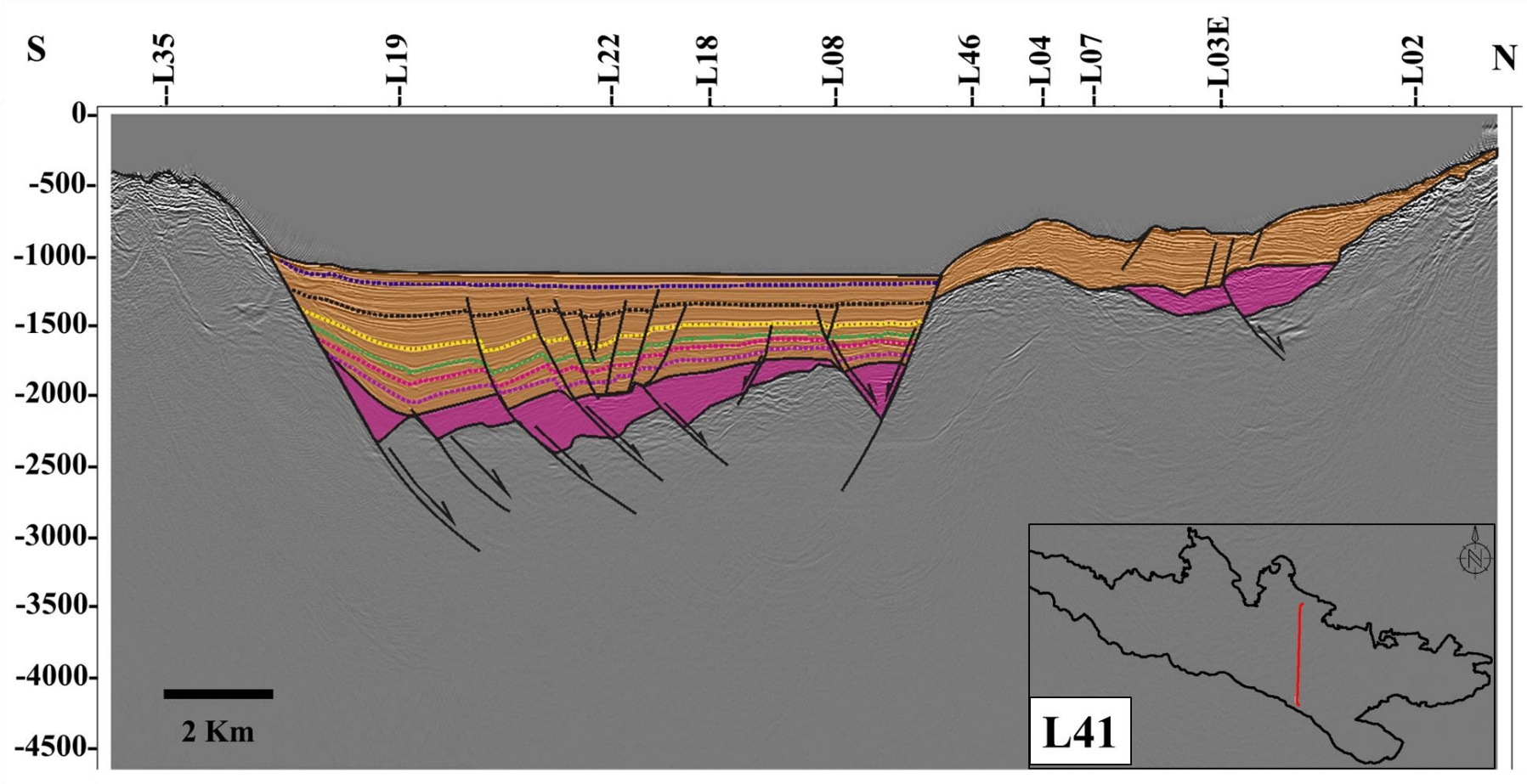
S
L35
L19
L22
L18
L08
L46
L04
L07
L03E
L02
N
0
-500
-1000
-1500
-2000
-2500
-3000
-3500
-4000
-4500
2 Km
L41

N
L02
L37
L03E
L46
L04
L23
L18
L09
L22
L19
S
0
-500
-1000
-1500
-2000
-2500
-3000
-3500
-4000
-4500
2 Km
L42

N
L02
L37
L03E
L46
L04
L23
L18
L09
L22
L19
S
0
-500
-1000
-1500
-2000
-2500
-3000
-3500
-4000
-4500
2 Km
L42

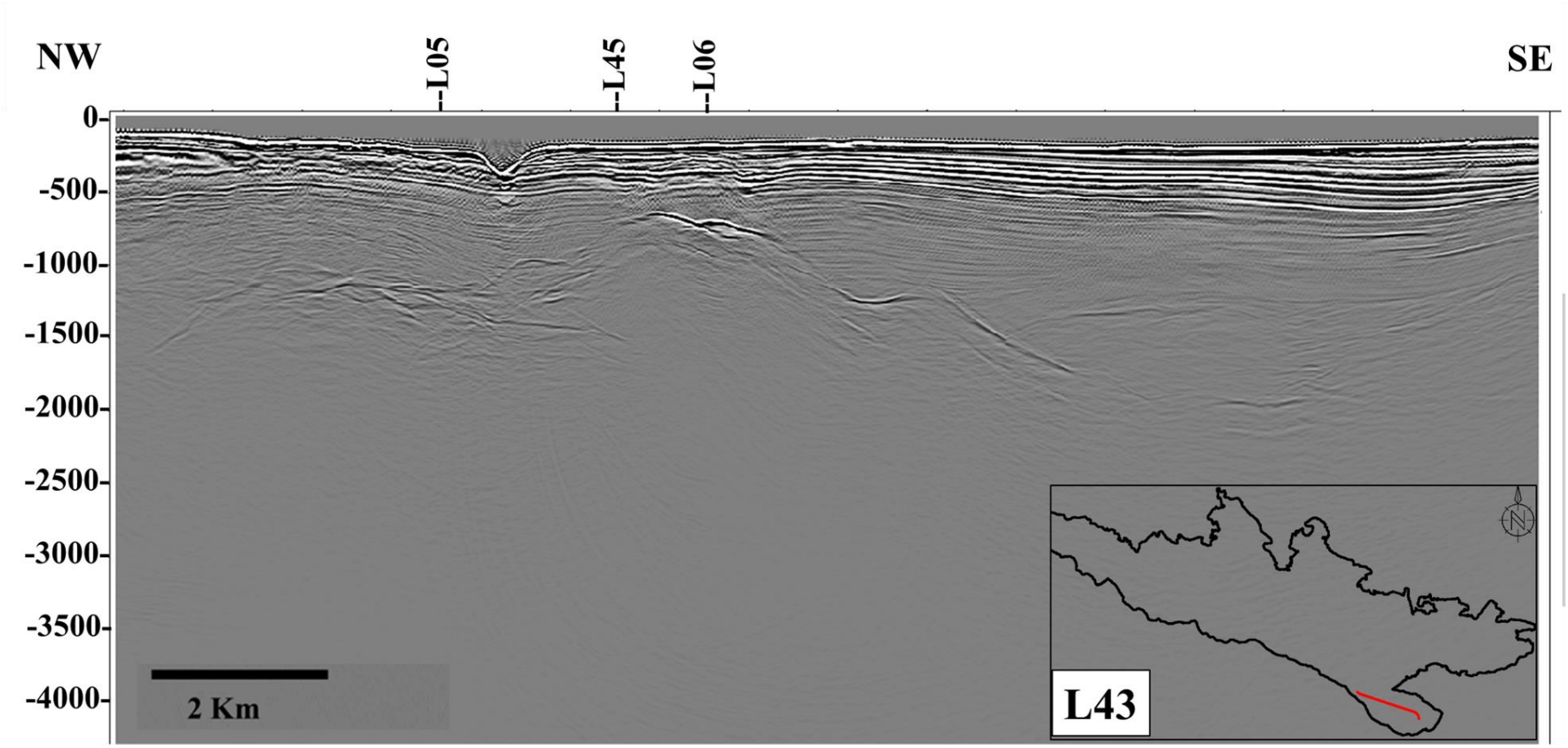
NW
SE
L05
L45
L06
0
-500
-1000
-1500
-2000
-2500
-3000
-3500
-4000
2 Km
L43

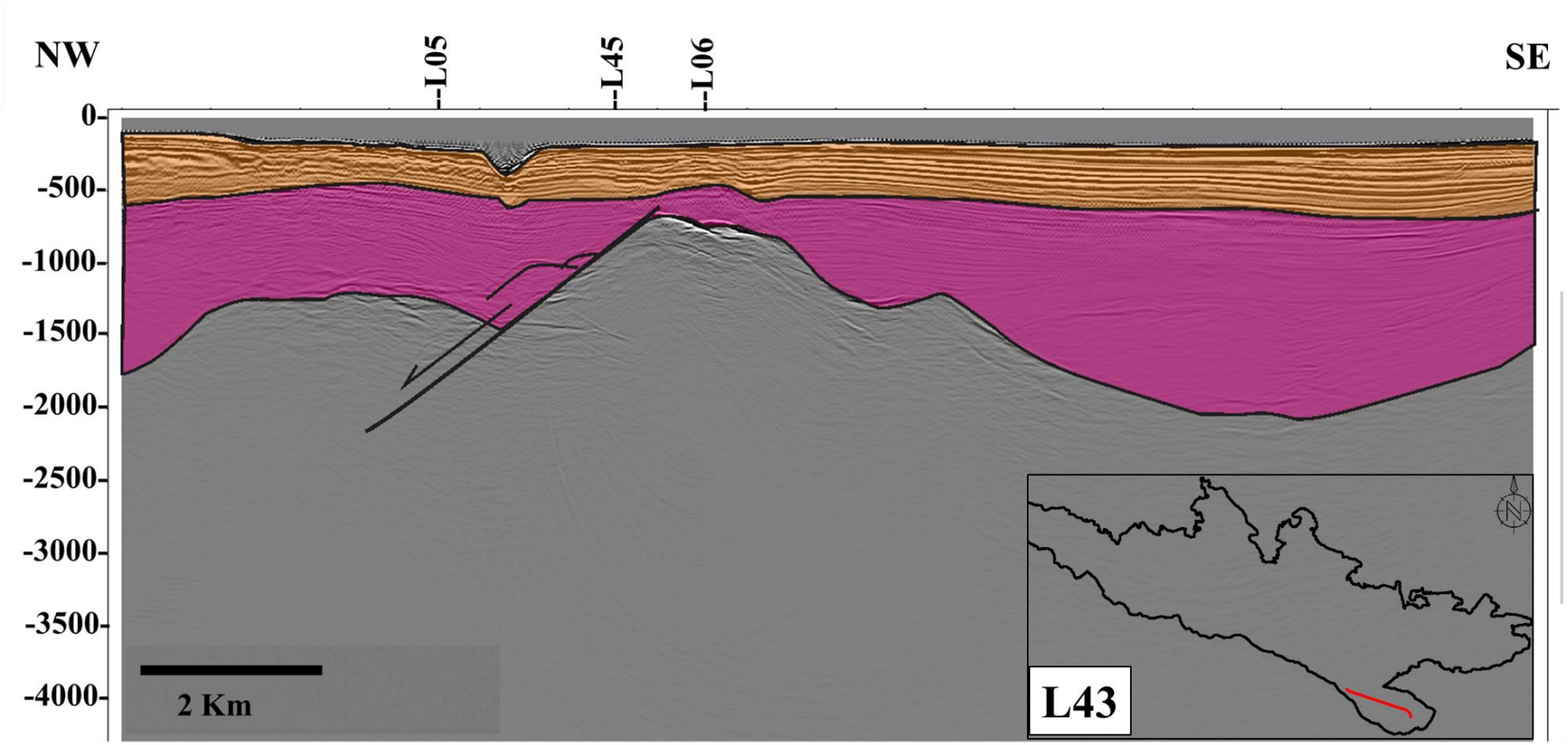
NW
L05
L45
L06
SE
0
-500
-1000
-1500
-2000
-2500
-3000
-3500
-4000
2 Km
L43

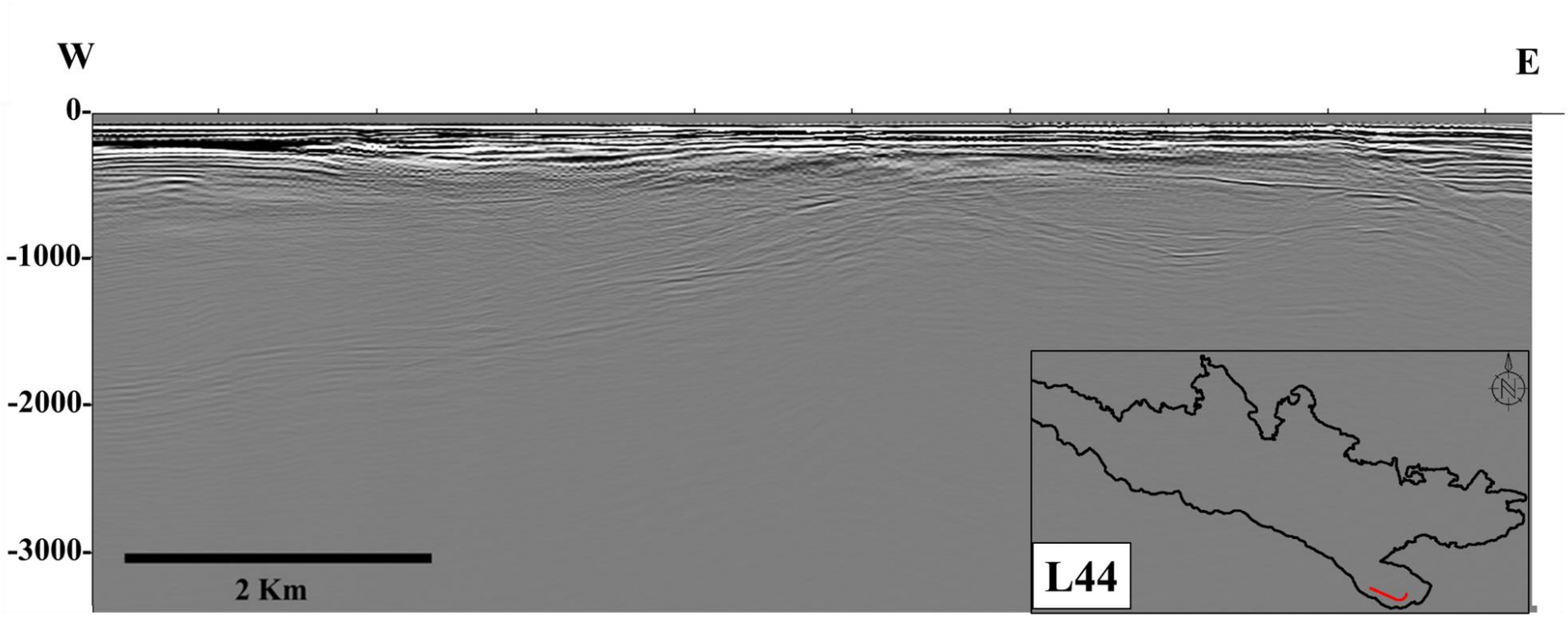
W
E
0-
-1000-
-2000-
-3000-
2 Km
L44

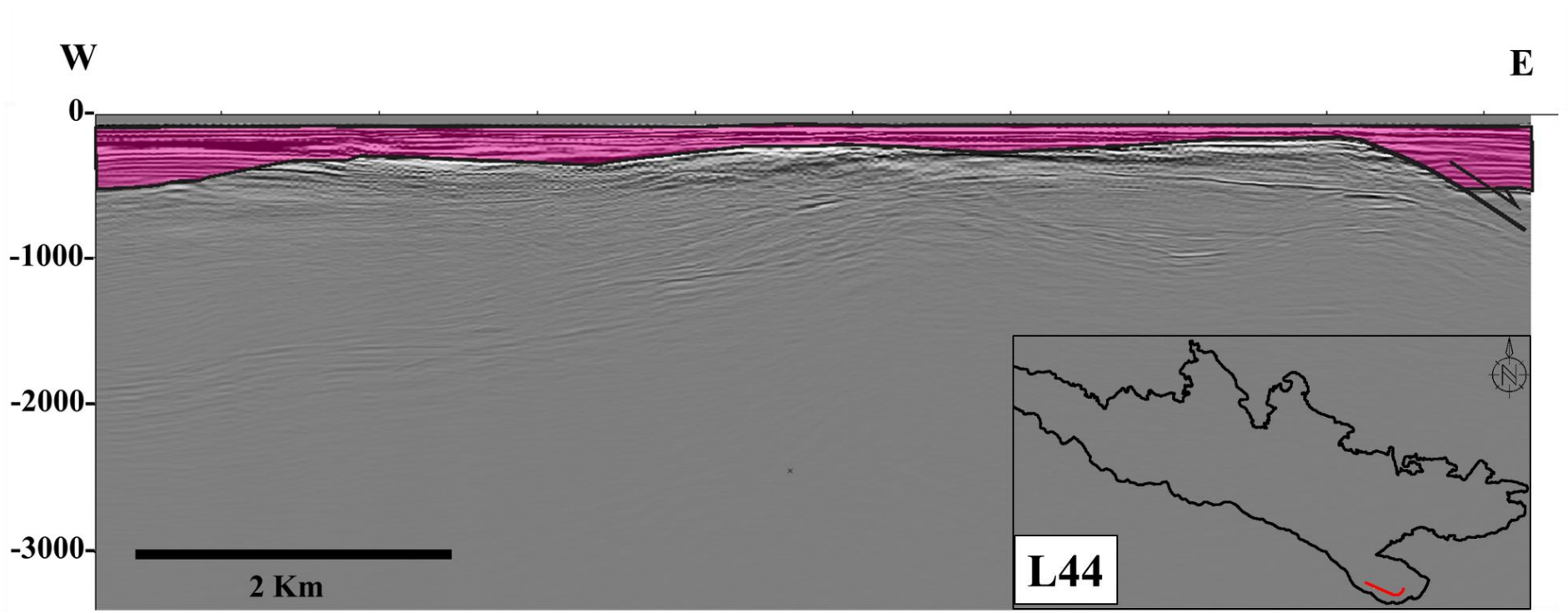
W
E
0
-1000
-2000
-3000
2 Km
L44

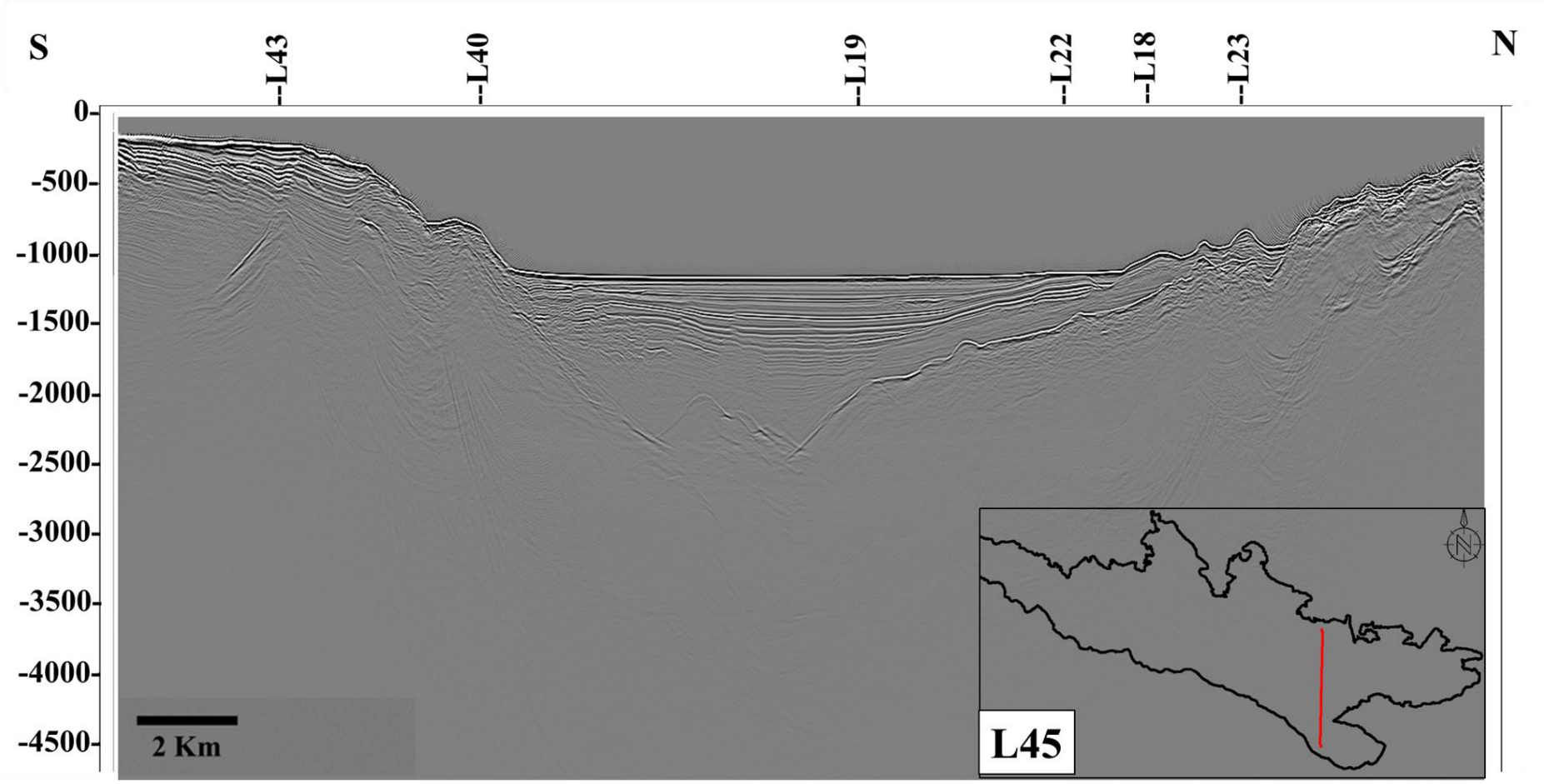
S
--L43
--L40
--L19
--L22
--L18
--L23
N
0
-500
-1000
-1500
-2000
-2500
-3000
-3500
-4000
-4500
2 Km
L45

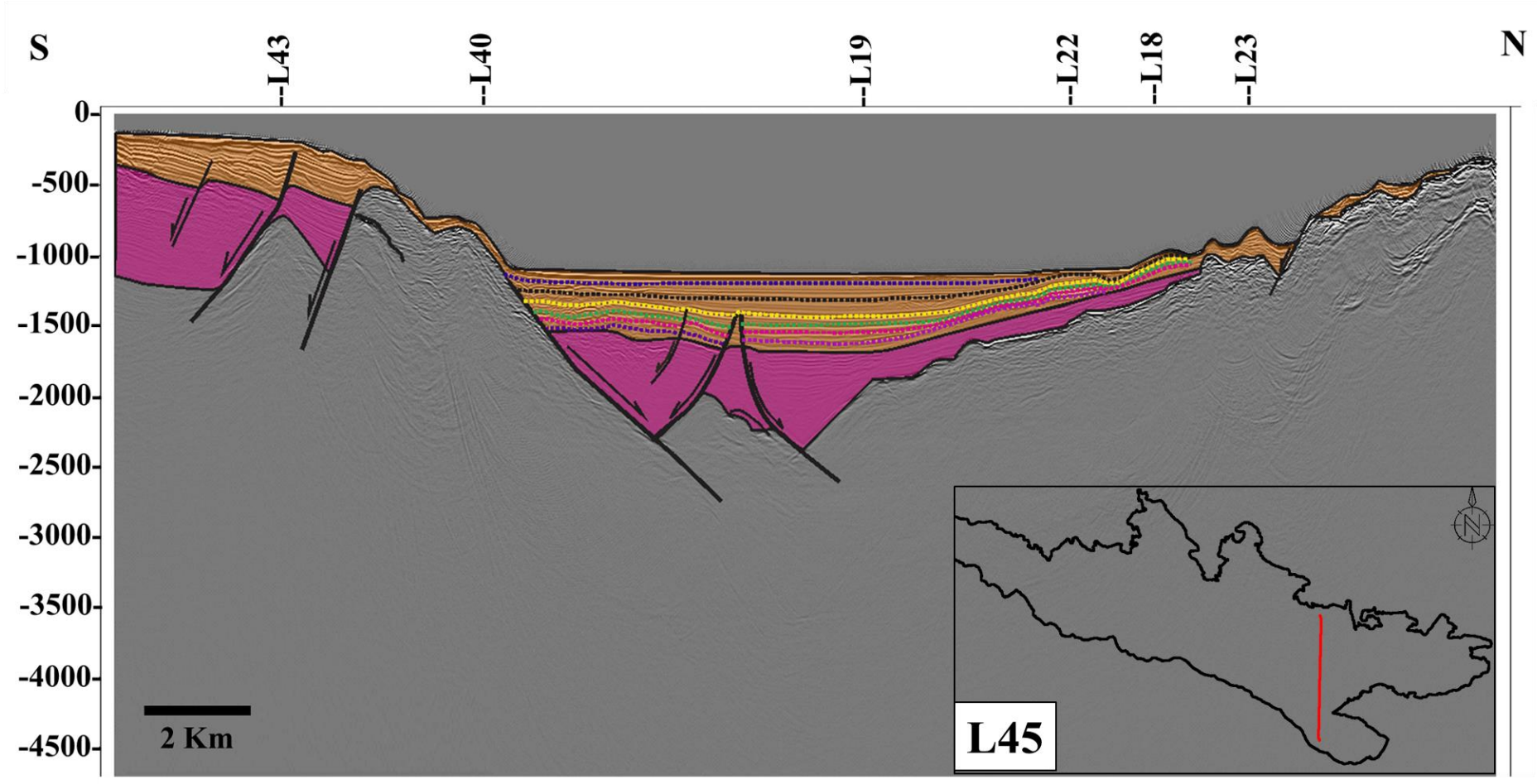
S
L43
L40
L19
L22
L18
L23
N
0
-500
-1000
-1500
-2000
-2500
-3000
-3500
-4000
-4500
2 Km
L45

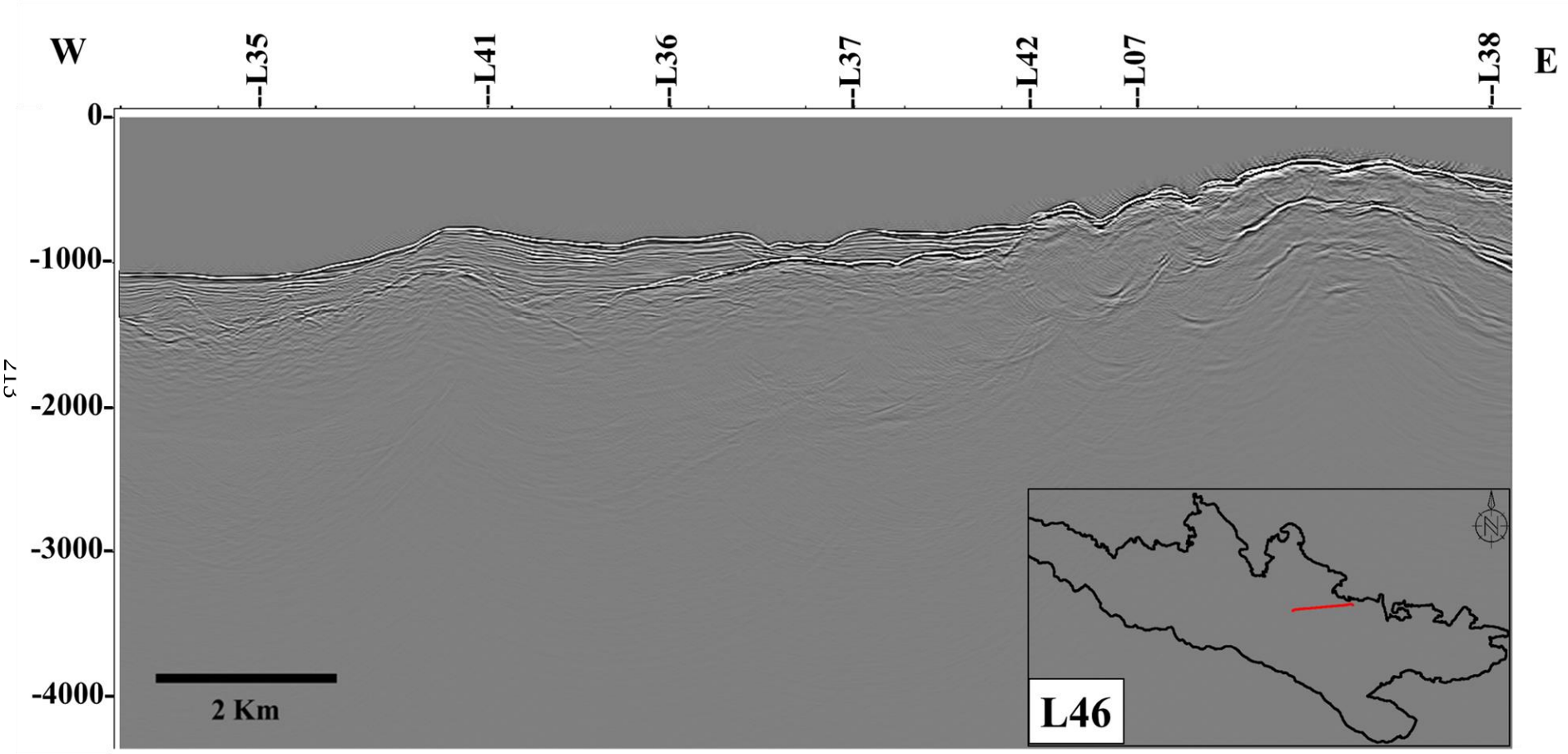
W
L35
L41
L36
L37
L42
L07
L38
E
0
-1000
-2000
-3000
-4000
2 Km
L46

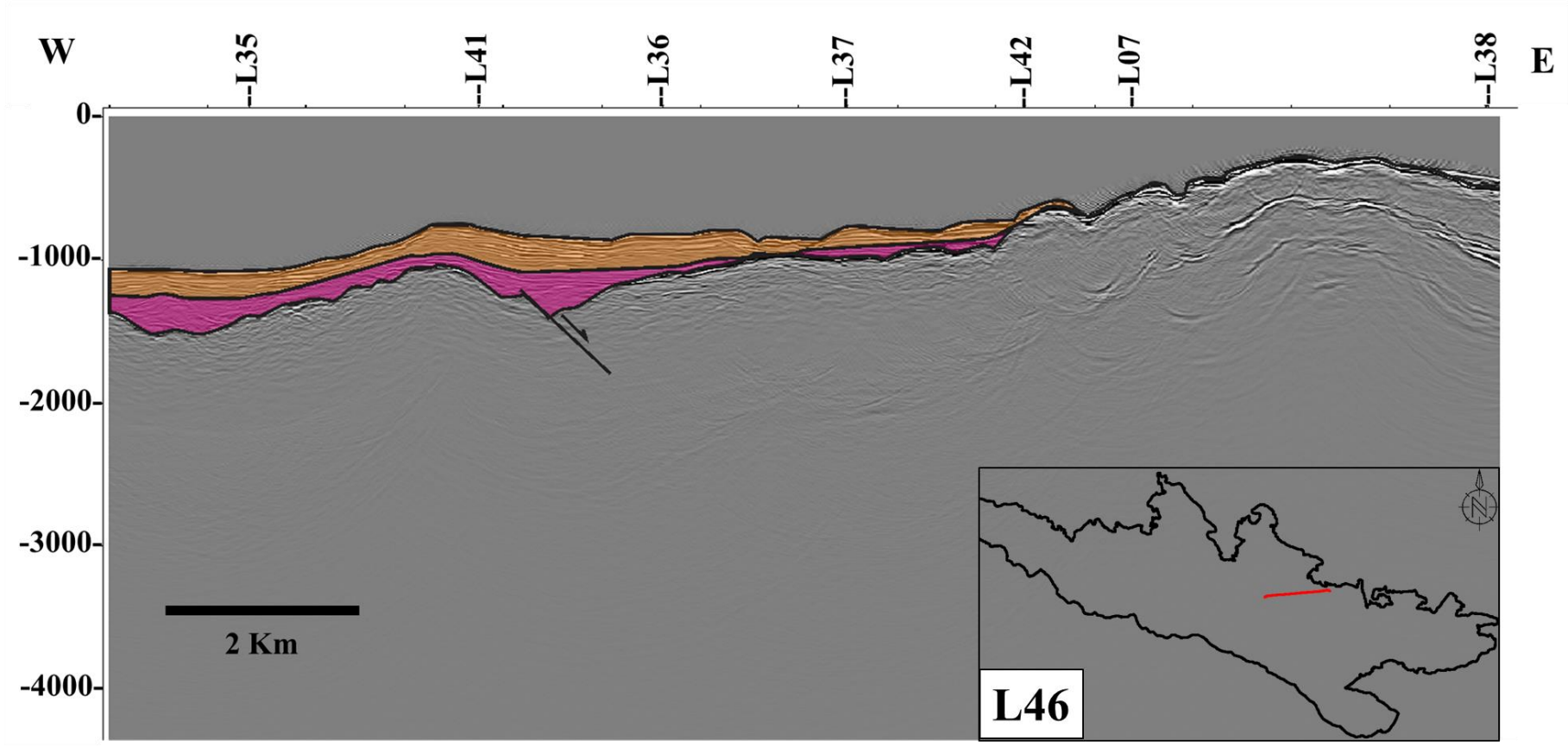
W
L35
L41
L36
L37
L42
L07
L38
E
0
-1000
-2000
-3000
-4000
2 Km
L46

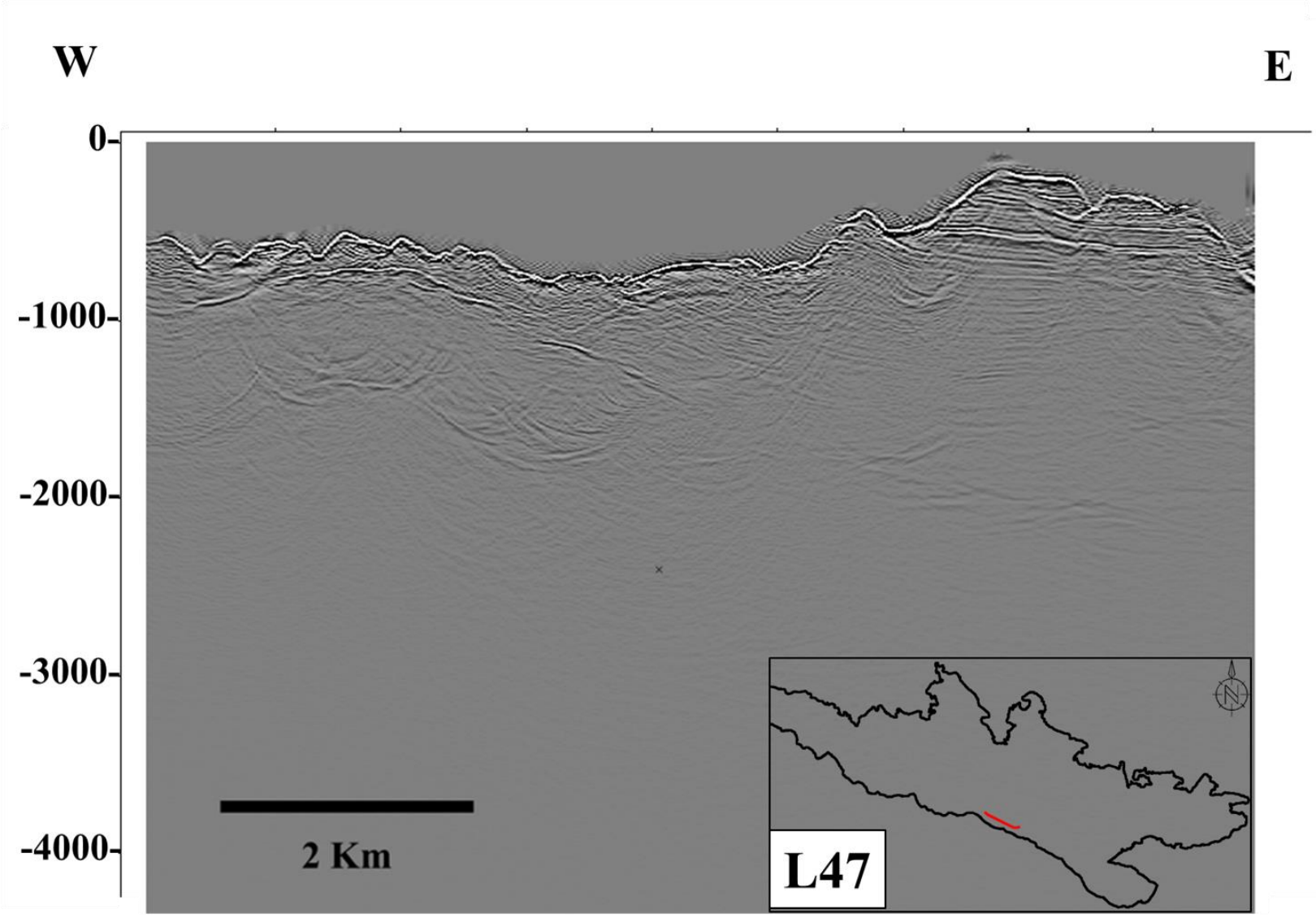
W
E
0
-1000
-2000
-3000
-4000
2 Km
L47

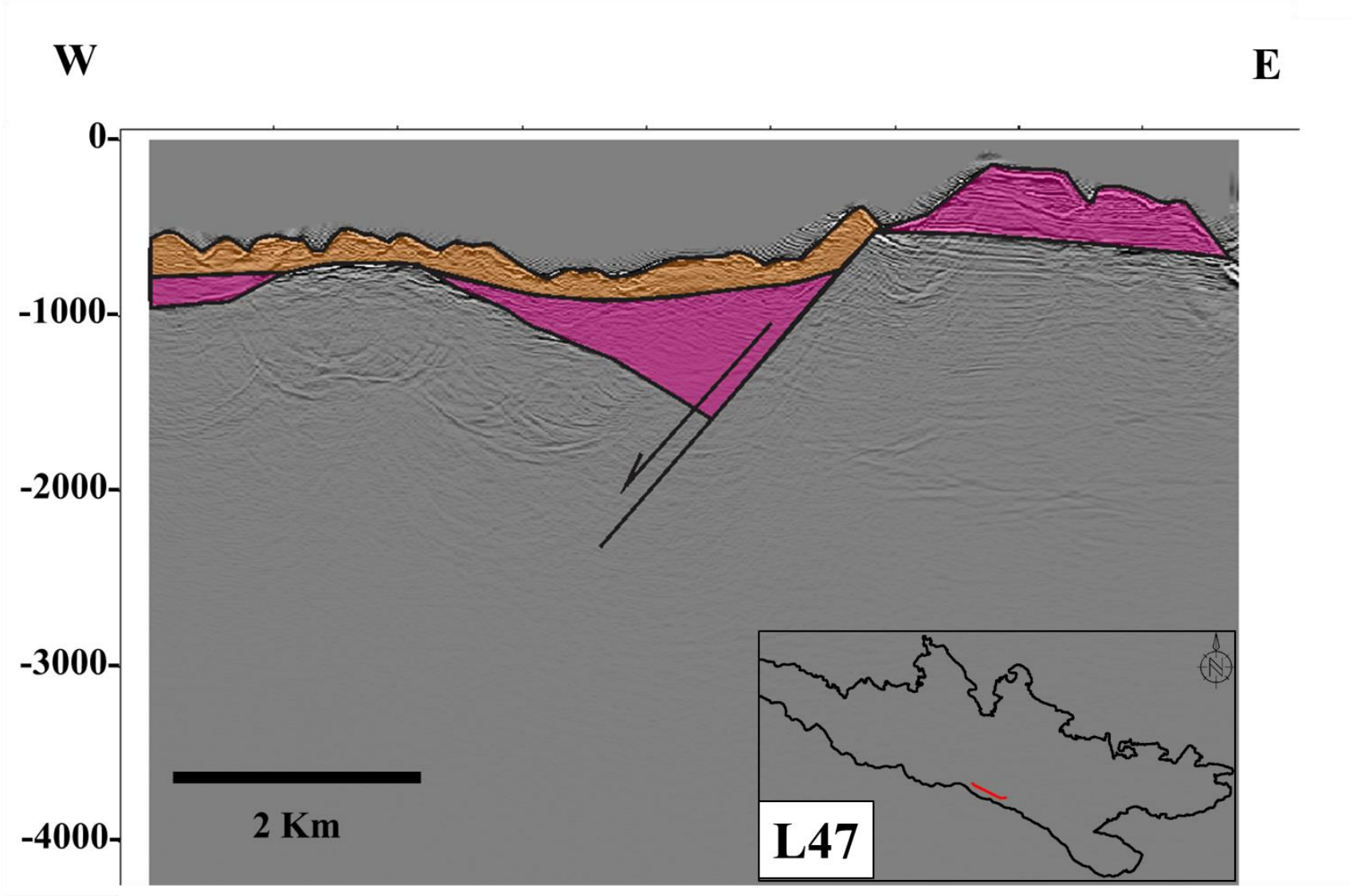
W
E
0
-1000
-2000
-3000
-4000
2 Km
L47

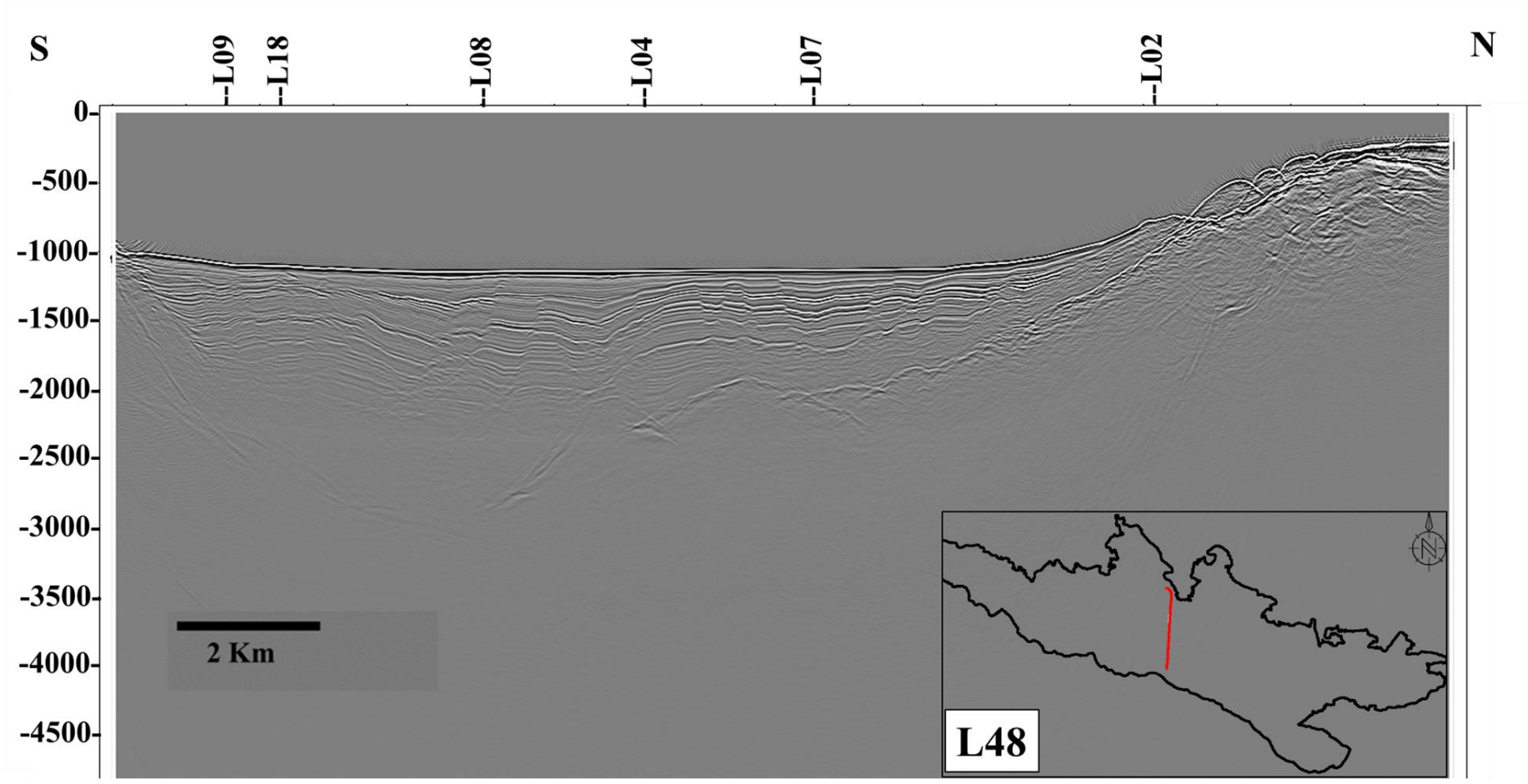
S
L09
L18
L08
L04
L07
L02
N
0
-500
-1000
-1500
-2000
-2500
-3000
-3500
-4000
-4500
2 Km
L48

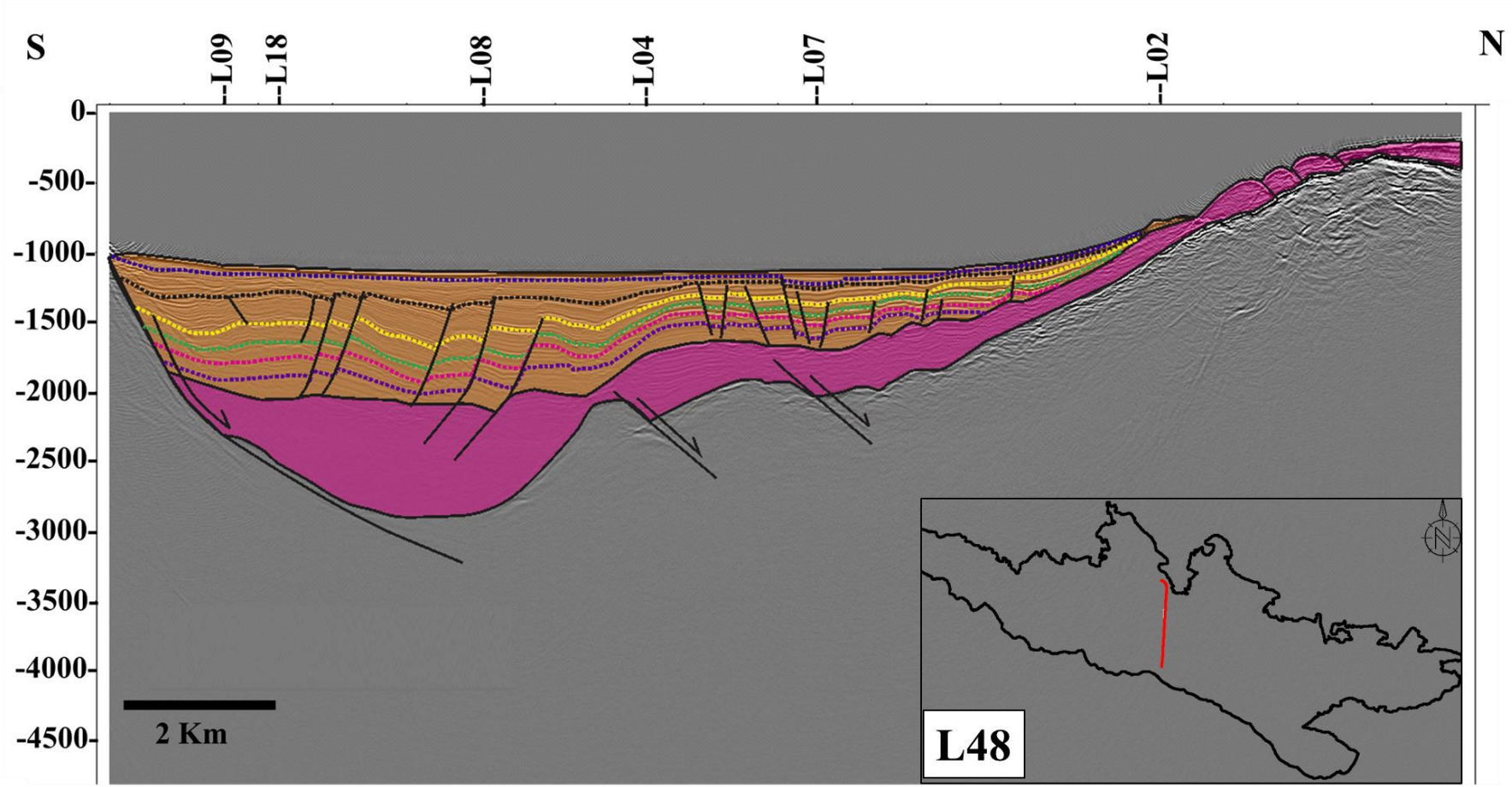
S
L09
L18
L08
L04
L07
L02
N
0
-500
-1000
-1500
-2000
-2500
-3000
-3500
-4000
-4500
2 Km
L48

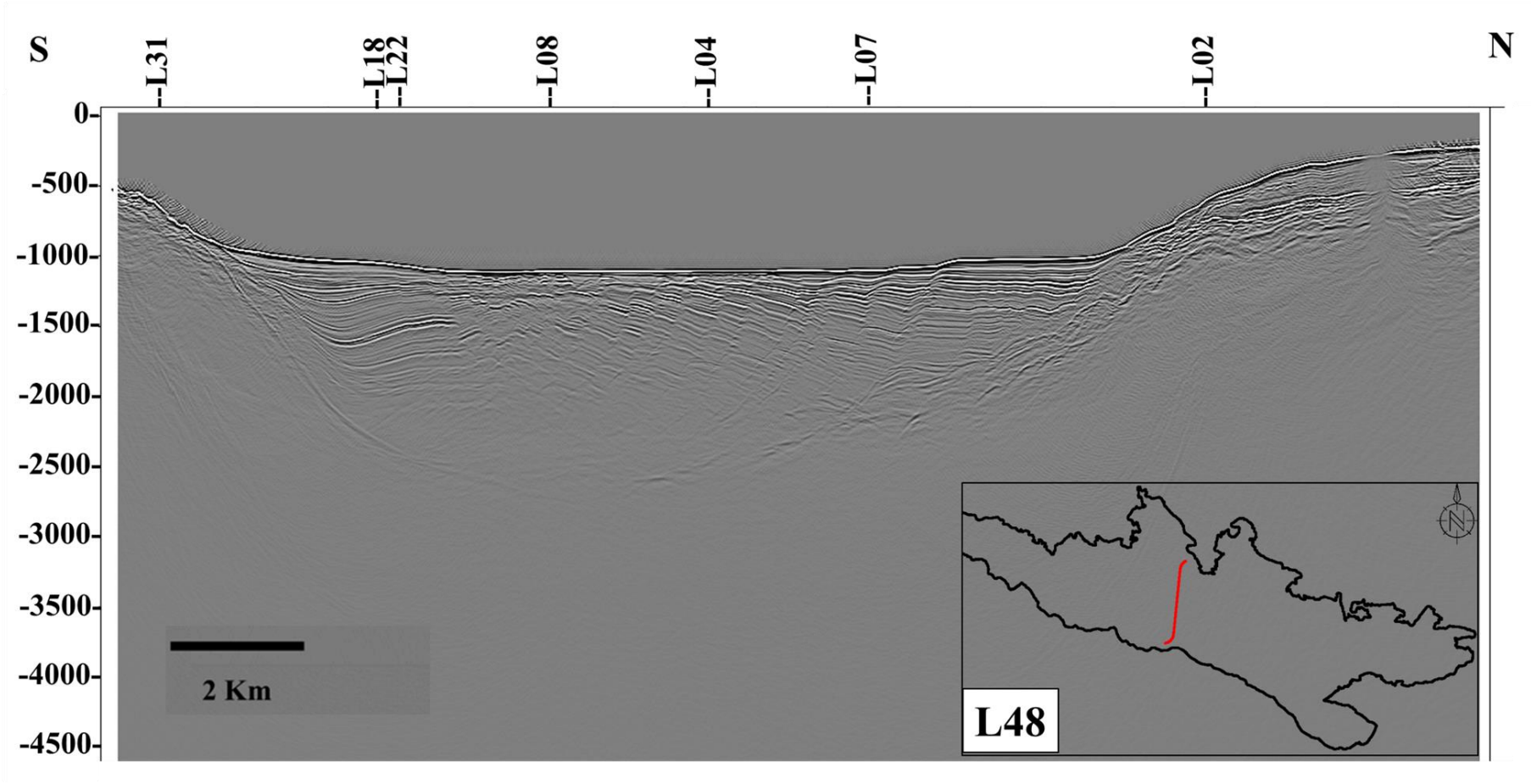
S
N
--L31
--L18
--L22
--L08
--L04
--L07
--L02
0
-500
-1000
-1500
-2000
-2500
-3000
-3500
-4000
-4500
2 Km
L48

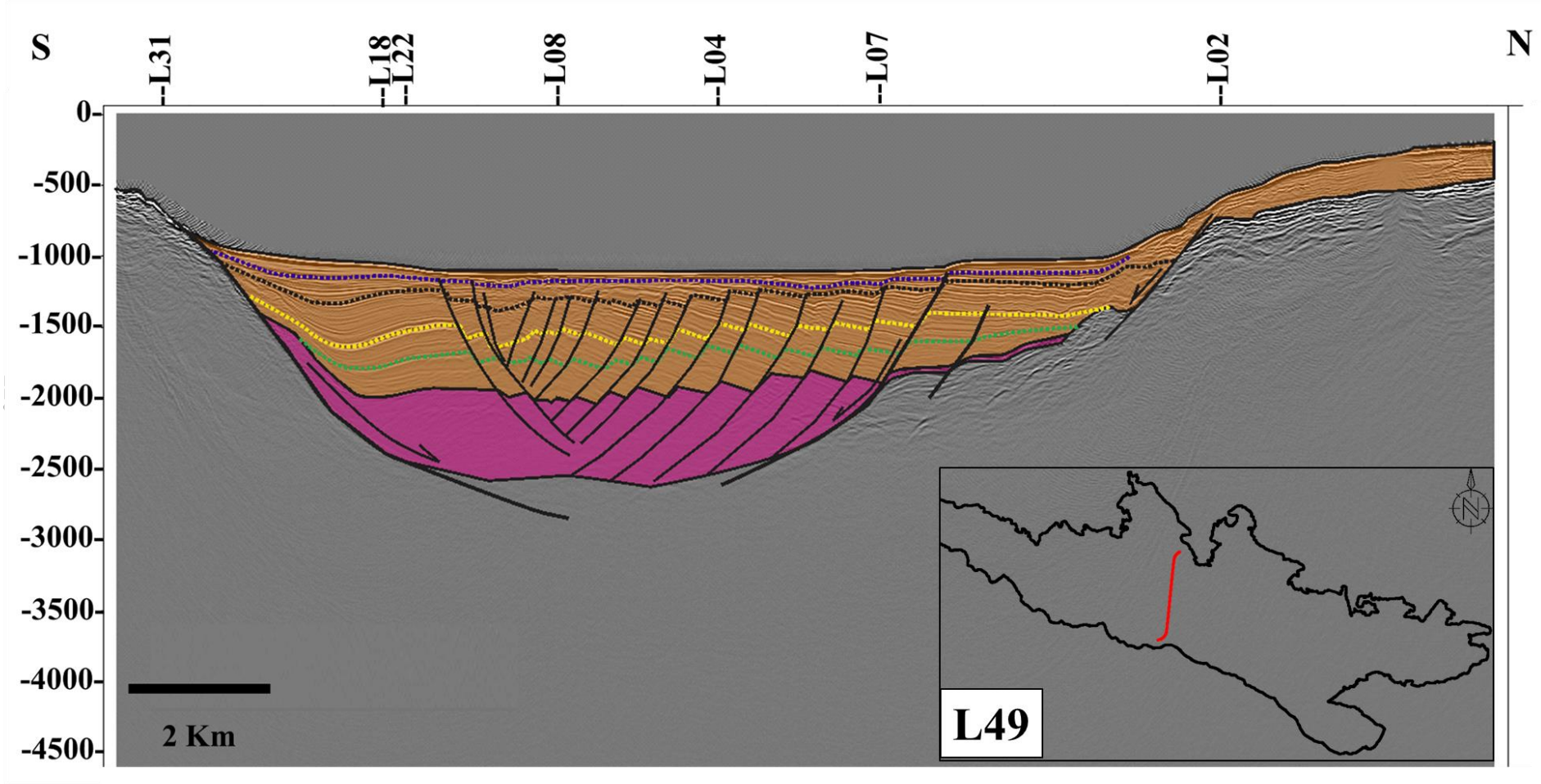
S
N
L31
L18
L22
L08
L04
L07
L02
0
-500
-1000
-1500
-2000
-2500
-3000
-3500
-4000
-4500
2 Km
L49

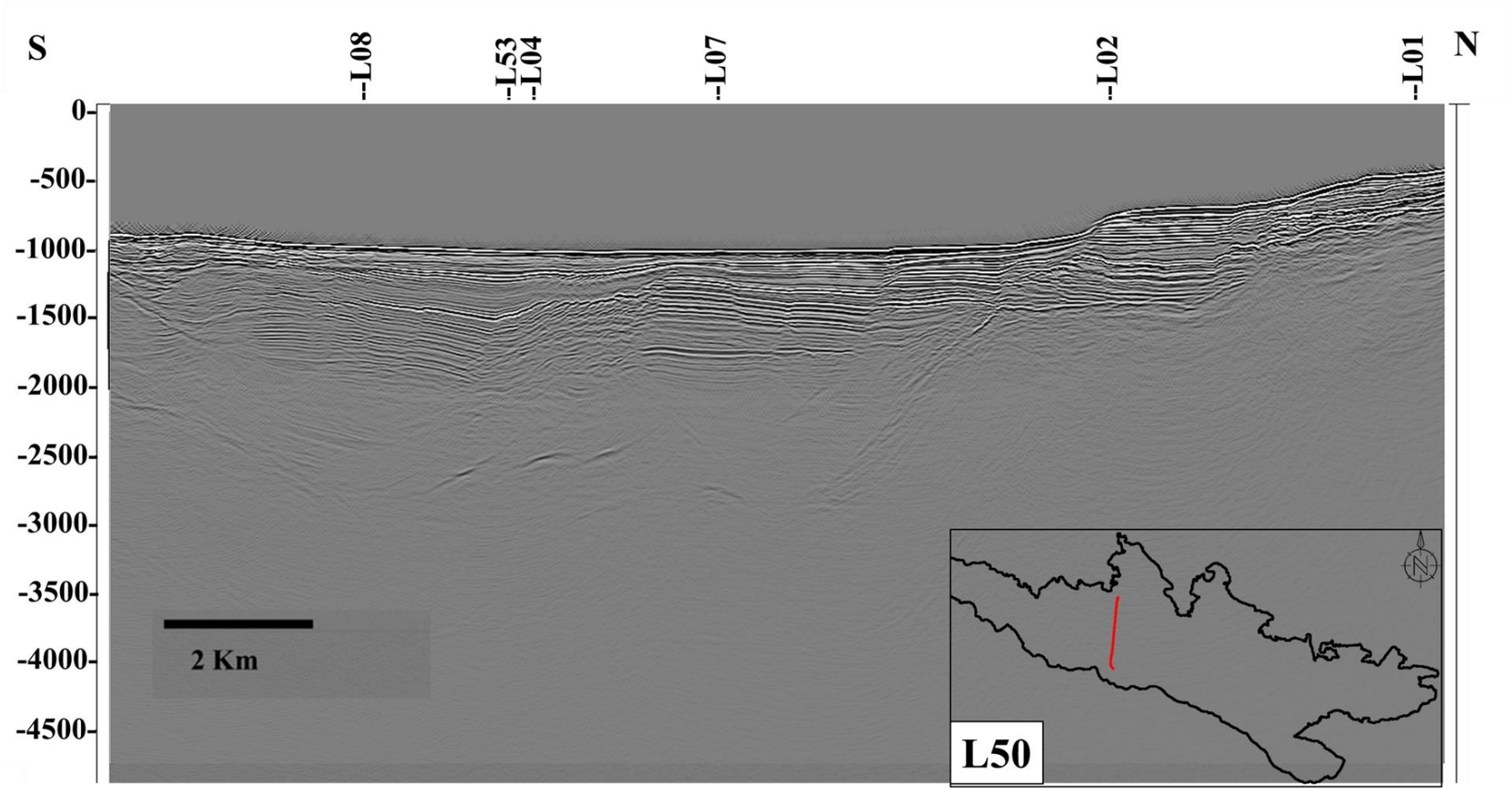
S
--L08
--L53
--L04
--L07
--L02
--L01
N
0
-500
-1000
-1500
-2000
-2500
-3000
-3500
-4000
-4500
2 Km
L50

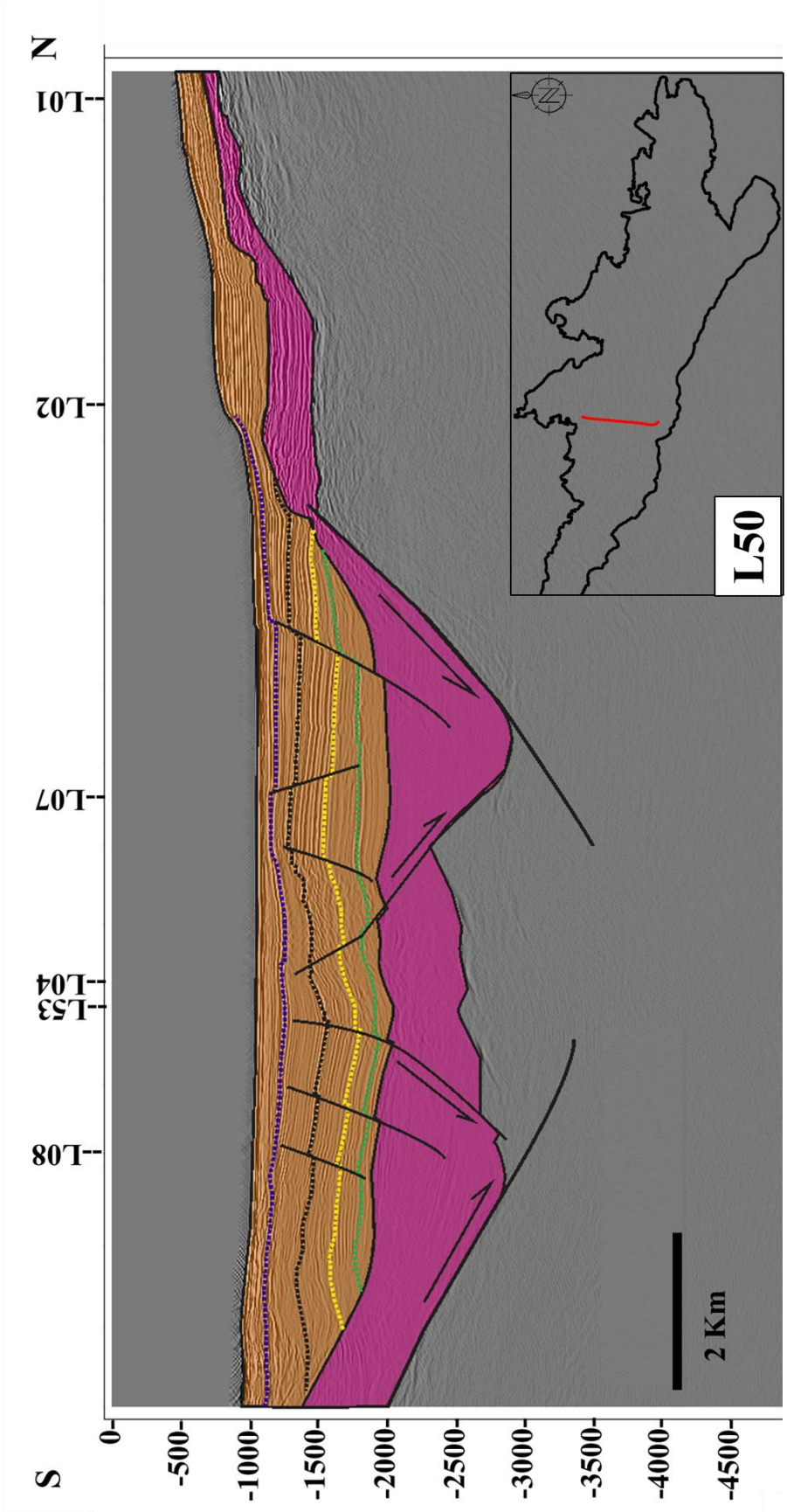
N
L01
L02
L07
L04
L53
L08
S
0
-500
-1000
-1500
-2000
-2500
-3000
-3500
-4000
-4500
2 Km
L50

E
L14
L16
L50
L04
L30
L24
L29
L25
L28
L07
L26
L27
W
0
-1000
-2000
-3000
-4000
N
2 Km
L53

E
L14
L16
L50
L04
L30
L24
L29
L25
L28
L07
L26
L27
W
0
-1000
-2000
-3000
-4000
L53
2 Km